SURFACE PROPERTIES AND SELECTIVE FLOTATION OF INHERENTLY HYDROPHOBIC MINERALS

by

Sadan Kelebek

A thesis submitted to the Faculty of Graduate Studies and Research in partial fulfilment of the requirements for the degree of Doctor of Philosophy

Department of Mining and
Metallurgical Engineering
McGill University
Montreal, Quebec, Canada.

© December 1984

Ph.D.

Metallurgical Engineering

SURFACE PROPERTIES AND SELECTIVE FLOTATION OF INHERENTLY HYDROPHOBIC MINERALS

by

Sadan Kelebek

ABSTRACT

Surface properties of a number of minerals including talc, graphite and sulphides such as chalcopyrite and galena were investigated. A new method of surface preparation for the layer-type, inherently hydrophobic minerals was developed. A correlation has been shown between contact angle, zeta potential and flotation behaviour. The hydrophilic-to-hydrophobic ratios of various minerals were estimated and their role in this correlation discussed.

Critical surface tensions of wetting (γ_c) were determined using pure liquids as well as aqueous solutions. Adsorption densities of methanol ($\Gamma_{\ell v}$) and viscosities were used to explain the mechanism of wetting and the frequently observed γ_c value of $\simeq$ 30 mN/m for a number of hydrophobic samples. The adhesion tension diagrams were used to identify the critical surface tension range within which preferential wetting occurs between two inherently hydrophobic minerals. This range has been exploited for the flotation separation of binary mixtures of the minerals. Induction periods estimated as a function of surface tension ($\gamma_{\ell v}$) have been discussed with reference to the separation tests. The separations employing the methanol solutions have been compared with those obtained using a more conventional system of Lignosol-MIBC solutions.

The effect of sulphur formation and hydrocarbon chain length on the wettability and floatability of sulphides were also determined as a function of $\gamma_{\ell v}$.

Doctorat

Génie
Métallurgique

PROPRIETES SUPERFICIELLES ET FLOTTATION SELECTIVE DE MINÉRAUX NATURELLEMENT HYDROPHOBES

RESUME

On a étudié les propriétés superficielles d'un certain nombre de minéraux incluant le talc, le graphite et des sulfures, telle la chalcopyrite et la galène. Une nouvelle méthode de préparation des surfaces et minéraux stratifiés, hydrophobes de nature, fut mise au point. On a établi une corrélation entre l'angle de contact, le potentiel zêta et les comportements lors de la flottation. Les rapports hydrophile/hydrophobe de divers minéraux furent estimés et leur rôle dans cette corrélation analysé.

Les tensions superficielles critiques de mouillage (γ_c) ont été déterminées en utilisant des liquides purs et des solutions aqueuses. Les densités d'adsorption du méthanol ($\Gamma_{\ell v}$) ainsi que les viscosités ont été utilisées pour expliquer le méchanisme du mouillage ainsi que la valeur de ≈ 30 mN/m fréquemment constatée chez une quantité d'échantillons hydrophobes. Des diagrammes de tension-adhésion furent utilisés pour délimiter la tension critique superficielle à laquelle un mouillage préférentiel se produit entre deux minéraux naturellement hydrophobes. Cette limite fut mise à profit lors du traitement par flottation de composés binaires de minéraux. Se basant sur les tests de séparation, on analyse les périodes d'induction en fonction de la tension superficielle ($\gamma_{\ell v}$). Les séparations obtenues en employant des solutions de méthanol ont été comparées à celles de solutions plus conventionnelles tel le Lignosol-MIBC.

L'effet qu'a la formation de sulfure et la longueur de la chaîne d'hydrocarbure sur le mouillage et la flottation des sulfures est donné en fonction de l'$\gamma_{\ell v}$.

Doktora

Metalurji Mühendisliği

KENDİLİĞİNDEN SUYU-DEFEDEN CEVHERLERİN YÜZEY ÖZELLİKLERİ VE SEÇİMLİ YUZDÜRÜLMESİ

Şadan Kelebek

ÖZET

Talk, grafit ve kükürtlülerden kalkoprit ve galen dahil birçok cevherin yüzey özellikleri araştırıldı. Tabaka yapılı, kendiliğinden suyu-defeden tür cevherler için yeni bir yüzey hazırlama usûlu geliştirildi. Temas açısı, elektrokinetik potansiyel ve yüzme davranışı arasındaki ortak ilişki belirtildi. Çeşitli cevherlerin suyu-seven-ve-defeden bölgelerinin oranı tesbit edilip bu ortak ilişkideki payı tartışıldı.

Saf sıvılar ve hem de sulu çözeltileri kullanarak cevherlerin kritik ıslanma-yüzey-gerilim (γ_c) değerleri belirlendi. Metanolün adsorpsiyon yoğunlukları ($\Gamma_{\ell v}$) ve sulu çözeltilerinin vizkoziteleri ıslatma olayını ve birçok örnek için sık sık gözlenen ≃ 30 mN/m lik γ_c değerini açıklamada kullanıldı. Suyu-defeden tür iki cevher arasındaki tercihi ıslanmanın vuku bulduğu kritik yüzey gerilim uzanımlarını belirlemek için yapışma gerilimi şemaları kullanıldı. İkili cevher karışımlarını yüzdürme usûlü ile ayırmak için bunlardan yararlanıldı. Değişik yüzey gerilimlerinde belirlenen enduksiyon süreleri ayırma deney sonuçları eşliğinde irdelendi. Metanol çözeltileri ve daha kullanışlı Lignosol-MIBC çözeltileriyle elde edilen ayırma sonuçları karşılaştırıldı.

Ayrıca, yüzeylerde kükürt oluşumu ve hidrokarbon zincir uzunluğunun kükurtlü cevherlerin ıslanabilirlik ve yüzdürülebilirliğindeki etkisi de değişik $\gamma_{\ell v}$ değerlerinde belirlendi.

TABLE OF CONTENTS

	page
ABSTRACT, RESUME and ÖZET	i-iii
TABLE OF CONTENTS	iv
LIST OF FIGURES	xi
LIST OF TABLES	xviii
ACKNOWLEDGEMENTS	xxii
CHAPTER 1 INTRODUCTION	
1.1 General Introduction	1
1.2 Inherent Hydrophobicity and Naturally Floatable Minerals	3
1.3 Natural Floatability of Common Sulphides	5
1.4 Minerals Studied and Their Crystal Structures	6
1.5 The Partial Ionic Character of the Metal-Sulphur Bonds	17
1.6 Statement of Problem and Objectives	21
1.7 Scope of the Work	22
1.8 REFERENCES	25
CHAPTER 2 SURFACE PROPERTIES OF VARIOUS NATURALLY FLOATABLE MINERALS	
2.1 INTRODUCTION	30
2.2 THEORETICAL REVIEW	33
2.2.1 Electrokinetics	33
2.2.1.1 The Mechanism of Surface Charging	33
2.2.1.2 Electrical Double Layer	36

page

2.2.2 Contact Angle and Wetting 41
2.2.2.1 Classical Wetting Equations 41
2.2.2.2 The Critical Surface Tension of Wetting 46
2.2.2.3 Degree of Polarity of Inherently Hydrophobic Surfaces 52
2.2.3 Flotation 56
2.2.3.1 Stages in Flotation . . . 56
2.2.3.2 Disjoining Pressure and its Components. 62

2.3 EXPERIMENTAL MATERIALS AND PROCEDURES 64

2.3.1 Mineral Samples 64
2.3.2 Electrokinetic Mobility Determination . 66
2.3.2.1 Apparatus 66
2.3.2.2 Procedure 67
2.3.2.3 Calculation of Zeta Potential 68
2.3.3 Contact Angle Measurements. 71
2.3.3.1 Sample Preparation . . . 71
2.3.3.2 Apparatus 74
2.3.3.3 Procedure 74
2.3.4 Flotation Tests 78
2.3.4.1 Apparatus 78
2.3.4.2 Procedure 80

2.4 RESULTS 81

2.4.1 pH-Dependent Surface Properties 81
2.4.2 Octane Contact Angles. 98
2.4.3 Critical Surface Tension of Wetting . . 101

2.5 DISCUSSION 105

2.5.1 Layer Type Inherently Hydrophobic Minerals. 105

page

2.5.1.1 Electrokinetic Behaviour 105
2.5.1.2 Flotation Behaviour. 108
2.5.1.3 Contact Angle Behaviour. 114
2.5.1.4 Correlation Between the pH-Dependent Surface Properties of Layer Type Minerals. 121
2.5.2 Common Sulphides: Chalcopyrite and Galena 122
2.5.2.1 Electrokinetic Behaviour 122
2.5.2.2 Flotation Behaviour. 126
2.5.3 Octane Contact Angles and Polar Characteristics of the Minerals. 133
2.5.4 Critical Surface Tension of Wetting. . . 135
2.6 REFERENCES 142

CHAPTER 3 PROPERTIES OF AQUEOUS METHANOL SOLUTIONS

3.1 REVIEW 154
3.1.1 Chemistry of Methanol. 154
3.1.2 Molecular Structures of Water and Methanol 156
3.1.3 Hydrogen-Bond Formation. 156
3.1.4 Viscosity. 161
3.1.5 Thermodynamics of Mixing 164
3.1.6 Vapor Pressures. 167
3.1.7 Surface Tension and Molecular Surface Orientation 170
3.1.8 Frothing and Collecting Properties . 173
3.2 EXPERIMENTAL MATERIALS AND PROCEDURES. . . 174
3.2.1 Solutions. 175
3.2.2 Method of Surface Tension Measurement 176
3.2.3 Bubble-Size Distribution Cell. . . . 177
3.2.4 Procedure. 178

page

3.3 RESULTS 180

3.3.1 Surface Tension Measurements. . . . 180

3.3.2 Bubble Size Measurements. 183

3.4 DISCUSSION. 196

3.4.1 Surface Tension of the Methanol Solutions 196

3.4.2 Thermodynamics of Adsorption at the Methanol Solution Surface 200

3.4.3 Bubble Size Distribution 209

3.4.4 Correlations Between Various Properties 216

3.5 REFERENCES. 221

CHAPTER 4 CRITICAL SURFACE TENSION OF WETTING AND OF FLOATABILITY

4.1 INTRODUCTION. 225

4.2 EXPERIMENTAL MATERIALS AND PROCEDURES . . 226

4.2.1 Reagents. 226

4.2.2 Wettability Tests 228

4.2.3 Floatability Tests. 230

4.3 RESULTS 232

4.3.1 Wettability Tests 232

4.3.2 Floatability Tests. 240

4.4 DISCUSSION 249

4.4.1 Wettability 249

4.4.1.1 Representation of the Experimental Data 249

4.4.1.2 Adhesion Tension Behaviour 252

4.4.1.3 Selective Wetting Between Inherently Hydrophobic Minerals. 255

4.4.1.4 Mechanism of Wetting. . . . 259

page

4.4.2 Floatability 265
4.4.2.1 Typical Flotation Behaviour 265
4.4.2.2 Reproducibility. 268
4.4.2.3 Critical Surface Tension Range of Floatability. . . 270
4.4.2.4 Selective Flotation and Efficiency of Separation . 274
4.4.2.5 Estimation of Induction Periods During Flotation . 284

4.5 REFERENCES. 289

CHAPTER 5 EFFECT OF ELEMENTAL SULPHUR FORMATION ON THE FLOTATION RATE OF GALENA AND CHALCOPYRITE

5.1 INTRODUCTION 293
5.2 FLOTATION RATE. 295
5.3 EXPERIMENTAL MATERIALS AND PROCEDURES . 297
5.3.1 Mineral Samples. 297
5.3.2 Infrared Spectra. 297
5.3.3 Pretreatment of Galena. 298
5.3.4 Extraction and Determination of Sulphur 299
5.3.5 Flotation Tests 300
5.4 RESULTS 301
5.4.1 Infrared Spectra. 301
5.4.2 Sulphur Extraction Tests. 304
5.4.3 Flotation Tests 304

5.5 DISCUSSION 308
5.5.1 Formation of Elemental Sulphur on Chalcopyrite and Galena 308
5.5.2 Effect of Surface Tension on the Kinetics of Flotation 310
5.5.3 Correlation Between the Amount of Liberated Sulphur and Flotation Rate of Chalcopyrite and Galena . 316

5.6 REFERENCES 322

page

CHAPTER 6 GALENA-XANTHATE SYSTEM

6.1 INTRODUCTION 325
6.2 EXPERIMENTAL MATERIALS AND PROCEDURES. . 326
6.2.1 Reagents 326
6.2.2 Galena Sample. 327
6.2.3 Infrared Spectra 327
6.2.4 Surface Tension Measurements . . . 328
6.2.5 Contact Angle Measurements. . . . 329
6.2.6 Flotation Tests. 331
6.3 RESULTS. 332
6.3.1 Infrared Spectra 332
6.3.2 Contact Angle Measurements 336
6.3.3 Flotation Tests 341
6.4 DISCUSSION 343
6.4.1 Adsorption of Alkyl Xanthates on Galena 343
6.4.2 Contact Angles 349
6.4.3 Adhesion Tensions in Aqueous Methanol Solutions 353
6.4.4 Polarity Level of Xanthated Galena Surfaces 357
6.4.5 Adhesion Tensions of Air Bubbles and Octane Droplets in Water . . . 359
6.4.6 Wettability of the Galena-Decyl Xanthate System 363
6.4.7 Flotation Tests 364
6.5 REFERENCES 370

CHAPTER 7 CONCLUSIONS, CLAIMS TO ORIGINAL RESEARCH AND SUGGESTIONS FOR FURTHER WORK

7.1 CONCLUSIONS. 373
7.1.1 Fundamental Surface Properties of Minerals Studied 373
7.1.1.1 Layer-Type Minerals. . . . 373
7.1.1.2 Sulphide Minerals. 373

page

7.1.1.3 Polar Characteristics . . . 375

7.1.1.4 Critical Surface Tension of Wetting 375

7.1.1.5 Surface Pressures 376

7.1.2 Methanol-Water System 376

7.1.3 Critical Surface Tension of Wetting and of Floatability 377

7.1.4 Selective Flotation 378

7.1.5 Induction Periods 378

7.1.6 Kinetics of Flotation 378

7.1.7 Presence of Elemental Sulphur on Sulphide Minerals 379

7.1.8 Correlation Between Sulphur Content and Flotation Rate 379

7.1.9 Behaviour of Xanthated Galena . . . 379

7.2 CLAIMS TO ORIGINAL RESEARCH 380

7.3 SUGGESTIONS FOR FURTHER WORK. 384

APPENDICES 386

LIST OF FIGURES

Figure		Page
1.1	Crystal Structure of Molybdenite (a) and Stibnite (b)	11
1.2	Crystal Structure of Realgar (a) and Orpiment (b)	13
1.3	Crystal Structure of Chalcopyrite (a), Pyrite (b) and Galena (c)	16
1.4	Crystal Structure of Sulphur (a), Graphite (b) and Talc (c)	18
2.1	A Schematic Representation of the Electrical Double Layer	40
2.2	Solid-Vapour-Liquid System in Equilibrium.	42
2.3	Wettability of Polytetrafluoroethylene, Polyethylene and Polyvinylchloride (by pure liquids) and Polystyrene (by aqueous methanol solutions)	49
2.4	A Schematic Representation of Rank Brothers' Electrophoresis Apparatus. . . .	68
2.5	A Schematic Representation of the Contact Angle Apparatus	75
2.6	Main Features of the Micro-Flotation Cell.	79
2.7	Contact Angle and Flotation Recovery (Woodfill, 1966) of Talc as a Function of pH .	83
2.8	Contact Angle and Zeta Potential of Talc as a Function of pH.	84
2.9	Contact Angle, Flotation Recovery and Zeta Potential of Stibnite as a Function of pH.	86
2.10	Contact Angle and Zeta Potential (Chander et al., 1975) of Graphite as a Function of pH	87
2.11	Contact Angle and Flotation Recovery of Molybdenite as a Function of pH.	89
2.12	Contact Angle and Zeta Potential of Molybdenite as a Function of pH	90

Figure		Page
2.13	Zeta Potential and Flotation Recovery of Chalcopyrite as a Function of pH (dashed line is for elemental sulphur)	92
2.14	Zeta Potential vs. pH Relationship for Galena and Elemental Sulphur Prepared Under Various Conditions	94
2.15	Flotation Recovery vs. pH Relationship for Galena Prepared and Floated Under Various Conditions	96
2.16	Zisman Plots of Minerals Including Non-Sulphides.	102
2.17	Zisman Plots of Various Sulphide Minerals	103
2.18	Molybdenite Face Sample Used in the Flotation Experiments	111
2.19	Contact Angle and Flotation Recovery of Talc and Molybdenite as a Function of pH (Flotation sample consisted of pieces of cut layers. See Figure 2.18 for molybdenite sample)	112
2.20	Variation of Contact Angle of Molybdenite as a Function of Residence Time in Distilled Water	116
2.21	Photomicrographs of Sulphur and Molybdenite Discs	118
3.1	Schematic Drawings of Water (left) and Methanol (right) Molecules	156
3.2	(a) Cluster Model for Water, (b)Mean Size of Hydrogen Bonded Aggregates, $\bar{n}$ in Liquid Water and Methanol	159
3.3	Hydrogen Bonded Formations in Methanol; Open (top) and Cyclic (bottom) Structures.	160
3.4	Viscosity of Aqueous Methanol Solutions as a Function of Methanol Mole Fraction .	163
3.5	Thermodynamic Excess Functions for Mixing Between Water and Methanol (25°C)	166
3.6	The Equilibrium Partial Pressures of Methanol and Water Over Aqueous Methanol Solutions (25°C)	169
3.7	Vapour Composition of Aqueous Methanol Solutions as a Function of Methanol Mole Fraction.	171

Figure		Page
3.8	Flat Cell Constructed for the Determination of Bubble Size Distribution	179
3.9	Surface Tensions of Aqueous Methanol Solutions of Varying Composition	181
3.10	Temperature Dependence of Surface Tension for Aqueous Methanol Solutions	184
3.11	Temperature Dependence of Surface Tension for Aqueous Methanol Solutions (Cont'd.) .	185
3.12	Photographs of Air Bubbles Produced in Aqueous Methanol Solutions - Concentration Range; 0-1.0% (vol.)	186
3.13	Photographs of Air Bubbles Produced in Aqueous Methanol Solutions - Concentration Range; 2-63% (vol.)	187
3.14	Photographs of Air Bubbles Produced in Aqueous Methanol Solutions - Concentration Range; 72-100% (vol.)	188
3.15	Bubble Size Distribution in Aqueous Methanol Solutions - Concentration Range; 0-1% (vol.).	191
3.16	Bubble Size Distribution in Aqueous Methanol Solutions - Concentration Range; 2-18% (vol.)	192
3.17	Bubble Size Distribution in Aqueous Methanol Solutions - Concentration Range; 27-63% (vol.)	193
3.18	Bubble Size Distribution in Aqueous Methanol Solutions - Concentration Range; 72-100% (vol.)	194
3.19	Number of Bubbles Produced per cm^3 of Solution vs. log (molar concentration of methanol, C_M)	195
3.20	Surface Tensions of the Aqueous Solutions of the Homolog Series of Monohydric Alcohols Illustrating the Validity of Traube's Rule	198
3.21	Activity Coefficients of Methanol and Water in Aqueous Methanol Solutions . . .	206
3.22	Adsorption of Methanol of the Solution-Gas Interface, Area per Adsorbed Molecule and Surface Tension as a Function of ln (activity of methanol, α)	207

Figure		Page
3.23	Number of Bubbles Produced per cm^3 of Solution as a Function of Methanol Concentration	213
3.24	Relationship Between the Adsorption Densities at the Solution-Gas Interface and the Number of Bubbles Produced in Aqueous Methanol Solutions	217
3.25	Relationship Between Heat of Mixing, Adsorption Density and Viscosity in Aqueous Methanol Solutions	218
4.1	(a) Suggested Structure of Lignosulphonate	227
	(b) Structure of Syntex	228
4.2	Adhesion Tension Diagram for Talc, Coal and Graphite in Aqueous Methanol Solutions	234
4.3	Adhesion Tension Diagram for Stibnite in Aqueous Methanol and Decyl Xanthate Solutions	235
4.4	Adhesion Tension Diagram for Molybdenite in Aqueous Decyl Xanthate and Syntex Solutions	236
4.5	Adhesion Tension Diagram Illustrating the Upper and Lower Limits of Critical Surface Tension Range of Wettability and Floatability for Sulphur and Molybdenite.	238
4.6	Adhesion Tension Diagram for Talc and Molybdenite in Aqueous Lignosulphonate and MIBC Solutions	239
4.7	Floatability of Various Polymers in Aqueous Methanol Solutions of Various Surface Tension	241
4.8	Floatability of Pretreated Sulphide Minerals in Aqueous Methanol Solutions of Various Surface Tension.	243
4.9	Floatability of Sulphur, Talc, Graphite and Molybdenite in Aqueous Methanol Solutions of Various Surface Tension	245
4.10	Separation Efficiencies for the binary Mixtures (50:50) of Various Inherently Hydrophobic Minerals in Aqueous Methanol Solutions of Various Surface Tension	247
4.11	Separation Efficiencies for the Binary Mixtures (50:50) of Talc and Molybdenite in Lignosol-XD & MIBC Solutions of Various Surface Tension	248

Figure		Page
4.12	Zisman Wettability Diagram (top) and Adhesion Tension Diagram (bottom) for Sulphur in Aqueous Methanol Solutions	250
4.13	Crystal and Disc Samples of Sulphur (left) and Molybdenite (right) with Their γ_s^p Values Indicated	258
4.14	Surface Tension, Adsorption Density and Viscosity Variation in Aqueous Methanol Solutions.	261
4.15	Schematic Representation of the Wetting Mechanism in Aqueous Methanol Solutions . .	264
4.16	Floatability vs. Surface Tension Curves for Sulphur and Graphite Samples and Their Functional Expressions; R^S and R^G respectively .	278
4.17	Comparison of Observed and Estimated Values for the Fractional Recoveries of the Inherently Hydrophobic Mineral Samples Within Their Critical Surface Tension Range of Floatability	279
4.18	Zeta Coefficients for Molybdenite and Talc at pH=7.2 Due to Lignosol-XD.	283
4.19	Induction Periods as a Function of Surface Tension of Aqueous Methanol Solutions. . . .	287
5.1	Infrared Spectra of Sulphur and Galena . . .	302
5.2	Infrared Spectra of Sulphur and Chalcopyrite	303
5.3	Amount of Liberated Sulphur Extracted from Sulphide Minerals	305
5.4	Graphical Representation of the First Order Rate Data for the Flotation of Sulphur in Aqueous Methanol Solutions	311
5.5	Graphical Representation of the First Order Rate Data for the Flotation of Chalcopyrite in Aqueous Methanol Solutions.	312
5.6	Graphical Representation of the First Order Rate Data for the Flotation of Galena in Aqueous Methanol Solutions	313
5.7	Variation of $\ln K$ as a Function of γ_{lv} within the Critical Surface Tension Range of Floatability of Sulphur, Chalcopyrite and Galena	315
5.8	Relationship between the Specific Surface Area and Particle Size of Galena	318

Figure		Page
6.1	Infrared Spectra of Lead Methyl Xanthate (dotted line), Dimethyl Dixanthogen (dashed line) and the Galena Sample Treated with Potassium Methyl Xanthate Solution at Natural pH	333
6.2	Infrared Spectra of Lead Hexyl Xanthate (dotted line), Dihexyl Dixanthogen (dashed line), and the Galena Sample Treated with Potassium Hexyl Xanthate Solution at Natural pH	334
6.3	Infrared Spectra of Lead Dodecyl Xanthate (dotted line), Didodecyl Dixanthogen (dashed line), and the Galena Sample Treated with Potassium Dodecyl Solution at Natural pH . .	335
6.4	Contact Angles of Air Bubbles and Octane Droplets on Xanthated Galena as a Function of the number of Carbon Atoms in the Hydrocarbon Group	337
6.5	Adhesion Tension Diagram for Galena Pretreated with n-Alkyl Xanthates of Increasing Hydrocarbon Chain Length in Aqueous Methanol Solutions.	339
6.6	Adhesion Tension Diagram for Galena in Aqueous Potassium Decyl-Xanthate Solutions .	340
6.7	Flotation of Bulk Lead Alkyl Xanthates in Methanol Solutions as a Function of Surface Tension	342
6.8	Flotation of Xanthated Galena in Methanol Solutions as a Function of Surface Tension .	344
6.9	Representation of a Chemisorbed Monomolecular Film of Xanthate on Galena	346
6.10	Polar Component of the Surface-Free Energy of Xanthated Galena as a Function of the Number of Carbon Atoms in the Hydrocarbon Group.	358
6.11	The Linear Relationship Between $\ell n\ \gamma_s^p$ and the Number of Carbon Atoms for Xanthated Galena	360
6.12	Adhesion Tension of Air Bubbles (o) and Octane Droplets ( ) for Xanthated Galena in Distilled Water as a Function of the Number of Carbon Atoms.	361

Figure		Page
A.I.1	Calibration Curves for the Determination of Iron and Copper by Atomic Absorption . .	388
A.I.2	Calibration Curves for the Determination of Antimony and Arsenic by Atomic Absorption.	389
A.I.3	Calibration Curves for the Determination of Lead and Molybdenum by Atomic Absorption.	390
A.III.1	Correction Factor Chart for Surface Tension Determination	404
A.III.2	Fisher Autotensiomat for the Measurements of Solution Surface Tension	405
A.V.1	Calibration Curve for the Determination of the Concentration of Sulphur in Ethanol Using UV Spectrophotometer	436
A.V.2	Typical UV Spectra of Sulphur in Ethanol .	437

LIST OF TABLES

Table		Page
1.1	Percentage Ionic Character of the Covalent Bonds Present in the Samples Studies	20
2.1	Mineral Samples Studied	55
2.2	Natural Flotation Response of Galena (After Aerative Washing) in Air-Saturated Solutions	99
2.3	Contact Angles of Octane Droplets on Various Minerals in Distilled Water . .	100
2.4	Values of the Zisman Parameters of Various Mineral Samples	104
2.5	Contact Angles and Fraction of Hydrophobic Sites on Inherently Hydrophobic Minerals.	120
2.6	The Polar Component of the Surface-Free Energy, γ_s^p and Relative Non-Polarity, n_R of the Samples	135
2.7	Surface Pressure of Water Vapour on Inherently Hydrophobic Minerals	139
3.1	Molecular Structures of Methanol and Water	156
3.2	Temperature Dependence of Surface Tension for Aqueous Methanol Solutions . .	183
3.3	A Comparison of the Experimental Surface Tension Values of Aqueous Methanol Solutions with those Calculated using the Szyszkouski Equation	201
4.1	Flotation of Silica Sand in Methanol Solutions of Various Surface Tension. .	242
4.2	Comparison of β, γ_s^p (average) and $X_{h\ell}$ Values for Various Inherently Hydrophobic Minerals	253
4.3	Reproducibility of Flotation Tests in the Critical Surface Tension Range of Floatability and Above for Talc and Chalcopyrite Samples.	269

Table		Page
4.4	Comparison of γ_{Clf} and γ_{cmf} Values of Floatability and Wettability Tests . . .	274
4.5	Results of Polynomial Regression of Second Degree for the Surface Tension of Floatability Curves of the Samples . . .	277
4.6	Comparison Between Experimental and Predicted Results of the Separation . . .	281
5.1	Flotation of Sulphur in Aqueous Methanol Solutions of Various Surface Tensions as a Function of Time.	305
5.2	Flotation of Chalcopyrite in Aqueous Methanol Solutions of Various Surface Tensions as a Function of Time	306
5.3	Flotation of Pretreated Galena in Aqueous Methanol Solutions of Various Surface Tensions as a Function of Time. . .	307
5.4	Amount of Elemental Sulphur Formed on Sulphide Minerals	319
5.5	Correlation Between the Quantity of Liberated Sulphur and Flotation Rate Constants of Chalcopyrite and Galena . .	320
6.1	The Values of Critical Surface Tension of Wetting and Slopes of Wettability Lines for Xanthates of Various Chain Length Adsorbed on Galena	341
6.2	Comparison Between Observed and Predicted Contact Angle of Octane Droplets on Inherently Hydrophobic Minerals in Water.	362
A.I.1	Results of Ignition Tests.	386
A.I.2	Results of Acid-Leaching Tests	386
A.I.3	Operating Conditions of the Atomic Adsorption Spectrophotometer	387
A.II.1	Results of Electrophoretic Measurements for Talc and Molybdenite	391
A.II.2	Results of Electrophoretic Measurements for Chalcopyrite and Sulphur	392
A.II.3	Results of Electrophoretic Measurements for Galena	393
A.II.4	Contact Angles Measured on Disc Samples of Talc.	394

Table		Page
A.II.5	Contact Angles Measured on Disc Samples of Molybdenite	395
A.II.6	Contact Angles Measured on Disc Samples of Stibnite and Graphite	396
A.II.7	Contact Angles of Various Liquid Droplets on Mineral Samples	396
A.II.8	Flotation of Molybdenite as a Function of pH	397
A.II.9	Natural Flotation Response of Galena and Chalcopyrite as a Function of pH	397
A.III.1	Thermodynamic Excess Functions of Mixing Between Water and Methanol	398
A.III.2	Concentration of Methanol Vapour Inside Air Bubbles Produced in Methanol Solutions.	401
A.III.3	Apparent Surface Tensions of Aqueous Methanol Solutions	410
A.III.4	Correction Factors and Surface Tension Values as a Function of Methanol Concentration	411
A.III.5	Temperature Dependence of the Surface Tension for the Water-Methanol System. . .	413
A.III.6	Apparent Surface Tension of Decyl Xanthate Solutions.	415
A.III.7	Surface Tension of Potassium Decyl Xanthate Solutions.	416
A.III.8	Surface Tension of Lignosol-XD Solutions .	417
A.III.9	Surface Tension of Syntex Solutions. . . .	418
A.III.10	Data for the Polynomial Regression and a Comparison with Estimated Surface Tensions	420
A.III.11	Surface Excess Values of Methanol at the Solution-Gas Interface	421
A.III.12	Surface Excess and Deficiencies at the Aqueous Methanol Solution-Gas Interface According to Gibbs and Guggenheim-Adam Conventions.	422
A.III.13	Bubble Size Distributions in Methanol Solutions	423
A.III.14	Number of Bubbles Produced per cm^3 of Methanol Solutions	425

Table		Page
A.III.15	Some Physical Parameters of the Water-Methanol System	428
A.III.16	Dimensionless Parameters for Bubbles of 0.5 mm Diameter in Aqueous Methanol Solutions	429
A.IV.1	Wettability Data for Various Minerals Aqueous Methanol Solutions.	430
A.IV.2	Wettability Data for Stibnite and Molybdenite in Decyl Xanthate Solutions. . .	431
A.IV.3	Wettability Data for Molybdenite Face in Aqueous Syntex Solutions	431
A.IV.4	Separation Efficiencies (SE) of Binary Mixtures of Inherently Hydrophobic Minerals	432
A.IV.5	Induction Periods According to Sutherland's Equation	433
A.V.1	Absorbance Values of UV by Elemental Sulphur in Ethanol (at 275 mμ).	434
A.V.2	Absorbance Values of UV by Elemental Sulphur in Ethanol (at 262 mμ).	435
A.VI.1	Chemical Reagents Used in the Preparation and Purification of Potassium Alkyl Xanthates	440
A.VI.2	Contact Angle and Adhesion Tension Data for Xanthated Galena in Aqueous Methanol Solutions	443
A.VI.3	The Data Cont'd. for Propyl- and Butyl-Xanthated Galena.	444
A.VI.4	The Data Cont'd. for Pentyl- and Hexyl-Xanthated	445
A.VI.5	The Data Cont'd. for Decyl-Xanthated Galena	446
A.VI.6	Polar Component of the Surface-Free Energy of Xanthate Coatings on Galena .	446

ACKNOWLEDGEMENTS

The author wishes to thank his supervisor, Dr. G.W. Smith for reading the written manuscript and making helpful comments.

The financial assistance offered by the Faculty of Graduate Studies of McGill University, Alcan and the National Research Council of Canada during the 1980-84 academic years has been greatly appreciated.

Acknowledgement is extended to Dr. J.E. Gruzleski, chairman of the department, for his understanding and arranging a leave of absence for the author's military duty in Turkey which had to be done during the 1982-83 academic year; to Dr. J.A. Finch for his interest and encouraging comments; to Mr. I. Karakaya, a Ph.D. candidate in the department, for his discussions on the thermodynamic aspects of the work; to Dr. S. Yörük of Fırat University for discussions and translations from German; to Mr. M. Leroux of the department for translations from French, and finally, to Dr. S.R. Rao, a senior research scientist in the department, for his interest and discussions on various topics, and to other staff, fellow graduate students and technicians of the department for their help on many occasions.

Thanks are also due Mrs. Joan Kaylor of Redpath Museum (McGill Univ.), Mr. L.A. Marshall of Badische Canada Ltd., Dr. J.M. Dealy (Chem. Eng., McGill Univ.), Mr. G. Fortin of Reed Ltd. and Climax Co. (Colorado) for supplying pure mineral samples, Nylon-6, Polyethylene and polystyrene, lignosulphonates and Syntex respectively.

CHAPTER 1

INTRODUCTION

1.1. General Introduction

Flotation is a physico-chemical process for separating finely divided solids from one another in an aqueous suspension. Presently it is the most commonly used mineral processing technique for the concentration of valuable constituents from ore body.

The term flotation was first used for all concentration processes in which the levitation of particles heavier than water was accomplished. When large quantities of oil were involved, the process was termed "bulk-oil flotation". When the process was carried out using only small quantities of oil, it was called "skin flotation". When gas bubbles were introduced as particle carriers, due to surfactant additions, they produced a layer of froth at the suspension-gas interface and thus the process was appropriately called "froth flotation". There are other prefixes in use such as ion flotation, precipitate flotation and flocco-flotation to denote the removal of ions, precipitates and flocculated fine particles respectively, from solutions by using froth

flotation. Today, the term flotation in general refers to froth flotation.

The operating mechanism in flotation is that finely divided particles, rendered hydrophobic by the adsorption of suitable reagents, are captured by the rising stream of bubbles upon collisions with them and carried to the froth layer where they can be removed. The particles that are not sufficiently hydrophobic cannot be captured and remain in the bulk suspension.

Flotation practice was developed long before the theory. Because of its multi-variable nature and complexity, the phenomenon taking place during the flotation process is still not fully understood. Besides surface hydrophobicity, other conditions which are physical in nature have to be fulfilled for the recovery of valuable mineral particles. The events prior and subsequent to the bubble-particle attachment (e.g. approach of particle to a bubble, collisions and survival of bubble-particle aggregates before reaching the froth removal stage) may be determined by such physical parameters as the size of the particles and bubbles, their velocities, the specific gravity of the particles, the hydrodynamics in the cell, etc. However, the attachment event itself is primarily dependent upon the surface properties of the particles and the bubbles. Some degree of hydrophobicity at the particle surface is a prerequisite to the bubble-particle attachment. Minerals to be separated sometimes have the

suitable surface properties to render the valuable one inherently floatable. For instance, the success of coal flotation is a consequence of inherent hydrophobicity of the organic part and the hydrophilicity of the associated inorganic ash forming minerals.

1.2. Inherent Hydrophobicity and Naturally Floatable Solids

Inherent hydrophobicity describes, for a clean solid surface, a condition of incomplete wetting by water. This property is such that it is thermodynamically favorable for air to partially displace water from the surface. The particles of such a solid will float (if not oxidized or physically covered by hydrophilic contaminants) naturally without a flotation collector. There are a number of inherently hydrophobic solids. These include molybdenite, graphite, stibnite, talc, sulphur, realgar, orpiment, solid hydrocarbons such as paraffin, coals and plastics. Attempts have been made by researchers to explain the natural floatability of these solids. Consideration has been given to chemical composition, nature of surface bonds and crystal structure of the solids. Streltsin (1952, 1953) classified the minerals based upon the bonds between atoms and groups of atoms and emphasized the weak hydration of naturally floatable mineral surfaces by water. Later, Gaudin et al. (1957) classified the crystal types extensively in a similar fashion and proposed that natural floatability results when at least some fracture or cleavage surfaces form without rupture of interatomic bonds other than residual bonds (i.e. van der Waals'

bonds). The presence of the broken interatomic bonds in the surface gives rise to the hydrophilic character of the surface. In water, such a surface will be subjected to a strong hydration by polar water molecules. On the other hand, a surface which is formed by the rupture of weak van der Walls' bonds only (e.g. molybdenite and graphite) will be subjected to weak hydration, resulting in a predominantly hydrophobic surface. Presence of highly electrophilic atoms such as oxygen in the surface layer (e.g. due to oxidation) increases the water binding power through hydrogen bond formation between surface oxygen atoms and polar water molecules. Thus, oxidation, which all non-oxide solids are to some extent subject to, tends to destroy the inherent hydrophobicity of solids.

Inherent hydrophobicity has been investigated by contact angle measurements and also micro-scale flotation tests. Recent studies have dealt mainly with molybdenite, graphite, talc (Arbiter et al., 1975; Chander et al., 1975) and various coals (Kelebek et al., 1982; Yarar, 1983). The purpose of these studies was, in part, to examine the correlation between contact angle, electrokinetic potential and flotation response rather than verifying the inherent hydrophobicity of these minerals which had already been established (Gaudin, 1957; Klassen and Mokrousov, 1963). What still needs to be established is whether the common sulphides such as galena, chalcopyrite, chalcocite, pyrite, etc. are naturally floatable. There exists a considerable number of conflicting reports in the literature on this topic.

1.3. Natural Floatability of Common Sulphides

In the early days of flotation practice, it has been known that sulphide minerals were poorly wettable by water so that their selective separation from oxide gangue minerals was possible. The historical book by Hoover (1916) gives many examples of the separation processes by skin and bulk-oil flotation and describes the first patents granted on the subject. Gaudin (1932) also pointed out that some sulphides such as galena and chalcopyrite could be floated without using a collector. Ravitz and Porter (1933), Ravitz (1940) and Herd and Ure (1941) on the basis of flotation tests with galena, cleaned of hydrophilic oxidation products, claimed the first experimental evidence in favor of the natural flotability of galena. However, these findings were opposed by various investigators including Knoll and Baker (1941) and Sutherland and Wark (1955) mainly on the grounds of accidental contamination of the samples.

A completely different view was proposed by Plaksin from the U.S.S.R. He suggested that the apparent inherent hydrophobicity of the sulphides was a consequence of adsorbed molecular oxygen which promoted the dehydration of the surface. According to Plaksin (1959), in the absence of oxygen, the sulphide minerals are not naturally floatable. This is in sharp contradiction with the observations of Herd and Ure who had noted that the 'cleaned' galena is naturally floatable in the absence of oxygen. It is interesting that Plaksin

neither commented on these observations nor did he refer to any other related work carried out outside the U.S.S.R. He only emphasized the important role played by the gases, primarily oxygen, in the flotation of sulphide and non-sulphide minerals, a fact first recognized by MacLaclan (1926).

Over the years, research papers referring to the natural floatability of various sulphide minerals increased (Rey and Formanek, 1960; Paterson and Salman, 1968; Suwanasing and Salman, 1970; Boyce et al., 1970; Gutierrez, 1973; Lepetic, 1974; Finkelstein et al., 1975; Heyes and Trahar, 1977; Yoon, 1981; Gutierrez and Martin-Poveda, 1981; Fuerstenau and Sabacky, 1981). In a few of these studies, the use of a frother was reported. In most of them, no reagents were used. The reason given for the natural floatability was the formation of elemental sulphur which has a strongly hydrophobic character. However, Heyes and Trahar (1977) who found that natural floatability of chalcopyrite was brought about in an oxidizing environment, could not analytically detect any sulphur in acetone after leaching floated particles. Gardner and Woods (1979) in an electrochemical study confirmed the results observed by Heyes and Trahar and suggested that elemental sulphur formation was responsible for hydrophobicity. Yoon (1981) claimed that natural floatability of chalcopyrite was promoted in a reducing environment but again, the presence of elemental sulphur at the surfaces could not be detected this time using ESCA. However, in a more detailed study

Luttrell and Yoon (1983) agreed on the necessity of an oxidizing environment for the natural floatability of chalcopyrite and showed the presence of elemental sulphur by various spectrometric methods. Previously, Finkelstein et al. (1975) had also shown the presence of elemental sulphur at sulphide surfaces. However, there was no clear relationship between the amount of sulphur found and the floatability of the samples. Gutierrez (1973) was of the opinion that galena was naturally floatable because of its inherent hydrophobicity. He argued that this hydrophobicity was so weak that it could not be detected by captive bubble experiments due to the difficulty of measuring finite contact angles below 20° on a flat polished specimen. This point was previously made by Ravitz (1940). Another point Gutierrez (1973) made to reconcile the natural floatability of galena particles with the non-measurable contact angles on polished surfaces is based on the research work by Eigeles and Volavo (1960) who noted that the attraction forces necessary for the contact of a large bubble with a polished surface was much greater than those required for bubble-particle attachment in actual flotation. Poling and Leja (1972) called attention to the fact that galena has a non-stoichiometric composition often containing trace impurities and is very reactive towards the environment. They expressed the view that depending upon its precise composition and the environment, a galena sample may show natural floatability or non-floatability. It is clear that the oxygen

content of the environment is a decisive factor in this respect. The results demonstrating natural floatability of most common sulphides by Fuerstenau and Sabacky (1981) were obtained in a stainless steel glove box which reportedly had less than 10^{-6} mole fraction oxygen in the gas and less than 5 ppb oxygen in the water. This paper is important in that the oxygen content of the environment was precisely defined for the first time. It would be interesting to see if the results presented by Fuerstenau and Sabacky could be reproduced by other researchers. It would be interesting to find out also whether the samples were still naturally floatable upon introducing some oxygen deliberately into the flotation cell say, at the conditioning stage. A recent study by Trahar (1983) on the influence of oxygen on the natural floatability of chalcopyrite suggested evidence against the observations of Fuerstenau and Sabacky. Trahar showed that chalcopyrite samples which were not floatable under reducing conditions became naturally floatable only when oxygen was made available. Thus, there appears to be established a relationship between the oxidizing or reducing condition of the suspension and the natural floatability of chalcopyrite (Heyes and Trahar, 1977; Gardner and Wood, 1979; Luttrell and Yoon, 1983). Continuing research (Trahar, 1984) shows that behavior of galena is essentially not very different from that of chalcopyrite. In a way, these findings are in line with those of Plaksin and his coworkers (Plaksin, 1959). However, the U.S.S.R.

researchers did not seem to propose any distinct surface entity responsible for natural floatability, whereas recent work in the non-communist part of the world has established the presence of elemental sulphur liberated on naturally floatable sulphide surfaces (Finkelstein et al., 1975; Luttrell and Yoon, 1983). This is confirmed by the results obtained in the present work. (See Chapter 5.)

1.4. Minerals Studied and Their Crystal Structures

The research program involved the use of the following metallic sulphide minerals: molybdenite, stibnite, orpiment, realgar, chalcocite, chalcopyrite and galena. All of these were included in the determination of critical surface tension of wetting by pure liquids. However, of these, only molybdenite, chalcopyrite and galena were used extensively in other related experiments. Two elemental minerals, graphite and sulphur, were also studied. In addition, due to its well-known, inherently hydrophobic character, talc, a silicate mineral, was included in the experiments. A brief description of the crystal structures of these minerals is appropriate because of the apparent relationship between natural floatability and crystal structure (Gaudin et al., 1957).

a) Molybdenite (MoS_2)

Molybdenite has a hexagonal layer type structure (Dickinson and Pauling, 1923). A rhombohedral structure has also been reported (Bell and Herfert, 1957), but the hexagonal form of natural MoS_2 predominates. The natural laminar

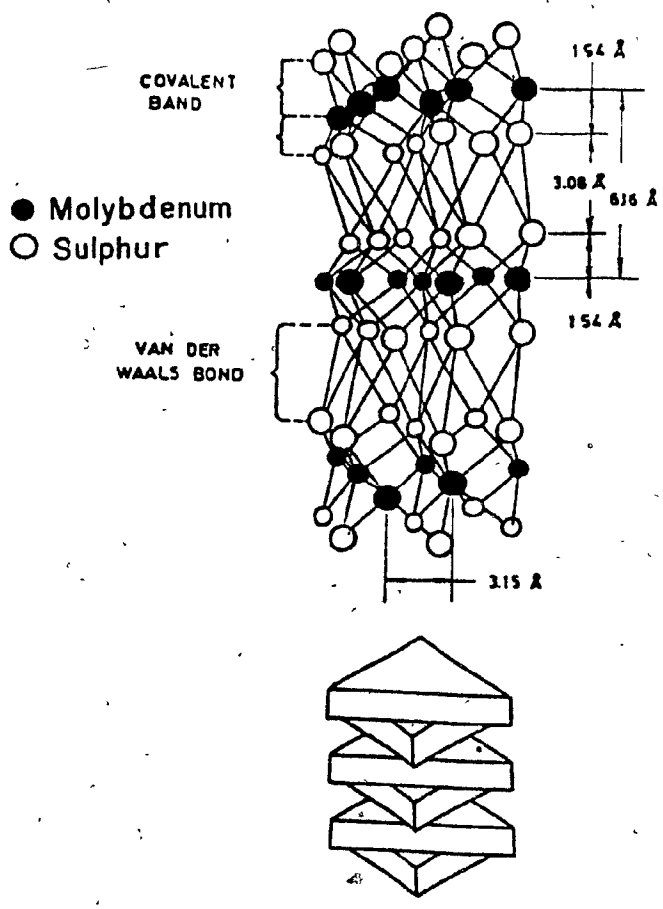
composition consists of two sheets of sulphur atoms between which is sandwiched a single sheet of molybdenum atoms. Each molybdenum atom is surrounded by six equidistant sulphur atoms at the corners of a triangular prism (Figure 1.1 a). The Mo-S distance within the prism is about 2.4.1 Å . There are strong covalent bonds within the S-Mo-S layers of triangular prisms, but only weak van der Waals forces between them to yield relatively large S-S interlayer distances. These bonds are easily ruptured, giving rise to characteristic cleavage along planes parallel to the layers.

b) Stibnite (Sb_2S_3)

Stibnite consists of slightly distorted polyhedra (orthohombic) which are connected through common sulphur atoms to form a ribbon-like (or chain type) structure. The ribbon-like $(Sb_4S_6)_n$ polymers may be regarded as forming a zig-zag sheet. The Sb-S bonds linking the polymeric ribbons together are comparatively weaker (at distances from 3.20 to 3.60 Å) than the Sb-S bonds within the ribbons (at distances ranging from 2.49 to 2.83 Å). However, they are not considered as van der Waals' type in spite of their weak character. The crystal structure is illustrated schematically in Figure 1.1 b Scavnicar, 1960).

c) Realgar (AsS) and Orpiment (As_2S_3)

Realgar consists of puckered ring molecules (As_4S_4) held together by van der Waals forces. The molecule is



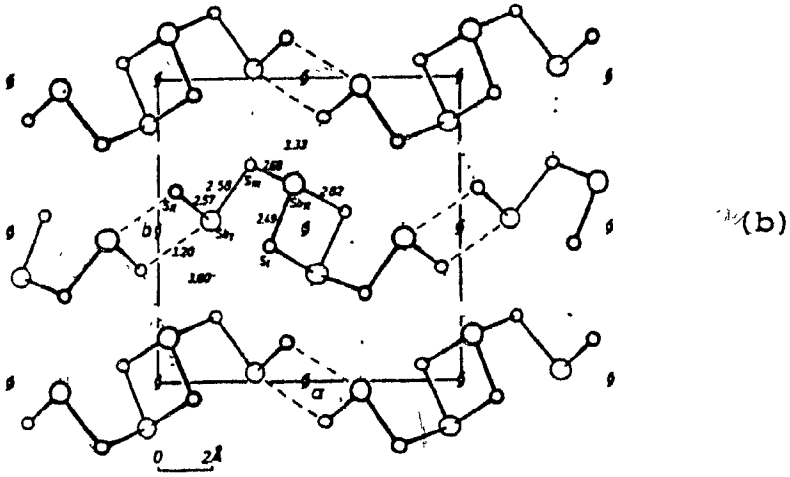
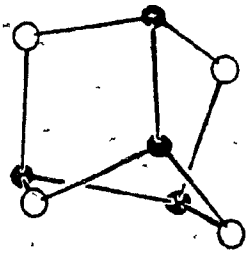


Figure 1.1 Crystal Structure of Molybdenite (a) and Stibnite (b)

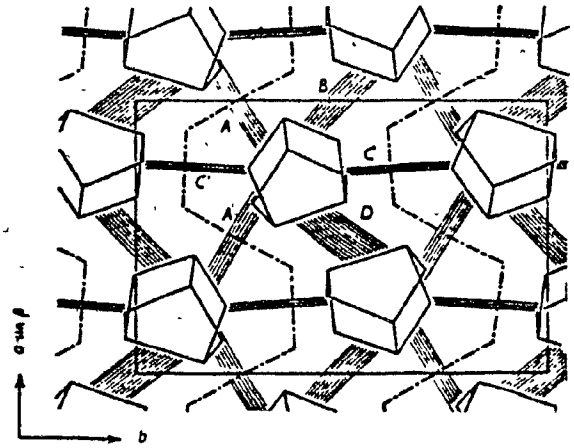
commonly called the cradle model. Four sulphur and four arsenic atoms in the molecule are bound to one another by covalent bonds. The mean values of the covalent As-As and As-S distances are 2.59 and 2.24 Å respectively (Ito et al., 1952). The intermolecular As-As, As-S and S-S distances range from 3.40 to 3.95 Å (in the regions A, B, C and D shown in Figure 1.2.a). The structure of orpiment is made up of superimposed As_2S_3 layers in which each arsenic atom is surrounded by three sulphur atoms and each sulphur atom is shared by two arsenic atoms. The layers are linked to each other by weak van der Waals forces. The crystal system of both realgar and orpiment is monoclinic. On exposure to light, realgar changes easily to orpiment. The layer structure of orpiment is reproduced in Figure 1.2b (Wuensch, 1974).

d) Chalcocite (Cu_2S)

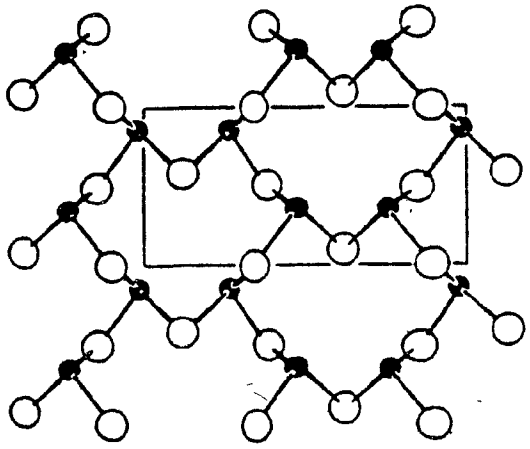
Chalcocite is reported to have an extremely complicated monoclinic structure. A cell contains 48 Cu_2S. The structure is based on hexagonal close-packing of sulphur atoms. Above 103°C, the copper atoms become disordered and the structure transforms into a hexagonal form which is known as high chalcocite. In the room temperature form (low chalcocite) one-third of the copper atoms occupy triangular interstices within the close-packed sulphur layers. The remaining copper atoms occupy triangular sites between the close-packed sulphur layers. The existence of van der Waals' bonds or any kind of cleavage is not reported (Wuensch, 1974; Vaughan and Craig, 1978).



(a)



● Arsenic
○ Sulphur



(b)

Figure 1.2 Crystal Structure of Realgar (a) and Orpiment (b)

e) Chalcopyrite ($CuFeS_2$)

The structure of chalcopyrite is tetragonal (Figure 1.3a). Each atom in chalcopyrite is tetrahedrally bonded to four other atoms. Every copper and iron atom is bonded to four sulphur atoms, each sulphur is bonded to two copper and two iron atoms, the result being that no copper and iron atoms touch each other. The Cu-S and Fe-S distances are 2.32 and 2.20 Å respectively. The bondings between the atoms are covalent with some ionic character (see Table 1.1). Chalcopyrite does not exhibit predominant cleavage planes (Wuensch, 1974; Vaughan and Craig, 1978).

f) Pyrite (FeS_2)

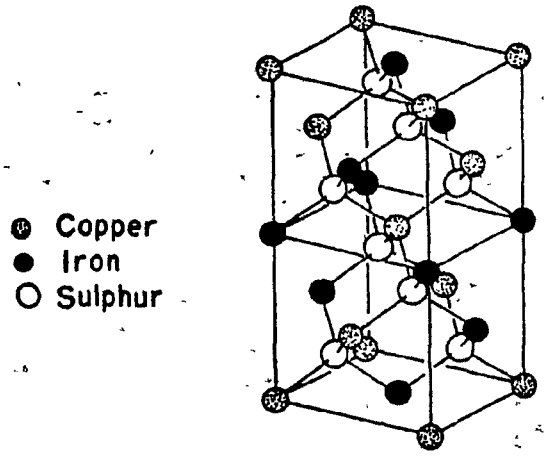
Pyrite has a cubic structure (Figure 1.3b). The structure is comparable to that of rock salt (NaCl). Iron atoms are in a face-centered cubic array. A covalently-bonded S_2 pair occupy the positions of the chlorine ions, and the iron occupy the sodium ion positions. The iron atoms form an octahedron about the S_2 pair. The S-S and Fe-S distances are 2.14 and 2.26 Å . The former is entirely covalent (since there is no electronegativity difference between the two S atoms). The latter has some ionic character. Each sulphur atom is linked to a sulphur on one side and to iron atoms on the other. Each iron atom touches six sulphur atoms. Sulphur species appear to dominate the surface (Wuensch, 1974; Vaughan and Craig, 1978).

g) Galena (PbS)

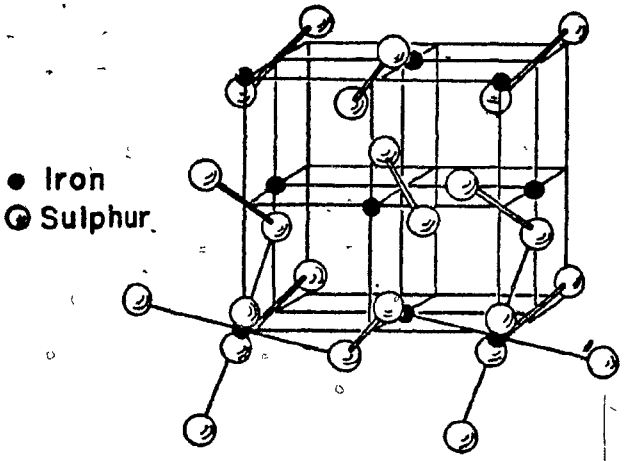
Galena has the rocksalt crystal structure which is a double face-centered cube as shown in Figure 1.3c (Vaughan and Craig, 1978). The lead atoms form a face-centered cubic structure. The sulphur atoms form another face-centered cubic structure of the same cell size displaced 1/2 a unit-cell distance in one cell direction. The Pb-S distance is 3.1 Å. The bond is predominantly covalent. Cubic cleavage is commonly observed and is highly perfect. The metallic luster is attributed to the lead-lead bonds (Pauling, 1960).

h) Sulphur (S)

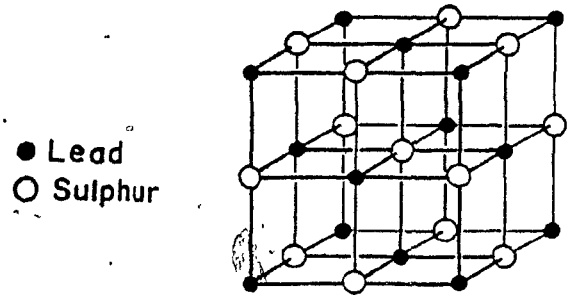
A number of different allotropic forms of sulphur are known. At room temperature, the stable form is orthorombic sulphur. Above 96°C, it changes to a monoclinic form. The crystalline orthorombic form consists of the S_8 ring molecules (Abrahams, 1955). The ring (Figure 1.4a) is puckered, that is, all the atoms are not coplanar. The mean S-S distance within the rings is about 2.04 Å. The closest distance of approach of atoms in neighboring molecules is about 3.3 Å. The ratio of these distances is similar to that observed in molybdenite. It may, therefore, be inferred that the forces holding the molecular rings together should be relatively weak. The structure may be cleaved through these weak bondings but the cleavage is not easily accomplished and it is not perfect (perhaps because of puckered structure).



(a)



(b)



(c)

Figure 1.3 Crystal Structure of Chalcopyrite (a), Pyrite (b) and Galena (c)

i) Graphite (C)

The structure of graphite consists of hexagonal layers (Figure 1.4b) which are separated by a distance so large (3.40 Å) that there can be no covalent bonds between them (Wells, 1962). The C-C distance within the layers is 1.42 Å . As in the case of molybdenite, each layer is considered as a giant molecule and the superimposed layer molecules are held together only by weak van der Waals forces. However, contrary to the case of molybdenite, in graphite there is some Coulombic attraction between the layers due to the interplanar Π electron pair distribution.

j) Talc ($3MgO{\cdot}4SiO_2{\cdot}H_2O$)

Talc is a hydrous magnesium silicate and is thought to form when silica tetrahedra condenseswith $MgO{\cdot}H_2O$. Like molybdenite talc structure (Figure 1.4c) is made of layers which are electrically neutral. A review (McHardy, 1972) indicates that monoclinic and also triclinic forms of the layers may exist. The elements (or ions) such as magnesium, hydroxyl, silica, and oxygen within a layer of talc molecules are held together through ionic/electrostatic forces which are much stronger than the weak van der Waals forces present between the oxygen atoms of the layers. Cleavage is expected to occur along planes parallel to these layers.

1.5 - The Partial Ionic Character of the Metal-Sulphur Bonds

The previous section has shown that the bond between

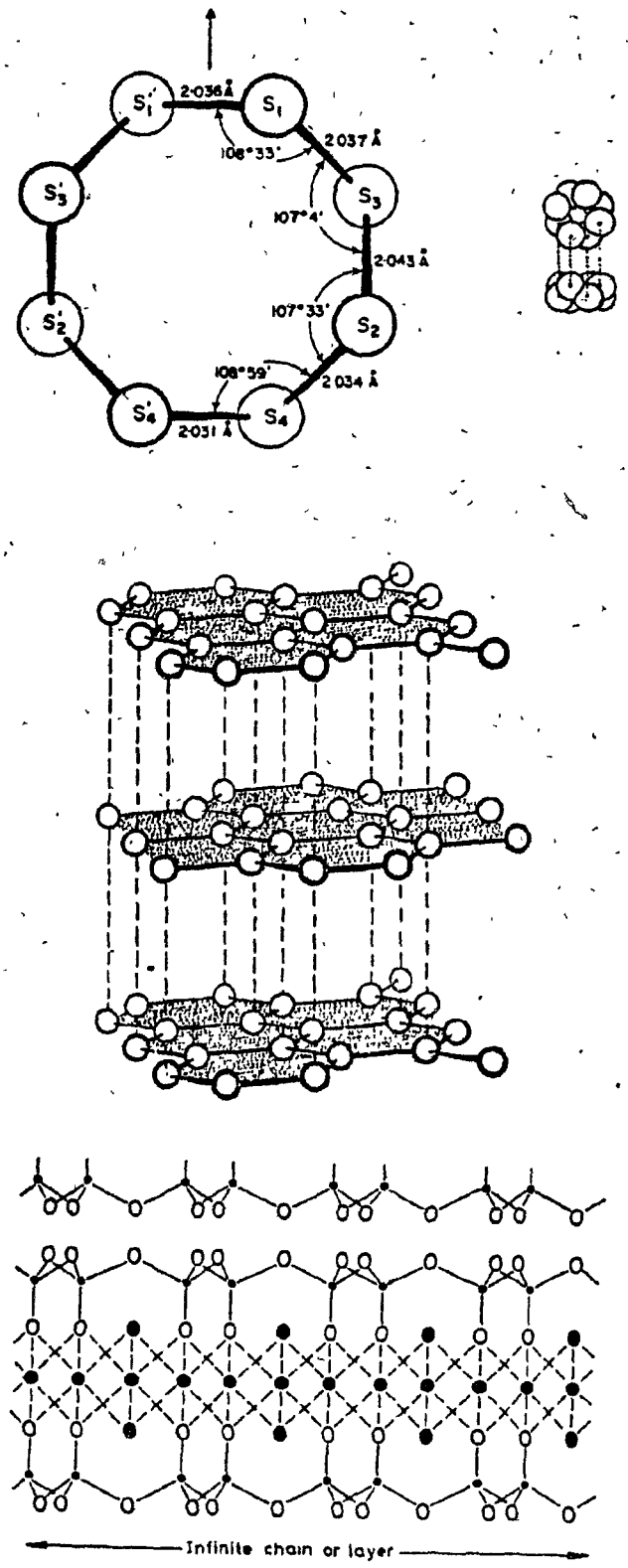


Figure 1.4 Crystal Structure of Sulphur (a), Graphite (b) and Talc (c)

the metal and the sulphur atoms in sulphide minerals is the covalent type (i.e. the bond involves the sharing of an electron pair by the two atoms). However, due to a difference in electronegativity (the power of an atom in a molecule to attract electrons to itself) between sulphur and various metal atoms, the electrons are not shared equally. Thus, almost all covalent bonds should have some degree of ionic character because of this unequal sharing of electrons. According to the empirical formula of Pauling (1960), the amount of ionic character of a single bond between atoms A and B, with electronegativities x_A and x_B is

$$\text{partial ionic character} = 1 - e^{-1/4(x_A - x_B)^2}$$

However, as reported by Wells (1962), the following equation by Hannay and Smyth (1946) can give a better estimate.

$$\text{partial ionic character} = 16\,|x_A - x_B| + 3.5(x_A - x_B)^2$$

Using these two equations, the percentage ionic character for each mineral sample was calculated (Table 1.1). The electronegativity values were taken from Pauling (1960).

From the table it can be noted that the ionic character of the covalent bonds between the metal and the sulphur atoms considered is less than 13 percent. The bonds of the elemental minerals such as sulphur and graphite do not have any ionic character unless they are broken and subsequently oxidized. Oxidation is expected to increase the water avidity of an

Table 1.1

Percentage Ionic Character of the Covalent Bonds Present in the Samples Studied

Bond	$\lvert x_A - x_B \rvert$	Percentage Ionic Character	
		Pauling (1960)	Hannay and Smyth (1946)
Mo-S	0.7	11.5	12.9
Sb-S	0.06	9.1	10.9
As-S	0.05	6.1	8.9
Cu-S	0.6	9.1	10.9
Fe-S	0.7	11.5	12.9
Pb-S	0.7	11.5	12.9
S-S	0	0	0
C-C	0	0	0
Mo-O	1.7	51.4	37.3
Sb-O	1.6	47.3	34.6
S-O	1.0	22.1	19.5
Mg-O	2.3	73.4	55.3
Si-O	1.7	51.4	37.3

inherently hydrophobic sulphide surface. With oxidation, the electrostatic fields on such surfaces become strong enough to attract the water dipoles. This is supported by the higher percentage ionic character of the metal-oxygen bonds. The molybdenite edges are known to be completely hydrophilic. This is presumably due to the creation of the Mo-O bonds which have a large percentage ionic character as seen in Table 1.1. The ionic nature of the Mg-O and the Si-O bonds within a layer of talc molecules is also apparent from the table.

1.6 - Statement of Problem and Objectives

In the minerals industry, flotation and agglomeration are two important examples of separation processes which depend upon a difference in the wettability among the contacting phases (liquid-solids-gas in the former and liquid 1 - solids-liquid 2 in the latter). Much of the flotation research has been concentrated on the surface reactions between minerals and various reagents and reviewed periodically (Rao, 1969; Granville et al., 1972; Finkelstein and Poling, 1977; Hornsby and Leja, 1982). Comparatively little research work has been devoted to the surface properties of naturally floatable minerals. Relatively recent papers by Arbiter et al. (1975), Chander et al. (1975) and Finkelstein et al. (1975) are notable exceptions.

As pointed out by Leja (1982), in some ore deposits, inherently hydrophobic minerals such as talc, graphite, molybdenite, elemental sulphur and stibnite co-exist. The talcose molybdenite ores from mines in the Abitibi area of Quebec are an example (Mathieu and Bruce, 1974). Because of the natural co-flotation of these minerals serious difficulties are encountered in the beneficiation processes. Similar problems exist in the selective flotation separation of ever-increasing plastic wastes for recycling purposes (Saito et al., 1975).

This investigation had two main purposes which are

related. The first objective was to experimentally determine various surface properties of a number of naturally floatable minerals including the electrokinetic and contact angle phenomena with respect to pH variation and the critical surface tension of wetting for various sulphide and non-sulphide minerals and to compare the results with those obtained for coals (Parekh and Aplan, 1978). The second one was to find out the extent of applicability of Zisman's critical surface tension of wetting concept (Zisman, 1964) for the selective separation of inherently hydrophobic minerals by flotation. During the course of this investigation of these two objectives, experimental work was extended into several related areas to meet what may be referred to as secondary objectives which had arisen spontaneously. These included the adsorption of methanol at the solution-gas interface, the effect of sulphur liberation on the flotation of common sulphides such as galena and chalcopyrite and the relationship between the slope of wettability line and the degree of estimated polarity of hydrophobic surfaces.

1.7 - Scope of the Work

The experimental part of this research program is divided into five chapters.

In Chapter 2, the fundamental surface properties of inherently hydrophobic minerals are discussed. These include electrokinetic potentials, contact angles and natural flotation response as a function of pH. Also the critical surface

tension of wetting values for a number of minerals that show or that are claimed to show natural floatability have been determined using Zisman's method and the results are compared with those reported for coals.

Chapter 3 is devoted to a detailed discussion on the bulk and surface properties of aqueous methanol solutions which have been used extensively in the wettability and the floatability tests. The discussion includes the thermodynamics of methanol adsorption at the solution-gas interface and bubble size distributions in aqueous methanol solutions.

In Chapter 4, the wettability data obtained for aqueous methanol solutions are employed to define the critical surface tension range of wettability and of floatability for sulphur, molybdenite and talc. Selective separation of inherently floatable minerals from their binary mixtures is demonstrated and discussed on the basis of the critical surface tension of wetting and of floatability. The induction periods are estimated for the components of the mixtures which have been subjected to selective flotation as a function of surface tension.

In Chapter 5, the formation of elemental sulphur on realgar, galena and chalcopyrite is established and quantified using UV spectrophotometry. The amount of elemental sulphur extracted from the galena and chalcopyrite samples is correlated with the flotation rate constants within the critical surface tension range of floatability of these minerals.

In Chapter 6, wettability and floatability of galena, pretreated with xanthates of increasing hydrocarbon chain length from methyl- to decyl- is determined as a function solution surface tension. The relationship between the slope of wettability line and the degree of estimated polarity of the xanthate coatings is investigated. The natural floatability of lead xanthates is demonstrated and differentiated through the critical surface tension of floatability curves for various hydrocarbon chain lengths.

Finally in Chapter 7, conclusions reached in each chapter are collectively presented. Contributions to original knowledge are claimed and the areas of further research suggested.

References

Abrahams, S.C., (1955). The Crystal and Molecular Structure of Orthorhombic Sulphur, Acta Cryst., vol. 8, pp. 661-671.

Arbiter, N., Fuji, Y., Hansen, B., and Raja, A., (1975). Surface Properties of Hydrophobic Solids. In: Recent Advances in Interfacial Phenomena of Particulate/Solution/Gas Systems; Applications to Flotation Research. (P. Somasundaran and R.B. Grieves; Editors) AIChE Symposium Series, No. 150, vol. 71, pp. 176-182.

Bell, R.E. and Herfert, R.E., (1957). Preparation and Characterization of a New Crystalline Form of MoS_2. J. Am. Chem. Soc., vol. 79, pp. 3351-3354.

Boyce, J.R., Venter, W.J., and Adam, J., (1970). Beneficiation Practice at the Tsumeb Concentrator. In: World Symposium on Mining and Metallurgy of Lead and Zinc, (D.O. Raush and B.C. Mariacher; Editors) Vol. I., AIME, pp. 542-570.

Chander, S., Wie, J.M., and Fuerstenau, D.W., (1975). On Native Floatability and the Surface Properties of Naturally Hydrophobic Solids. In: Recent Advances in Interfacial Phenomena of Particulate/Solution/Gas Systems; Applications to Flotation Research. (P. Somasundaran and R.B. Grieves; Editors) AIChE Symposium Series, No. 150, vol. 71, pp. 183-188.

Dickinson, R.G. and Pauling, L., (1923). The Crystal Structure of Molybdenite. J. Am. Chem. Soc., vol. 48, pp. 1466-1471.

Eigeles, M.A. and Volova, M.L., (1960). Kinetic Investigation of Effect of Contact Time, Temperature and Surface Condition on the Adhesion of Bubbles to Mineral Surfaces, paper 14, Int. Miner. Process. Congr., pp. 271-284, IMM, London.

Finkelstein, N.P., Allison, S.A., Lovell, V.M., and Stewart, B.V., (1975). Natural and Induced Hydrophobicity in Sulfide Mineral Systems. In: Recent Advances in Interfacial Phenomena of Particulate/Solution/Gas Systems; Applications to Flotation Research. (P. Somasundaran and R.B. Grieves; Editors) AIChE Symposium Series, No. 150, vol. 71, pp. 165-175.

Finkelstein, N.P., and Poling, G.W., (1977). The Role of Dithiolates in the Flotation of Sulphide Minerals. Miner. Sci. Eng., vol. 9, pp. 177-197.

Fuerstenau, M.C., and Sabacky, B.J., (1981). On the Natural Floatability of Sulphides, Int. J. Miner. Process., vol. 8, pp. 79-84.

Gardner, J.R., and Woods, R., (1979). An Electrochemical Investigation of the Natural Floatability of Chalcopyrite. Int. J. Miner. Process., vol. 6, pp. 1-16.

Gaudin, A.M., (1932,1957). Flotation, 1st and 2nd Edition, McGraw Hill Co., New York.

Gaudin, A.M., Miaw, H.L., and Spedden, H.R., (1957). Native Floatability and Crystal Structure. 2nd Int. Congr. Surf. Activity, vol. 3, pp. 202-216.

Granville, A., Finkelstein, N.P., and Allison, S.A., (1972). Review of Reactions in the Flotation System: Galena-Xanthate-Oxygen, Trans. I.M.M., vol. 81, C1-C30.

Gutierrez, C., (1973). The Mechanism of Flotation of Galena by Xanthates, Miner. Sci. Eng., vol. 5, No. 2, pp. 108-117.

Gutierrez, C. and Martin-Poveda, F., (1981). Flotation of Galena, Influence of Grain Size, of Pulp Deoxygenation, and of Cleaning with Ammonium Acetate. Int. J. Miner. Process., vol. 8, pp. 111-123.

Hannay, N.B. and Smyth, C.P., (1946). The Dipole Moment of Hydrogen Fluoride and the Ionic Character of Bonds. J. Am. Chem. Soc. vol. 68, pp. 171-173.

Herd, H.H. and Ure, W., (1941). Surface Chemistry in the Flotation of Galena. J. Phys. Chem., vol. 45, pp. 93-106.

Heyes, G.W., and Trahar, W.J., (1977). The Natural Floatability of Chalcopyrite. Int. J. Miner. Process, vol. 4, pp. 317-344.

Hoover, J.T., (1916). Concentrating Ores by Flotation, 3rd Edition, Chapters II and III, Mining and Scientific Press.

Hornsby, D. and Leja, J., (1982). Selective Flotation and its Surface Chemical Characteristics. In: Surface and Colloid Science, (E. Matijevic; Editor), vol. 12, pp. 217-301.

Ito, T., Morimoto, N., and Sadanaga, R., (1952). The Structure of Realgar, Acta Crystallogr., vol. 5, pp. 775-782.

Kelebek, S., Salman, T., and Smith, G.W., (1982). Interfacial Phenomena in Coal Flotation Systems. In: Phoenix of the 80's, Al-Taweel; Editor), vol. I, pp. 145-152, Chem. Inst. Canada.

Klassen, V.I. and Mokrousov, V.A., (1963). An Introduction to the Theory of Flotation, Trans. by J. Leja and G.W. Poling, Butterworths, London.

Knoll, A.F. and Baker, D.B., (1941). Adsorption of Potassium Xanthate by Galena in Oxygen-Free Atmosphere, AIME Tech. Publ.; 1313.

Leja, J., (1982). Surface Chemistry of Froth Flotation, p. 758, Plenum Press, New York.

Lepetic, V.M., (1974). Flotation of Chalcopyrite Without Collector after Dry Autogenous Grinding, C.I.M. Bull., June, pp. 71-77.

Luttrell, G.H. and Yoon, R.H., (1983). Surface Chemistry of Collectorless Flotation of Chalcopyrite, paper; 193, 112th AIME Annual Meeting, Atlanta, Georgia, March 6-10.

MacLaclan, C.G., (1926). Synthetic Testing for Flotation, C.I.M. Bull., vol. 17, September, pp. 273-

Mathieu, G.I. and Bruce, R.W., (1974). Getting the Talc out of Molybdenite Ores, Can. Min. J., vol. 95, No. 6, pp. 75-77.

McHardy, J.C., (1972). Surface Chemistry of Talc Flotation, Masters Thesis, Dept. Min. Metall. Eng., McGill Univ., Montreal.

Parekh, B.K. and Aplan, F.F., (1978). Critical Surface Tension of Wetting of Coal. In: Recent Developments in Separation Science, (N.N. Li; Editor), vol. IV, pp. 107-113.

Paterson, J.G. and Salman, T., (1968). Interaction of Xanthate with Chalcocite, C.J.M. Bull., January, pp. 1-5.

Pauling, L., (1960). The Nature of the Chemical Bond and the Structure of Molecules and Crystals, 3rd Edition, p. 644, Cornell Univ. Press.

Plaksin, I.N., (1959). Interaction of Minerals with Gases and Reagents in Flotation, Min. Eng., March, pp. 319-324, AIME.

Poling, G.W. and Leja, J., (1972). Discussion on the paper by Granville et al. (1972), Trans. I.M.M., C125-126.

Rao, S.R., (1969). The Collector Mechanism in Flotation, Sep. Sci., vol. 4, pp. 357-411.

Ravitz, S.F., (1940). Oxygen-Free Flotation II - Further Experiments with Galena. AIME Tech. Publ.; 1147.

Ravitz, S.F. and Porter, R.R., (1939). Oxygen-Free Flotation I - Flotation of Galena in Absence of Oxygen, AIME Tech. Publ.; 513.

Rey, M. and Formanek, V., (1960). Some Factors Affecting Selectivity in the Differential Flotation of Lead-Zinc Ores. Particularly in the Presence of Oxidized Lead Minerals, paper 18, Int. Miner. Process. Congr., pp. 343-353, I.M.M., London.

Saito, K., Nagano, I., and Izumi, S., (1975). New Separation Techniques for Plastics, Japan Plastics Age, March, pp. 25-30.

Scanvicar, S., (1960). The Crystal Structure of Stibnite; A Redetermination of Atomic Positions, Zeits. Krist., vol. 114, pp. 85-97.

Sergio, C., (1979). Flotation of Molybdenite. In: International Molybdenum Encyclopaedia, (A. Sutalov; Editor), vol. II, p. 165. Intermet Publ., Santiago de Chile.

Streltsin, G.S., (1952, 1953). As quoted in: Klassen and Mokrousov (1963), pp. 10, 41-42, 63-64.

Sutherland, K.L. and Wark, I.W., (1955). Principles of Flotation, Australasian I.M.M., Melbourne.

Suwanasing, P. and Salman, T., (1970). Particle Size in Flotation Studies, Can. Min. J., vol. 91, No. 12, pp. 55-62.

Trahar, W.J., (1983). A Laboratory Study of the Influence of Sodium Sulphide and Oxygen on the Collectorless Flotation of Chalcopyrite, Int. J. Miner. Process, vol. 11, pp. 57-74.

Vaughan, D.J. and Craig, J.R., (1978). Mineral Chemistry of Metal Sulfides, p. 493, Cambridge Univ. Press, London.

Wells, A.F., (1962). Structural Inorganic Chemistry, 3rd Edition, Clarendon Press, Oxford.

Wuensch, B.J., (1974). Sulfide Crystal Chemistry, Ch. 2. In: Sulfide Mineralogy. (P.H. Ribbe; Editor), Mineralogical Soc. Am., Short Course Notes, vol. I, pp. 21-44.

Yarar, B., (1983). Correlation of Zeta-Potential and Floatability of Weathered Coal, Trans. AIME, vol. 272, pp. 1978-1983.

Yoon, R.H., (1981). Collectorless Flotation of Chalcopyrite and Sphalerite Ores by Using Sodium Sulfide, Int. J. Miner. Process., vol. 8, pp. 31-48.

Zisman, W.A., (1964). Relation of Equilibrium Contact Angle to Liquid and Solid Constitution. In: Contact Angle, Wettability and Adhesion - Advances in Chemistry Series (R.F. Gould; Editor), vol. 43, pp. 1-51.

CHAPTER 2

SURFACE PROPERTIES OF VARIOUS NATURALLY FLOATABLE MINERALS

2.1 INTRODUCTION

In the preceding chapter, the crystal structures of minerals that exhibit an apparent inherent hydrophobicity were described. The explanations for the inherent hydrophobicity were summarized.

Inspection of the literature indicates that there is a meager amount of research work reported on the surface properties of these minerals. In two simultaneous publications, Arbiter et al. (1975) and Chander et al. (1975) discussed the results of zeta potential contact angle and flotation response of molybdenite, talc, stibnite, sulphur and graphite, paying particular attention to whether or not a correlation existed between them. Previously, a correlation between these pH-dependent surface properties had been clearly demonstrated for the quartz-dodecylammonium acetate system (Fuerstenau; 1957). A similar correlation may be sought for an inherently hydrophobic mineral in a surfactant-free system. Derjaguin and Shukakidse (1961) were first to note a correlation between zeta potential and flotation recovery of stibnite as a function of pH. As the zeta potential became less negative, the

recovery increased. They explained the correlation theoretically and proposed a quantitative floatability criterion including the zeta potential term (section 2.2.4.3). Their experimental findings were verified by Arbiter et al. using contact angle and flotation tests. However, there was only qualitative agreement with theory. For minerals like molybdenite, graphite, they found no correlation. In a general discussion of these studies Arbiter (1975) emphasized the following:-

> *"Any correlation between zeta potential and floatability for stibnite may be more fortuitous than real. Paraffin, graphite and unoxidized molybdenite, which show qualitatively similar zeta potential against pH behaviour to stibnite, show little or no parallelism between floatability and zeta potential."*

In contrast with the results of Arbiter et al., Chander and Fuerstenau (1972) did find a correlation between the zeta potential and the natural flotation response of the KOH-leached and unleached molybdenite samples. However, interestingly, they did not include the correlation obtained with the latter sample in the discussion of a later publication (Chander et al., 1975). The latter authors put emphasis on the surface anisotropy due to bond breakage on fracture and to surface oxidation to explain the observed lack of correlation for the majority of the samples.

For coals which possess various degrees of inherent

hydrophobicity, there appears to be a similar conflict regarding the correlation between the zeta potential and natural floatability. Brown (1962) proposed that maximum floatability and hydrophobicity of coal should take place at the point-of-zero-change (PZC). However, experimental results obtained by Jessop and Stretton (1969), Edwards (1972) and Celik and Somasundaran (1980) showed that the floatability of coal was either independent of pH over a wide range or was maximum at a pH value not corresponding to its PZC value. In general, PZC value of coals occurs in the acidic solutions. Iskra and Laskowski (1967) reported that flotation response of coals in salt flotation was maximum at low pH, nearly 2. Kelebek et al. (1982a, 1982b) showed that maximum contact angles were developed in the vicinity of the PZC values of the coal samples which ranged from pH 2 to 5. Floatabilities of the PZC values were among the highest but there appeared to be no distinct maximum in the case of high rank coals. Similarly, Yarar and Leja (1982) reported results in favour of correlation between the zeta potential and floatability of weathered coal.

The reasons for these differing observations may be connected to remarkably heterogeneous character of coals and differences in the experimental procedures employed. Another likely reason may be the differences in the hydrophobic-to-hydrophilic ratios of the samples used in the zeta

potential, contact angle and flotation tests. This is in accordance with the concept of surface anisotropy hypothesized by Chander et al. (1975). An anisotropic surface is defined as consisting of two types: one formed by the rupture of van der Walls bonds, is hydrophobic and the other formed by rupture of ionic or covalent bonds, is hydrophilic. Surface anisotropy is considered to be an inherent characteristic of most hydrophobic solids. This hypothesis explains the lack of correlation observed by Arbiter et al. (1975) between the zeta potential, contact angle and the natural flotation response of various inherently hydrophobic minerals especially of layer type structure such as talc and molybdenite.

This chapter is intended in part to re-examine this correlation and how it can be demonstrated using new and relatively simple techniques. The experimental work provides a test for the hypothesis put forward by Chander et al. (1975).

2.2 THEORETICAL REVIEW

2.2.1. Electrokinetics

2.2.1.1. The Mechanism of Surface Charging

All the solid particles carry an electrical charge when in contact with an aqueous environment. This is demonstrated by the electrokinetic migration of the fine particles under the influence of an applied voltage (i.e. electrophoresis)

(Kruyt, 1952). If the crystal structure of a solid is such that the surface layer does not contain ruptured interatomic bonds it should be strongly hydrophobic as deduced from the work of Gaudin et al. (1957). The electrical charge at such a surface may be determined primarily by the aqueous phase (i.e. the solid may not participate in determining the electrical charge) (Arbiter et al., 1975). However, this is an unlikely case. There are usually impurities present; most minerals have a degree of ionic bonding, hence lattice sites are occupied by ions which may be released into the solution. More importantly, size reduction (e.g. grinding to liberate the valuable minerals) can produce an appreciable number of ionic (hydrophilic) sites due to bond breakage. Therefore, the magnitude of the electrical charge at an originally hydrophobic surface depends upon both the surface chemistry of the solid and the solution chemistry of the aqueous environment.

Potential-determining ions represent the type of ions which cause the establishment of a certain surface at a particle surface. In the case of oxide minerals, they are the hydrogen and hydroxyl ions along with some hydroxy-complexes (hydrolysed metal ions) (Parks, 1965). For hydrophobic solids such as graphite, coal and molybdenite, which are susceptible to oxidation, these ions also play a primary role in establishing surface charge. Oxide surfaces acquire their charge in two stages: formation of a hydroxyl ion layer as a result of

surface hydration, followed by a second step in which a surface charge is established either by amphoteric dissociation of the previously hydrated oxide surface or by adsorption of hydrogen and/or hydroxyl ions (Parks and de Bruyn, 1962; Aplan and Fuerstenau, 1962; Smith and Salman, 1966). Parks (1965) states that a positive surface charge may originate either by adsorption of hydrogen ions or the desorption of hydroxyl ions or vice versa, but that this cannot be distinguished experimentally. In the context of present knowledge, the following mechanisms are distinguishable in the establishment of a surface charge:

I. Adsorption of specific ions from solution, nature of the adsorption being strong or weak. Adsorption of potential-determining ions can cause a negative or a positive surface charge.

II. Loss of ions from the surface of an ionic solid. For example, a barite surface may acquire a negative or positive electric charge by losing Ba^{++} or $SO_4^{=}$ ions into solution. A definite concentration of these potential-determining ions determines zero surface charge (Buchanan and Heyman, 1949).

III. Surface charge may also result from dissociation of surface functional groups such as -COOH and -SiOH. This mechanism is important in the surface charging of organic colloids (Abramson, 1942) and low rank coals (Kelebek et al., 1982a).

The surface charge of a certain sign thus created will be subjected to the attraction of counter-ions present in

hydrated forms in the aqueous solution. An equilibrium distribution will be set up between the solid surface and the solution which results in the formation of an electrical double layer.

2.2.1.2. Electrical Double Layer

The development of the theory of the electrical double layer began with the work of Helmholtz (1879) who introduced the first model of electrical double layer structure. In this model, the electrical double layer is presumed to be a flat condenser; one plate of which is the solid surface and the other one, which carries the counter-ions, is in the solution a very small distance from the first plate. The main shortcoming of the model is the fact that the thickness of the double layer is very small and approximates molecular dimensions which means that the charges are so rigidly held that an external field could not affect this arrangement of the double layer. It is unlikely that such a structure is held so tightly due to the electrostatic repulsion between charged particles and the thermal motion of the liquid.

Gouy (1910) and Chapman (1913) independently proposed a diffuse counter-ion layer concept. According to the Gouy-Chapman theory, counter-ions are not only concentrated at the interface, but also may be dispersed in the liquid phase at a distance away from the interface. Thus, the

formation of a double layer is determined by an equilibrium between the thermal motion of counter ions and their attraction by the electric field of the solid phase. The Gouy-Chapman theory can run into difficulties when the surface potential (ψ_o) is large because of the theory's inherent assumption of point charges and the consequent neglect of ionic diameters. One of the deficiencies of the Gouy-Chapman theory is that there are large differences between the experimental and predicted values of the capacitance of the double layer (Leja, 1982).

Consequently, neither the Helmholtz nor the Gouy-Chapman model is satisfactory to represent the structure of the electrical double layer. The former over-emphasized the rigidity of the ionic environment, and the latter overemphasized its mobility.

An improved double layer structure is described by Stern (1924) who modified the Gouy-Chapman model by replacing the point charge approximation with ions of finite size and combined it with the Helmholtz model. Secondly, Stern introduced the concept of specific adsorption of ions from solution which is caused by a field of molecular adsorption forces in the immediate vicinity of the solid surface. According to Stern's theory, the first layer of counter ions is attracted to the surface under the action of both electrostatic and adsorption forces. This results in the formation of a plane

condenser having a thickness of Δ, as envisaged by the Helmholtz theory. This layer, in which the electrical potential decrease sharply, is variously known as "the Stern layer", "the Helmholtz layer" or "the adsorption layer." The remaining counter-ions, as a result of thermal motion, form the diffuse part of the double layer as in the Gouy-Chapman theory. As a further improvement, Graham (1954) sub-divided the Stern layer into two parts. The internal part which was termed "inner Helmholtz plane" contains ions which are specifically adsorbed by the solid surface with the loss of their hydration shells. The external part termed "outer Helmholtz plane" contains weakly adsorbed hydrated ions. More details concerning various aspects of the electrical double layer are discussed elsewhere (Adamson, 1976; Leja, 1982).

Figure 2.1 represents a schematic illustration of the electrical double layer with the exception of the sub-division of the Stern layer qualitatively described above. The surface potential, ψ_o, is the potential difference between the solid surface and the bulk of the solution. By convention, the potential of the bulk solution is defined as zero, so that in the absence of specific adsorption, ψ_o is zero at the point of zero charge. At a given activity of potential determining ions, a_+ and a_-, ψ_o is given by the Nernst equation:-

$$\psi_o = \frac{RT}{z_+F} \ln\left(\frac{a_+}{a_+^o}\right) = \frac{RT}{z_-F} \ln\left(\frac{a_-}{a_-^o}\right) \qquad 2.1$$

where R is the gas constant, T is the absolute temperature, F is the Faraday constant, a_+^o, a_-^o are the activities of the potential-determining ions at the PZC, and z_+ and z_- are the corresponding ionic charges. For small potentials ($zF\Psi_o \ll RT$, or $\Psi_o \ll 25$ mv) in the absence of specific adsorption, the following equations can be obtained (Adamson, 1976) for the potential (Ψ) and the surface charge density (σ):-

$$\Psi_{(x)} = \Psi_o e^{-\kappa x} \qquad 2.2$$

$$\sigma = \frac{\Psi_o \varepsilon \kappa}{4\Pi} \qquad 2.3$$

where x is the distance from the interface into the solution, ε is the dielectric constant of the medium, and κ is the reciprocal of the double layer thickness which represents the distance of the center of gravity of the electrical charge in the diffuse layer from the solid surface. If n_i and z_i represent respectively the bulk concentration and the charge on the i-th ion, then κ is expressed as:-

$$\kappa = \sqrt{\frac{4\Pi e^2 \sum_i n_i z_i^2}{\varepsilon kT}} \qquad 2.4$$

where e is the electronic charge and k is the Boltzmann constant. This equation indicates that the effective thickness of the diffuse double layer (i.e. $1/\kappa$) varies inversely with the square root of ionic concentration of the solution (e.g. compression of double layer with an increase in electrolyte concentration).

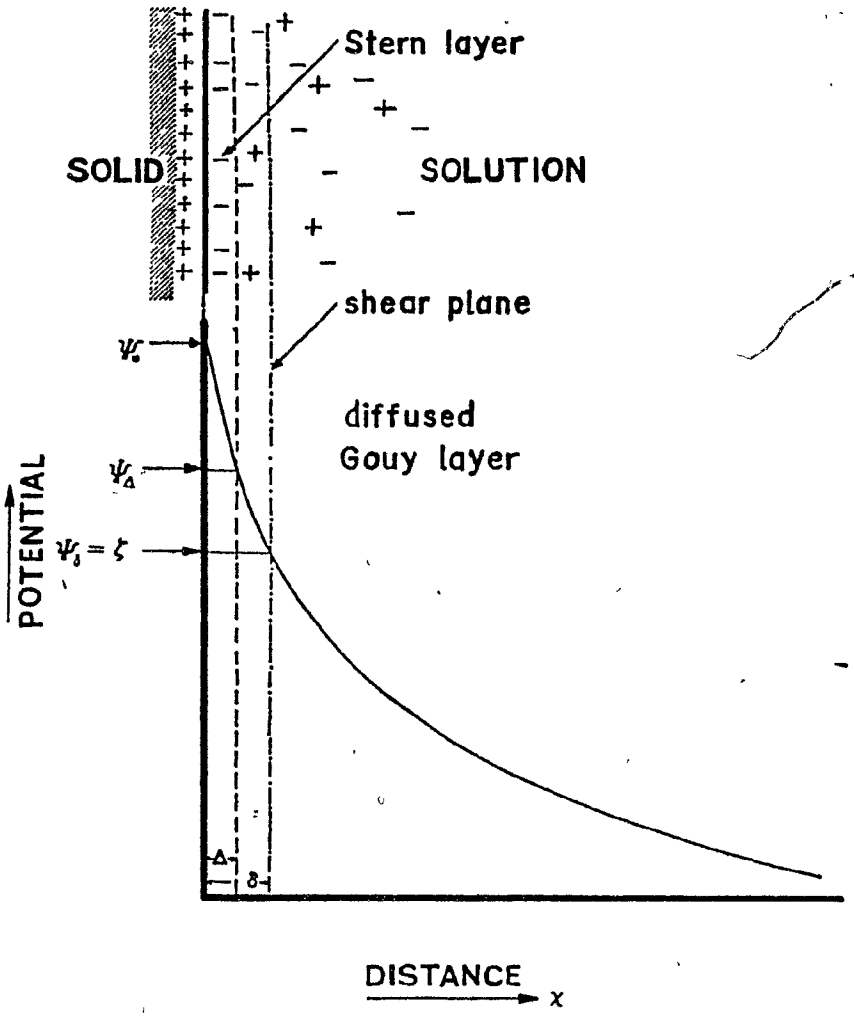


Figure 2.1 A Schematic Representation of the Electrical Double Layer

As previously noted, the Stern layer (or the Helmholtz layer) is rigidly held and is considered to be immobile in the sense of resisting shear. This type of immobility refers to the medium as a whole and hence primarily to the solvent (Adamson, 1976). It means that some residual water is carried along with the hydrated ions held in the outer Helmholtz plane of the Stern layer during the electrokinetic migration of fine particles. The zeta potential (ζ) is the electrical potential at the shear plane between the fixed and flowing liquid constituting the bulk solution (Figure 2.1).

2.2.2. Contact Angle and Wetting

2.2.2.1. Classical Wetting Equations

There are a number of different ways to express the degree of wetting of a solid against liquids. Often, it is expressed simply in terms of an equilibrium contact angle (θ) between a liquid and a solid (Figure 2.2). The higher the contact angle in the air-solid-liquid system, the lower the wettability of the solid by the liquid. That is, the contact angle is an inverse measure of wettability. The equilibrium state at the point of three-phase contact is described by the well-known Young equation which relates the contact angle to the interfacial tensions of the energies (γ) involved:-

$$\gamma_{sv} - \gamma_{s\ell} = \gamma_{\ell v}\cos\theta \qquad 2.5$$

where the subscripts s, v and ℓ refer to solid (smooth and

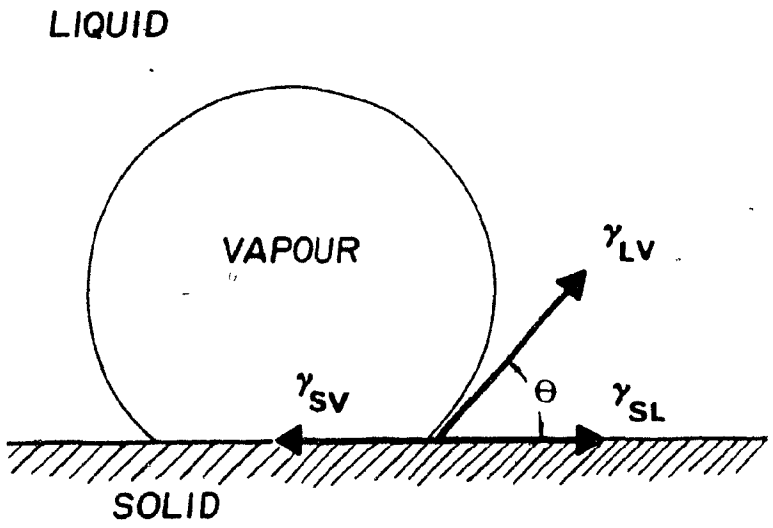


Figure 2.2 Solid-Vapour-Liquid System in Equilibrium.

undeformable), vapour and liquid respectively. This equation indicates that for a three-phase line of contact the following condition must be fulfilled:-

$$\gamma_{sv} - \gamma_{s\ell} < \gamma_{\ell v} \qquad 2.6$$

Flotation collectors perform their task by modifying the interfacial tensions to satisfy Equation 2.6.

Freundlich (1926) expressed wettability by $\gamma_{\ell v} \cos\theta$ and called it adhesion tension which is simply the difference between the non-measurable interfacial tensions of the solid in the Young expression (Equation 2.5). For spontaneous

bubble-particle adhesion, adhesion tension must be less than liquid surface tension.

The work of adhesion of liquid to solid W_A and the work of cohesion of the liquid W_c are given by: -

$$W_A = \gamma_{sv} + \gamma_{\ell v} - \gamma_{s\ell} \qquad 2.7$$

$$W_c = 2\,\gamma_{\ell v} \qquad 2.8$$

Combining Equations 2.5 and 2.7 yields:-

$$W_A = \gamma_{\ell v}\ (1 + \cos\theta) \qquad 2.9$$

which may be divided by Equation 2.8 termwise, and subsequently rearranged to give the following relation:-

$$\cos\theta = 2\left(\frac{W_A}{W_c}\right) - 1 \qquad 2.10$$

It follows from Equation 2.10 that no vapour/solid contact is established if $W_c \leq W_A$. However, a three-phase line of contact is established when $W_c > W_A$. This condition is met naturally for a number of minerals such as molybdenite, graphite, sulphur, etc. which exhibit various degrees of inherent hydrophobicity. Theoretically, the maximum hydrophobicity implies a complete absence of interaction of solid with water (i.e. $W_A = 0$). However, such a solid does not exist in nature. Every solid has dispersion forces to interact with a contacting phase involved (e.g. water). The work of adhesion for a solid-liquid pair can be represented by the sum of terms for the different kinds

of interactions (Fowkes, 1967):-

$$W_A = W_A^d + W_A^h + W_A^{\Pi} + W_A^p + W_A^e \qquad 2.11$$

where superscripts are d for London dispersion forces, h for hydrogen-bonding, Π for interfacial pi-bonds, p for other polar interactions and e for the electrical double layer effects. A liquid may spread out on a solid surface or form a finite contact angle θ, depending upon the relative magnitude of the forces operating on the liquid. For a strongly hydrophobic mineral such as a molybdenite cleavage plane containing no ruptured Mo-S bonds, the components of the work of adhesion for specific interactions (e.g. W_A^h) may be negligibly small. But the work of adhesion as a whole cannot be negligible because of the interfacial contribution by the London dispersion forces.

Other wetting terms include the spreading coefficient, S (Harkins, 1952) which is defined as:-

$$S = \gamma_{sv} - (\gamma_{s\ell} + \gamma_{\ell v}) \qquad 2.12$$

If $S > 0$, the liquid spreads out on the solid surface. A negative S value, corresponds to partial spreading and hence to a floatable condition. This conclusion may be drawn from the following equation which is obtained from Equations 2.7, 2.8 and 2.12:-

$$S = W_A - W_C \qquad 2.13$$

For partial spreading, $S < 0$, cohesion within the liquid is greater than the adhesion of the liquid to the solid surface.

When the solid and vapour phases are mutually saturated as the equilibrium requirement, the solid surface is often covered with a film of adsorbed vapour phase. This lowers the surface-free energy of solid by an amount Π^v which is known as the surface pressure of the adsorbed film.

$$\gamma_{sv} = \gamma_s - \Pi^v \qquad 2.14$$

where γ_s is the surface-free energy or surface tension of solid in the absence of any adsorbate (i.e. in vacuum). For a solvent-solute system, a similar equation involving the surface pressure of the surface active solute (Π^s) may be written:-

$$\gamma_{sg} = \gamma_{wg} - \Pi^s \qquad 2.15$$

where the subscripts sg and wg refer to the solution-gas and the water-gas interfaces. Combining Equations 2.5 and 2.14 yields:-

$$\gamma_{\ell v} \cos\theta = \gamma_s - \gamma_{s\ell} - \Pi^v \qquad 2.16$$

which indicates that an increase in Π^v results in a larger contact angle.

The contact angle which is described by Young's equation (2.5) corresponds to thermodynamic equilibrium conditions. It is often difficult experimentally to determine the true value of this angle. At a surface over which liquid is advancing,

the angle is greater than at a surface from which it is receding. The difference between these two was termed the hysteresis of the contact angle by Sulman (Gaudin, 1932). It is the opinion of many authors, including Wark and Cox (1934) and Wenzel (1936), that hysteresis is brought about by surface roughness. Wenzel defined a roughness factor, r, as the ratio of the actual surface area to the geometric plane area and used it as a correction factor in the following expression:-

$$\cos\theta = \frac{1}{r}\cos\theta' \qquad 2.17$$

where θ' is apparent or measured contact angle and θ is the true contact angle. The effect of surface roughness may be minimized by careful polishing. Another frequent cause of hysteresis is unintentional contamination of the system. Fowkes and Harkins (1940) found that, when dealing with pure liquids and smooth and very clean solid surfaces (e.g. graphite), the hysteresis disappeared.

The literature reveals that the flotation behaviour may be correlated with contact angle (Fuerstenau, 1957), adhesion tension (Somasundaran, 1968), and surface pressure of surfactant solutions (Kulkarni and Somasundaran, 1975; Bleir et al., 1976).

2.2.2.2 The Critical Surface Tension of Wetting

The relationship between wettability of a solid and the surface tension of a wetting liquid dates back for many decades.

As early as 1926, Freundlich qualitatively expressed this relationship as follows:-

> *". . . liquids in general wet the better the lower their surface tension. This we know to be born out by experience; liquids with a small surface tension such as ether, alcohol, and generally the majority of organic liquids, wet most solid bodies better than water or sulphuric acid, and these again better than mercury or molten metal."*

Bartell and Osterhof (1928), and Bartell and Zuidema (1936) determined the wettability of various solids (e.g. carbon black, silica, wax) using liquids of different surface tensions and noticed a number of regularities in contact angle behaviour with respect to the surface tension of the liquids but apparently did not seek a quantitative correlation between these two relevant properties.

Zisman and his co-workers (Zisman, 1964) were able to take advantage of this relationship. They found that the contact angle of a sessile liquid drop on a smooth and homogeneous polymeric solid surface decreased as the surface tension of liquid decreased. They defined a new term "the critical surface tension of wetting", γ_c, as that value of surface tension below which liquid wets the surface completely (by spreading spontaneously).

In general, a linear relationship was found between the cosine of the slowly advancing contact angle and the liquid surface tension, γ_{Lv}, for a series of homologous liquids (e.g.

n-alkanes, di[n-alkyl] esters). An approximate of γ_c value is obtained by extrapolating the straight-line plot of cos θ vs. γ_{Lv} to cos θ = 1. Linear relationships have also been found for a variety of nonhomologous liquids on some polymer samples. Figure 2.3 illustrates the results obtained with the n-alkanes of various hydracarbon chain length on polytetrafluoroethylene (i.e. Teflon) and with a series of miscellaneous liquids on polyethylene and polystyrene. A greater scatter of experimental data is notable in the latter case. In addition to various polymeric solids which are of the low-surface-energy by their nature, the high-surface-energy solids such as glass, polished metals (Zisman, 1964) and various minerals (Parekh, 1972; Parekh and Aplan, 1974) coated with a variety of heteropolar surfactants also exhibit a linear relationship between cosθ and γ_{Lv}.

The Zisman relationship (i.e. cosθ vs. $\gamma_{\ell v}$ may be described by the following equation:-

$$\cos \theta = 1 - b\ (\gamma_{\ell v} - \gamma_c) \qquad 2.18$$

where b is the slope of the line. In some cases, deviations from linearity have been found, particularly for values of $\gamma_{\ell v}$ above 50 mN/m. In the linear part of the plot, especially for n-alkanes on strongly hydrophobic solids such as Teflon (Figure 2.3), the interaction between the solid and the liquid is thought to result from London dispersion forces only.

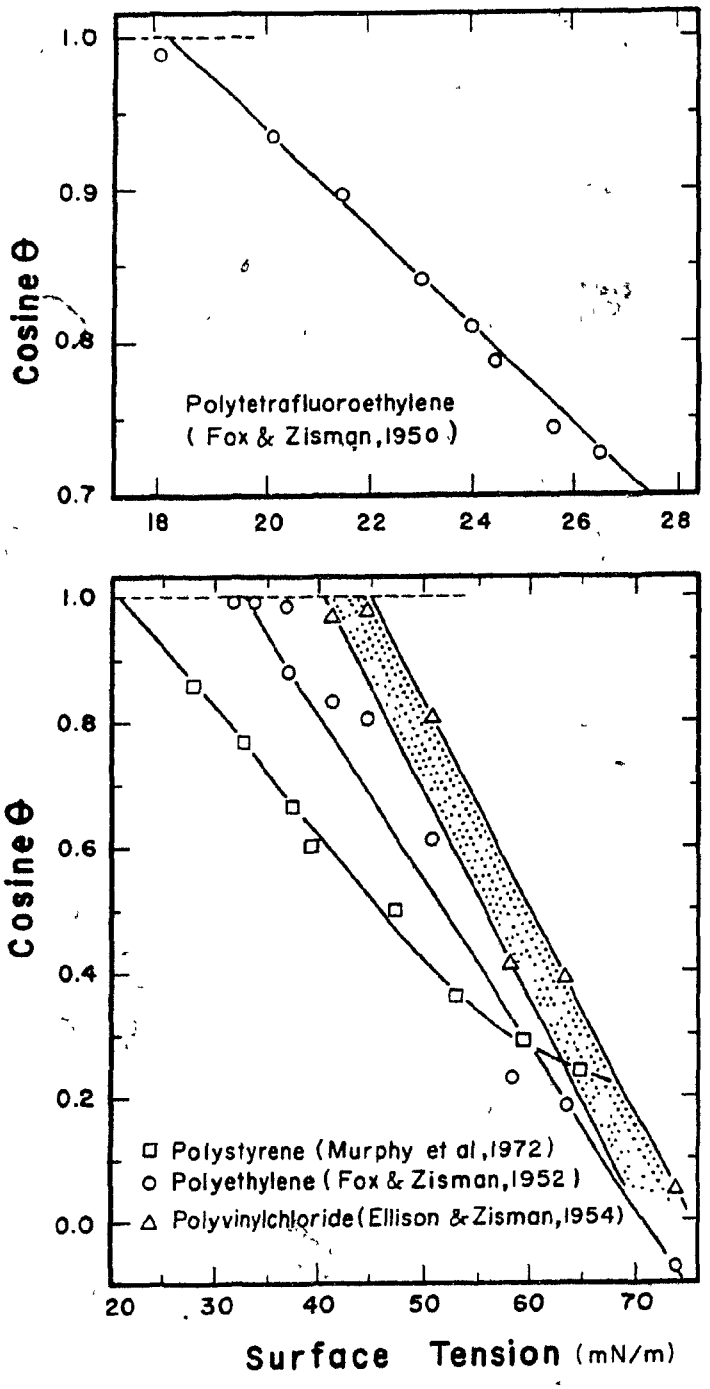


Figure 2.3 Wettability of Polytetrafluoroethylene, Polyethylene and Polyvinylchloride (by pure liquids) and Polystyrene (by aqueous methanol solutions)

Reference wetting liquids of high surface tension (i.e. $\gamma_{\ell v}$ > 50 mN/m) can interact with the solid through additional forces such as hydrogen bonding. According to Zisman (1964), the curvature results from weak hydrogen bond formation between the molecules of liquid and those in the solid surface.

Both γ_c and b values have been utilized effectively to characterize the relative hydrophobicities of solids. The former was used by Shafrin and Zisman (1960) as a criterion to classify the highly non-polar organic polymers with respect to their atomic constitution. According to this classification, the surfaces comprised of closest packed $-CF_3$ groups have the lowest surface energy (γ_c = 6 mN/m). As the surface fluorine atoms are substituted by hydrogen atoms, γ_c increases in a regular fashion. In general, the critical surface tension of wetting values of carbon-containing surfaces have been found to increase in the order of fluorocarbons (γ_c = 6 - 28 mN/m), hydrocarbons (γ_c = 22 - 35 mN/m), chlorocarbons (γ_c = 39 - 43 mN/m) and the nitrated hydrocarbons (γ_c = 40 - 45 mN/m). The success of this classification appears to be partly due to the fact that the slope values (b) of the Zisman plot for most solids remained constant at 0.035±0.005.

For coals which are solid hydrocarbons containing various quantities of oxygen, nitrogen, sulphur and some other elements depending mainly upon their rank, the γ_c values have been found to be nearly constant at 45 mN/m but the b values have been

indicative of hydrophobicity level of the coal type (Parekh and Aplan, 1978). When γ_c is constant for a series of hydrophobic solids, a high value of b means a higher contact angle for liquids with $\gamma_{\ell v} > \gamma_c$. Therefore, a correlation between the rank of the coals and the b value of their respective Zisman plot is expected. As pointed out by Gray (1962), a higher value of b indicates a greater difference of wettability by liquids of high and low surface tension. That is, a high value of b means that a surface will be readily wetted by low surface tension liquids but difficult to wet by high surface tension liquids.

In general, γ_c determined by surfactant solutions is lower than that obtained by pure reference liquids. Two exceptions are polyethylene and Teflon studied by Bernett and Zisman (1959). Various surfactant solutions produced the same γ_c values for these solids as those established by pure liquids, but the cos θ vs. $\gamma_{\ell v}$ relationship was no longer linear. The rest of the polymeric solids studied by Dann (1970) and Murphy et al. (1972) exhibited lower γ_c values when solutions were used. Figure 2.3 shows the results obtained for a polystrene sample using methanol solutions. Murphy et al. claimed that the γ_c value for this system was 21 mN/m as compared to 33-34 mN/m obtained with pure liquids. Dann attributed this difference to an interaction between the polar components of the solid and solution surface tensions. Alternatively, Murphy

et al., proposed that the reduction in γ_c was due to preferential adsorption of the alcohol molecules at the solid/liquid and solid/vapour interfaces through the hydroxyl group. However, such an adsorption mechanism does not seem to be realistic (Ottewill and Vincent, 1972; Brooks et al., 1977).

2.2.2.3. Degree of Polarity of Inherently Hydrophobic Surfaces

The Zisman parameters (γ_c and b) are useful in characterizing the degree of non-polarity of low-surface-energy solids. These surfaces, however, invariably possess some polar sites. They may be generated by oxidation of the surface of a polymer-like polyethylene, catalyzed by light or heat (Allan, 1959; Baskin et al., 1977). Or they could be due to impurities like surfactant molecules used in emulsion polymerization, as in the production of Teflon. The surface concentration of the polar sites can vary enormously. On Teflon 6, about one in 200 surface sites is polar and can accept highly polar adsorbates such as water (Zettlemoyer, 1968). As the surface concentration of polar sites on polyethylene was increased by various pretreatments, γ_c was found to increase regularly. This was accompanied by a decrease in b. Such changes in the Zisman parameters may thus be employed to indicate the extent of polar character of low-surface-energy solids. Alternatively, this can be accomplished by recently developed semi-empirical approaches. The approach suggested by Hamilton (1972, 1974) involves the use of octane contact angles measured on polymeric solids in distilled water. This method makes use of the

concept of the components of the interfacial free energy by Fowkes (1964).

According to Fowkes a solid-liquid interfacial free energy ($\gamma_{s\ell}$) can be expressed by the following equation when only dispersion forces are in operation between the solid and liquid phases.

$$\gamma_{s\ell} = \gamma_s + \gamma_\ell - 2\sqrt{\gamma_s^d \cdot \gamma_\ell^d} \qquad 2.19$$

where γ_s^d and γ_ℓ^d are the dispersive components of the surface free energies in air for the solid (γ_s) and liquid phases (γ_ℓ).

Tamai et al. (1967) extended Fowkes' treatment to include a term $I_{s\ell}$ to account for non-dispersion forces (e.g. polar interactions). Thus:-

$$\gamma_{s\ell} = \gamma_s + \gamma_\ell - 2\sqrt{\gamma_s^d \cdot \gamma_\ell^d} - I_{s\ell} \qquad 2.20$$

They combined this equation with Young's equation for two solid-liquid-liquid-combinations and obtained two equations in two unknowns. I_{sw}, the interfacial free energy component for polar interactions at the solid-water interfaces could thus be obtained by this method.

Hamilton proposed that the same information can be obtained using octane contact angle only. The Young equation for the solid-octane-water contact angle (θ_{ow}) is:-

$$\cos\theta_{ow} = (\gamma_{sw} - \gamma_{so}) / \gamma_{ow} \qquad 2.21$$

γ_{so} and γ_{sw}, the interfacial free energies for the solid-octane and solid-water interfaces, can be estimated from Equations 2.19 and 2.20 respectively. When these are inserted in Young's expression the resulting equation becomes:-

$$\cos\theta_{ow} = (\gamma_w - \gamma_o - 2\sqrt{\gamma_s^d \cdot \gamma_w^d} + 2\sqrt{\gamma_s^d \gamma_o^d} - I_{sw}) / \gamma_{ow} \quad 2.22$$

γ_w and γ_o are measurable surface free energies (or surface tensions) of the water and octane phases which are saturated with each other and γ_{ow} is the interfacial free energy between the two phases. γ_s^d, γ_w^d and γ_o^d are the dispersion components of the surface free energies of the solid, water and octane, respectively. The reason for Hamilton's selection of octane as the hydrocarbon phase was that the dispersion component of water and octane were the same ($\gamma_o^d = \gamma_w^d = 21.8$ mJ/m^2). As shown previously by Fowkes (1964), the surface free energy value for octane is due to dispersion forces only, but that for water consists of two components, dispersion forces ($\gamma_w^d = 21.8$ mJ/m^2) and polar forces ($\gamma_w^P = 50.8$ mJ/m^2). The only forces which contribute to the interfacial free energy between two liquids are those forces which exist in both liquids. Since $\gamma_o = \gamma_o^d = \gamma_w^d$, the two square root terms in Equation 2.22 cancel for a given solid. Hamilton (1972) inferred that θ_{ow} (measured through the octane phase) would be 50° for solids capable of dispersion interactions only and higher for solids which may interact also by polar sites. This conclusion was found to be invalid due to the use of erroneous surface tension values.

Bagnall and Green (1979) introduced necessary corrections and replaced the term I_{sw} in Equation 2.22 by a geometric mean in which γ_s^P and γ_w^P are the polar components of the surface free energies of the solid and water, respectively. The modified equation was as follows:-

$$\cos \theta_{ow} = (\gamma_w - \gamma_o - 2\sqrt{\gamma_s^P \cdot \gamma_w^P}) / \gamma_{ow} \qquad 2.23$$

Using the values γ_w = 72.6 mJ/m^2, γ_o = 21.8 mJ/m^2, γ_{ow} = 50.8 mJ/m^2 and γ_w^P = 50.8 mJ/m^2, the polar component of the surface free energy of solid, γ_s^P can be estimated from Equation 2.23 which is rearranged to:-

$$\gamma_s^P = 12.70 \times (1 - \cos \theta)^2 \qquad 2.24$$

Equation 2.22 and alternative expressions have frequently been used as an attempt to characterize various solid surfaces (Tamai, 1976; Busscher et al. 1983). These expressions have been discussed by Andrade et al. (1979). Although θ_{ow} can experimentally be measured without major difficulty, the derivation of γ_s^P and γ_s^d from experimental data is in general complicated. Since these components cannot be measured directly by experiment, a fruitful discussion concerning the validity of any theoretical expression requires the estimation of γ_s^P and γ_s^d by independent experimentation. This type of study appears to be lacking in the literature. An exception is the γ_s^d value of graphite sample considered by Fowkes (1967). He found that the γ_s^d value obtained from the contact angle of water on

graphite was about 109 mJ/m^2. This result was checked by γ_s^d values for graphite obtained by heats and free energies of adsorption of alkanes on Graphon, and by heats of immersion of Graphon in alkanes. A convincing agreement was reported between these values. More recently, a study of a similar nature has been reported for marble (Janczuk et al., 1983).

The γ_s^d values for sulphur and graphite were recently determined by Janczuk and Chibowski (1983) using the following expression:-

$$\gamma_s^d = \left[\frac{\gamma_w \cos \theta_{wa} - \gamma_{hw} \cos \theta_{hw} + 2\gamma_w - \gamma_h}{2(2\sqrt{\gamma_w^d} - \sqrt{\gamma_h^d})}\right]^2 \qquad 2.25$$

where θ_{wa} and θ_{hw} are the solid-water-air and solid-hydrocarbon-water contact angles and the subscripts h and w refer to hydrocarbon (saturated) and water respectively. Here the underlying assumption is the absence of interfacial polar interactions. The γ_s^d values were reported to be 124.1 and 121.7 mJ/m^2 for sulphur and graphite, respectively.

2.2.3. Flotation

2.2.3.1. Stages in Flotation

The events leading to the recovery of particles under dynamic flotation conditions are usually considered to occur in three main stages (Derjaguin and Dukhin, 1961; Laskowski, 1975):

(a) bubble-particle collision

(b) thinning and rupture of the disjoining film which separates the colliding bubble and particle for the bubble-particle attachment to occur

(c) formation of the stable bubble-particle aggregate capable of withstanding considerable disruptive forces operating in the cell.

The collision frequency can be said to depend upon the flotation cell hydrodynamics and related solution chemistry for the production of bubbles of suitable size, while the attachment efficiency depends mainly upon the physicochemical conditions, particularly the degree of hydrophobicity of the particle surfaces.

Thermodynamic criterion for bubble-particle attachment is given by:-

$$\Delta G = \gamma_{sv} - \gamma_{\ell v} - \gamma_{s\ell} = \gamma_{\ell v} (\cos \theta - 1) < 0 \qquad 2.26$$

where ΔG denote the change in the Gibbs free energy of the system. Therefore, the more negative the ΔG value, the greater is the probability of flotation. However, this criterion alone is not sufficient to describe a dynamic process such as flotation. There are kinetic resistances to the establishment of a finite three-phase contact angle (Sheludko, 1963). The contact angle becomes important in the third stage, namely, the establishment of the aggregate stability and in determining the maximum floatable size (Gaudin, 1957; Sheludko et al. 1976).

The second stage - the thinning and rupture of the disjoining film - is regarded as the most important stage in flotation (Derjaguin and Skukakidse, 1961; Blake, 1972). It has been known for a long time that a layer of liquid, after thinning to a certain critical value, becomes unstable and is subsequently ruptured. The lifetime of the disjoining film between a bubble and particle from the onset of bubble deformation to film rupture is known as the induction time. When this time is greater than the bubble-particle contact time the particle capture would be impossible even if, after contact, the contact angle was large. The contact time is known to be in the order of a few milliseconds (Sutherland and Wark, 1955). The thinning and rupture of the wetting film depends not only upon the degree of hydrophobicity of the surface but also upon other parameters such as the viscosity of the film.

Eigeles and Volova (1960) measured the induction times between bubbles and particles of various sizes under various conditions. They found that collector additions to the solution shortened the induction time from infinity (for strongly hydrophilic minerals) to the range of 1-10 milliseconds. This effect was much more pronounced when mixtures of surfactants were used. They also showed that the induction time decreased exponentially with increasing temperature and ordinarily with decreasing particle size. Lekki and Laskowski (1971) furnished further evidence on the beneficial effect of the joint

action of frother (α-terpineal) and collector (ethyl xanthate) in the flotation of chalcocite.

2.2.3.2. Disjoining Pressure and its Components

The study of the thinning process of a wetting liquid layer on a surface of a mineral appears to be vital for the development of the theory of flotation. By extending the theory of interaction between colloidal particles first given by Derjaguin and Landau (1941) and by Verwey and Overbeek (1946) (commonly known as the DLVO theory), Derjaguin and Dukhin (1961) analysed conditions for the stability of the thin film existing between a particle and a bubble as they collide. Within this concept, basically three kinds of interactions are considered to be significant in flotation:-

(a) forces due to the presence of an electrical double layer around the particles;
(b) the attractive forces arising from the van der Waals forces between atoms and molecules;
(c) forces related to structural changes in the boundary layers (e.g. hydration).

Due to a lack of quantitative understanding of the forces of the third kind, they were neglected in the mathematical treatment of the theory.

The concept of a disjoining pressure was developed to explain the changes in the thermodynamic properties and in the stability of the thin liquid film. Disjoining

pressure is considered to be the equilibrium pressure set up within the thin liquid film separating two phases (e.g. solid-solid, solid-gas, etc.), opposing direct contact between the phases (Klassen and Mokrousov, 1963). A positive disjoining pressure in a liquid film is considered to cause the film to thicken or cause the two phases to "disjoin". The disjoining pressure, P_d, is thought to consist of several components, each representing a specific type of interaction:-

$$P_d = P_{el} + P_{vw} + P_h \qquad 2.27$$

where P_{el}, P_{vw} and P_h are the components of the total disjoining pressure due to the electrical double-layer repulsion, van der Waals' attraction and hydration steric repulsion forces, respectively. Depending upon the individual contribution of these components, a particle surface may or may not acquire a stable film in an aqueous suspension. Air bubbles cannot attach to the particles if the overall disjoining pressure is positive and relatively large. This leads to a description of hydrophilic solids (e.g. gypsum, silica, etc.) as having indefinitely stable aqueous liquid layers attached to their surface. However, if the particle surface is such that it causes the offsetting of attractive forces between solid and the liquid, that surface is expected to be hydrophobic (hence floatable). The liquid films on such surfaces are characterized by small positive disjoining pressures or negative ones. The magnitude of the disjoining pressure is

a function of the film thickness Kitchener and his co-workers (Blake and Kitchener, 1972) studied the disjoining films of various thicknesses on the methylated silica in aqueous electrolyte solutions and concluded that over the range of 60-220 nm, the stability of the film was due to the electrical double-layer forces. It appears that dispersion forces and more specific interactions like hydrogen bonding are relatively unimportant at these thicknesses. The film instability at smaller thicknesses (especially below 20 nm) was attributed basically to reduced hydrogen bonding between methylated silica surface and the water molecules. Under these circumstances, the term P_{el} alone predominantly contributes to the positive disjoining pressure in Equation 2.27. Conversely, it can be stated that hydrogen bonding is primarily responsible for the existence of indefinitely stable disjoining films on naked silica (i.e. non-methylated) in an aqueous environment.

The thinning of the wetting film below 20 nm may be said to depend mainly upon the capability of hydrogen-bond formation and also the magnitude of the van der Waals' constants of attraction in the system. Sulphide minerals, when un-oxidized, do not participate in hydrogen bond formation with water . Therefore, the magnitude of their van der Walls' constants can influence the rate of film thinning considerably in the absence of significant electrical double

layer forces. A measure of attractive force is expressed in terms of the Hamaker constant, A_{12}:-

$$A_{12} = \Pi^2 N_1 N_2 C_{12} \qquad 2.28$$

where N_1 and N_2 are the numbers of atoms per unit volume in the materials 1 and 2 and C_{12} is the London dispersion force constant between atom 1 and atom 2. The method of the determination of the Hamaker constants have been reviewed by Rao (1974). It appears that the Hamaker constants are so far available only for a few minerals. Furthermore, in general, the available ones lack reliability. Rao implies this by comparing the Hamaker constants (for the attraction of a mineral to water) of graphite ($A_{12} = 3.2\ 10^{-13}$ erg) and some oxides such as hematite ($A_{12} = 3.0\ 10^{-13}$ erg) and stating the usual hydrophobicity of the former and the hydrophilicity of the latter. Kitchener (1974) is of a similar opinion. He draws attention to the possible invalidity of the approximations made in the mathematical formulation of the DLVO theory and states the following:-

> *"There is, at present, not a single mineral for which the van der Walls' component of the disjoining pressure can be stated with confidence."*

2.2.3.3. Floatability Criterion

Derjuguin and Shukakidse (1961) studied the conditions for the flotation of a "bulk" hydrophobic (i.e. inherently

hydrophobic) mineral in the absence of a collector. Assuming that the disjoining pressure in the wetting film between bubble and particle is equal to the sum of the electrical double layer force and the van der Walls force, they proposed a quantitative criterion of floatability:-

$$m \equiv \frac{D\varepsilon\zeta^2}{A} \quad ; \qquad A = A_{11} - A_{12} \qquad 2.29$$

In this expression, D is the Debye thickness of the ionic atmosphere, ε is the dialectric constant, ζ is the zeta-potential, and A is the Hamaker constant which is the difference between the Hamaker constants for the attraction of water to water (A_{11}) and of water to the mineral (A_{12}). The value of "m" should be less than 3 for the condition of disappearance of the repulsive force barrier and thus for good flotation. This equation predicts that floatability should increase as the zeta potential is decreased. To test the validity of this expression, Derjaguin and Shukakidse determined flotation recoveries and zeta potentials of antimonite (i.e. Stibnite, Sb_2S_3) as a function of pH and calculated the criterion "m" for each pH value. They found quantitative agreement between the theory and the experimentally determined floatability. When the value of m was less than 3, the flotation recovery exceeded 90%. As a result, it was concluded that "the value of the zeta potential can serve as one of the characteristics in determining the flotation activity of antimonite".

This conclusion and in general, the theory has since been tested by other research groups. Arbiter et al. (1975) carried out the contact angle tests in addition to flotation experiments. They found that while the contact angle and floatability of stibnite did increase as the zeta potential was decreased, there was no quantitative agreement with theory. The recovery values obtained by Arbiter et al. were much lower than those obtained by Derjaguin and Shukakidse. The use of a frother (n-hexyl alcohol) by the latter was thought to be a possible reason for the differences observed. For other inherently hydrophobic solids (molybdenite, graphite, paraffin), Arbiter et al. could not observe even a qualitative agreement with the floatability criterion expressed by Equation 2.29.

The topics reviewed in this section have necessarily been brief and selective. Many other aspects of wetting and related surface phenomena have been comprehensively covered in various publications (Johnson and Dettre, 1969; Finch and Smith, 1981; Leja, 1982).

2.3 EXPERIMENTAL MATERIALS AND PROCEDURE

2.3.1. Mineral Samples

With the exception of talc and sulphur, the mineral samples were obtained from Ward's Natural Science Establishment, Inc. The talc sample was from an unknown location in

Quebec. Acid leaching and ignition loss tests (McHardy, 1972) showed a high purity form of talc sample. Sulphur (in fragmented form) was purchased from A.D. Mackay Inc. In addition, individual specimens of cleaved talc (Holly Springs, Oregon) and sulphur (Girgenty, Sicily) were obtained from the Redpath Museum, McGill University. Another sample of sulphur possessing smooth faces was synthetically prepared by recrystallization from carbon disulphide. The coal sample included in the contact angle measurements was obtained from a bituminous type of coal from Sydney, Nova Scotia. It contained about 2.5% ash. A list of the minerals with their original location and approximate purity is shown in Table 2.1.

Table 2.1

Mineral Samples Studied

Sample	Source	Purity (%)
Molybdenite	Ontario	99.4
Talc	Quebec/Oregon	-
Sulphur	A.D. Mackay Inc./Sicily	~ 100
Graphite	Sri Lanka	-
Coal	Sydney, Nova Scotia	~ 96
Stibnite	Borneo/Japan	80.2
Orpiment	Geltchell, Nevada	85.3
Realgar	Manhattan, Nevada	-
Galena	Kansas	99.6
Chalcocite	Butte, Montana	99.2
Chalcopyrite	Rouyn, Quebec	97.4
Pyrite	-	97.0

The samples were received in the form of large lumps and crushed to about 1-2 cm and stored under nitrogen for later use. The samples of orpiment, chalcocite, and molybdenite were old due to long periods of storage (up to four years) in closed cardboard boxes. Therefore, these were specially pretreated before use in flotation experiments. However, for molybdenite, leaching did not seem to produce a significantly better floating sample and thus leaching was discontinued for the subsequent tests. The cleavage specimens from this particular molybdenite sample were prepared from the interior parts of relatively large lumps. The purity levels of the samples were determined by conventional methods of analysis using atomic adsorption (Appendix I).

2.3.2. Electrokinetic Mobility Determination

2.3.2.1. Apparatus

Electrokinetic mobility was measured by using a Mark II micro-electrophoresis apparatus (Rank Brothers). It consists of a transparent chamber comprising a flat type quartz cell in which observations of moving particles are made under an applied voltage through platinum electrodes which are platinized periodically. The flat cell (of cross-section 1mm x 10 mm) was used in preference to the cylindirical type because the mineral particles, although very small, settled at appreciable velocities. The electrical cell lenth was determined

to be 8.29 cm using standard potassium chloride solutions at 25°C (0.01, 0.1, and 1.0 N), and an AC bridge. Movements of particles were observed through the eye-piece micrometers, which were located on each side of a binocular and were timed by means of a timer sensitive to 1/5 of a second. One of the eye-pieces is fitted with a scale of 104 μm/division, and the other 36 μm/division. The apparatus and the cell are schematically shown in Figure 2.4.

The pH determinations were made using a digital pH-meter having a single combined electrode (Orion Research Co.).

2.3.2.2. Procedure

About ten grams of each sample were manually selected from pure fragments of freshly crushed mineral. The sample was ground under distilled water in an agate mortar and the fine fraction was obtained by sedimentation.

The electrokinetic mobility determinations were carried out by observing the movement of particles 2-3 μm in size at the locations of zero fluid velocity in the cell. This location was determined optically by means of the binocular and the micrometer (Lozyk, 1978).

For each pH value, about twenty different particles were observed to calculate an average mobility value. Depending upon the pH value and the electrokinetic mobility,

the voltage applied to the electrodes varied from 20 to 80 volts. Lower voltages were used for strongly acidic or alkaline suspensions when the electrolysis of the water was experienced at the higher voltates.

The sign of the apparent charge on the particles was determined by observing the direction of the motion of the particles under the influence of the applied field and taking into consideration the reversal of the image by the lens. All the measurements were carried out at a constant temperature of 25±0.5°C which was controlled by the water bath of the apparatus.

2.3.2.3. Calculation of Zeta Potential

Smoluchowski (1914) showed that the electrokinetic mobility per unit field strength of a particle u, moving through a liquid of viscosity μ, and dielectric constant ε, is related to the zeta potential ζ by the following equation:-

$$u = \frac{\zeta \varepsilon}{4 \Pi u} \qquad 2.30$$

An average u value was obtained using the relation given below:-

$$u = \frac{\text{Particle Velocity}}{\text{Potential Gradient}} \qquad 2.31$$

The particle velocity was determined as the distance travelled by the particles (cm) per unit time (sec.), and the

A - electrophoretic cell
B - microscope
C - transparent chamber filled with water
D - heater
E - micrometer
F - glass cell filled with water
G - lamp

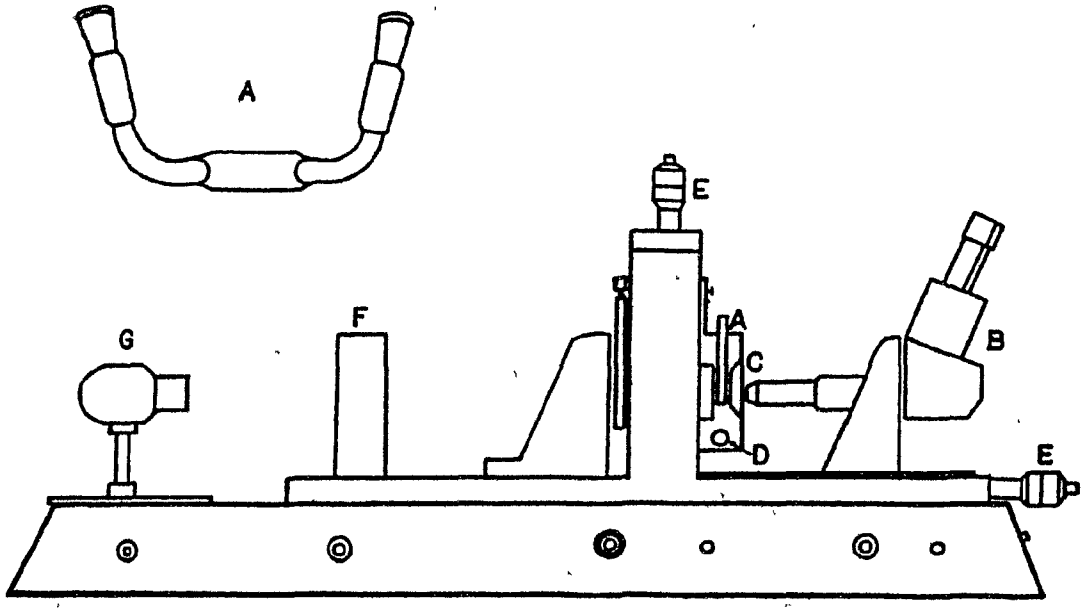


Figure 2.4 A Schematic Representation of Rank Brothers' Electrophoresis Apparatus.

potential gradient as the voltage applied through the electrodes (volts) per unit length of the inter-electrode distance (cm). Substituting the values of the dielectric constant and viscosity of water ta 25°C in Equation 2.29, the zeta potential may be obtained from the following relation:-

$$\zeta = 1.285 \times 10^5 \, u \qquad (2.32$$

where u is in (cm/sec)/(volt/cm) and ζ is in mV.

The ζ value calculated from Equation 2.32 might not necessarily represent the absolute zeta potential of the system studied. This is due to certain assumptions involved in the derivations of the equations pertaining to the electrical double layer theory (Leja, 1982). Nevertheless, the electrokinetic measurements continue to retain their importance as research tool in many applications of surface chemistry, including the mineral flotation.

In general, the reproducibility of the electrokinetic data were found to depend upon the sample used and the pH value. For minerals such as talc and molybdenite, which are regarded as relatively unreactive towards the environment, the reproducibility was good. For example, the average of four measurements carried out using molybdenite resulted in a zeta potential value of -32±2 mV at pH = 6.0±0.2. However, for freshly ground galena four measurements at pH = 6.2±0.3

gave the following zeta potentials; +28.7, -11.2, +14.7, -13.4 mV. This large spread in the zeta potentials are related possibly to well known surface reactivity of galena and of all common sulphides in general.

2.3.3. Contact Angle Measurements

2.3.3.1. Sample Preparation

Four surface preparation techniques were employed. These were (1) cleaving the layer type minerals, (2) crystallization, (3) compacting the powdered sample into a disc, and (4) grinding and polishing.

The first method was suitable for molybdenite, talc and graphite which have layer-type crystal structures (section 1.4). Cleavage was most easily accomplished for the molybdenite sample. The talc sample from Quebec did not yield smooth cleavage planes. The other talc sample (Holly Springs, Oregon) was cleavable with relatively smooth planes, but with some difficulty. The graphite sample was the most difficult to cleave. After many trials, only one cleavage sample could be obtained from this particular graphite, which was not as perfect as that of molybdenite. The cleavage was done using a razor-sharp thin metal or wooden plate, and forceps which had been thoroughly cleaned before use.

The use of the second method was limited to sulphur. In orthorhombic form, sulphur consists of molecular rings

(S_8) in which the intermolecular distance is about 1.5 times the interatomic distance in the rings (Donohue, 1974). However, it does not have a layer structure as easily cleavable as that of molybdenite. Therefore, the sample was prepared by recrystallization from the saturated sulphur solution of carbon disulphide. A number of tiny crystals obtained in the preliminary trials were used as the seeds to grow larger crystals. General methods of crystal growing suggested by Holden and Singer (1960) were followed. After many attempts, two crystals possessing smooth surfaces were obtained. They were kept in a desiccator under oxygen-free nitrogen gas at low pressure for 24 hours during which the gas was changed periodically to remove any possible solvent residue that might have evaporated from the crystals. Then, the crystals were washed repeatedly with freshly distilled water. The surface tension of water before and after washing showed no variation. The samples were stored in the desiccator under oxygen-free nitrogen gas until required.

In contrast with the previous two methods which produced samples representing the least wettable surfaces, the third method was used to obtain samples with more wettable surfaces. This method involved pressing 0.8-1.0 gram of deslimed, dry sample into a circular flat plate (disc) employing a hydraulic press. Unless mentioned otherwise, the samples were prepared from the flotation feed itself. A load of 20 tons was applied on a 1.3 cm diameter disc.

Before and during pressing, the sample compartment in the mould was kept connected to a mechanical pump. The disc sample obtained this way was immediately placed into an all-glass cell containing distilled water or aqueous solution for contact angle measurements.

The last method was used for minerals which produce either non-smooth cleavage planes or do not have cleavage planes at all. These included all the mineral samples listed in Table 2.1 with the exception of molybdenite and sulphur. The samples, with sides ranging from 0.3 to 1.5 cm in length, were prepared on graded emery paper with a variable speed polishing wheel. The final preparation was by polishing on cloth laps with aqueous slurries of alumina of successively decreasing particle size, the smallest size being 0.1 micrometer, and finally with distilled water. The polished specimens were rinsed under a strong current of distilled water to remove traces of alumina and stored temporarily under distilled water. Specimens were handled with cleaned surgical latex rubber gloves or clean crucible tongs at all times. Alumina powder (Micro Metallurgical Ltd.) used had been heated in a porcelain crucible to a red heat (~ 700°C) for an hour to remove any possible organic contaminant (e.g. grease). Then, it was mixed in distilled water to form a slurry of 5-15% solids by volume.

2.3.3.2. Apparatus

The construction of the contact angle apparatus was based upon the original design due to Taggart et al. (1930). Since the present study involved the use of highly concentrated methanol solutions up to 80% (by vol.) commonly used contact angle cells which are usually made of lucite would not be suitable against the solvent power of these solutions. Therefore, the construction and use of a glass cell was essential. The ease of cleaning glass made this choice even more attractive. The bubble holder consisted of a 1.0 mm diameter glass capillary tube mounted on an independent mechanical stage positioned on top of the microscope stage. Behind the cell containing the specimen in solution, a light source was placed in the horizontal plane passing through the face of the specimen in order to illuminate the point of contact between the bubble and the specimen. The bubble was observed through the microscope and the angle of contact was directly read by means of a built-in protractor. The apparatus is shown diagramatically in Figure 2.5.

2.3.3.3. Procedure

The measurements of contact angle may be considered in three groups. The first group involved the determination of the influence of pH on the contact angle of air bubbles on the cleavage planes and disc samples obtained from the layer-type minerals as well as on sulphides such as stibnite

A - goniometer eyepiece
B - microscope
C - sample
D - bubble holder
E - vertical and horizontal adjustment screws
F - main support
G - lamp
H - light filter

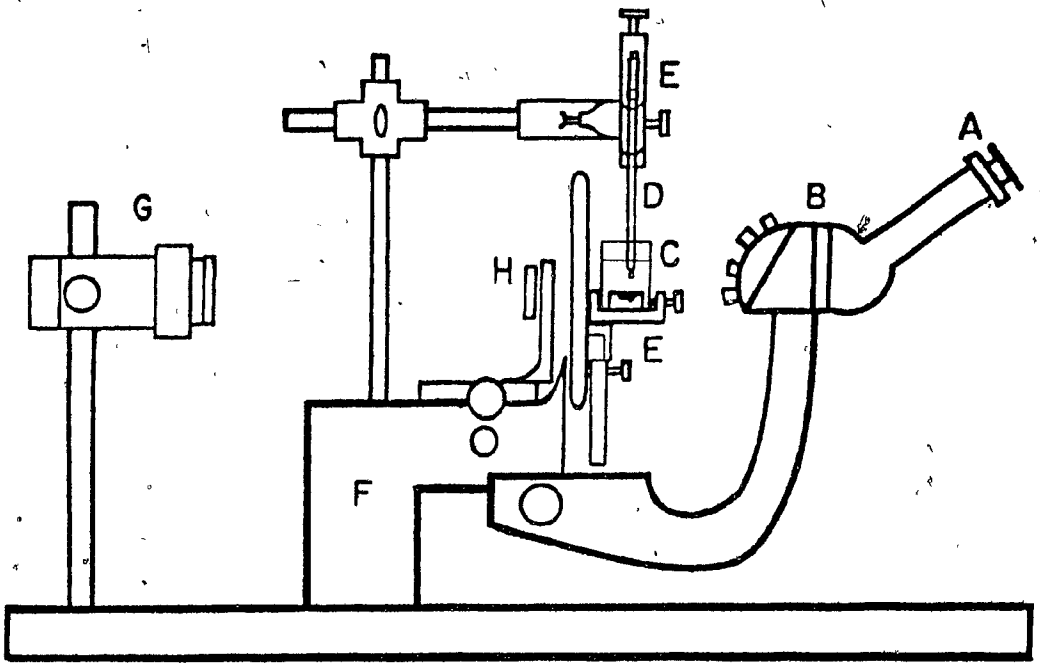


Figure 2.5 A Schematic Representation of the Contact Angle Apparatus

and chalcocite. The second group consisted of the determination of the Zisman parameters using the contact angles measured with pure reference liquids. Finally, the last group was concerned with the determination of the polar character of various samples by estimating the polar component of their solid-vapor interfacial free energy from the octane contact angles.

The influence of pH on contact angle was determined using the captive bubble technique (Taggart et al., 1930). Each sample was allowed to equilibrate for about 15 minutes in each solution of different pH value. Then, successively, air columns of measured length in the capillary tube of 1.0 mm diameter were introduced into the cell to make contact with different regions of the sample surface. The bubbles produced this way were calculated to be 1.5±0.2 mm in diameter. The stage upon which the cell rests was tapped lightly to obtain an equilibrium value of contact angle (Sutherland and Wark, 1955) and to be comparable, all bubbles were kept in contact with the surfaces for about twenty minutes, prior to the angles being read to the nearest degree. Five to eight pairs of readings for each surface were averaged and plotted against pH. The adjustment of pH was not done by direct addition of hydrochloric acid and/or potassium hydroxide solutions into the cell containing the sample. Instead, beakers filled with distilled water were

brought to predetermined pH values from about 2 to 12 with alkali and/or acid addition. After the first measurement of contact angle, which was carried out always at the natural pH of distilled water (5.7-6.2), the solution was transferred by a suction system to its original beaker. Then the next solution of either higher or lower pH value was added to the cell without exposing the sample to air and the contact angle values were measured in the same way. Subsequently, the solution was returned to its original beaker. The pH value was changed gradually in the same direction as the preceding one. Finally, when the measurements were completed for the most alkaline (or acidic) pH value, the direction of the pH change was reversed to re-examine the pH dependence of contact from the highest to the lowest pH value (or vice versa).

The reference liquids used in the contact angle measurements for the determination of the critical surface tension of wetting were water ($\gamma_{\ell v}$ = 72.6 mN/m), (glycerol ($\gamma_{\ell v}$= 63.4 mN/m), formamide ($\gamma_{\ell v}$ = 58.2 mN/m), methylene iodide ($\gamma_{\ell v}$ = 50.8 mN/m), and 1-Bromonaphthalene ($\gamma_{\ell v}$ = 44.6 mN/m). The samples which had been stored after preparation for 24 hours under oxygen-free nitrogen gas in desiccators, were studied two at a time. The contact angles were measured using the sessile drop method of Fox and Zisman (1950). The procedure was similar to that followed by Parekh and Aplan (1978) for various coals. Drops of reference liquids were placed on different regions of the specimens in

air by means of a syringe and the slowly advancing angles were measured. These angles were found to be reproducible within ±3° for different specimens of the same mineral. A test was made to check for any organic contamination by comparing the contact angles of water on galena, cinnabar, pyrite and chalcopyrite before and after ether washing. In all cases, the contact angles before and after washing were similar (i.e. ±2°). For each sample, four to six pairs of contact angles were measured and the cosine of the average contact angle was plotted in the Zisman graph. The average deviation from the mean was ±2°.

The procedure followed for octane contact angle measurements was the same as that described for the air bubbles. The octane and water phases had been presaturated with each other (section 6.25). Each data point was the average of between four and nine pairs of readings. The average deviation from the mean was in general, ±2°.

All the measurements were carried out at room temperature of 23±2°C.

2.3.4. Flotation Tests

2.3.4.1. Apparatus

Flotation tests were performed in an all glass microflotation cell. Main features of the cell are shown in Figure 2.6. It was similar in form to that reported by

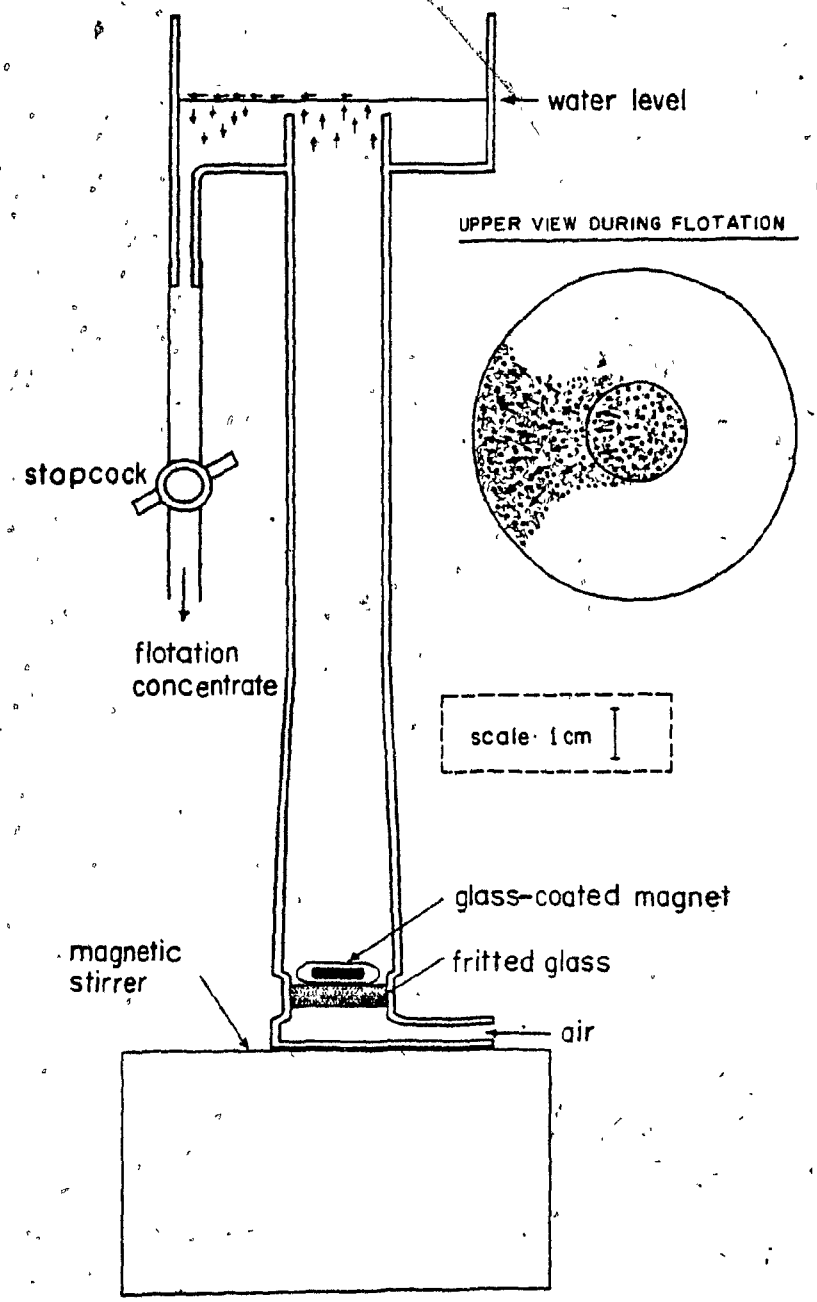


Figure 2.6 Main Features of the Micro-Flotation Cell.

Partridge and Smith (1972). The cell had an 18 cm long cylindrical body (1.8 cm in diameter). The volume of the central flotation column was about 50 cm^3. The collection chamber had a capacity of about 60 cm^3. The fritted glass disc at the bottom of the cell to disperse the flotation gas in the cell was originally of fine porosity (~ 1-5 μm). The pores were enlarged later by circulating a hydrofluoric acid solution (15% by volume) using a suction system. In general, the flotation gas was air. However, for the galena sample, nitrogen, oxygen and hydrogen were also used as the flotation gas. The gas passed through two gas washing bottles. The gas flow rate was regulated by a plastic Gilmont flow control valve and measured by a glass Gilmont flow meter. The cell contents were agitated with a glass coated magnetic bar (1.6 cm) using a magnetic stirrer (Fisher Sci.).

2.3.4.2. Procedure

Hand-picked specimens were ground dry (unless mentioned otherwise) in batches of 1 to 1.5 grams in a small size agate mortar and sized to 100x200 mesh (75-150 μm) immediately before desliming and floating. For convenience, micro-sieves (Allen-Bradley) were used for screening such small samples. In the case of talc, sulphur, and molybdenite, the feed size was 80x150 mesh (105-177 μm).

The following procedure was followed for each flotation test: ~ 0.65 gram of freshly prepared sample was

transferred to a small beaker and mixed in water with a magnet intermittently for a period of 2 minutes. At each interval suspension was deslimed till free of visible fines. At the end it was mixed with a small quantity of flotation solution of predetermined pH value and the suspension was then transferred to the flotation cell by means of a specially made funnel. The cell was filled with the remaining solution to such a level that once the particles floated up to the surface, they could not recirculate back to the central flotation column. (In the preliminary tests with light particles such as coal, recirculation was experienced when the water level in the collection chamber was too high.) The feed was conditioned for 5 minutes and the pH value of the suspension was remeasured and recorded. The flotation time was one minute at a gas flow rate of 50 ml/min, standardized for all tests. This gas flow rate did not generate excessive turbulence so as to cause the collection of non-floatable particles by any hydrodynamic carry-over mechanism. After the test was completed, the concentrate and tailing products were filtered, dried, and weighed to determine the percent recovery by weight.

2.4. RESULTS

2.4.1. pH-Dependent Surface Properties

Specifically, these properties include the zeta potential, contact angle, and the natural flotation response as a

function of the pH of the aqueous phase. Since one of the objectives of this work was to re-examine the nature of the relationship among these distinct surface properties, the results obtained from different types of experiments were plotted in common graphs to facilitate the comparison. However, in order to avoid crowding, they were usually plotted in pairs.

Figures 2.7 and 2.8 illustrate the results obtained with the talc sample from Quebec. The former is a plot of the contact angle variation on a disc sample prepared from the 100 x 150 mesh size fraction along with the flotation results of Woodfill (1966). As seen, with pH increasing, both the recovery and contact angle decrease. The latter figure is a plot of the contact angles obtained using another disc sample prepared from a finer size (-200 mesh) and the zeta potential. As pH increases, contact angle decreases continuously, and, as opposed to the previous case, it vanishes at pH $\geq$ 10.5. However, upon decreasing the pH, the hydrophobicity reappears (θ~15°) at about pH = 10.5 and continues to increase as the pH decreases. A decrease in pH causes the zeta potential to become less negative as indicated by all the zeta potential curves shown in Figure 2.8. The results obtained in the present work indicate that the PZC value for talc is located at about pH=3. At lower pH values the surface acquires a positive charge. The zeta potential variation of the other talc sample from

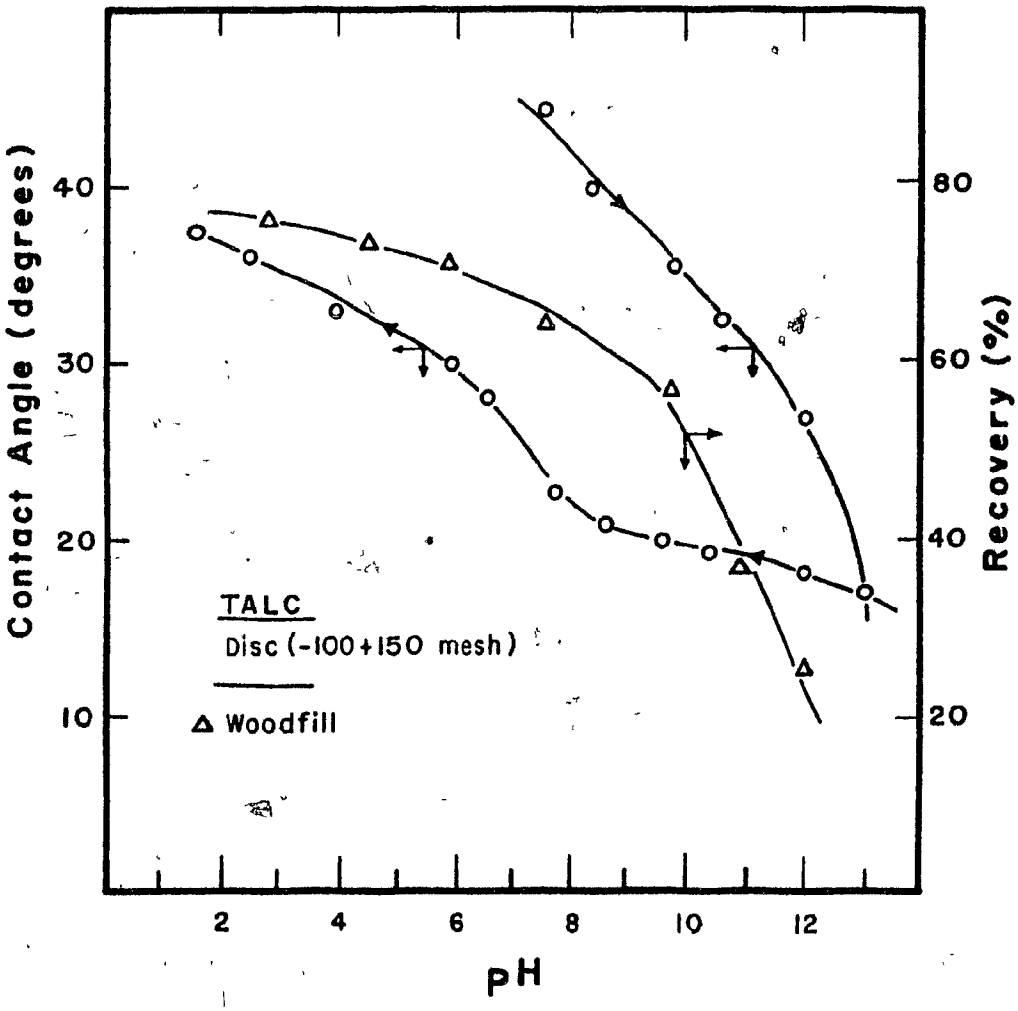


Figure 2.7 Contact Angle and Flotation Recovery (Woodfill, 1966) of Talc as a Function of pH

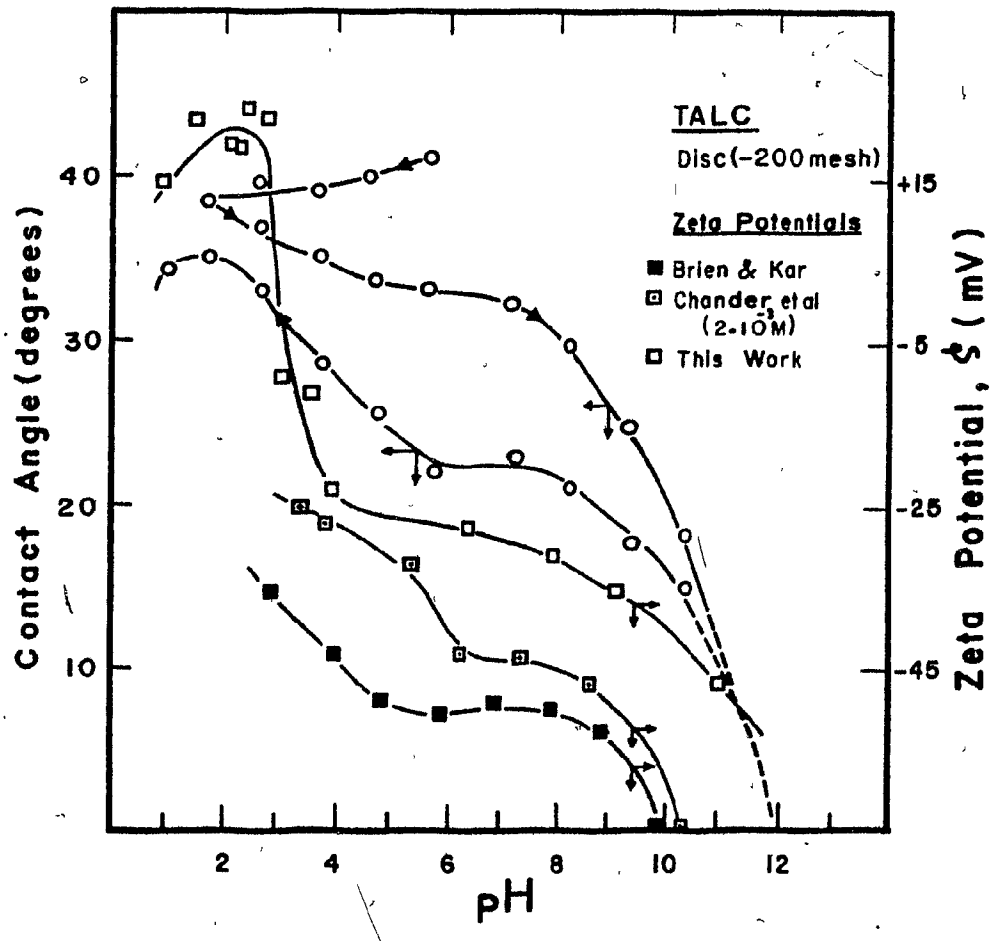


Figure 2.8 Contact Angle and Zeta Potential of Talc as a Function of pH

Holly Springs, Oregon (not shown in the figure) was essentially similar.

Figure 2.9 shows the zeta potential, recovery, and contact angle variation of various stibnite samples as a function of pH. The contact angles of the samples (Sarawak, Bornea) reported in the present work were measured on a disc specimen and on a relatively smooth cleavage surface obtained accidentally during crushing. The zeta potentials were taken from the data by Derjaguin and Shukakidse (1961) who used an electroosmosis technique on a sample from Georgia, U.S.S.R. The flotation and contact angle data by Arbiter et al. (1975) were obtained with samples from Japan and Portugal. Depending upon the experimental conditions employed, the magnitude of the contact angles and flotation recoveries is seen to be significantly different from each other (e.g. the flotation recoveries reported by Derjaguin and Shukakidse and Arbiter et al.). However, relative pH dependence of these surface properties remain generally the same as observed for talc. That is, both the contact angles and flotation recoveries increase and the zeta potentials become less negative as the pH values decrease.

The results of the zeta potentials (Chander et al., (1975) and contact angles obtained with a disc sample (prepared from the -200 mesh fraction) of graphite show a similar pH dependence (Figure 2.10). The zeta potentials (determined with -270 mesh sample by electrophoresis) change

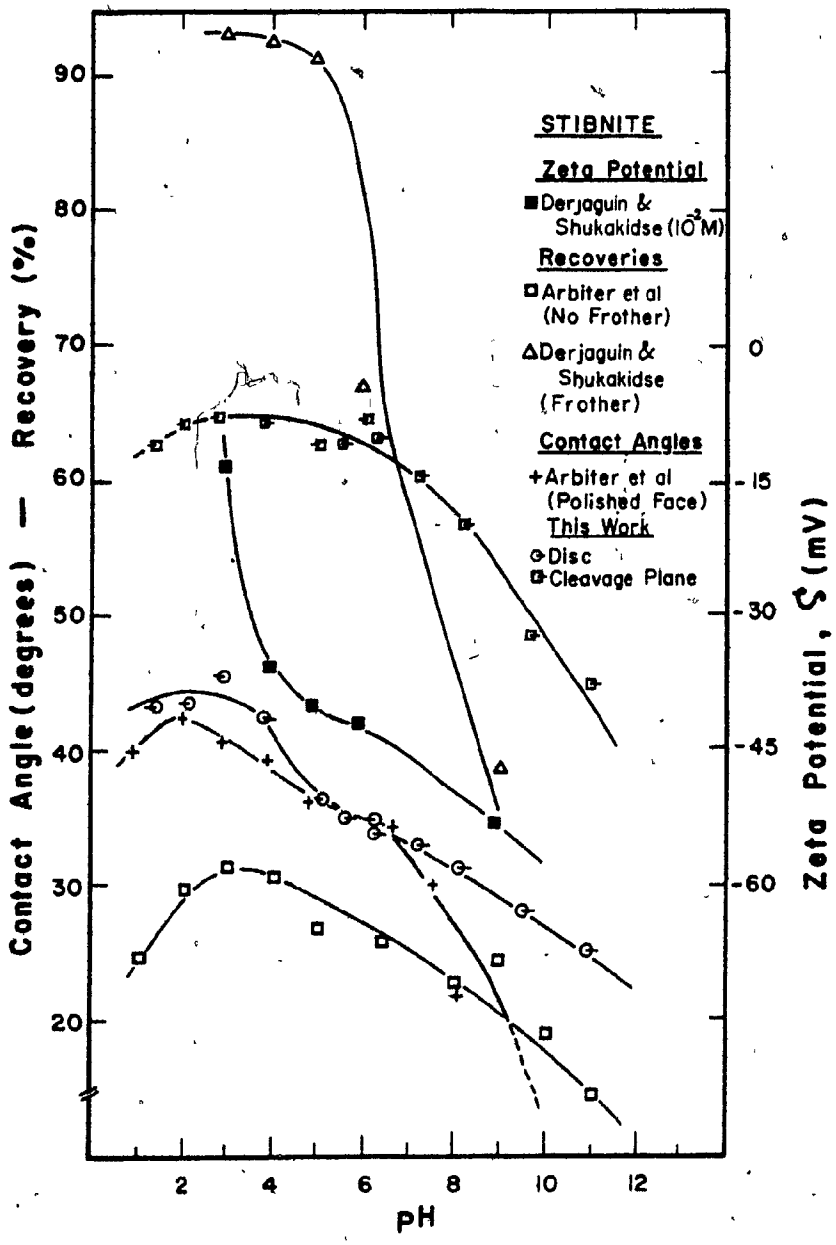


Figure 2.9 Contact Angle, Flotation Recovery and Zeta Potential of Stibnite as a Function of pH.

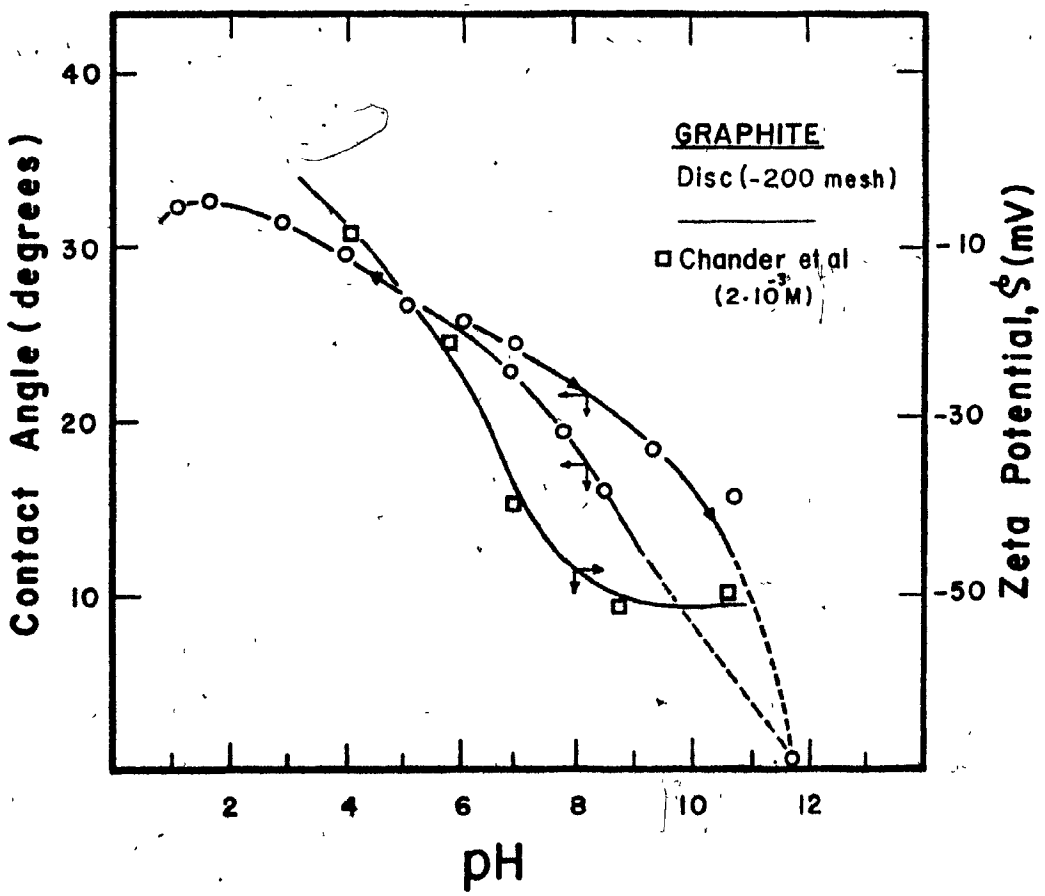


Figure 2.10 Contact Angle and Zeta Potential (Chander et al., 1975) of Graphite as a Function of pH

from -50 to ~ -10 mv as the pH decreases from ~ 11 to 4. This change in the zeta potential is accompanied by a gradual increase in contact angle from nearly 0 to 30°.

The behaviour of the molybdenite is shown in Figures2.11 and 2.12. Figure 2.11 compares contact angle and flotation test results. The contact angles decrease from 50° to 20° as the pH increases from 5.5 to ~ 11. The most dramatic decrease in hydrophobicity occurs above pH=8. Below this value down to a pH of 2, the change in contact angle is relatively small. The recoveries of molybdenite also show a decrease with increasing pH value. The percentage of the recovery depends on whether or not a frother is used. In the absence of methyl isobutyl carbinol (MIBC), it decreases gradually from 40% to less than 10% as the pH value increases from 2 to 11. In the presence of MIBC (~ 1 mg/100 ml), the recoveries are remarkably large at all pH values (e.g., ~ 100% at a pH of 3). However, the recovery still decreases with increasing pH.

The contact angles obtained using a disc specimen prepared from the -200 mesh sample show (Figure 2.12) that upon decreasing the pH value from ~ 5.5 to 1.5 and increasing it from 1.5 to ~ 8, the hydrophobicity continuously decreases and finally vanishes at pH $\geq$ 8.5. Subsequent decreases in pH indicate that a reverse transition back to hydrophobicity occurs only at a pH value of ~ 1.3. Figure

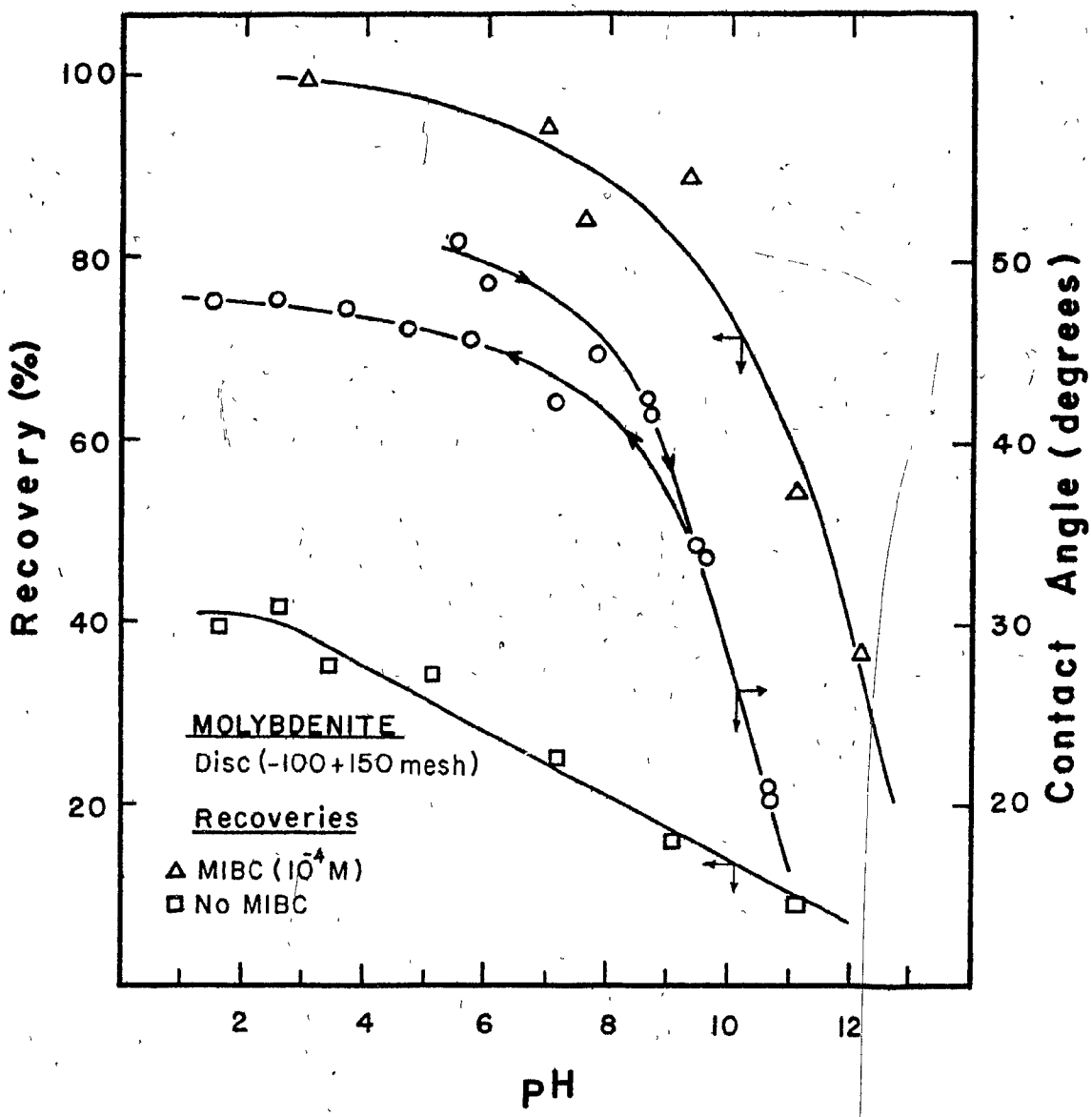


Figure 2.11 Contact Angle and Flotation Recovery of Molybdenite as a Function of pH

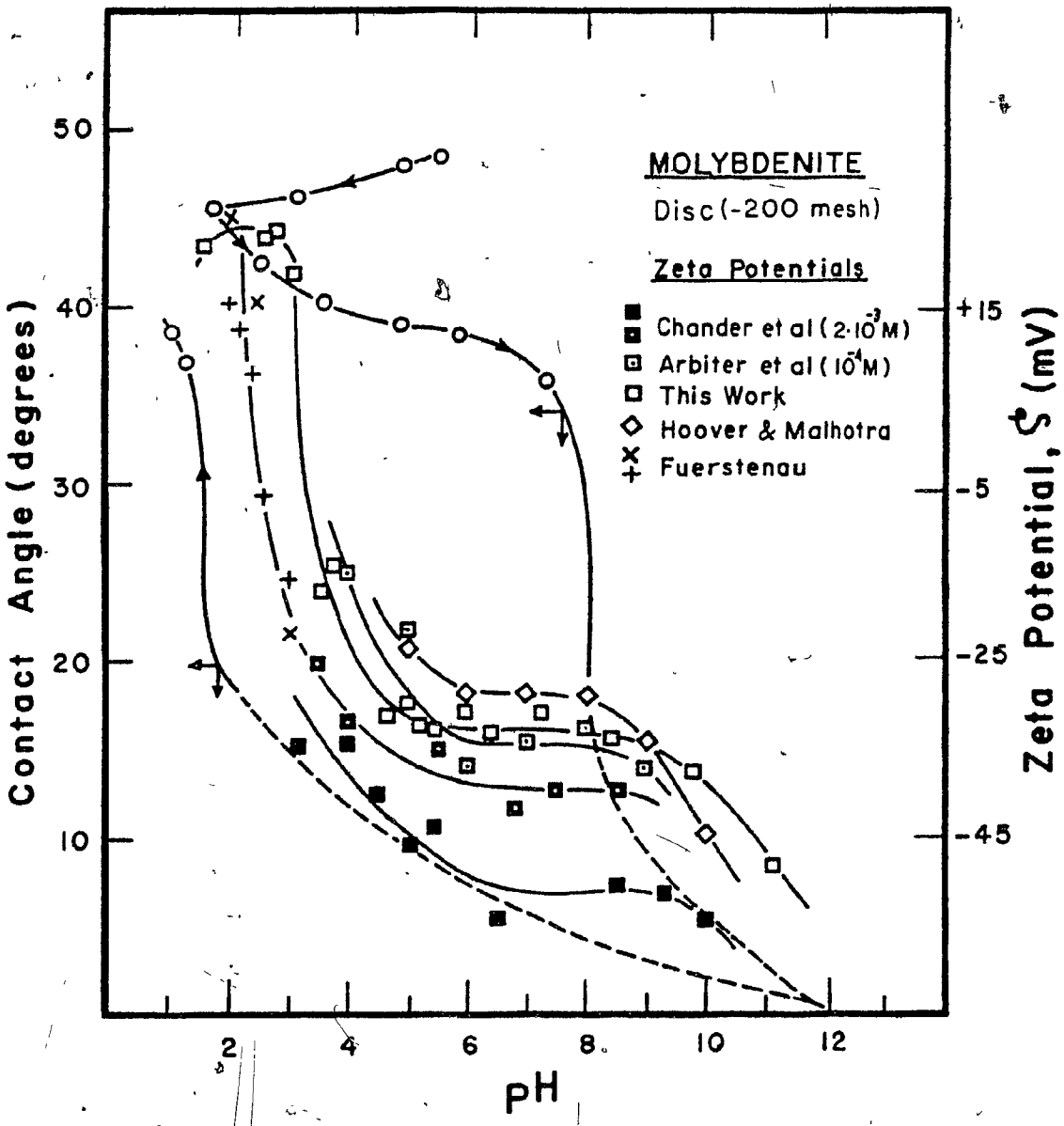


Figure 2.12 Contact Angle and Zeta Potential of Molybdenite as a Function of pH

2.12 illustrates also the zeta potential values determined in the present work and also those reported previously by various investigators. In the pH range ~ 5 - 9, generally, there is relatively small change in the zeta potentials. In the more alkaline and more acidic pH range the zeta potentials become less negative with decreasing pH. The sample employed in the present work has a PZC value of about pH=3.3 as compared with 2.5 (the PZC value by Fuerstenau, (1980)). Reducing the pH below these values causes the surfaces to acquire positive zeta potentials up to +20 mV.

The zeta potential and flotation recovery of chalcopyrite is shown as a function of pH in Figure 2.13. The recoveries were obtained in oxygen-saturated solutions using freshly-ground (dry) samples and deslimed feed. The zeta potential of elemental sulphur (dashed line) is included for comparison. As in the case of the previous results, the recoveries are seen to be inversely related to the zeta potential. Increases in pH are accompanied by increases in the zeta potentials and decreases in the flotation recoveries (especially within the pH range 2 to 5). The recoveries seem to be unaffected in the pH range 5 to 9. The PZC value for both chalcopyrite and sulphur occurs at about pH=2.1 which corresponds to the maximum chalcopyrite recovery of 91%. It was found that pre-washing the deslimed

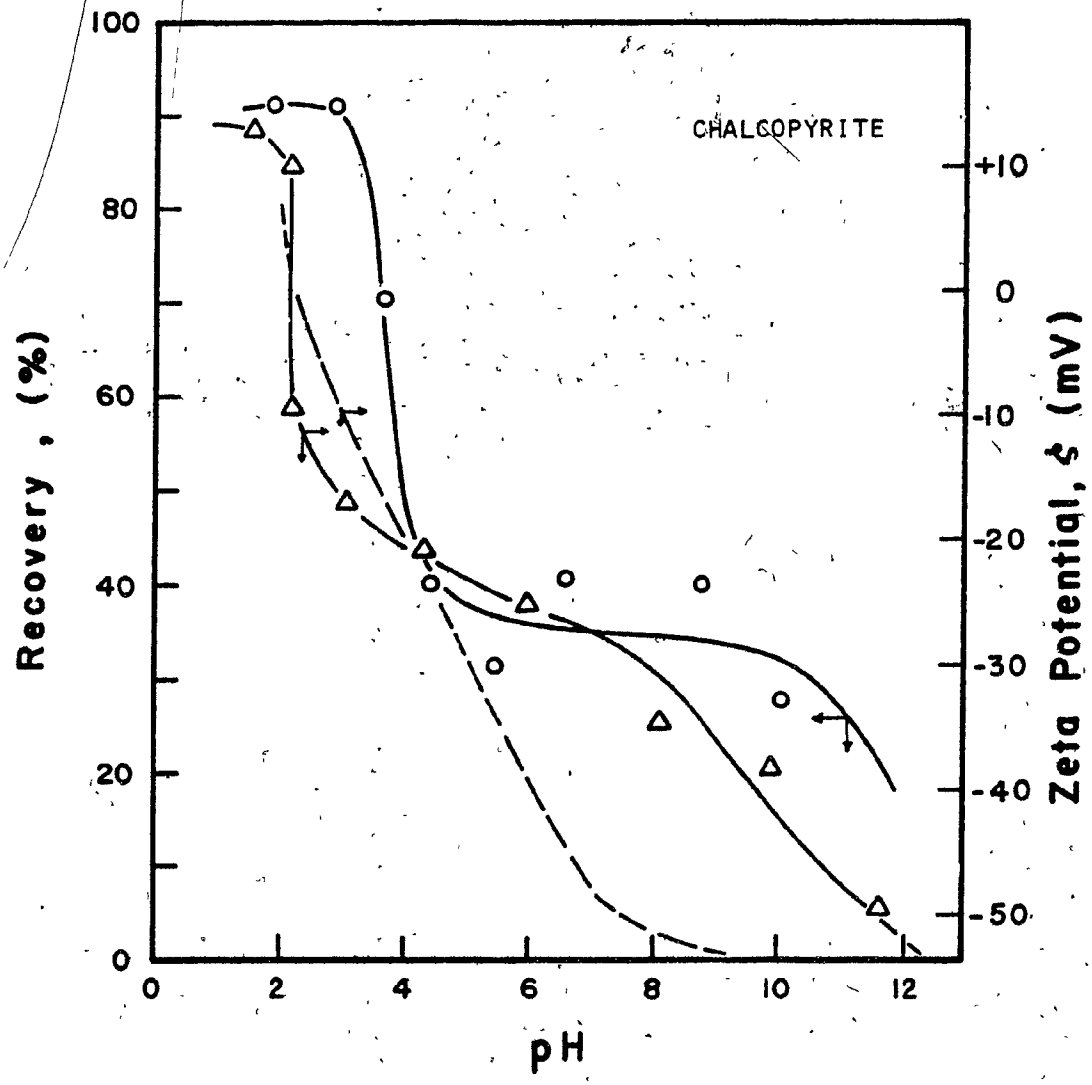


Figure 2.13 Zeta Potential and Flotation Recovery of Chalcopyrite as a Function of pH (dashed line is for elemental sulphur)

flotation feed rigorously with distilled water (arbitrarily referred to as aerative washing) had a significant effect in increasing the flotation recovery. This effect was observed in both acidic and alkaline solutions. For example, at pH = 5.5, the recovery without aerative washing was about 30%, but, with the aerative washing it was 96% at the same pH. The recovery at pH=10.1 was ~ 28% without aerative washing. The tailing material was filtered and refloated at the same pH value, after an aerative washing. The recovery was ~ 90%.

Figure 2.14 shows the zeta potentials of the galena and sulphur samples prepared under various conditions. The PZC of the first sample (o) occurs in a neutral pH range (i.e. pH=6 - 8). The precise location of this point, however, is not well defined. Each data point was obtained using a fresh sample prepared by grinding pure crystals of galena under distilled water. The sample used immediately after dry grinding was found to have smaller positive zeta potentials and a lower PZC value (i.e. pH = 5.2) than the sample ground under distilled water. Pre-treatment of the dry ground sample with an ammonium chloride solution described by Gaudin and Wilkinson (1933) decreased the positive zeta potentials further and the PZC value to about pH=4.2 (□). The zeta potentials of the sample which had been dry ground and stored in a closed container for about five months (Δ) are shown to be negatively charged at most

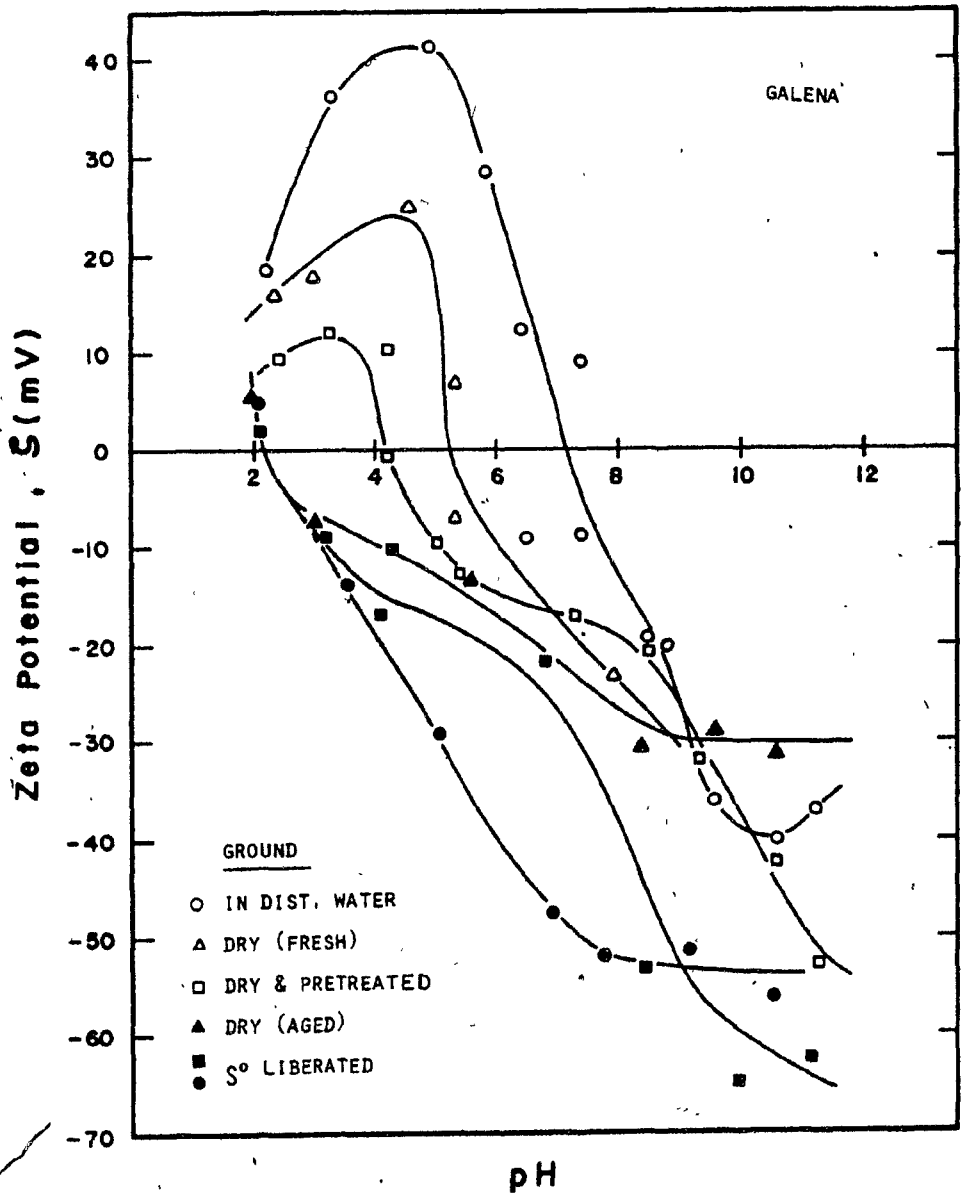


Figure 2.14 Zeta Potential vs. pH Relationship for Galena and Elemental Sulphur Prepared Under Various Conditions

pH values. The sample acquired a very small positive charge at pH=2.1. An apparent PZC value occurs around pH 2.2. Figure 2.14 also includes the zeta potential change of two sulphur samples both produced by oxidation of sulphide samples in concentrated acid solutions. One sample was the sulphur liberated from galena when it was boiled in sulphuric acid. The zeta potential data obtained from this sulphur sample are indicated by filled squares. The other sample was the sulphur liberated from a lead/zinc concentrate during its dissolution in boiling nitric acid. The zeta potentials determined using this sulphur sample* are shown by filled circles in the figure. Both samples have a common PZC value at pH 2.2 although the dependence of zeta potential on pH is different.

Figure 2.15 illustrates the natural flotation response of galena sample as a function of pH. The flotation feed was prepared by wet grinding and screening using distilled water which was previously saturated with air, nitrogen, or oxygen. In addition, one experiment was conducted using a sample prepared in a hydrogen atmosphere using distilled water pre-saturated with hydrogen. The feed thus prepared was never allowed to contact air. The flotation tests were carried out in solutions pre-saturated with the same gas as that used in the sample preparation. The

---

*The sample was furnished by Gregg Hill, a fellow graduate student in the department.

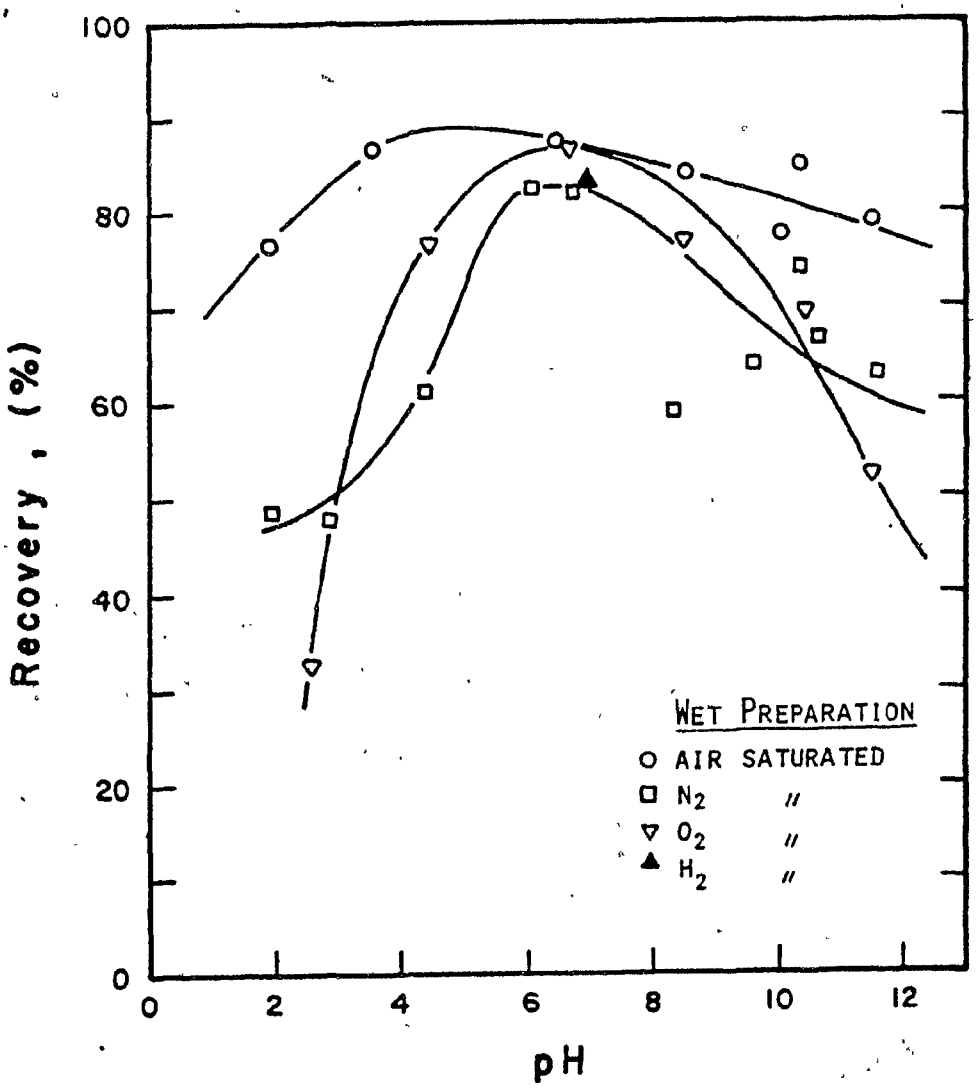


Figure 2.15 Flotation Recovery vs. pH Relationship for Galena Prepared and Floated Under Various Conditions

recovery obtained at natural pH (~ 7.0) using hydrogen gas is comparable to that obtained with the other gases. The recovery vs. pH curves of the samples floated with nitrogen and oxygen show maximum recoveries of 83 to 86% in the pH range of 6 to 7. Outside this pH range, the recoveries decrease as the solutions become more acidic or alkaline. The recoveries appear to be less pH dependent in the flotation tests conducted in air-saturated solutions. The difference between the highest and the lowest recovery observed with respect to pH is about 10% (as compared to the recovery differences of 35 ~ 50% observed using other gases).

As in the case of chalcopyrite, the aerative washing was found to significantly increase the recovery of the galena prepared by dry grinding and screening. To illustrate this, two observations are noted. (a) When the sample, which had been exposed to air for about 30 minutes during dry grinding and sizing, was transferred directly into the flotation cell containing distilled water (pH = 6.3), conditioned for 5 minutes and floated for 1 minute, the recovery was less than 10%. (b) When the sample, prepared in the same way as in (a), was subjected to an aerative washing prior to flotation in distilled water (pre-saturated with air), the recovery was greater than 95%. To find out more about the effect of this aerative washing, additional

flotation tests were conducted using samples prepared under various conditions and floated at various pH values. The results and experimental conditions are summarized in Table 2.2. The description consists of three lines. The first line indicates the grinding conditions. For example, "dry, in s. steel crucible" means that the sample was ground dry in a stainless steel crucible. The second line indicates the type of screen used in sizing the ground sample. The third line indicates the type of air-saturated solution. The feed weight for these tests was 1.0 _ 0.2 gram. The tap water used was found to have a conductivity of 370 micromhos at 21°C, as measured by a conductivity bridge and a cell with a cell constant of 0.1.

2.4.2. Octane Contact Angles

Contact angles of octane droplets measured through the solid/water/octane is given in Table 2.3. The sulphur crystal face formed an average contact angle of 135° with octane droplets, which is the highest angle measured. The octane contact angle for molybdenite cleavage plane was determined to be 120°C. This value was found fo be characteristic of various cleavage specimens prepared from the same sample. On the other hand, two cleavage specimens of talc, obtained with varying degrees of success, produced different contact angles with notable hysteresis. It was speculated that if the sample were perfectly cleaved, the resulting contact angles would be higher than the present highest

Table 2.2

Natural Flotation Response of Galena (After Aerative Washing) in Air-saturated Solutions

pH	Description	R (%)
2.1 ± 0.1	Dry, in Agate Mortar Allen Bradley Sieve Distilled Water	92.1
3.2 ± 0.2	Wet, in S. Steel Crucible, Tyler Sieve Tap Water	91.9
5.0 ± 0.1	Dry, in S. Steel Crucible, Tyler Sieve Distilled Water	98.4
5.9 ± 0.2	Dry, in Agate Mortar Allen Bradley Sieve Distilled Water	97.7
6.7 ± 0.1	Wet, in S. Steel Crucible, Tyler Sieve Distilled Water	98.6
8.1 ± 0.1	Wet, in S. Steel Crucible, Tyler Sieve Tap Water	97.2
10.2 ± 0.2	Dry, in S. Steel Crucible, Tyler Sieve Tap Water	72.7
11.8 ± 0.1	Wet, in Agate Mortar Allen Bradley Sieve Distilled Water	85.9

Notes

1. All the samples (100x200 mesh) were freshly prepared and deslimed before flotation.
2. Average time elapsed before flotation including grinding, screening, desliming and conditioning is about 30 minues.

Table 2.3

Contact Angles of Octane Droplets on Various Minerals in Distilled Water

Crystal Face or Cleavaged sample	Contact Angles (Degrees)
Sulphur	135
Molybdenite	120
Talc*	108-116
Graphite*	78-90
Polished Samples	
Orpiment	75
Realgar	72
Stibnite	45
Chalcocite	0-37
Chalcopyrite	0-34
Galena	0-32
Coal	78

* Samples obtained by fracture.

value of 116° and the hysteresis eliminated. Similar problems existed in cleaving the graphite sample. The angles reported are those measured on relatively smooth fracture faces. Again, the contact angles representing a perfectly cleaved graphite specimen are presumably much higher than the reported values in Table 2.3.

The polished mineral samples have relatively low octane contact angles. The angles formed on two arsenic sulphide minerals, namely orpiment (As_2S_3) and realgar (AsS) were comparable at values of 75 and 72°, respectively.

Stibnite had an average angle of 45°. The angles formed on such common sulphides as chalcocite, chalcopyrite, and galena were found to be related to the surface age. On freshly prepared samples octane angles ranging from 32° to 37° were observed. These samples were prepared at the expense of obtaining samples with high polish. When the surface was relatively old due to long periods of polishing and storage in distilled water, no finite value of contact angle could be measured. In general, the contact angle behaviour of these sulphide samples was found to be unpredictable, inconsistent, and poorly reproducible (see section 2.5.2.3 for details). The contact angle measured on the coal sample is comparable with that of orpiment.

2.4.3. Critical Surface Tension of Wetting

For clarity, the Zisman plots for the minerals studied are given in two different graphs. Figure 2.16 illustrates the results for talc, (Quebec sample), orpiment, graphite, cinnabar, stibnite, and molybdenite. The Zisman plots for the rest of the minerals including galena, realgar, chalcopyrite, pyrite, and chalcocite are given in Figure 2.17. For some samples (e.g. pyrite) the data points are quite scattered. However, as in the case of the polymeric materials (Zisman, 1964), a linear trend between cosine θ and $\gamma_{\ell v}$ is apparent. The values of the critical surface tension of wetting, γ_c, and of the slopes, b, are collectively given in Table 2.4.

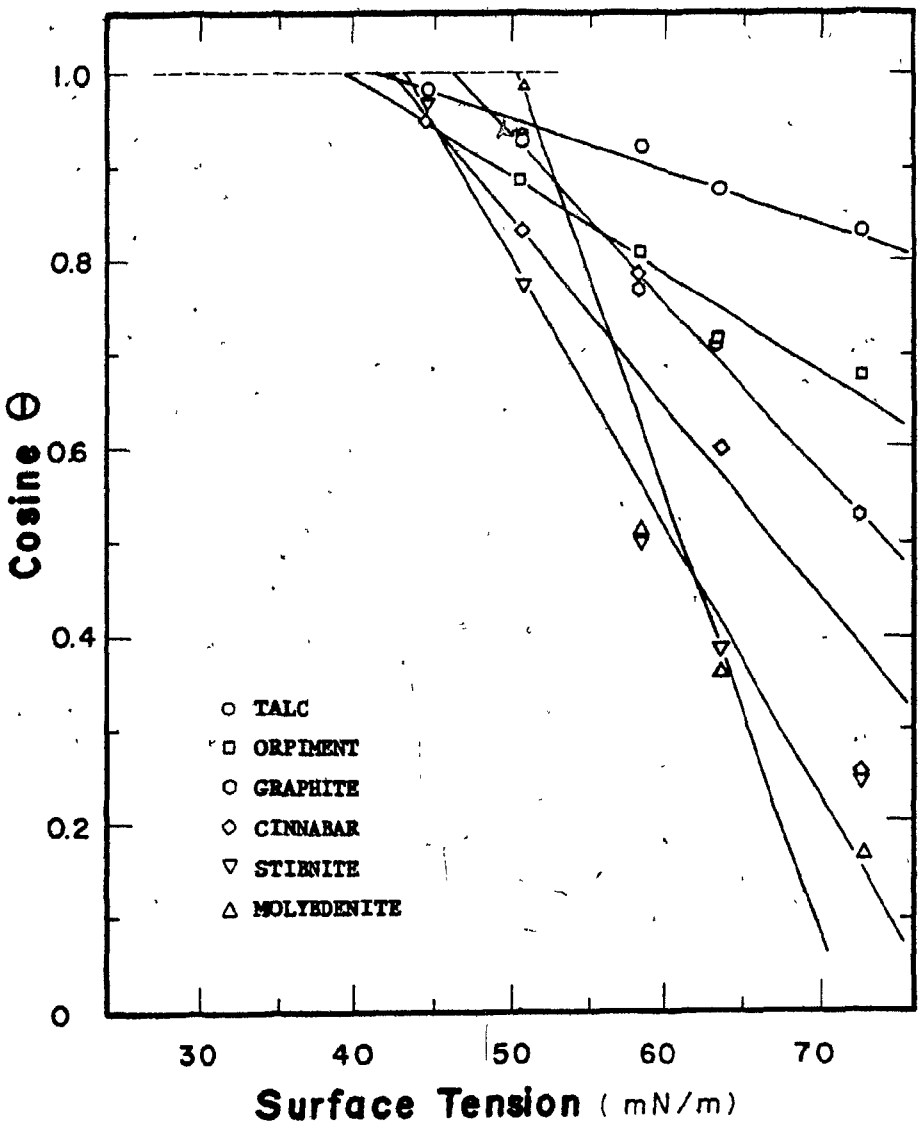


Figure 2.16 Zisman Plots of Minerals Including Non-Sulphides.

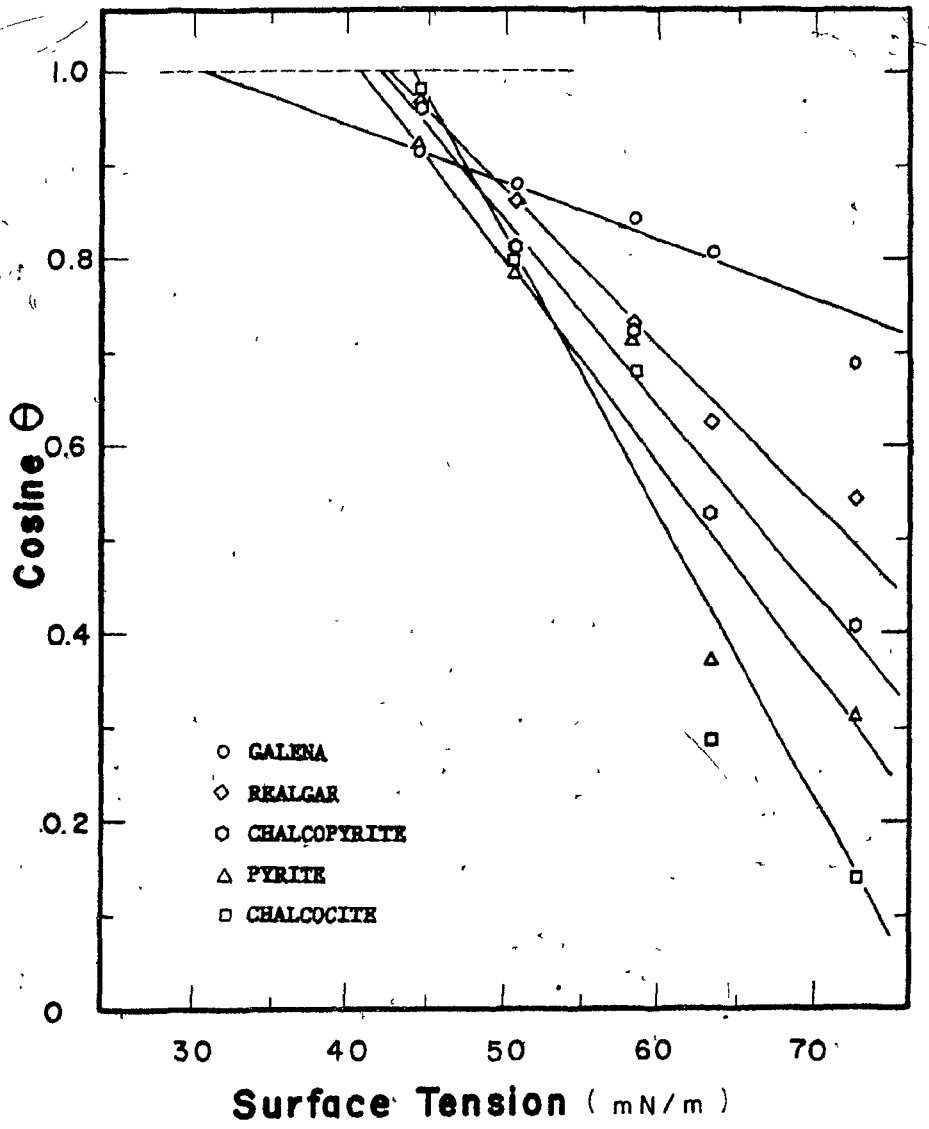


Figure 2.17 Zisman Plots of Various Sulphide Minerals

Table 2.4

Values of the Zisman Parameters of Various Mineral Samples

Mineral	γ_c (mN/m)	bx(10^2)
Talc	41.5	0.57
Galena	31	0.63
Orpiment	39.5	1.12
Realgar	42.5	1.68
Graphite	46.5	1.83
Chalcopyrite	42	2.00
Pyrite	41	2.22
Stibnite	43	2.86
Chalcocite	44	3.00
Molybdenite	50	4.65

Two characteristics may be noted: First, with the exception of two minerals, all the samples studied have γ_c values ranging from ~ 40 to 46 mN/m. One of the exceptions is galena which has the lowest γ_c value of 31 mN/m. The other one is molybdenite with a γ_c value of ~ 50 mN/m which is the highest among others. The second point is that the slope values vary significantly as opposed to relatively constant γ_c values. In the table, the slopes are shown in the order of increasing values from 0.57×10^{-2} for talc to 4.65×10^{-2} for molybdenite.

2.5 DISCUSSION

2.5.1. Layer Type Inherently Hydrophobic Minerals

2.5.1.1. Electrokinetic Behaviour

The surface properties of talc, graphite, and molybdenite are expected to be similar due to their layer type crystal structures. Because these minerals have weak van der Waals' bonds between the layers, size reduction produces characteristically flat particles. The flatness of the particles is evident from the visual observations of coarse particles and from the examination of scanning electron micrographs (Chander and Fuerstenau, 1974; Yokoyama et al., 1983) of fine sizes. The particles of these minerals consist of two distinct portions: faces, created by the rupture of the van der Waals' bonds along the cleavage plane; and edges, created by the rupture of strong interatomic bonds. The edges and faces characterize the surface anisotropy of these particles. The edges, and to some extent, the faces, produce a number of ionic surface species which form the hydrophilic regions of the mineral. The pH dependence of the electrical charge on the particles may be explained by the presence of these ionic surface species.

For talc, the species of SiO^- were suggested at the hydrophilic edges while the hydrophobic faces contained mainly uncharged Si-O-Si units (McHardy and Salman, 1974).

The surface may acquire an electrical charge by a similar mechanism suggested for quartz (Aplan and Fuerstenau, 1962). The broken bonds at the edges react with water molecules to form a surface silicic acid. The ionization of this surface silicic acid gives rise to a negative charge on the surface as follows:-

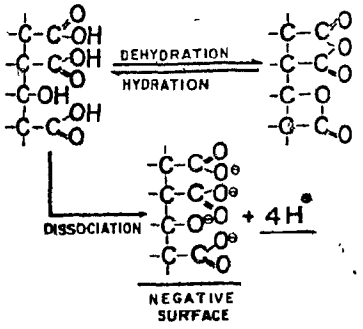
$$-\overset{|}{\underset{|}{Si}}-OH \rightleftharpoons -Si-O^- + H^+ \qquad 2.33$$

In the case of molybdenite, the existence of thiomolybdate ions $[MoS_xSO_y]^{-n}$ was suggested at the edges (Chander and Fuerstenau, 1974). Depending upon the pH of the solution, the charge of surface thiomolybdate species may change according to the following reaction:-

$$[MoS_xO_y]^{-n} + H^+ \rightleftharpoons [MoS_xO_yH]^{-n+1} \qquad 2.34$$

For graphite, the broken interatomic bonds (i.e. C-C) during the creation of the edges and faces react with oxygen to form various carbon-oxygen complexes which may include familiar weakly acidic groups such as phenolic -OH and -COOH. Equation 2.34, which has been suggested as representation of surface charging of coal (Kelebek et al., 1982b), may also explain the change of electrical charge on the graphite particles in aqueous solutions.

The presence of negatively charged ionic surface species explains the negative zeta potentials at the natural pH of the solution. As the pH is lowered, the zeta potentials



2.35

become progressively less negative and finally positive due presumably to the adsorption of hydrogen ions.

Equations 2.33-35 may be said to represent the surface reactions occurring at locations where the strong interatomic bonds within or on the layers are ruptured. These locations constitute the hydrophilic sites on the particle surface. Due to the surface anisotropy, the density of the electrical charge is not expected to be uniformly distributed over the surface. The contribution to the establishment of an overall zeta potential of the particles is presumably much lower from the faces than from the edges.

The zeta potential vs. pH curves for molybdenite samples investigated by various researchers exhibit a qualitative resemblance to each other (Figure 2.12). The results obtained recently by Raghavan and Hsu, (1984) indicate a similar pH dependence of the zeta potentials. In general, in the pH range 5 to 9, the zeta potentials are little

affected by pH variations. This trend is also apparent for talc samples (Figure 2.8). At similar pH values, the magnitude of the negative zeta potentials is different for different samples. A greater negative zeta potential value can be attributed to the samples having a larger edge-to-face ratio. This ratio is influenced by the way the sample is prepared (Chander and Fuerstenau, 1974).

Stibnite differs significantly in structure from the previous three minerals. The structural unit is a chain rather than a sheet. Cleavage of stibnite is formed by the rupture of Sb-S bonds. Although these interatomic bonds are not strong they are not of van der Waals' type (section 1.4). Like molybdenum, antimony is known to form anionic species in aqueous solutions (Bailar et al., 1975). Chander et al. (1975) postulated the presence of ionic groups with the general formula, $[SbSxO_yH_z]^{-n}$. Arbiter et al. (1975) postulated a reversible hydrolytic scission of the Sb-S bonds in alkaline solutions, resulting in formation of SbOH and SH sites in equilibrium with SbO^- and S^- sites as determined by the pH. Because of the more isotropic nature of stibnite as compared to molybdenite, the electrical charge, hence the hydrophilic sites are more uniformly distributed over the stibnite surfaces.

2.5.1.2. Flotation Behaviour

In general, the pH dependence of flotation recoveries

is similar to that of contact angles measured on disc samples (Figures 2.7 and 2.11). Two important features may be noted:- (a) the recoveries gradually decrease as the pH increased and (b) the use of frother increases the recovery levels at all pH values without changing their general pH dependence (Figures 2.9 and 2.11).

The stability of the wetting film surrounding the particles should be affected differently by the hydrophobic and hydrophilic parts of the particles. For a layer type inherently hydrophobic particle, the disjoining pressure, P^P may be written as:-

$$P^P = P^E + P^F \qquad 2.36$$

where P^E amd P^F are disjoining pressures for edges and faces. The faces can be considered as consisting of oxidized and un-oxidized parts

$$P^F = P^{F(ox)} + P^{F(unox)} \qquad 2.37$$

In aqueous solutions, the nature of the oxidized part of the faces are expected to be similar to that of the edges since their formation involves the rupture of the interatomic bonds and oxidation to produce hydrophilic sites consisting of ionic species (e.g. $Si\text{-}O^-$ and $[MoS_xO_y]^{-n}$ for talc and molybdenite respectively). Considering the components of the disjoining pressure (section 2.2.4.2.) for each different part of these particles and using Equations 2.27, 2.36 and 2.37 the following expression is obtained:-

$$P_t^P = (P_{el}^E + P_{el}^{F(ox)} + P_{el}^{F(unox)}) + (P_{vw}^E + P_{vw}^{F(ox)} + P_{vw}^{F(unox)}) + (P_h^E + P_h^{F(ox)} + P_h^{F(unox)})$$

2.38

For good flotation, the particles must have zero or negative disjoining film pressures. The change in the zeta potentials on the particles manifest itself in the P_{el} terms of Equation 2.38. In general, P_{el}^E, $P_{el}^{F(ox)} >> P_{el}^{F(unox)} > 0$. The zeta potential on unoxidized parts of the faces is expected to be low, probably about -10mV (Chander et al., 1975). This results in a small positive value of $P_{el}^{F(unox)}$. For these regions, the van der Waals' term of the disjoining film pressure, $P_{vw}^{F(unox)}$ is always negative. Thus, the attractive force between bubble and the surface is expected to be greater than the electrical double layer repulsion forces. Since the disjoining film on such regions is expected to be unstable, the particle capture by a bubble should be relatively easy. To check the validity of these statements, flotation tests were carried out using a specially prepared sample. The samples were freshly prepared as follows: a few layer thick cleavage surfaces from molybdenite and talc were cut in the form of squares and rectangular with sides ranging from 0.5 to 3.5 mm (see Figure 2.18 for molybdenite sample). The samples were found to be readily floatable at all pH values tested (Figure 2.19). The bubble-particle attractive forces being great is apparent also from large contact angles which are generally independent of pH. However, the particles



Figure 2.18 Molybdenite Face Sample Used in the Flotation Experiments

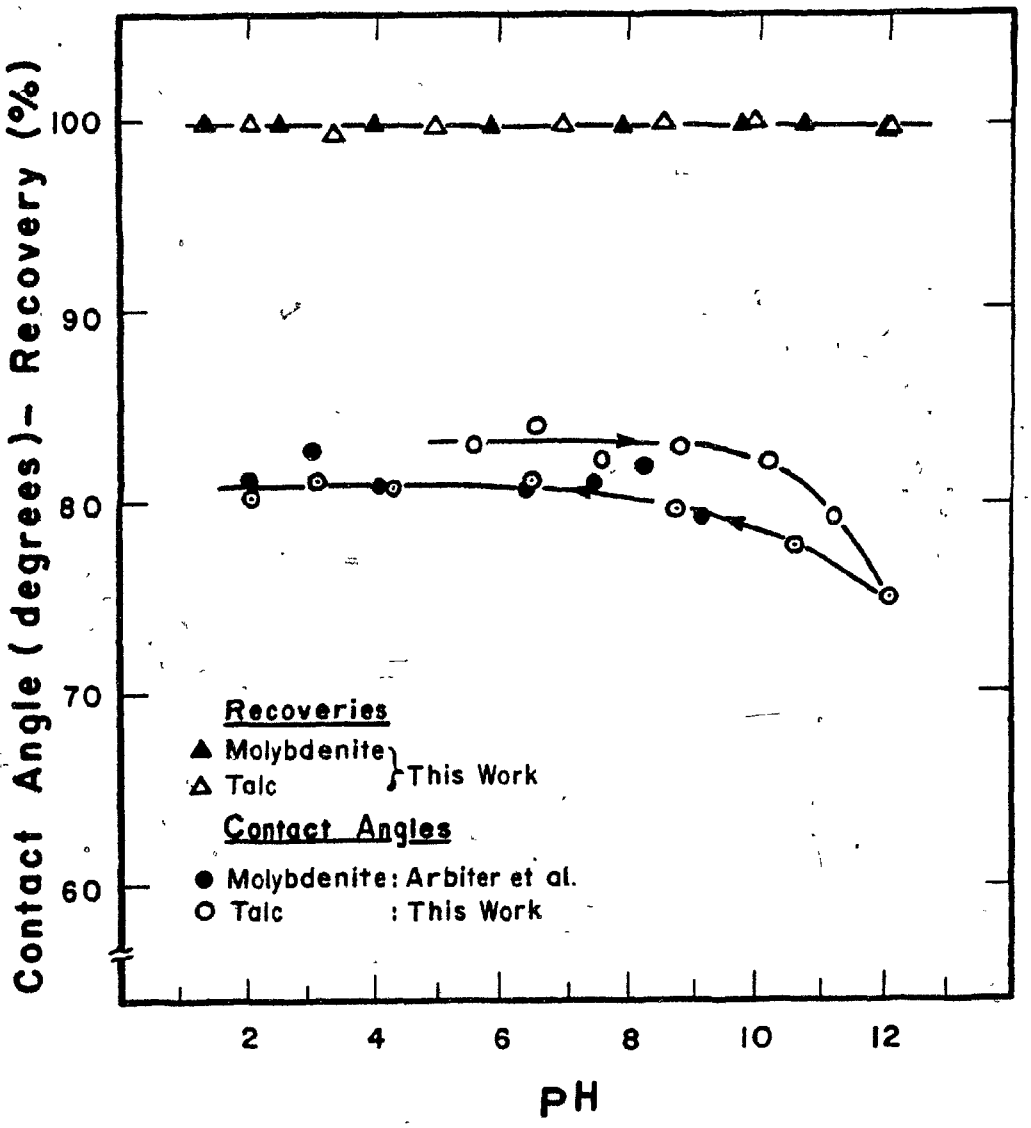


Figure 2.19 Contact Angle and Flotation Recovery of Talc and Molybdenite as a Function of pH (Flotation sample consisted of pieces of cut layers. See Figure 2.18 for molybdenite sample)

encountered in actual flotation practice have the faces which invariably contain hydrophilic sites. The natural flotation response of these particles is determined to a large degree by the concentration of these hydrophilic sites. Since the edges are completely hydrophilic regardless of the pH variation, the pH dependence of flotation should be shaped primarily by the variation of $P^{F(ox)}$. The value of $P^{F(ox)}$ should become relatively more positive with increasing pH while, as judged from the results given in Figure 2.19, $P^{F(unox)}$ remains essentially unchanged. Therefore, the electrical double-layer forces of repulsion as suggested by increased zeta potentials appear to dominate the attraction forces in alkaline solutions. Thus, the particles whose faces acquire relatively more stable wetting films cannot be captured at high pH.

The recoveries of molybdenite in the presence of MIBC are much higher at all pH values than in the absence of it (Figure 2.11). This is similar to the case of stibnite (Figure 2.9). The presence of frother molecules do not affect the zeta potentials (Derjaguin and Shukakidse, 1961) nor the magnitude of the contact angles (Arbiter et al., 1975). The latter authors attributed the increases in recoveries to the possible decrease in the induction period by frothers. However, this is difficult to verify by direct measurement. It is believed that there are other factors

involved. An important factor not considered by previous researchers is the variation in cell hydrodynamics, and the probability of collisions and attachment. In the absence of frother, the bubble size distribution in the cell is very wide (Chapter 3). The presence of large bubbles (usually non-spherical) creates turbulence due to their high upward velocity which disturbs the smaller bubbles with lower upward velocity. Due to more violent conditions in the cell without a frother, some particles with weak hydrophobic character cannot be captured by the bubbles. With the use of frothers, the number of bubbles increases considerably (hence higher probability of collisions) and the bubbles are more homogeneously distributed within a much narrower size range. This creates more favourable hydrodynamic conditions for the collection of weakly hydrophobic particles.

2.5.1.3. Contact Angle Behaviour

From the contact angles measured on disc samples of talc, graphite and molybdenite with respect to pH (Figures 2.7, 2.8, 2.10-12), two features are apparent: (a) the hydrophobicity as a function of pH is, generally, reversible, but, usually with some degree of hysteresis occurring in certain pH ranges. Indeed, it is clear that when the pH value is changed in the reverse direction the data points do not fall on the initial contact angle curves, but, they usually follow a path of smaller angles. This may be

attributed to a relatively rapid rate of hydration due to the presence of the hydrophilic edges on the disc samples. Adsorption of water molecules on such heterogeneous surfaces and the formation of wetting films by hydrogen bonding between the adsorbed water and the bulk water molecules are time-dependent. The water molecules are thought to form clusters on the hydrophilic sites in the hydrophobic surfaces (Zettlemoyer, 1968). With an increase in the thickness of the water film the contact angles decrease (Klassen and Mokrousov, 1963). Therefore, the contact angles on disc samples are expected to decrease as a function of their residence time in water. This is verified experimentally (Figure 2.20). The decrease in contact angle is negligible for the cleavage planes. Accompanying this decrease is the increase in induction period for the bubble attachment. The rate of decrease in contact angle with the residence time in water is faster as the ratio of edge-to-face increases.

Secondly, (b) the contact angles measured on disc samples are not only low in magnitude but also pH-dependent. They show a regular decrease as the solution pH increases. This is contrary to the contact angle behaviour of the cleavage surfaces (Arbiter et al., 1975). In order to explain these observations, consideration must be given to the heterogeneous structures of the disc surfaces. Because the discs were prepared directly by compacting the particles, their surfaces should contain large edge-to-face ratios. In

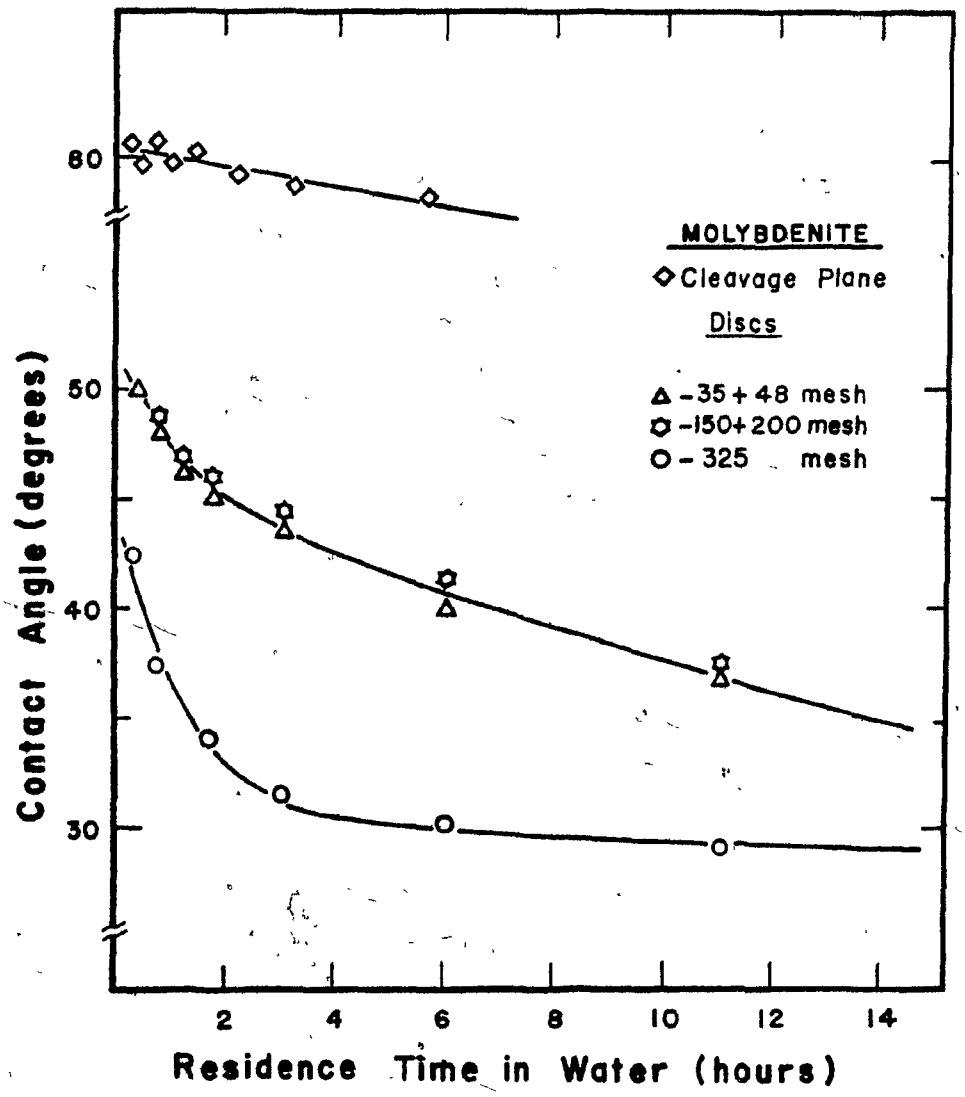


Figure 2.20 Variation of Contact Angle of Molybdenite as a Function of Residence Time in Distilled Water

general, cleavage planes of these layer-type minerals should contain none or the least possible number of hydrophilic sites. However, when the sample is polished, hydrophilic sites are created due to the rupture of interatomic bonds. Thus, the surface acquires a heterogeneous character and, due to the presence of these hydrophilic sites, the contact angles are lower. The fractional area occupied by hydrophilic sites is a very difficult factor to assess experimentally. However, a measure of this parameter can be obtained using the equation first developed by Cassie (1948) for composite surfaces:-

$$\text{Cos } \theta_{he} = x_{hb} \text{ Cos } \theta_{hb} + x_{h\ell} \text{ Cos } \theta_{h\ell} \qquad 2.39$$

where θ_{he}, θ_{hb} and $\theta_{h\ell}$ represent the contact angles for the heterogeneous surface, hydrophobic and hydrophilic sites in the surface respectively. x_{hb} and $x_{h\ell}$ are the fractions of the hydrophobic and hydrophilic sites respectively. This equation has been used for the purpose of predicting the surfactant coverage on inherently hydrophilic minerals (Philippoff et al., 1952; Yen et al., 1973) and is directly applicable to the inherently hydrophobic surfaces. The underlying assumption in using this equation is that two components occur as evenly distributed areas at the surface which are small compared to the area of the bubble used to measure the contact angle. The micrographs of the sulphur and molybdenite discs (Figure 2.21) indicate

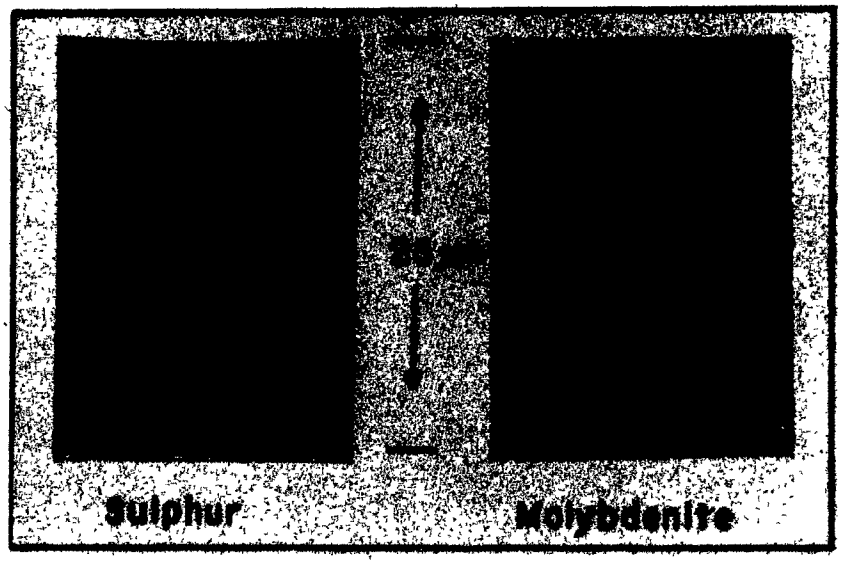


Figure 2.21 Photomicrographs of Sulphur and Molybdenite Discs

the nature of the surface heterogeneity of the samples. Isolated dark and bright areas are indeed very small (i.e. ~ < 5μm). This supports the validity of the assumption. For hydrophilic sites, the contact angle is assumed to be zero ($\text{Cos } \theta_{h\ell} = 1$). This was verified by contact angle tests using the polished edges of talc and molybdenite. Since $x_{hb} + x_{h\ell} = 1$, Equation 2.39 becomes:-

$$\text{Cos } \theta_{he} = \text{Cos } \theta_{hb} - x_{h\ell} \ (\text{Cos } \theta_{hb} - 1) \qquad 2.40$$

Rearranging this equation yields the following:-

$$x_{h\ell} = \frac{\text{Cos } \theta_{he} - \text{Cos } \theta_{hb}}{1 - \text{Cos } \theta_{hb}} \qquad 2.41$$

Equation 2.41 can be employed to predict the ratios between hydrophilic and hydrophobic sites on the samples which may be used for comparison purposes to examine the nature of pH dependence of the contact angles of the samples.

Contact angle for the cleavage plane of molybdenite was found to be ~ 80°. This value is in excellent agreement with the values of 80 and 81° previously reported by Chander and Fuerstenau (1972) and Arbiter et al., (1975) respectively. The latter authors found that if the molybdenite is polished parallel to cleavage plane the angle is reduced to 70°. Using $\theta_{hb} = 80°$ and $\theta_{he} = 70°$ the fraction of the hydrophilic sites introduced by polishing can be calculated from Equation 2.41 as $x_{h\ell} = 0.20$ (i.e. due to polishing, the hydrophilic sites increases by 20%).

For this surface, the contact angles remain independent of pH in the pH range 1 - 9. The results of the calculations for the specimens from various mineral samples are given in Table 2.5. The values of θ_{hb} for talc and stibnite

Table 2.5

Contact Angles and Fraction of Hydrophilic Sites on Inherently Hydrophobic Minerals

Sample	θ_{he}	$x_{h\ell}$	$x_{h\ell}/x_{hb}$
Talc (θ_{hb}=88°)			
Cleavage (1)	84	0.07	0.08
Cleavage (2)	78	0.18	0.22
Cleavage (3)	68	0.35	0.54
Disc (1)	46.5	0.68	2.13
Disc (2)	39	0.77	3.35
Graphite (θ_{hb}=80°)			
Fracture face	61	0.38	0.61
Disc (1)	44	0.68	1.94
Disc (2)	26	0.88	7.33
Molybdenite (θ_{hb}=80°)			
Polished sample	70	0.20	0.25
Disc (1)	54	0.50	1.00
Disc (2)	48	0.60	1.50
Stibnite (θ_{hb}=84°)			
Fracture face (1)	64	0.37	0.59
Fracture face (2)	50	0.60	1.50
Polished sample (1)	35	0.80	4.00
Polished sample (2)	31	0.84	5.25

were taken from Fowkes and Harkins (1940), and for graphite from Arbiter et al., (1975). The specimens Disc 1 and Disc 2 were prepared from the 100 x 150 and -200 mesh size fractions. As the hydrophilic-to-hydrophobic ratios increase, the pH dependence of contact angles of the samples become more apparent.

2.5.1.4. Correlation Between the pH Dependent Surface Properties of Layer Type Minerals

An examination of the results presented reveals that a correlation between contact angle, the zeta potential and the natural flotation response has been established. As the pH increases, both the flotation recovery and contact angles decrease while the negative value of the zeta potential increase and vice versa. In order to demonstrate such a corelation, special attention has been given to the sample preparation. The correlation is better observed when the samples used in these various tests have comparable hydrophilic-to-hydrophobic ratios. In this correlation, the effect of both the hydrophilic and hydrophobic sites on the establishment of zeta potential, contact angles and stability of the disjoining films has been taken into consideration. An attempt by Arbiter et al., (1975) to observe a correlation between the zeta potential and contact angle of molybdenite was unsuccessful apparently because of the low hydrophilic-to-hydrophobic ratio (i.e. 1:4, Table 2.5) of their sample used for contact angle measurements. Using Cassie's equation, the hydrophilic-to-hydrophobic ratios of various samples were predicted (Table 2.5).

For talc, graphite and molybdenite the correlation between contact angles and the zeta potentials or flotation recoveries becomes more apparent if the hydrophilic-to-hydrophobic ratio on the contact angle sample is at least 1:1. In the previous studies no attempt was made to determine or predict this ratio. The variability of this ratio from sample to sample may be mainly responsible for conflicting reports on the correlation between the zeta potential and floatability (Derjaguin and Shukakidse, 1961; Jessop and Stretton, 1969; Arbiter et al., 1975; Collins and Jameson, 1977; Kelebek, 1980; Yarar and Leja, 1982). Among these, only Jessop and Stretton and Arbiter et al. reported non-correlation.

As pointed out by Chander et al. (1975) who were first to call attention to the anisotropic nature of layer type hydrophobic minerals, quantitative agreement is not expected. The zeta potentials are strongly affected by the presence of the ionic, hydrophilic sites, whereas flotation or contact angle is determined primarily by the hydrophobic sites on the surface and only secondarily by the zeta potential.

2.5.2. Common Sulphides: Chalcopyrite and Galena

2.5.2.1. Electrokinetic Behaviour

The electrokinetic behaviour of chalcopyrite and galena are more complicated to interpret. One of the reasons for difficulty is the number of ions that may participate in

determining the zeta potential. The metallic cation, S^{2-}, HS^-, H^+, OH^- anions and H_2S may all be responsible for surface charging of a base metal sulphide but the HS^- ion, the first hydrolysis product of the S^{2-} ion presumably play a chief role in determining the potential on such surfaces. According to de Bruyn and Agar (1962), the process by which the sulphide surface is electrically charged, may be represented by any of the following reactions:-

$$S^{2-}\ (\text{solid}) \rightleftharpoons S^{2-}\ (\text{aq.}) \qquad 2.42$$

$$S^{2-}\ (\text{solid}) + H_2O \rightleftharpoons HS^-\ (\text{aq.}) + O\bar{H} \qquad 2.43$$

$$S^{2-}\ (\text{solid} + 2H_2O \rightleftharpoons H_2S(\text{aq.}) + 2O\bar{H} \qquad 2.44$$

$$S^{2-}\ (\text{solid}) + H^+ \rightleftharpoons HS^-\ (\text{aq.}) \qquad 2.45$$

The electrokinetic behaviour changes rapidly due to the oxidation of freshly exposed sulphide surfaces. Plante and Sutherland (1949) found that oxidation of these minerals produced soluble cations and sulphate in neutral or acidic solutions and polythionates, sulphate, sulphite and thiosulphate in alkaline solutions. Due to the presence of other potential determing ions in addition to H^+ and OH^-, the use of the term PZC is to be preferentially replaced by the IEP (i.e. Iso Electric Point).

The zeta potentials of freshly prepared chalcopyrite (dry grinding) are presented as a function of pH in Figure 2.13. They become increasingly more negative as the pH

increases. According to McGlashan et al. (1968), various ionic sites involving copper, iron and sulphur atoms created on fracture react with oxygen to produce negatively charged surface species. This may explain why chalcopyrite yields a negative zeta potential at most pH values. Figure 2.13 also includes the zeta potential variation of a sulphur sample for comparison purposes. The IEP values for both chalcopyrite and sulphur occur at a pH of ~ 2.2. This similarity in the electrokinetic behaviour of the two supports the view of McGlashan et al. that the surface of chalcopyrite is dominated by sulphur and that the surface reactions are primarily dependent upon sulphur and secondarily dependent upon the metal atoms. The IEP of pH=2.2 seems to be in fair agreement with the previously reported values of pH=2-3 for chalcopyrite (Healy and Moignard, 1976).

The variation of the zeta potentials for galena with respect to pH has been found to depend significantly upon the preparation and pretreatment of the sample (Figure 2.14). The sample prepared freshly in distilled water has an IEP value between pH=6-8. Dry grinding causes a shift in IEP towards a lower value (pH ~ 5.2) probably because of the formation of oxidation products (e.g., S°, $PbSO_4$, etc.). The sample ground dry and subsequently pretreated with an ammonium chloride solution (Chapter 5) for the removal of $PbSO_4$ from the surface has been found to have an even lower

IEP value (pH ~ 4.2) and lower zeta potentials. This pretreatment should have caused a significant decrease in the hydrophilic surface compounds (e.g. $PbSO_4$) on the surface. The flotation feed pretreated with the same solution has been readily floatable in distilled water. Another important finding was that floated particles contained appreciable amount of elemental sulphur on their surfaces (Chapter 5). Two sulphur samples obtained from the sulphide minerals have an IEP value at pH ~ 2.2 which also represents the galena sample aged after grinding to a fine size. Liberation of elemental sulphur on galena samples due to oxidation should be responsible at least partially for the gradual decrease in IEP towards lower values. $PbSO_4$, the final product of oxidation of galena can be converted to $PbCO_3$ in solutions open to the air since the solubility of the latter is much lower than that of the former (Weast, 1981-82). The zeta potentials of freshly precipitated $PbSO_4$ amd $PbCO_3$ were found to be lower than 20 mV at all pH values up to pH ~ 11. This might explain the relatively low zeta potentials in the case of the aged galena sample.

There are a number of different IEP values reported for galena. An IEP at pH ~ 3 has been found by Gaudin and Sun (1946), Yarar and Kitchener (1970) and Yücesoy and Yarar (1974). Neville and Hunter (1976) have found that the way of conditioning has a significant effect on the IEP of the

samples. The IEP of their galena sample is in the pH range 2 to 4. They have observed that the samples conditioned at pH=4 exhibit two IEP values between pH 6 to 10, due probably to hydroxide or basic sulphate precipitation on the particles. The above studies have been reviewed in more detail by Healy and Moignard (1976). More recent studies by Fuerstenau and his co-workers (Fuerstenau, 1978) show that in the virtual absence of oxygen, a galena sample has an IEP at pH=2.6. In the presence of oxygen, the IEP value is at about pH=8. The details of the sample preparation and the mechanism of surface charging at these two different conditions have not been given. Aplan et al. (1978) have found that various galena samples including synthetic ones yield IEP values at pH=2.0-2.1 which agree well with the IEP value of aged galena obtained in the present study. They also report that a natural galena sample from Kansas has an IEP value at pH ~ 6.7 which is in good agreement with the IEP value of the freshly prepared (wet) galena sample also from Kansas (Figure 2.14).

Considering all these reported results, it appears that the electrokinetic properties of galena can vary according to the sample (surface stoichiometry, type of semiconductivity, etc.) and the sample preparation (method of conditioning, aging in the air or solution, various pretreatments, etc.).

2.5.2.2. Flotation Behaviour

The natural flotation response of chalcopyrite is seen

to increase in acidic solutions reaching a maximum of ~ 90% at pH=2-2.8 which represents relatively low zeta potentials (Figure 2.13). Although McGlashan et al. (1968) have recognized the importance of the domination of the chalcopyrite surface by sulphur in determining its interfacial reactions, they have not suggested that this may lead to chalcopyrite's natural floatability. For this to occur, the surface sulphur has to be oxidized to its elemental form, S°, on the chalcopyrite particles. This has been established by sulphur extraction tests which have indicated the presence of appreciable amount of elemental sulphur on the chalcopyrite sample (Chapter 5). The presence of sulphur on chalcopyrite is also supported by the fact that the IEP value of the chalcopyrite sample is the same as that of elemental sulphur. These results establish a definite role played by the liberated sulphur in the observed natural floatability of chalcopyrite. The E_h-pH diagram of sulphur (Garrels and Christ, 1965) indicates that elemental sulphur is more stable at low pH values than at high pH values. In alkaline solutions, it is oxidized to higher oxidation states forming negatively charged sulphoxy ions (e.g. $S_2O_3^{2-}$, SO_4^{2-}) which constitute hydrophilic sites at the surface. Thus, the recoveries should decrease in alkaline solutions as observed.

The natural flotation response of galena with respect to pH is different from that of chalcopyrite in that the maximum recoveries are obtained in neutral solutions. These

flotation tests have been conducted using fresh samples prepared in distilled water pre-saturated with various gases (Figure 2.15). No attempt has been made to determine the elemental sulphur on these particular galena samples. However, the extraction tests have shown the presence of elemental sulphur on galena samples prepared in several different ways (Chapter 5). It is not certain if the elemental sulphur alone is responsible for the natural flotation of galena in these tests. In acidic pH range where the elemental sulphur is known to be stable, the recoveries are low. This is contrary to the observations using chalcopyrite.

The oxygen-saturated distilled water contains ~ 20 ppm dissolved oxygen (Douglas, 1965) whereas the air and nitrogen saturated water has an oxygen content of 8-9 and 0.1-0.2 ppm respectively (Gilroy and Mayne, 1962). Apparently, in acidic solutions saturated with oxygen, some soluble sulphoxy ions and virtually insoluble lead sulphate (pK_s=7.8) are formed. The galena surface is probably dominated by the hydrophilic surface species, but may contain also hydrophobic regions where oxidation produces some elemental sulphur. In the case of chalcopyrite, hydrophilic oxidation products (e.g. $FeSO_4$, $CuSO_4$) are soluble. Their dissolution into solution changes the hydrophobic-to-hydrophilic balance of the surface in favour of a more hydrophobic one. In nitrogen-saturated solutions, due to the deficiency of oxygen, the elemental sulphur may not form sufficiently on the galena

surface. As the solutions become more acidic the surface S^{2-} and/or HS^- ions can participate in the formation of H_2S leaving the surface richer in Pb^{2+}. During some experiments using strongly acidic solutions, the characteristic odour of H_2S was noted. Further interaction of the particles with such solutions produce ionic surface species which may account for the relative decrease in recoveries. In alkaline solutions, the recoveries decrease with increasing pH probably due to the adsorption of HS^-/OH^- ions on the particle surfaces. In air-saturated solutions, due to the presence of oxygen, the galena particles should develop, as previously suggested, both bydrophobic and hydrophilic oxidation products. Presumably the particle surfaces are dominated by hydrophobic oxidation product, namely sulphur, so that the recoveries are relatively higher at all pH values. In general, the maximum recoveries observed at natural pH values of 6-7 may be related to the low charge density on the particle surfaces. Freshly (wet) prepared galena sample has shown an IEP in the same pH range (Figure 2.14). In this regard, it is interesting to note a conclusion by Richardson and Edelstein (1978) who stated that both the charge at the surface and the exact chemical composition should determine the natural floatability of galena. By chemical composition, they refer specifically to the surface stoichiometry of galena, namely the sulphur-lead balance, which determines the type of semiconductivity (i.e. p-type if the sample has a slight excess of sulphur, otherwise n-type).

Preliminary tests with galena have shown that the recoveries obtained with prewashed feed are notably higher than those obtained with unwashed feed. Subsequent tests conducted using samples prepared and floated under different conditions have indicated that the aerative washing was the most important single factor in increasing the flotation recovery (Table 2.2). The aerative washing may have functioned in two ways. First, various water soluble sulphoxyl-ions (e.g. $S_2O_3^{2-}$, SO_3^{2-}, etc.) are at least partially removed from the galena surface. Due to insoluble nature of liberated sulphur, the ratio of hydrophobic-to-hydrophilic regions on the surface increases. Secondly, the sulphur-liberated regions, relatively free of water-soluble ions of higher oxidation state are saturated with air and thus sensitized to air bubble attachment during flotation.

2.5.2.3. Contact Angle Behaviour

The natural floatabilities of chalcopyrite and galena were clearly demonstrated by the flotation tests. However, this could not be verified consistently by classical contact angle tests. The majority of tests with polished specimens indicated no apparent bubble attachment to the surface. This is in general agreement with the previous results. Traditionally, attachment of air bubbles on polished sulphides in water during contact angle experiments was attributed to an oily contamination of the system (Sutherland and Wark, 1955).

However, classifying a mineral as hydrophilic due to the failure of the bubble-polished surface attachment may be misleading. A finite contact angle below ~ 15° which is generally nonmeasurable using the usual captive bubble technique, may still be sufficient for the flotation of particles. The following observations may be presented as evidence in favour of the natural floatability of chalcopyrite, galena and chalcocite. Three details were specific to these tests: (a) avoiding long periods of polishing to prevent aging the samples, (b) using the specimens freshly immediately after their preparation (i.e. no temporary storage in distilled water), and (c) washing the polished specimens with distilled water rigourously immediately prior to measurements. In distilled water (pH ~ 6.1), each sample gave finite contact angles on various regions of the surface after an induction period of approximately one minute. The average of five measurements on each sample was 16 ± 2° (chalcopyrite), 15 ± 1° (galena), and 18 ± 1° (chalcocite). During the initial minutes of observation, it was noted that the volumes of the attached bubbles decreased slowly with time. This was relatively more pronounced in the case of chalcopyrite. The affinity of freshly formed sulphide surfaces for gases (particularly for oxygen) has been known for many years (Plaksin, 1959). However, to the author's knowledge, such a phenomenon (i.e. consumption of the attached air bubbles) has not been noted previously. The mechanism

of this phenomenon is presently unknown.

A small finite contact angle on these sulphides is in agreement with the observations of Poling and Leja (1960) who suggested "a threshold hydrophobicity" for galena. They noted that on standing in water for more than 15-20 minutes, the slight hydrophobicity of a freshly formed galena film disappeared. In the present study, this hydrophobicity was persistent for longer times.

The effect of acidic and alkaline pH on the contact angles of these three samples was tested. The pH of the solution was reduced to about 2.3. The bubble attachment was achieved in a much shorter time (5-15 seconds), and an increase in the magnitude of the contact angles was observed. The average of six pairs of measurements on each sample was 36 ± 2° (chalcopyrite), 21 ± 1° (galena), and 24 ± 1° (chalcocite). The samples were washed to remove the acidic solution without exposing them to air and the contact angles were re-measured in distilled water to check for reproducibility. There was an apparent decrease in the number of hydrophobic regions. However, the average angles remained nearly the same as the previous values in distilled water; 16 ± 2° (chalcopyrite), 14 ± 1° (galena), and 19 ± 2° (chalcocite). By this time at least one hour has passed since the start of the experiments. The pH was then increased to 10.8. In this solution, the surfaces of all the three

samples became so hydrophilic that no contact angle was measurable even after ten minutes of contact time. Finally, the contact angle tests were repeated in distilled water after washing the samples. There was no contact angle formation for all regions of chalcopyrite and for most regions of galena and chalcocite surfaces. The average contact angles measurable on two regions were 12 ± 2° and 16 ± 2° for galena and chalcocite respectively.

The increase in contact angle at pH ~ 2.3 could be due to a decrease in the zeta potentials, the presence of elemental sulphur with increased stability or both. The disappearance of the finite contact angles in alkaline solution (pH=10.8) may be attributed to the formation of sulphoxyl ions $[S_xO_y]^{-n}$ and/or metal hdyroxides on the surface. In general, these observations give support for the natural floatability of these sulphides. But, the question whether or not they owe this apparent natural floatability totally to the liberation of the elemental sulphur on their surfaces remains uncertain.

2.5.3. Octane Contact Angles and Polar Characteristics of the Minerals

There appears to be no literature data with which to compare the octane contact angle data except a recent study by Janczuk and Chibowski (1983). They have reported contact angles of saturated hydrocarbon liquids on sulphur, graphite

and Teflon. The values given for the octane contact angles are 131 and 120.5° on sulphur and graphite respectively. The former value is in reasonable agreement with the value of 135° which was measured on the crystal face of sulphur. However, the angle for graphite is much larger than those obtained for two graphite samples used in the present work (Table 2.3). The sample description was not given by Janczuk and Chibowski. However, large value for graphite would indicate that their sample was probably a well-cleaved graphite plane. Lower contact angle values should be the result of the presence of relatively large number of hydrophilic sites on the samples used.

The polar component of the surface free energy of the samples, γ_s^P as determined from Equation 2.24 are listed in Table 2.6. The larger the octane contact angle, the smaller the γ_s^P value for solid. Octane can interact with a solid surface only with its dispersion forces since its surface-free energy does not have a polar component. The failure of the solid surface to form a finite contact angle with octane droplet in water indicates that the interaction through dispersion forces is negligible. Such a solid interacts with liquids like water through its non-dispersion forces (e.g. polar forces). The polar forces (i.e. hydrogen bonding and dipole interactions) account for about 70% of the surface-free energy of water (Fowkes, 1964). Since for solids

interacting only with polar forces, γ_s^P is equal 50.8 mJ/m^2, for each sample a measure of non-polarity, n_R may be obtained from the following expression:-

$$n_R(\%) = 100 \left(1 - \frac{\gamma_s^P}{50.8}\right) \qquad 2.46$$

The values of $n_R(\%)$ are given also in Table 2.6.

Table 2.6

The Polar Component of the Surface-Free Energy, γ_s^P and Relative Non-Polarity, n_R of the Samples

Crystal Face or Cleaved Sample	γ_s^P (mJ/m^2)	n_R (%)
Sulphur	1.1	98
Molybdenite	3.2	94
Talc	4.0/6.1	92/88
Graphite	12.7/18.5	75/64
Polished Samples		
Orpiment	20.1	60
Realgar	21.8	57
Stibnite	37.0	27
Chalcocite	41.1/50.8	19/0
Chalcopyrite	42.5/50.8	16/0
Pyrite	45.5/50.8	10/0
Galena	43.4/50.8	15 0
Coal	18.5	64

2.5.4. Critical Surface Tension of Wetting

The critical surface tension of wetting values, γ_c,

are reported in Table 2.4. For galena, the γ_c value of about 31 mN/m is nearly the same as those reported by Olsen et al. (1967) for both allotropic forms of sulphur. This may suggest the presence of elemental sulphur on the galena due to oxidation. The γ_c and b values obtained for graphite are 46.5 mN/m and 1.83×10^{-2} respectively as compared with 47.5 mN/m and 2.08×10^{-2} reported by Parekh and Aplan (1978). Both samples were from Sri Lanka. A γ_c value of 41.5 mN/m for a polished specimen of a talc sample (Quebec) is also in good agreement with the value of 41.0 mN/m for a talc sample (origin and preparation technique not specified) studied by Parekh (1972). However, the data by Bartell and Zuidema (1936) indicates that for a well cleaved talc sample γ_c is about 35.5 mN/m. The rest of the mineral samples have γ_c values which are similar to those of various coals (γ_c = 49 - 47.5 mN/m obtained by Parekh and Aplan. This would place these minerals and coals as the low surface energy solids near the nitrated hydrocarbons in the wettability "spectrum" of various solid hydrocarbons which have a similar range of γ_c values (Shafrin and Zisman, 1960). This might imply additional support for the inherently hydrophobic character of common sulphides such as pyrite, chalcopyrite. However, this range of γ_c values can hardly be regarded as evidence of inherent hydrophobicity of common sulphides.

In defining low- and high-energy surfaces, Zisman (1964) refers to the hardness of the solids and cites metal

sulphides as being among the high-surface-energy solids. Indeed, an indication of the relative surface tension of solids may be judged from their relative hardness. The well-known softness of talc and graphite is in agreement with their inherently hydrophobic (i.e. low surface energy) character. In these solids, the elementary units (e.g. layers) are apart from each other, and hence forces of attraction are weak. Therefore, the work of cohesion and the surface tension of soft solids should be relatively small. In hard solids, however, the atoms or ions are close together. The force of attraction between the structural units comprising these solids is large, and the work of cohesion, and hence the surface tension is expected to be high. The hardness of common sulphides is several times that of talc. On the Moh hardness scale the hardness of 1 is for talc as compared to 2.6, 3.5 and 6.2 for galena, chalcopyrite and pyrite respectively (Taggart, 1945). Therefore, it seems unrealistic to expect similar surface-free energies, and hence γ_c values between talc and these common sulphides.

The reason why most of the mineral samples and coals have similar γ_c values (~ 45 mN/m) is not clearly understood. The liberation of elemental sulphur on sulphide minerals is likely. The indication for this appears to be provided particularly for galena. The presence of sulphur on freshly ground galena, chalcopyrite and realgar has been established (Chapter 5). If the elemental sulphur was formed on the polished

sulphides, it would be in the form of a very thin film. Such a sulphur film can give large contact angles with water droplets due to its insolubility in water, but may be dissolved to some extent by the reference organic liquids thus causing comparable contact angles, and hence similar γ_c values. Alternatively, if a thin oxide-like film is formed on common sulphides the physical adsorption of water vapor may have played a decisive role in the establishment of similar γ_c values. Zisman and his co-workers discovered that adsorption of water as a monolayer or as a thicker film on the surface of high energy solids such as glass, quartz and metals considerably lower their surface-free energies. For twelve different metals and an oxide (Fe_3O_4), γ_c value was found to be ~ 45 mN/m when the surfaces are covered by even a fraction of a monolayer of adsorbed water (Bernett and Zisman, 1968). It was concluded that γ_c as well as γ_s of clean high energy solids after exposure to a humid atmosphere was dependent upon the surface concentration of water adsorbed on the surface, but that it was independent of the chemical nature of the underlying solid (Zisman, 1975). In the case of sulphides, gases (i.e. oxygen due to its particular affinity for sulphide surfaces) should also play a role in determining the wettabilities of surfaces (Rogers, 1962).

In an investigation of adsorption properties of hydrophobic surfaces, Kiselev (1968) concludes that the amount of

water vapor adsorption is low on hydrophobic solids which, according to him, includes the metal sulphides. The decrease in the surface tension of solids due to the adsorption of water vapor, that is, the surface pressure of adsorbed water film, Π^V is given by the following relation (Bagham and Razouk, 1937):-

$$\Pi^V = \gamma_s - \gamma_{sw} = RT \int_0^{P^\circ} \Gamma \, d\ell nP \qquad 2.47$$

where Γ is the amount of water adsorbed per unit area at a vapor pressure $P \cdot P^\circ$ is the saturated vapour pressure of water. Π^V can be obtained graphically by determining the area under the adsorption isotherm (Gregg, 1951; Harkins, 1952), provided that the surface area, A_s is known. Using the graphical method described by Gregg, the values of Π^V for the molybdenite and coal were determined from the available adsorption isotherms for water vapor. These are given in Table 2.7 which includes the Π^V values determined by Harkins (1952) for various graphite samples.

Table 2.7

Surface Pressure of Water Vapor on Inherently Hydrophobic Minerals

Sample	Π^V(mN/m)	T(°C)	A_s(m^2/g)	Reference
Graphite (1)	19	25	4.18	Harkins
Graphite (2)	19	25	6.2	Harkins
Graphite (3)	58	25	27.6	Harkins
Molybdenite (1)	14	20	9.1	Ballou and Ross
Molybdenite (2)	97	30	12.0	Johnson and Moore
Coal (sub-bitum.)	143	20	200	Şenkan and Fuller

The values of Π^V are high and dependent upon the nature of the sample. The samples of graphite (1), (2), and (3) were reported to contain the ash contents of 0.004, 0.46, and 10% respectively (Harkins, 1952). Molybdenite (1) was reported to have an assay of 99% MoS_2. Before being used in the adsorption tests the powdered sample was sulphidized under a dry H_2S atmosphere for 12 hours (Ballou and Ross, 1953). Molybdenite (2) treated with HF to reduce the silica content to $< 0.02\%$ was dried in a stream of air (Johnston and Moore, 1964). Coal was a sub-bituminous-type containing 6.8% ash (Şenkan and Fuller, 1979). These Π^V values indicate the extent of high-energy impurities and artificial oxidation of the samples. Coal being a weakly hydrophobic and heterogeneous material has the greatest Π^V value. The value of Π^V for the air-dried molybdenite is much greater than that for the H_2S-treated-molybdenite probably due to the presence of a greater number of hydrophilic sites on its surface. It should be emphasized that these Π^V values represent the surface pressures on the powdered samples. On smooth surfaces used for contact angle measurements, the amount of water vapor adsorption is expected to be relatively smaller (Adam and Livingston, 1958).

Assuming the validity of smallest Π^V value for molybdenite sample (Table 2.7), one can calculate the dispersion component of its surface-free energy, γ_s^d from the following expression by Fowkes (1964):-

$$\text{Cos } \Theta = -1 + 2 \sqrt{\gamma_\ell^d \gamma_s^d} / \gamma_{\ell v} - \Pi^v/\gamma_{\ell v} \qquad 2.48$$

For water at 20°C on a molybdenite cleavage plane, Θ=80°, $\gamma_{\ell v}^d$ =21.8 mJ/m^2, $\gamma_{\ell v}$=72.8 mJ/m^2, and $\Pi^v \equiv$ 14 mJ/m^2. Using these values in Equation 2.48 yields a γ_s^d value of ~ 113 mJ/m^2. Fowkes (1967) determined the γ_s^d for graphite to be ~ 109 mJ/m^2. It is likely that talc, another layer-type hydrophobic mineral will have a comparable γ_s^d value.

2.6 REFERENCES

Abramson, H.A., Moyer, L.S., and Gorin, M.H. (1942). "Electrophoresis of Proteins and the Chemistry of Cell Surfaces", Reinhold Publ. Co., New York.

Adam, N.K., and Livingston, H.K. (1958). Contact Angles and Work of Adhesion, Nature, Vol. 182, No. 4628, p. 128.

Adamson, A.W. (1976). "Physical Chemistry of Surfaces" 3rd Ed., John Wiley and Sons, New York.

Allan, A.J.G. (1959). The Spreading of Liquids on Polyethylene Film. The Effect of Preprinting Treatments, J. Polymer. Sci., Vol. 38, No. 134, pp. 297-306.

Andrade, J.D., Ma, S.M., King, R.N., and Gregonis, D.E. (1979). Contact Angles at the Solid-Water Interface. J. Coll. Interface. Sci., Vol. 72, No. 3, pp. 488-94.

Aplan, F.F. and Fuerstenau, D.W. (1962). Principles of Nonmetallic Mineral Flotation. In: Froth Flotation 50th Anniversary Volume, (D.W. Fuerstenau; Editor) AIME.

Aplan, F.F., Simkovich, G., Spearin, E.Y., and Thompson, K.C. (1978). Effects of Point Defects on Fotattion. In: The Physical Chemistry of Mineral-Reagent Interactions in Sulfide Flotation. Proceedings of Symposium, April 6-7, 1978. Information Circular 8818, U.S. Bureau of Mines, pp. 25-34.

Arbiter, N. (1975). Discussion on the paper by Arbiter et al., (1975), p. 191.

Arbiter, N., Fujii, Y., Hansen, B., and Raja, A. (1975). Surface Properties of Hydrophobic Solids. In: Advances in Interfacial Phenomena of Particulate/Solution/Gas Systems: Applications to Flotation Research. (P. Somasundaran and R.B. Grieves; Editors) AICHE Symposium Series, No. 150, Vol. 71, pp. 176-182.

Bagnall, R.D. and Green, G.F. (1979). Some Observations on Octane Contact Angles in Aqueous Media. J. Coll. Interface Sci., Vol. 68, No. 2, pp. 387-388.

Bailar, J.D., Emeléus, H.J. Nyholm, R., and Dickenson, A.F.T. (Editors). (1975). Comprehensive Inorganic Chemistry, Vol. 2.

Ballou, E.V. and Ross, S. (1953). The Adsorption of Benzene and Water Vapor by Molybdenum Disulfide. J. Phys. Chem., Vol. 57, pp. 653-657.

Bangham, D.H. and Razouk, R.I. (1937). Adsorption and the Wettability of Solid Surfaces, Trans. Faraday Soc., Vol. 33, pp. 1459-63.

Bartell, F. E. and Osterhof, H.J. (1928). The Measurement of Adhesion Tension on Solid Against Liquid. In: Colloid Symposium Monograph, The Chemical Catalog Co., New York, pp. 113-133.

Bartell, F.E. and Zuidema, H.H. (1936). Wetting Characteristics of Solids of Low Surface Tension such as Talc, Waxes and Resins. J. Amer. Chem. Soc., Vol. 58, pp. 1449-1459.

Baskin, A., Nishino, M. and Ter-Minassian-Saraga, L. (1977). Solid-Liquid Adhesion of Oxidized Polyethylene Films. Effect of Temperature on Polar Forces. J. Coll. Interface Sci., Vol. 59, No. 3, pp. 516-524.

Bernett, M.K. and Zisman, W.A. (1959). Relation of Wettability by Aqueous Solutions to the Surface Constitution of Low-Energy Solids. J. Phys. Chem., Vol. 63, pp. 1241-1246.

Bernett, M.K. and Zisman, W.A. (1968). Effect of Adsorbed Water on the Critical Surface Tension of Wetting on Metal Surfaces. J. Coll. Interface Sci., Vol. 28, No. 2, pp. 243-249.

Blake, T.D. (1971). Current Problems in the Theory of Froth Flotation. In: Symposium on Bubbles and Foams, Nuremberg, W. Germany, Verlag des Vereins Deutscher Ing.

Blake, T.D. and Kitchener, J.A. (1972). Stability of Aqueous Films on Hydrophobic Methylated Silica. J. Chem. Soc. Faraday Trans. I., Vol. 68, pp. 1435-1442.

Bleier, A., Goddard, E.D. and Kulkarni, R.D. (1976). The Structural Effects of Amine Collectors on the Flotation of Quartz. In: Flotation, A.M. Gauidin Memorial Volume, Vol. 1, (M.C. Fuerstenau; Editor), AIME, New York, pp. 117-147.

Brien, F.B. and Kar, G. (1968). An Electrophoresis Study of the Flotation Properties of Talc. The Trend in Engng., Univ. of Washington, Vol. 20, pp. 8-12.

Brooks, J.H., Mingins, J and Owens, N.F. (1977). The Effect of the Film Pressure of an Insoluble Monolayer at an Air/Water Interface on the Wetting of Solid Surfaces, J. Coll. Interface Sci., Vol. 61, No. 2, pp. 215-222.

Brown, D.J. (1962). Coal Flotation. In: Froth Flotation 50th Anniversary Volume, (D.W. Fuerstenau; Editor), AIME, New York, pp. 518-538.

Buchanan, A.S., and Heymann, E. (1949). The Electrokinetic Potential of Sparingly Soluble Sulphates. I, J. Coll. Sci., Vol. 4, pp. 137-150.

Busscher, H.J., Van Pelt, A.W.J., De Jong, H.P., and Arends, J. (1983). Effect of Spreading Pressure on Surface Free Energy Determinations by Means of Contact Angle Measurements. J. Coll. Interface Sci., Vol. 95, No. 1, pp. 23-27.

Cassie, A.B.D. (1948). Contact Angles, Disc. Faraday Soc., Vol. 3, pp. 11-16.

Çelik, M.S. and Somasundaran, P. (1980). Effect of Pretreatments on Flotation and Electrokinetic Properties of Coal, Colloids and Surfaces, Vol. 1, No. 1, pp. 121-124.

Chander, S. and Fuerstenau, D.W. (1972). On the Natural Floatability of Molybdenite. Trans. SME/AIME, Vol. 252, No. 1, pp. 62-68.

Chander, S. and Fuerstenau, D.W. (1974). Effect of Potassium Diethyldithiophosphate on the Interfacial Properties of Molybdenite.

Chander, S., Wie, J.M., and Fuerstenau, D.W. (1975). On the Native Floatability and Surface Properties of Naturally Hydrophobic Solids. In: Advances in Interfacial Phenomena of Particulate/Solution/Gas Systems; Applications to Flotation Research (P. Somasundaran and R.B. Grieves; Editors), AICHE Symposium Series, No. 150, Vol. 71, pp. 183-188.

Chapman, D.L. (1913). A Contribution to the Theory of Electrocapillarity, Philos. Mag., Vol. 25, pp. 475-481.

Collins, G.L. and Jameson, G.J. (1977). Double-Layer Effects in the Flotation of Fine Particles, Chem. Eng. Sci., Vol. 32, pp. 239-246.

Dann, J.R. (1970). Forces Involved in the Adhesion Process. I. Critical Surface Tension of Polymeric Solids as Determined with Polar Liquids, J. Coll. Interface Sci., Vol. 32, No. 2, pp. 302-320.

de Bruyn, P.L. and Agar, G.E. (1962). Surface Chemistry of Flotation. In: Froth Flotation 50th Anniversary Volume, (D.W. Fuerstenau; Editor), AIME, New York, pp. 91-138.

Derjaguin, B.V. and Dukhin, S.S. (1961). Theory of Flotation of Small and Medium-Size Particles. Trans. IMM., Vol. 70, pp. 221-246.

Derjaguin, B.V. and Landau, L.D. (1941). Theory of the Stability of Strongly Charged Lyophobic Sols and Adhesion of Strongly Charged Particles in Solutions of Electrolytes. Acta. Physiocochim. USSR, Vol. 14, pp. 633-662.

Derjaguin, B.V. and Shukakidse, N.D. (1961). Dependence of the Floatability an Antimonite on the Value of Zeta Potential. Trans. IMM., Vol. 70, pp. 569-574.

Donohue, J. (1974). "Structures of Elements", John Wiley and Sons, New York, p. 331.

Douglas, E. (1964). Solubilities of Oxygen, Argon, and Nitrogen in Distilled Water, J. Phys. Chem., Vol. 68, pp. 169-174.

Edwards, G.E. (1972). Assessment of the Froth Flotation Characteristics of a Coal. J. Inst. Fuel., Vol. 45, pp. 514-521.

Eigeles, M.A. and Volova, M.L. (1960). Kinetic Investigation of Effect of Contact Time, Temperature and Surface Condition on the Adhesion of Bubbles to Mineral Surfaces. In: 5th Intern. Miner. Process. Congr., London, Trans. IMM, pp. 271-284.

Ellison, A.H. and Zeisman, W.A. (1951). Wettability of Halogenates Organic Solid Surfaces. J. Phys. Chem., Vol. 58, pp. 260-265.

Finch, J.A., and Smith, G.W. (1981). Contact Angles and Wetting. In: Anionic Surfactants/Physical Chemistry of Surfactant Action, (E.H. Lucassen-Reynders; Editor), Marcel Dekker, New York, pp. 317-384.

Fowkes, F.M. (1964). Attractive Forces at Interfaces, Ind. Eng. Chem., Vol. 56, No. 12, pp. 40-52.

Fowkes, F.M. (1967). Attractive Forces at Solid-Liquid Interfaces. In: Wetting, S.C.I. Monograph, No. 25, Soc. Chem. Ind., London, pp. 3-30.

Fowkes, F.M., and Harkins, W.D. (1940). The State of Monolayers Adsorbed at the Interface Solid-Aqueous Solution, J. Amer. Chem. Soc., Vol. 62, pp. 3377-3386.

Fox, H.W. and Zisman, W.A. (1950). The Spreading of Liquids on Low Energy Surfaces. I. Polytetrafluoroethylene, J. Coll. Sci., Vol. 5, No. 6, pp. 514-531.

Fox, H.W. and Zisman, W.A. (1952). The Spreading of Liquids on Low Energy Surfaces. III. Hydrocarbon Surfaces, J. Coll. Sci., Vol. 7, No. 4, pp. 428-442.

Freundlich, H. (1926). "Colloid and Capillary Chemistry", p. 158.

Fuerstenau, D.W. (1957). Correlation of Contact Angles, Adsorption Density, Zeta Potentials and Flotation Rate, Trans. AIME., Vol. 208, pp. 1365-1367.

Fuerstenau, M.C. (1978). Thiol Collector Adsorption Processes. In: The Physical Chemistry of Mineral-Reagent Interactions in Sulfide Flotation. Proceedings of Symposium, April 6-7, 1978, Information Circular 8818, U.S., Bureau of Mines, pp. 7-24.

Fuerstenau, M.C. (1980). Communicated by Hoover, M.R. (1980). In: Complex Sulphide Ores. IMM., (Jones, M.J.; Editor), London, p. 104.

Garrels, R.M. and Christ, C.L. (1965). "Solutions, Minerals and Equilibria", Harper and Row, New York.

Gaudin, A.M. (1932;1957). "Flotation", 1st and 2nd Edition, McGraw-Hill Book Co., New York.

Gaudin, A.M., Miaw, H.L. and Spedden, H.R. (1957). Native Floatability and Crystal Structure. In: Pro. 2nd Intern. Congr. of Surface Activity. Vol. III, (J.H. Schulman; Editor), Butterworths Sci. Publ., London, pp. 202-219,

Gaudin, A.M. and Sun, S.C. (1946). Correlation Between Mineral Behaviour in Catapharesis and in Flotation. Trans. AIME, Vol. 169, pp. 347-362.

Gaudin, A.M. and Wilkinson, W.D. (1933). Surface Actions of Some Sulfur-Bearing Organic Compounds on Some Finely-Ground Sulfide Minerals. J. Phys. Chem., Vol. 37, pp. 833-845.

Gilroy, D. and Mayne, J.E.O. (1962). The De-Aeration of Aqueous Solutions. J. Appl. Chem., Vol. 12, pp. 382-384.

Gouy, G. (1910). Constitution of the Electric Charge at the Surface of an Electrolyte, J. Phys., Vol. 9, No. 4, pp. 457-467.

Grahame, D.C. (1954). Differential Capacity of Mercury in Aqueous Sodium Fluoride Solutions. I. Effect of Concentration at 25°C, J. Amer. Chem. Soc., Vol. 76, pp. 4819-4823.

Gray, V.R. (1962). The wettability of Wood, Forest Prod. J., Vol. 12, p. 452.

Gregg, S.J. (1951). "The Surface Chemistry of Solids", Reinhold, New York.

Hamilton, W.C. (1972). A Technique for the Characterization of Hydrophilic Solid Surfaces, J. Coll. Interface Sci., Vol. 40, No. 2, pp. 219-222.

Hamilton, W.C. (1974). Measurement of the Polar Force Contribution to Adhesive Bonding, J. Coll. Interface Sci., Vol. 47, No. , pp. 672.

Harkins, W.D. (1952). "The Physical Chemistry of Surface Films", Reinhold, New York.

Healy, T.W. and Moignard, M.S. (1976). A Review of Electrokinetic Studies of Metal Sulphides. In: Flotation, A.M Gaudin Memorial Volume, Vol. 1, (M.C. Fuerstenau; Editor), AIME, New York, pp. 275-297.

Helmholtz, H.L.F. (1879). Wiss. Abh. Phys. Tech. Reichsanst, Vol. 1, p. 925.

Holden, A. and Singer, P. (1960). "Crystals and Crystal Growing". Science Study Series, Anchor Books, Doubleday and Company, Inc., New York.

Hoover, R.M. and Malhotra, D. (1976). Emulsion Flotation of Molybdenite. In: Flotation. A.M. Gaudin Memorial Volume, Vol. 1, (M.C. Fuerstenau; Editor), AIME, New York, pp. 485-505.

Iskra, J. and Laskowski, J. (1967). New Possibilities for Investigating Air-Oxidation of Coal Surfaces at Low Temperatures, Fuel, Vol. 46, No. 1, pp. 5-12.

Janczuk, B. and Chibowski, E. (1983). Interpretation of Contact Angle in Solid-Hydrocarbon-Water System. J. Coll. Interface Sci., Vol. 95, No. 1, pp. 268-270.

Janczuk, B., Chibowski, E., and Staszczuk, P. (1983). Determination of Surface Free Energy Components of Marble, J. Coll. Interface Sci., Vol. 96, No. 1, pp. 1-6.

Jessop, R.R. and Stretton, J.L. (1969). Electrokinetic Measurements on Coal and a Criterion for its Hydrophobicity, Fuel, Vol. 69, No. 1, pp. 317-320.

Johnson, R.E. and Dettre, R.H. (1969). Wettability and Contact Angles. In: Surface and Colloid Science, (E. Matijevic; Editor), Vol. 2, pp. 85-153.

Johnston, R.R.M. and Moore, A.J.W. (1964). Water Adsorption on Molybdenum Disulfide Containing Surface Contaminants. J. Phys. Chem., Vol. 68, pp. 3399-3405.

Kelebek, S. (1980). Surface Chemistry of Coal Flotation Systems. M. Eng. Thesis, Dept. Min. and Metall. Eng., McGill Univ., Montreal.

Kelebek, S., Salman, T., and Smith, G.W. (1982a). An Electrokinetic Study of Three Coals, Can. Met. Quart., Vol. 21, No. 2, pp. 205-209.

Kelebek, S., Salman, T., and Smith, G.W. (1982b). Interfacial Phenomena in Coal Flotation Systems. In: Proc. 64th CIC Coal Symposium, (A.M.Al Taweel; Editor), Can. Soc. Chem. Eng., pp. 145-152.

Kiselev, A.V. (1968). Adsorption Properties of Hydrophobic Surfaces. J. Coll. Interface Sci., Vol. 28, No. 314, pp. 430-442.

Kitchener, J.A. (1974). Discussion of the paper by Rao (1974). Minerals Sci. Engng., Vol. 6, No. 4, pp. 245-246.

Klasson, V.I. and Mokrousov, V.A. (1963). "An Introduction to the Theory of Flotation". (Transl.; J. Leja and G.W. Poling), Butterworths, London.

Kruyt, H.R., Editor, (1952). "Colloid Science", Elsevier, Amsterdam.

Kulkarni, R.D. and Somasundaran, P. (1975). Kinetics of Collector Adsorption at the Liquid/Air Interface and its Role in Hematite Flotation. In: Advances in Interfacial Phenomena of Particulate/Solution/Gas Systems; Applications to Flotation Research (P. Somasundaran and R.B. Grieves; Editors) AIChE Symposium Series, No. 150, Vol. 71, pp. 124-133.

Laskowski, J. (1974). Particle-Bubble Attachment in Flotation. Minerals. Sci. Engng., Vol. 6, No. 4, pp. 223-235.

Leja, J. (1982). "Surface Chemistry of Froth Flotation". Plenum Press, New York.

Leja, J. and Poling, G.W. (1960). On the Interpretation of Contact Angle. In: Proc. 5th Intern. Miner. Process. Congr. IMM, London, pp. 325-341.

Lekki, J. and Laskowski, J. (1971). On the Dynamic Effect of Frother-Collector Joint Action in Flotation. Trans. IMM., Vol. 80, pp. C174-180.

Lozyk, G.M. (1978). The Surface Chemistry of Sphalerite Flotation, M. Eng. Thesis, Dept. Min. Metall. Eng., McGill Univ., Montreal.

McGlashan, D.W., Rovig, A.D., and Podobnik, D.M. (1969). Assessment of Interfacial Reactions of Chalcopyrite. AIME., Vol. 244, pp. 446-452.

McHardy, J.C. (1972). Surface Chemistry of Talc Flotation. M. Eng. Thesis, Dept. Min. Metall. Eng., McGill Univ., Montreal.

McHardy, J.C. and Salman, T. (1974). Some Aspects of the Surface Chemistry of Talc Flotation. Trans. IMM., Vol. 83, pp. C25-30.

Murphy, W.J. Roberts, M.W., and Ross, J.R.H. (1972). Contact Angle Studies of Some Low Energy Polymer Surfaces. J. Chem. Soc. Faraday Trans. I, Vol. 68, pp. 1190-1199.

Neville, P.C. and Hunter, R.J. (1976). The Control of Slime Coatings in Mineral Processing. Paper presented to 4th RACI Electrochem. Conf., Adelaide, 1976.

Olsen, D.A., Moravec, R.W., and Osterhaas, A.J. (1967). The Critical Surface Tension Values of Group VIA Elements. J. Phys. Chem. Vol. 71, pp. 4464-4466.

Ottewill, R.H. and Vincent, B. (1972). Colloid and Surface Chemistry of Polymer Lattices. Part 1. Adsorption and Wetting Behaviour of n-Alkanols. J. Chem. Soc. Faraday Trans., Vol. 68, pp. 1533-1543.

Parekh, B.K. (1972). Contact Angle Studies of Minerals Coated with Surfactants, M. Sci. Thesis, Penn. State Univ., PA.

Parekh, B.K. and Aplan, F.F. (1974). Wetting Properties of Minerals Coated with Surfactants. In: Proc. CIC Flocculation and Dispersion Symposium, p. 21.

Parekh, B.K. and Aplan, F.F. (1978). The Critical Surface Tension of Wetting of Coal. In: Recent Developments in Separation Science, (N.N.Li; Editor), Vol. IV, pp. 107-113.

Parks, G.A. (1965). The Isoelectric Points of Solid Oxides, Solid Hydroxides and Aqueous Hydroxo Complex Systems. Chem. Reviews, Vol. 65, pp. 177-198.

Parks, G.A. and de Bruyn, P.L. (1962). The Zero Point of Charge of Oxides. J. Phys. Chem., Vol. 66, p. 967.

Partridge, A.C. and Smith, G.W. (1971). Small-Sample Flotation Testing: a New Cell. Trans. IMM, Vol. 80, pp. C199-200.

Philippoff, W., Cooke, S.R.B., and Cadwell, D.E. (1952). Contact Angles and Surface Coverage. Trans. AIME, Min. Eng., No. 4, pp. 283-286.

Plaksin, I.N. (1959). Interaction of Minerals with Gases and Reagents. Trans. AIME, Min. Eng., No. 4, pp. 319-324.

Plante, E.C. and Sutherland, K.L. (1949). Effects of Oxidation of Sulfide Minerals on their Flotation Properties. Trans. AIME, Vol. 183, pp. 160-188.

Raghavan, S. and Hsu, L.L. (1984). Factors Affecting the Flotation Recovery of Molybdenite from Porphyry Copper Ores. Intern. J. Miner. Process., Vol. 12, pp. 145-162.

Rao, S.R. (1974). Surface Forces in Flotation. Minerals Sci. Engng., Vol. 6, No. 1, pp. 45-53.

Richardson, P.E. and Edelstein, D.L. (1978). The Effect of the Space Charge Layer of Galena on the Kinetics of the Oxygen Reduction Reaction. In: The Physical Chemistry of Mineral-Reagent Interactions in Sulfide Flotation. Proceedings of Symposium. April 6-7, 1978, Information Circular 8818, U.S. Bureau of Mines, pp. 72-99.

Rogers, J. (1962). Principles of Sulphide Mineral Flotation. In: Froth Flotation-50th Anniversary Volume, (D.W. Fuerstenau; Editor), AIME, New York, pp. 139-169.

Senkan, S.M. and Fuller, Jr. E.L. (1979). Effect of NaOH Treatment on the Surface Properties of Coal, Fuel, Vol. 58, No. 10, pp. 729-731.

Shafrin, E.G. and Zisman, W.A. (1960). Constitutive Relations in the Wetting of Low Energy Surfaces and the Theory of the Retraction Method of Preparing Monolayers, J. Phys. Chem., Vol. 64, pp. 519-524.

Sheludko, A. (1963). Zur Theorie der Flotation, Kolloid Z., Vol. 191, pp. 52-58.

Sheludko, A., Tosheve, B.V., and Bojadiev, D. (1976). Attachment of Particles to a Liquid Surface, Faraday Trans. I, Vol. 72, pp. 2815-2828.

Smith, G.W. and Salman, T. (1966). Zero-Point-of-Charge of Hematite and Zirconia, Can. Met. Quart., Vol. 5, No. 2, pp. 93-107.

Smoluchowski, M.V. (1914). In: Handbook der Electrizidat und des Magnetismus. (L.L. Graetz; Editor), Vol. 2, Barth, Leipzig.

Somasundaran, P. (1968). The Relationship Between Adsorption at Different Interfaces and Flotation Behaviour, Trans. SME/AIME, Vol. 241, pp. 105-108.

Stern, O. (1924). The Theory of the Electrolytic Double Layer. Z. Electrochem., Vol. 30, pp. 508-516.

Sutherland, K.L. and Wark, I.W. (1955). "Principles of Flotation". Australasian IMM, Melbourne.

Taggart, A.F. (1945). "Handbook of Mineral Dressing-Ores and Industrial Minerals". John Wiley and Sons, Inc., New York, pp. (5) 118-119..

Taggart, A.F., Taylor, T.C., and Ince, C.R. (1930). Experiments with Flotation Reagents, Trans. AIMME, Vol. 87, pp. 285-386.

Tamai, Y. (1976). Surface Energy Analysis of Solids and its Application. Progr. Coll. Polymer Sci., Vol. 61, pp. 93-96.

Tamai, Y., Makuuchi, K., and Suzuki, M. (1967). Experimental Analysis of Interfacial Forces at the Plane Surface of Solids. J. Phys. Chem., Vol. 71, pp. 4176-4183.

Verwey, E.J.W. and Overbeek, J. Th.G. (1948). "Theory of the Stability of Lyophobic Colloids", Elsevier, Amsterdam.

Wark, I.W. and Cox, A.B. (1934). Principles of Flotation. I. An Experimental Study of the Effect of Xanthates on the Contact Angles at Mineral Surfaces. Trans. AIME, Vol. 112, pp. 189-244.

Weast, R.C. (Editor), (1981-82). Handbook of Physics and Chemistry, CRC Press, West Palm Beach, Florida.

Wenzel, R.N. (1936). Resistence of Solid Surfaces to Wetting by Water. Ind. Eng. Chem., Vol. 28, No. 8, pp. 988-994.

Woodfill, J.C. (1966). Flotation of Naturally Hydrophobic Minerals. M.Sc. Thesis, Univ. California, Berkeley.

Yarar, B. and Kitchener, J.A. (1970). Selective Flocculation of Minerals: 1. Basic Principles; 2. Experimental Investigation of Quartz, Calcite and Galena, Trans. IMM, Vol. 79, pp. C23-33.

Yarar, B. and Leja, J. (1982). Correlation of Zeta Potential and Floatability of Weathered Coal, paper presented at the SME/AIME Annual Meeting, Dallas, preprint No. 82-44.

Yen, W.T., Chahal, R.S., and Salman, T. (1973). Wettability of Modified Silica Surfaces, Can. Met. Quart., Vol. 12, No. 3, pp. 231-243.

Yokoyama, T., Urayama, K., and Yokoyama, T. (1983). Ultra-Fine Grinding and Consequent Changes of Power Characteristics. Kona; Powder Sci. Technol. in Japan, No. 1, pp. 53-63.

Yucesoy, A. and Yarar, B. (1974). Zeta Potential Measurements in the Galena-Xanthate-Oxygen System, Trans. IMM, Vol. 83, pp. C96-100.

Zettlemoyer, A.C. (1968). Hydrophobic Surfaces (Kendall Award Address, Amer. Chem. Soc.), J. Coll. Interface Sci., Vol. 28, No.3/4, pp. 343.369.

Zisman, W.A. (1964). Relation of Equilibrium Contact Angle to Liquid and Solid Constitution. In: Contact Angle, Wettability, and Adhesion, (R.F. Gould; Editor), Advances in Chemistry Series No. 43, Amer. Chem. Soc., pp. 1-51.

Zisman, W.A. (1975). Recent Advances in Wetting and Adhesion. Adhesion Sci. Technol. (L.H. Lee; Editor), Polym. Sci. Technol., Vol. 9A, Plenum Press, pp. 55-91.

CHAPTER 3

PROPERTIES OF AQUEOUS METHANOL SOLUTIONS

3.1 REVIEW

Methanol was the principal reagent employed in order to obtain wettability data for the construction of adhesion tension diagrams of a number of inherently hydrophobic solids. Also it has been used to control the bubble surface tension in flotation tests. Because of the importance of the liquid phase in these tests, a brief review of some essential properties of methanol and its aqueous solutions is provided. In the following section, both the bulk and surface properties of these solutions will be discussed. The data provided will be applied in the subsequent chapters.

3.1.1. Chemistry of Methanol

Methanol is the first member of the homolog series of monohydric alcohols. It was discovered in 1661 by Boyle among the distillation products of hardwood and its structure was identified in 1831 by Dumas and Peligot (Monick, 1968). It is also known by the names 'wood spirit' and 'carbinol'. The most important commercial process for the production of methanol is the catalytic reduction of carbon monoxide with hydrogen in the

Fischer-Tropsch reaction:

$$CO + 2H_2 \longrightarrow CH_3OH \qquad \Delta H_{298} = -5183 \text{ Joules} \qquad 3.1$$

It is one of the most commonly used alcohols in chemical industries as solvent, antifreeze additive, chemical intermediate etc. It is a colorless, neutral, flammable, volatile alcohol and is labeled a poison under federal and state laws because of its potential damage to the central nervous system (specifically to the optic nerve causing blindness ultimately).

3.1.2. Molecular Structures of Water and Methanol

Both methanol and water have polar molecules and are similar in structure. One might view the former as the methyl (CH_3-) derivative of the latter. Simple structural models are given in Figure (3.1). For water, the atoms are shown as spheres with radii equal to their van der Waals radii. The model for methanol was used recently by Pratt and Chandler (1980) in a study of hydrophobic interactions. It was constructed as a fusion product of a hard-sphere A representing the methyl group and a water molecule. The van der Waals' diameter of methyl group was taken as 3.7 A°, i.e. the same as that of methane. This figure is reported to be about 4.0 A° by Pauling (1960a). Molecular parameters of methanol as determined by Ivash and Dennison (1953) and Venkateswarlu and Gordy (1955) are compared with those of water in Table (3.1). The bond length for O-H and the values determined for the C-O-H and H-O-H angles in methanol and water respectively are very close to each other.

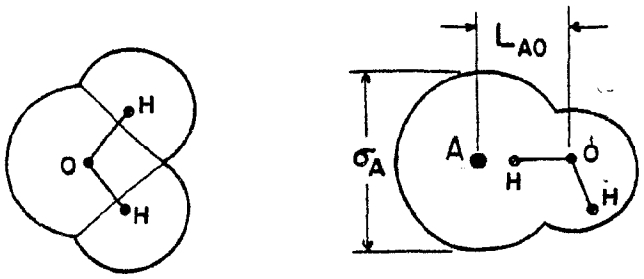


Figure 3.1 Schematic Drawings of Water (left) and Methanol (right) Molecules

Table 3.1

Molecular Structures of Methanol and Water

Methanol		Water
Ivash and Dennison (1953)	Venkateswarlu and Gordy (1955)	Pauling (1960)
d_{OH} = 0.0937 nm	0.0956 nm	0.096 nm
d_{CO} = 0.1434 nm	0.1427 nm	
d_{CH} = 0.1093 nm	0.1996 nm	
<HCH = 109° 30'	109°2'	<HOH = 104° 45'
<COH = 105° 56'	108°52'	

Structural similarity between methanol and water is reflected in some of their common behavior. They are both associated liquids and show hydrogen bond formation. An interesting feature of methanol is its ability to form crystalline structures with salts. For example, $MgCl_2.6\ CH_3OH$ is such a structure (Monick, 1968) similar to $MgCl_2.6\ H_2O$.

3.1.3. Hydrogen-Bond Formation

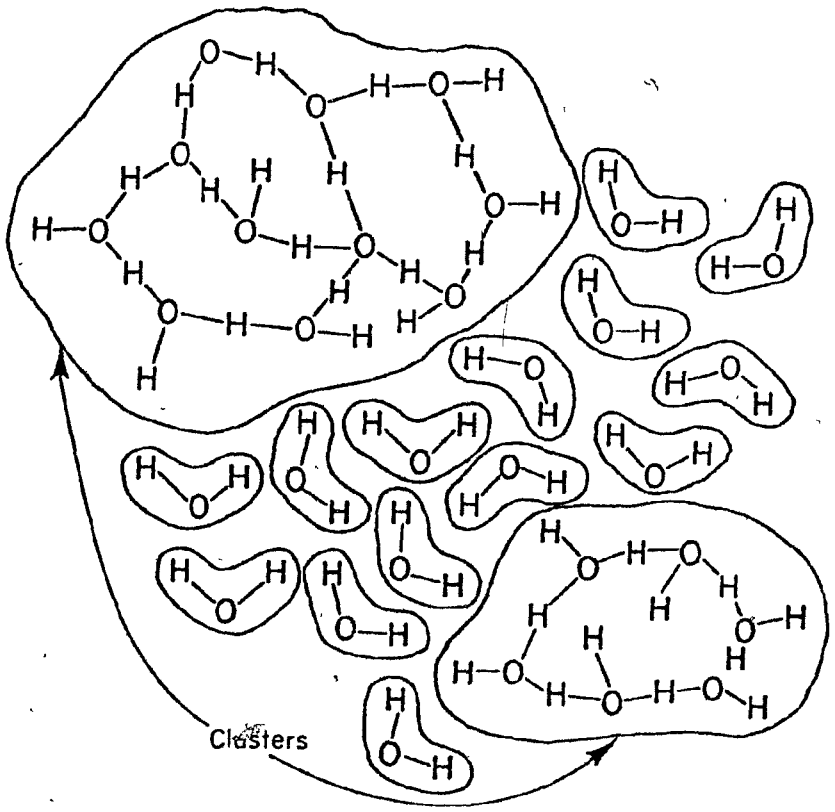
The bond formed when a proton (i.e. hydrogen) acts as a link between two electronegative atoms is known as a hydrogen bond. The ability and power of an atom to form a hydrogen bond increases with an increase in its electronegativity and with a decrease in its size (Pauling, 1960b). On the electronegativity scale of elements introduced by Pauling, oxygen with an assigned electronegativity of 3.5, is the second most powerful atom (to fluorine, 4.0) to participate in hydrogen-bond formation. Water and methanol are thus capable of a significant degree of hydrogen-bonding. The hydrogen bond is a distinctly directional and specific interaction. The enthalpy of hydrogen-bonds depending on the participating atoms falls in the range of 4.2 to 42 kJ/mole, i.e. 1-10 kcal/mole (Vinogradov and Linnell, 1971). In the case of water and methanol, it is about 21 kJ/mole (Pauling, 1960c) which translates into about $3.5x15^8$ pJ per single hydrogen-bond.

Formation or breakage of hydrogen-bonds is also temperature dependent. According to Luck (1967) 10-15% of hydrogen-bonds

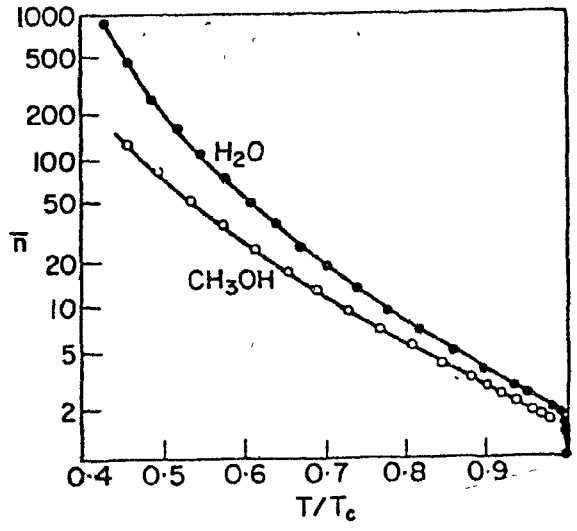
are ruptured when ice melts. At room temperature, as many as 80% of the hydrogen bonds may be in operation for liquid water. Some water molecules remain in the free state (monomer), the others may be in a dimer, trimer etc. or in a many molecular cluster form. Figure (3.2a) is the schematic illustration of cluster model for water proposed by Nemethy and Scheraga (1962) which shows monomer water molecules between two clusters with different sizes.

Methanol is expected to form more or less similar structures by hydrogen bonding. However, the degree of hydrogen-bonding may not be as large as that of water. One reason for this may be some degree of hydrophobic interaction due to non-polar methyl groups. These considerations are in line with the model calculations reported by Luck (1967) which are reproduced in Figure (3.2b). This illustrates that, at a given temperature T, the average number of methanol molecules in hydrogen-bonded aggregates, $\bar{n}$, in liquid is lower than those of water (i.e. the size of methanol clusters are smaller). The structure of the clusters is usually complex because of the large number of possible combinations. As shown in Figure (3.3) hydrogen-bonded formations can be open or cyclic (Vinogradov and Linnell, 1971) or combinations of both, thus creating the highly complicated clusters of varying sizes.

In binary mixtures of water and methanol, hydrogen-bonds are expected to function between water and methanol molecules



(a)



(b)

Figure 3.2 (a) Cluster Model for Water, (b) Mean Size of Hydrogen Bonded Aggregates, $\bar{n}$ in Liquid Water and Methanol

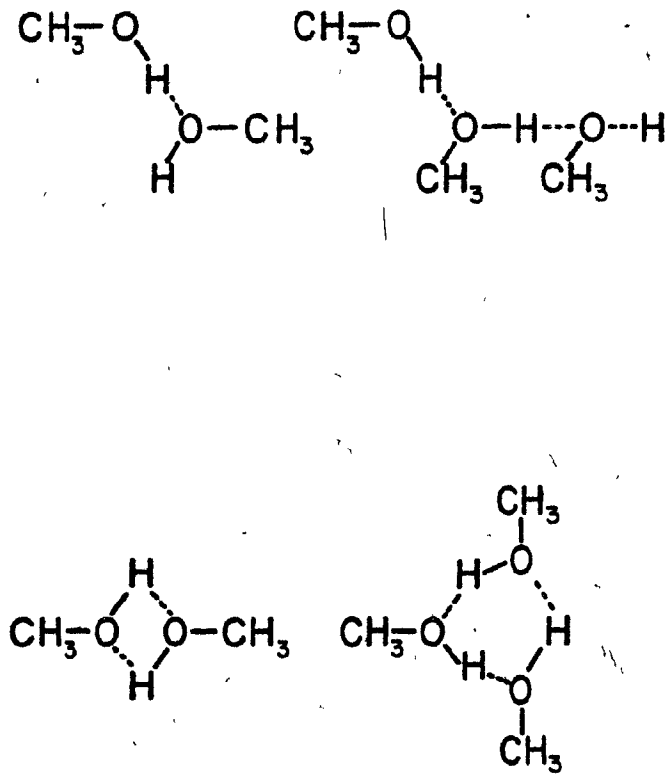
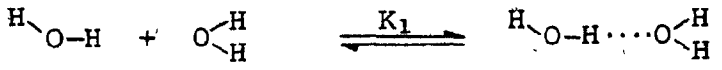
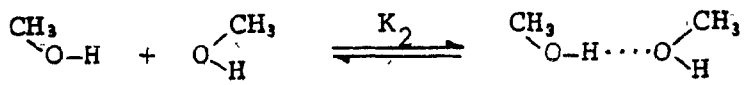


Figure 3.3 Hydrogen Bonded Formations in Methanol; Open (top) and Cyclic (bottom) Structures.

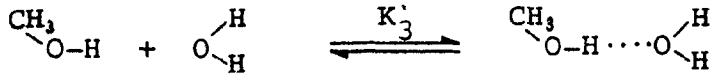
as well as between similar molecules. The reactions for hydrogen bond formation may be described as:-



3.2



3.3



3.4

These reactions produce the dimer structure which is the simplest case. The equilibrium constant for the association between methanol and water can be written as:-

$$K = \frac{[CH_3O\text{-}H...OHH]}{[CH_3OH]\,[H_2O]} \qquad 3.5$$

Equilibria concerning the formation of methanol-water multimers in binary solutions are presumably very complex. They involve rupture of some hydrogen-bonds in methanol and water aggregates first, then, the formation of hydrogen-bonds between water and methanol molecules. These structural rearrangements, accompanied by the liberation of heat (exothermic reactions) play a significant part in the determination of certain physical properties such as viscosity.

3.1.4. Viscosity

The viscosity of a liquid is a measure of its resistance to shear or angular deformation. The coefficient of viscosity, μ, expressed in poise is the ratio of the shearing stress to

rate of shear. At constant pressure, the viscosity of most liquids is given by the Arrhenius relation.

$$\mu = Ae^{E/RT} \qquad 3.6$$

where μ is the coefficient of viscosity, A a constant, E the activation energy for viscous flow, R the gas constant, and T is the the absolute temperature. E for water at 20°C is given as 1.0 KJoule/mol (Eisenberg and Kauzmann 1969). For methanol, it has been recently reported to be 0.62 KJ/mol in the range 0-30°C (D'Aprano et al. 1979).

Since viscosity is a measure of resistance of liquid to flow it should provide some information on the nature of structural arrangement of molecules. A greater viscosity means that hydrogen-bonded aggregates (clusters) in liquid have become more bulky, hence showing an increase in flow resistance. This is supported by the results given in Figure (3.2b) which simply indicates that the degree of polymerization in water ($\mu \triangleq$ 0.89 cp at 25°C) is larger than that in methanol ($\mu \triangleq$ 0.55 cp at 25°C). The viscosity of water-methanol mixtures was determined by Carr and Riddick (1951) as a function of methanol mole fraction (Figure 3.4)). It is interesting to note that the mixtures have higher viscosities than their individual components. Viscosity increases almost linearly with concentration in dilute range for both methanol-rich and water-rich solutions. It goes through a maximum at about 0.28 methanol mole fraction. The mechanism causing this behavior can be understood by considering the likely

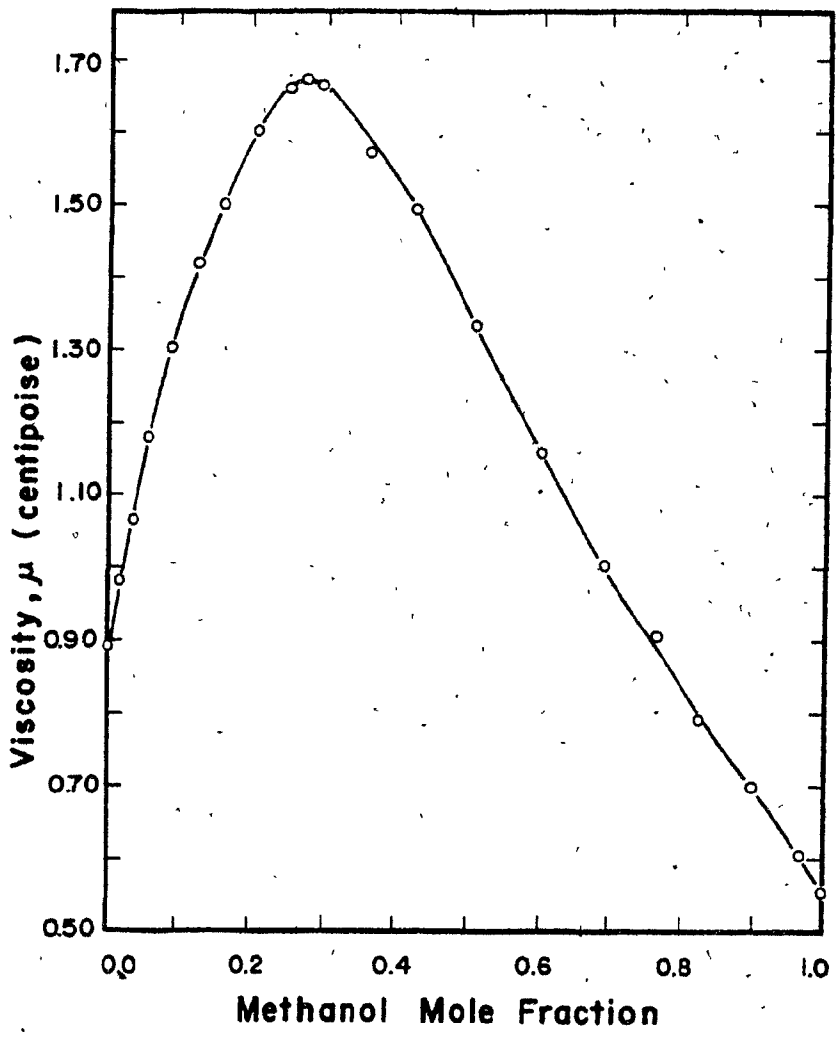


Figure 3.4 Viscosity of Aqueous Methanol Solutions as a Function of Methanol Mole Fraction

structural rearrangements taking place upon mixing.

It was stated in the previous section that both water and methanol have their characteristic molecular association constants (K_1 and K_2 respectively) describing complicated equilibria between hydrogen-bonded formations and free molecules. During mixing of the two species, individual equilibria change and finally a new equilibrium is set up as a result of newly formed clusters including water and methanol. It is mandatory, therefore, that structural rearrangements involve the rupture of some hydrogen bonds, i.e., $H_2O...H_2O$ and $CH_3HO...HOCH_3$ (depolymerization) and formation of new ones, i.e., $CH_3OH...H_2O$ (co-polymerization). Consequently, the increase in viscosity is probably due to the co-polymerization product (i.e. co-molecular cluster) which may have a larger molecular structure than the homo-molecular clusters of water and methanol prior to mixing. Generally, viscosity increases with an increase in molecular weight for a number of compounds in homolog series such as the alcohols (Monick, 1967).

3.1.5. Thermodynamics of Mixing

Methanol and water are completely soluble in each other. Dissolution occurs with great affinity and in certain compositions with significant evolution of heat. Thus, when a binary mixture is made an increase can be observed in its temperature. The heat that is liberated upon mixing two pure liquids to each other can be measured calorimetrically. The heat of mixing, ΔH^M for aqueous methanol solutions is available for various

compositions, temperatures and pressures (Christensen et al., 1982). The results obtained by Mato and Berrueta (1977) using an isothermal displacement calorimeter at 25°C are plotted as a function of methanol mole fraction in Figure (3.5). The experimental error is reported to be less than 0.4%. The empirical equation based on these measurements is as follows:

$$\Delta H^M = X_w X_m \ (-7229.3 + 13{,}071 X_m - 10{,}315 X_m^2 + 1040.6 X_m^3) \qquad 3.7$$

where ΔH^M is the heat of mixing (in Joule/mole). X_w and X_m are the mole fraction of water and methanol respectively.

For ideal solutions (i.e., obeying Raoult's law), $\Delta H^M = 0$. Thus, the measured ΔH values given above are known as excess heat of mixing, ΔH^{XS}, an important thermodynamic term characterizing the non-ideal behavior of binary solutions ($\Delta H^M \equiv \Delta H^{XS}$). Similarly, there is an excess free energy of mixing, ΔG^{XS} and an excess entropy of mixing, ΔS^{XS}. For any binary solution, the former can be expressed as follows (Reid et al., 1977):

$$\Delta G^{XS} = RT \ (X_m \ln f_m + X_w \ln f_w) \qquad 3.8$$

where f_m and f_w are the activity coefficients of two components making up the solution, R gas constant, T absolute temperature, X_m and X_w are the respective mole fractions. The activity coefficients were determined from the vapor pressure data. The ΔH^{XS} and ΔG^{XS} are related by the familiar equation,

$$\Delta G^{XS} = \Delta H^{XS} - T\Delta S^{XS} \qquad 3.9$$

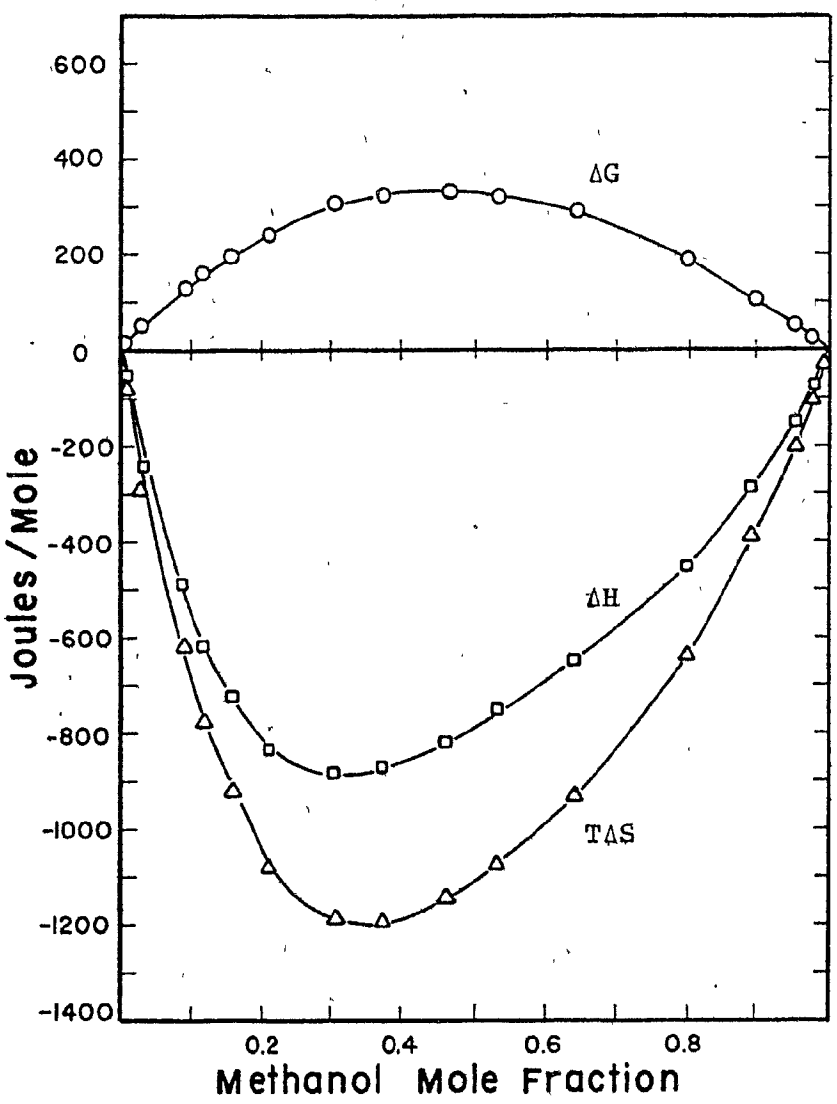


Figure 3.5 Thermodynamic Excess Functions for Mixing Between Water and Methanol (25°C).

which permits the calculation of excess entropy function for the mixing. Calculated ΔG^{XS} and $T\Delta S^{XS}$ values (Appendix III) are plotted on the same graph as ΔH^{M} values (Figure 3.5). The results are comparable with those obtained for the system ethanol-water(Frank and Ives, 1966). All the excess functions are similar in shape.

In general, negative heat of mixing values for both systems are attributed to the preferential hydrogen bonding between the alcohol and water molecules at the expense of the hydrogen bonds in the water and alcohol structures prior to mixing. However, a detailed examination of general thermodynamic properties of the alcohol-water mixtures (Franks and Ives, 1966; Franks, 1967) emphasizes that to what extent the breakdown of water structure occurs, if any, is not certain. It appears that the mechanisms leading to the formation of the alcohol-water structures may be different in alcohol-rich composition ranges than in water-rich ones. One of the main difficulties which arises is the lack of clear understanding of nature of individual liquid structures.

3.1.6. Vapor Pressures

For a solution which is in equilibrium with its vapor, the chemical potentials of any component of the solution in the vapor and in the solution are equal.

$$\mu_i^{vap} = \mu_i^{soln.} \qquad 3.10$$

Chemical potential of methanol in water can be expressed

by the following relation (Atkins, 1978).

$$\mu_M = \mu_M^o + RT \ln \left(\frac{P_M}{P_M^o}\right) \qquad 3.11$$

where P_M^o is the vapor pressure of pure methanol, P_M its vapor pressure for the aqueous solution, μ_M^o is the standard chemical potential of methanol, and R and T are the Universal gas constant and absolute temperature. For ideal solutions, Raoult's Law states that

$$\frac{P_i}{P_i^o} = X_i \qquad 3.12$$

where X_i is the mole fraction. However, few solutions behave ideally. In non-ideal behaviour the mole fraction X is replaced by the activity α. For the methanol-water binary system

$$\frac{P_M}{P_M^o} = \alpha_M = f_M \cdot X_M \qquad 3.13$$

$$\frac{P_W}{P_W^o} = \alpha_W = f_W \cdot X_W \qquad 3.14$$

where f_M and f_W are activity coefficients of methanol and water in solution respectively. Thus, the relationship between partial vapour pressures and activity coefficients for aqueous methanol solutions may be used to determine activity. The vapor pressure data at 25°C by Butler et al. (1933) and Hall et al. (1979) are plotted in Figure (3.6). It can be noted that Raoult's Law is obeyed only in very concentrated compositions (both for water and methanol).

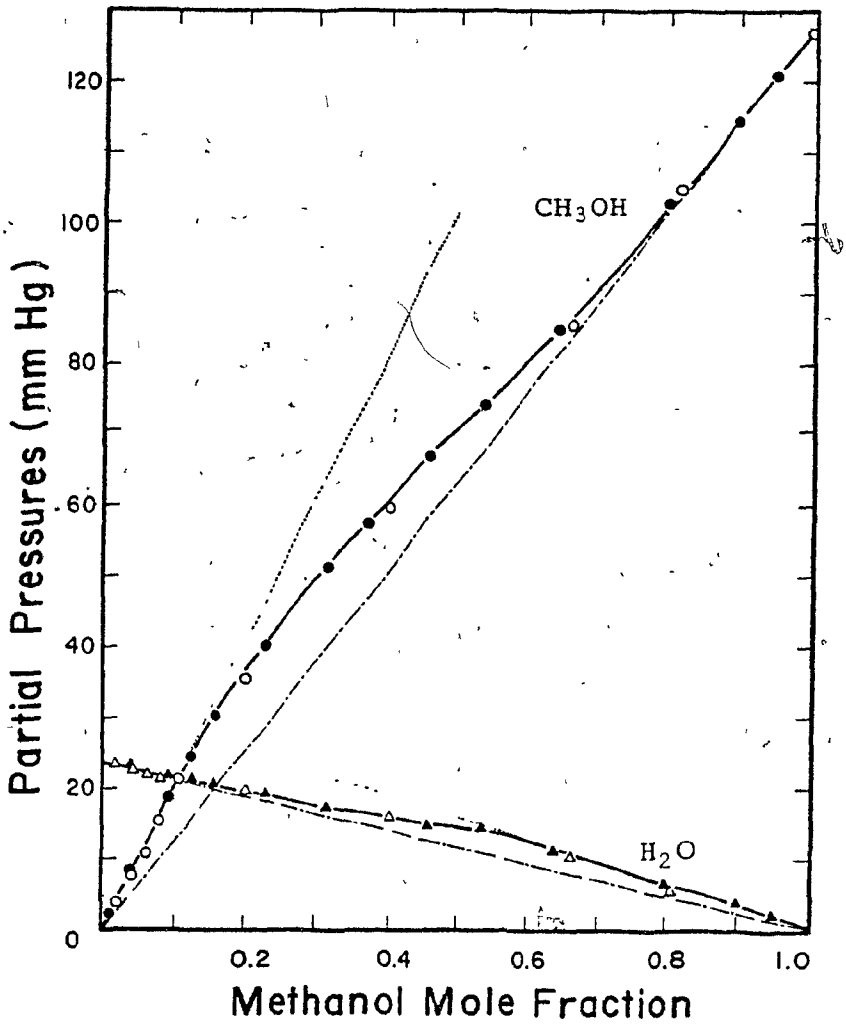


Figure 3.6 The Equilibrium Partial Pressures of Methanol and Water Over Aqueous Methanol Solutions (25°C)

In dilute solutions, Henry's Law (indicated by dotted line) is obeyed.

Figure 3.7 shows the amounts of methanol in vapor in equilibrium with the solutions of varying compositions (Hall et al. (1979)). This figure emphasizes the degree of volatility of methanol at various aqueous compositions and is useful in predicting the vapor composition of bubbles during flotation. For instance, consider an aqueous methanol solution at 0.12 methanol mole fraction (i.e. 23.5% methanol by volume). If enough vacuum is applied at the solution surface to generate a bubble in the solution it will be composed of approximately 52% methanol and 48% water vapor by mole or by volume. At this solution composition an air bubble produced in a flotation cell will contain about 3.0% (by vol.) methanol vapor in equilibrium with air and some moisture. As the methanol concentration in solution is increased say to 45%, the equilibrium vapor concentration of methanol inside the air bubbles will increase to about 5.9% (by vol.) (see Appendix III for calculations).

3.1.7. Surface Tension and Molecular Surface Orientation

Because of the unbalanced nature of molecular forces in the surface layer, an increase in surface area demands the expenditure of work. Surface tension is a measure of this work per unit area. Its dimension is dyne/cm (≡ mN/m) or erg/cm^2 (≡ mJ/m^2), the numerical values being equal in both units.

The molecules at the surface layer are distinctly oriented. If molecular orientation is to occur at a liquid

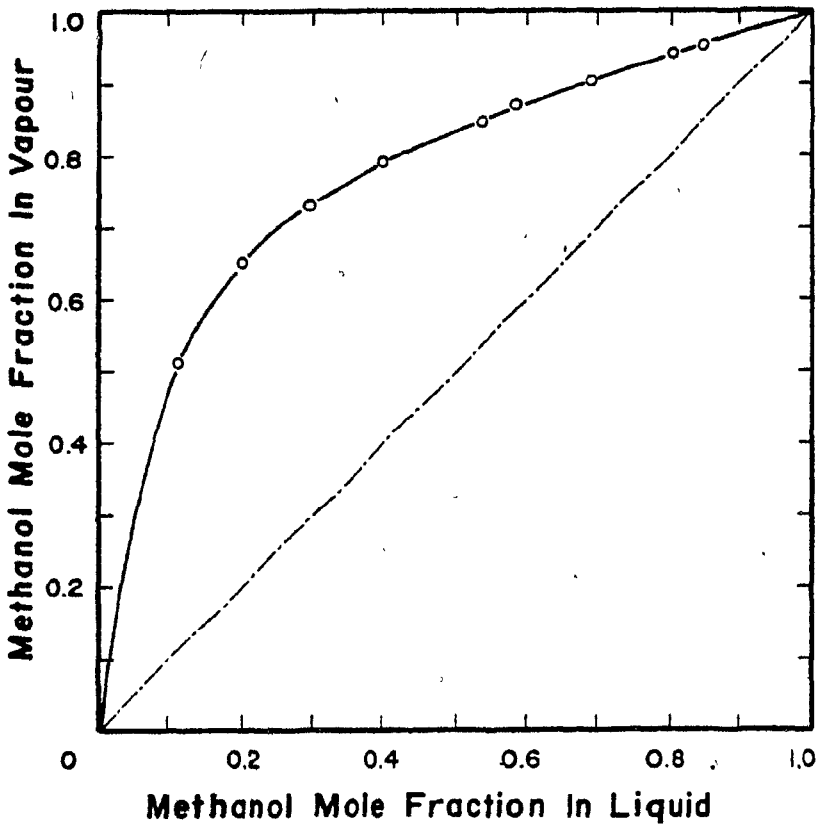


Figure 3.7 Vapour Composition of Aqueous Methanol Solutions as a Function of Methanol Mole Fraction.

surface there must be a decrease in the free energy of the system. In the case of methanol, the molecules are oriented with their methyl groups directed out from the surface. This can be predicted using Langmuir's principles of independent surface action in the same way as was applied to ethanol (Adamson, 1976). This type of orientation is further supported by the experimental observation that the actual surface tension of methanol (~ 22.6 mN/m) is in the order of that of liquid hydrocarbons. Orientation of heteropolar molecules like methanol at the surface is thus predictable. However, whether water molecules will be oriented or not cannot simply be predicted using the same approach as with methanol due to the symmetrical nature of the molecules. This question was studied by Fletcher (1968) who concluded that an oriented surface layer is thermodynamically more stable than is a completely random surface. The preferred surface orientation of water molecules, proposed by Fletcher is that with the hydrogen ions directed outwards at the surface and the driving force for this orientation comes from the long-range electrostatic interactions between water molecules.

In the case of binary mixtures of water and methanol, methanol molecules are concentrated at the solution surface and orient themselves with the hydroxyl groups directed towards the bulk solution. This kind of orientation stabilizes the bubbles and prevents their coalescence in aqueous solutions and also reduces the solution-gas interfacial tension. A wide range of

surface tensions (i.e. 72-23 mN/m) can thus be obtained by mixing the liquids at certain ratios. An important aspect of aqueous methanol solutions appears to be their ability to establish surface tension equilibrium very quickly. Addison (1945) pointed out that the equilibrium was reached so rapidly that dynamic surface tensions could not be measured by the vibrating jet method. A later study with an improved technique by Addison and Elliott (1949) implied that the time for the surface tension equilibrium could be as short as a few milliseconds. This suggests that, during the flotation tests, the air bubbles after their production at the bottom of the cell will presumably have enough time to establish an equilibrium surface tension prior to collisions with particles in flotation.

3.1.8. Frothing and Collecting Properties

It is generally known that frothing results from a change in solution surface tension which is caused by the adsorption and favorable orientation of ions or heteropolar molecules. In spite of having such molecules, methanol solutions do not produce any significant froth layer. Similarly, collecting ability of an alcohol is related to its adsorption and orientation at the solid-liquid interface so as to create at least a partial hydrophobic coating (by its own molecules) strong enough to permit collection by bubbles in flotation. The hydroxyl groups of alcohols are not reactive enough to form strong bonds with the solid surface. They can only attach

themselves through weak hydrogen bonds. In this way, they may enhance the floatability of a naturally hydrophobic mineral by causing a reduction in induction period. Generally, short chained alcohols are regarded as having insignificant collecting properties. Methanol, being the first member of the monodydric alcohols series, should have the least frothing and collecting properties. As noted by Klassen and Mokrousov (1963), frothability of monohydric alcohols depends mainly on the length of the hydrocarbon chain. Mainhood and Whelan (1955) concluded that, for the monohydric alcohols to be good frothers the hydrocarbon chain must contain at least five carbon atoms. Using the frothability index of Sun (1952), an aqueous methanol solution of 0.2% (by weight) was found to have a frothability index of 48. This is higher than that of distilled water which Sun (1952) reported to be 15.4, but lower than that of five carbon chain normal-amyl alcohol, 75. During the present investigation, increasing the methanol concentration caused no significant change in frothability although the surface tension decreased significantly.

3.2 EXPERIMENTAL MATERIALS AND PROCEDURES

Objectives

Surface tensions of aqueous methanol solutions are available only at a limited number of compositions. Handbook of Physics and Chemistry (1981-82) lists only seven surface tension values for methanol solutions. Since there is no model

accurately predicting the solution surface tensions, the use of interpolated values based on these known data lacks confidence. Therefore, for the purpose of the present work a number of surface tension measurements were made at different compositions which were to be used later for the adhesion tension determinations. Adsorption densities of methanol at the solution-gas interface were calculated to investigate their possible relationship with the bubble production.

A second series of experiments on the water-methanol solution involved the determination of bubble size distributions as a function of bubble surface tension. The average bubble size was used to estimate the induction periods during flotation tests.

3.2.1. Solutions

The solutions used in all experiments were prepared with single distilled water obtained from an all pyrex Corning Mega-Pure distillation apparatus. Conductivity of this water was measured to be in the range 0.5 to 1.85 μmhs/cm (22 ± 1.0°C) prior to use. A conductivity meter model RC 16B2 and a standard cell (cell constant 0.1) was used in these measurements.

The methanol (A.C.S. Spec.) was purchased from American Chemical Ltd. in 4-litre bottles. The aqueous methanol solutions were made up by mixing the required amounts of methanol and water. The solutions were cooled down to room temperature (22 ± 2°C) by applying cold tap water when necessary.

The glassware to be used in the experimental work was rigorously cleaned. A typical cleaning procedure involved repeated washing and rinsing operations using acetone (Anachemia, A.C.S. Spec.), hot and cold tap water, leaching in concentrated dichromic acid solution in a 220 Ultra-sonic Bath (Branson Instrument Co., Conn.), and finally thoroughly rinsing with distilled water. Dichromic acid solution was prepared from saturated potassium dichromate (Fisher Sci., cert.) and concentrated sulphuric acid (A.C.S. Spec.).

3.2.2. Method of Surface Tension Measurement

Surface tension of aqueous methanol solutions was determined using the du Noüy ring method (Adamson, 1976). It is a detachment method in common use and is suitable for solutions that achieve surface tension equilibrium rapidly, which appears to be the case for methanol solutions as stated in section 3.1.7. The technique involves the determination of the force required to detach a platinum ring from the solution-gas interface. The ring is pulled upward out of the liquid slowly by applying a steady force. The detachment force may be expressed by the following equation:

$$W_t = W_r + 4\pi R\gamma \qquad 3.15$$

$$W_t - W_r = f = m.g = 4\pi R\gamma \qquad 3.16$$

$$F.f = 4\pi R\gamma \qquad 3.17$$

where

W_t = total weight at the point of detachment

W_i = the weight of the ring

f = the maximum force applied; f=m.g (m:mass, g:980.8 cm s^{-2})

R = the radius of the ring (cm)

γ = surface tension (mN/cm)

F = correction factor

In its elementary form, Equation 3.15 was found to be in error. Harkins and Jordan (1930), and Quidema and Walters (1941) introduced an empirical correction factor which depended upon the radius of the ring, the radius of the wire of the ring, density of the solution, and density of the gas phase above the solution. The platinum ring employed was of 4.009 cm circumference. The radius of the wire was measured to be 0.0135 cm. Densities of the aqueous methanol solutions were taken from Carr and Riddick (1951). Thus, it was possible to obtain a correction factor for each methanol solution prepared. In addition to determination of surface tensions as a function of methanol concentration temperature dependence of surface tension was measured at several compositions. Temperature of the solutions was controlled by means of a water jacket surrounding the beaker containing the solution. At least three measurements were done and the average value obtained was used for the correction. Details concerning the measurement of surface tensions and the calculation of correction factors are given in Appendix III.

3.2.3. Bubble-Size Distribution Cell

In order to determine the bubble size variations as a function of methanol concentration (and thus surface tension), a special glass cell was constructed. Essential features of

this cell were similar to that used for flotation testing. The fritted disc at the bottom of the cell to introduce the bubbles into the cell was originally of fine porosity (1 - 5 μm). The pores were enlarged later by circulating a hydrofloric acid solution (15% by volume) using a suction system. This treatment was applied to both cells simultaneously to keep the pore size distribution approximately the same. This was secured by observing the movement of the air-water interfaces in the cells (both connected to a water pump through a three-way stopcock) with equal speed. A distinguishing feature of the cell (Figure 3.8) is that it has a flat body as opposed to circular body of usual micro-scale flotation cells. For practical purposes, the bottom part of the cell was built circular to facilitate mixing with a magnetic bar. The thickness of the flat part was 1.2 cm. This cell permitted better quality pictures to be taken so that the bubbles could be sized correctly in their original shape. The pictures obtained with circular cells produced distorted bubbles.

3.2.4. Procedure

The bubble size was measured by taking photographs of the front half of the flat cell. The bubbles were produced at an air flow-rate of about 50 ml/min which was kept constant for all bubble size measurement experiments as well as flotation tests. The mineral phase was excluded in these experiments in order not to introduce any complications to the size measurements. As demonstrated by Grainger-Allen (1970), the presence

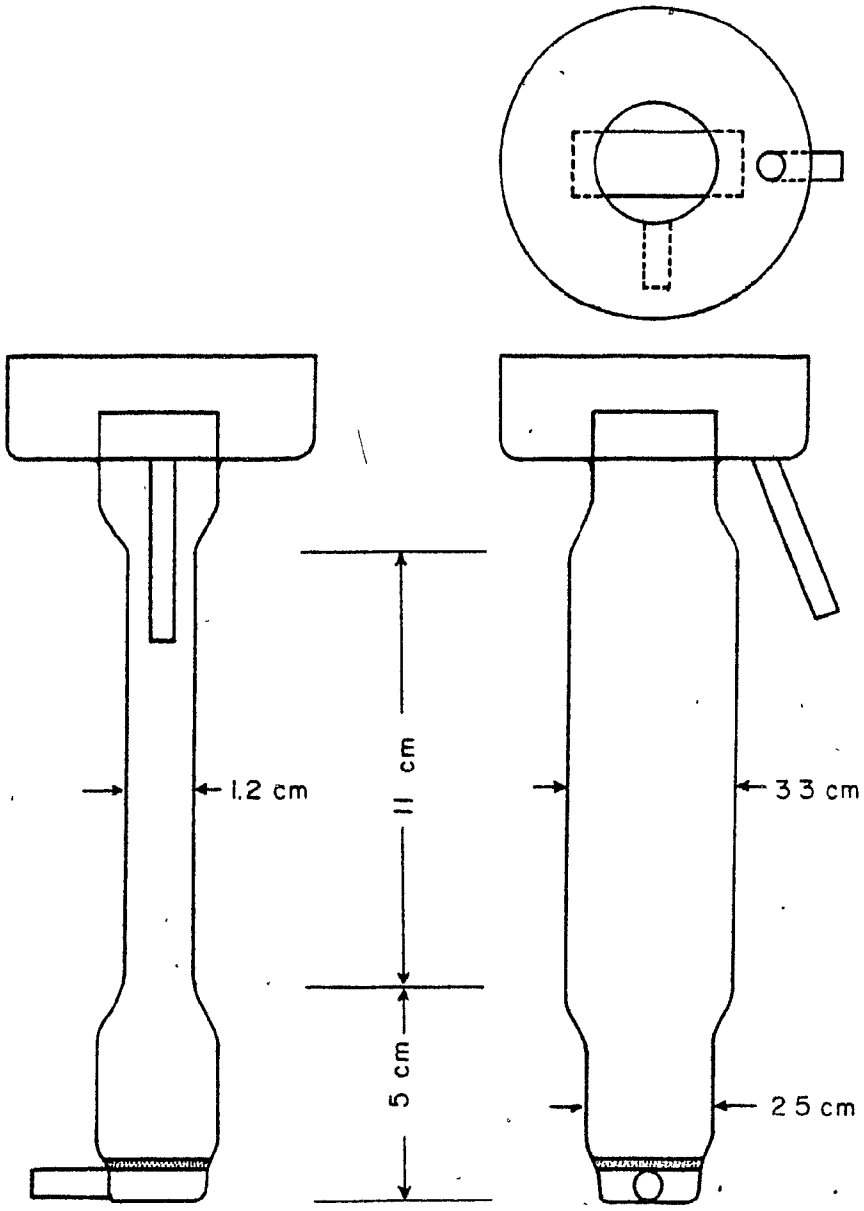


Figure 3.8 Flat Cell Constructed for the Determination of Bubble Size Distribution

of a mineral phase does not affect the bubble formation mechanism. The bubbles were measured visually by means of a grid which was placed at the back wall of the cell as a background. When required, size measurements were carried out under a magnifying glass. To enhance the focussing during the photography the thickness of the cell was limited further by suspending a plate of glass in the cell. The focussing was performed in reference to two scratches made on the front side of the plate of glass and the front wall of the cell respectively. 2 to 4 pictures were taken for each methanol solution using a Minolta camera, (1 millisecond exposure). Bubble diameters were determined for each size class and the size distributions were expressed in the form of block diagrams.

In addition to pictures taken for bubble size determination, traces of bubbles ascending in the cell were photographed at longer exposures (1/30 sec.). However, at this longer shutter speed due to blurry appearance of the bubbles themselves precise diameter measurements were not possible although the velocity of ascent could be determined with sufficient accuracy.

3.3 RESULTS

3.3.1. Surface Tension Measurements

The effect of methanol concentration on the surface tension of its aqueous solutions is shown in Figure 3.9. For practical purposes, the methanol concentration was expressed as per cent by volume. The results are tabulated in Appendix III which

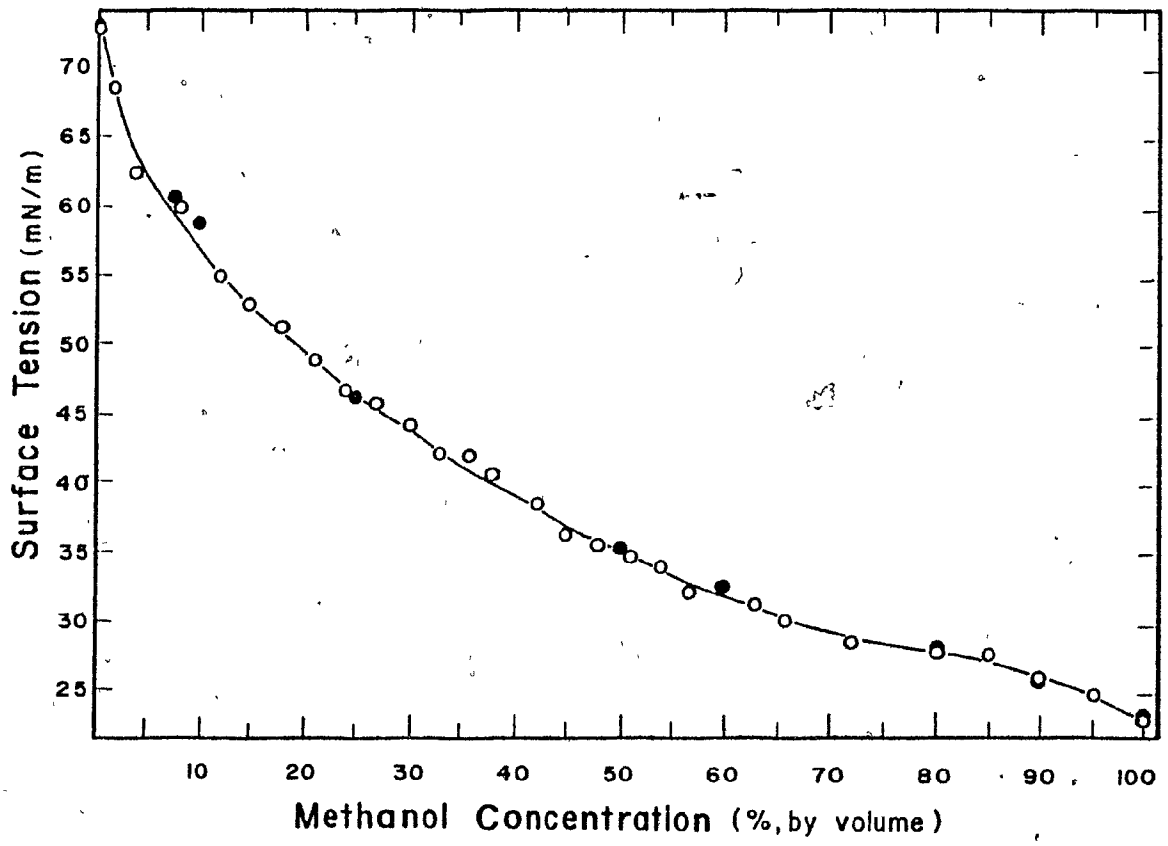


Figure 3.9 Surface Tensions of Aqueous Methanol Solutions of Varying Composition

includes the correction factors calculated as a function of concentration. Each point on the diagram is the average of at least three measurements. The surface tension of the distilled water was determined to be 72.53±0.19 mN/m at the 95% confidence level. This value agrees reasonably well with 72.88 mN/m (20°C) reported in the literature (Weast, 1981-82). The value for methanol employed in the present work was found to be 22.63±0.16 mN/m (95% confidence interval) in close agreement with the literature value of 22.50 mN/m (20°C). Standard deviations for the surface tensions of the solutions were less than 0.21 in all cases. Confidence intervals varied in the range ± 0.13 to ± 0.32 (at 95% confidence level). The surface tension values listed in the Handbook of Physics and Chemistry (1981-82) are included in the figure (filled circles). In spite of some difference in the temperature of the measurements, the literature values are in good agreement with those measured in the present work. The reduction in surface tension due to methanol additions was much more pronounced at low concentration than that at higher concentrations. For example, if the methanol concentration is increased by 5% (vol.) by additions to distilled water and methanol solutions of 50 and 90%, the surface tension will be decreased nearly by 10, 2.5 and 1 mN/m respectively. This effect is similar to that obtained with ethyl alcohol which shows a greater surface activity as will be discussed later.

The effect of temperature on the surface tensions of

water, methanol and some of their solutions is illustrated in Figures 3.10 and 3.11. Surface tension decreases linearly with increasing temperature not only for the two liquids but also for their binary mixtures. Variation of the slopes of the straight lines is given as a function of methanol concentration in the following table.

Table 3.2

Temperature Dependence of Surface Tension for Aqueous Methanol Solutions

% Methanol (vol.)	$d\gamma/dT$
0 (dist. water)	-0.167
2	-0.147
8	-0.132
18	-0.133
40	-0.107
57	-0.098
100 (methanol)	-0.094

The slope value obtained for distilled water (-0.167) compares with the value of -0.16 reported by Adamson (1976). As the methanol percentage increases the temperature dependence of the solution, surface tensions decreases and becomes similar to that of methanol itself.

3.3.2. Bubble Size Measurements

Figures 3.12-14 show the photographs of the air bubbles for aqueous methanol solutions of decreasing surface tension. The bubbles produced in distilled water and methanol are also included for comparison. In distilled water the shapes and

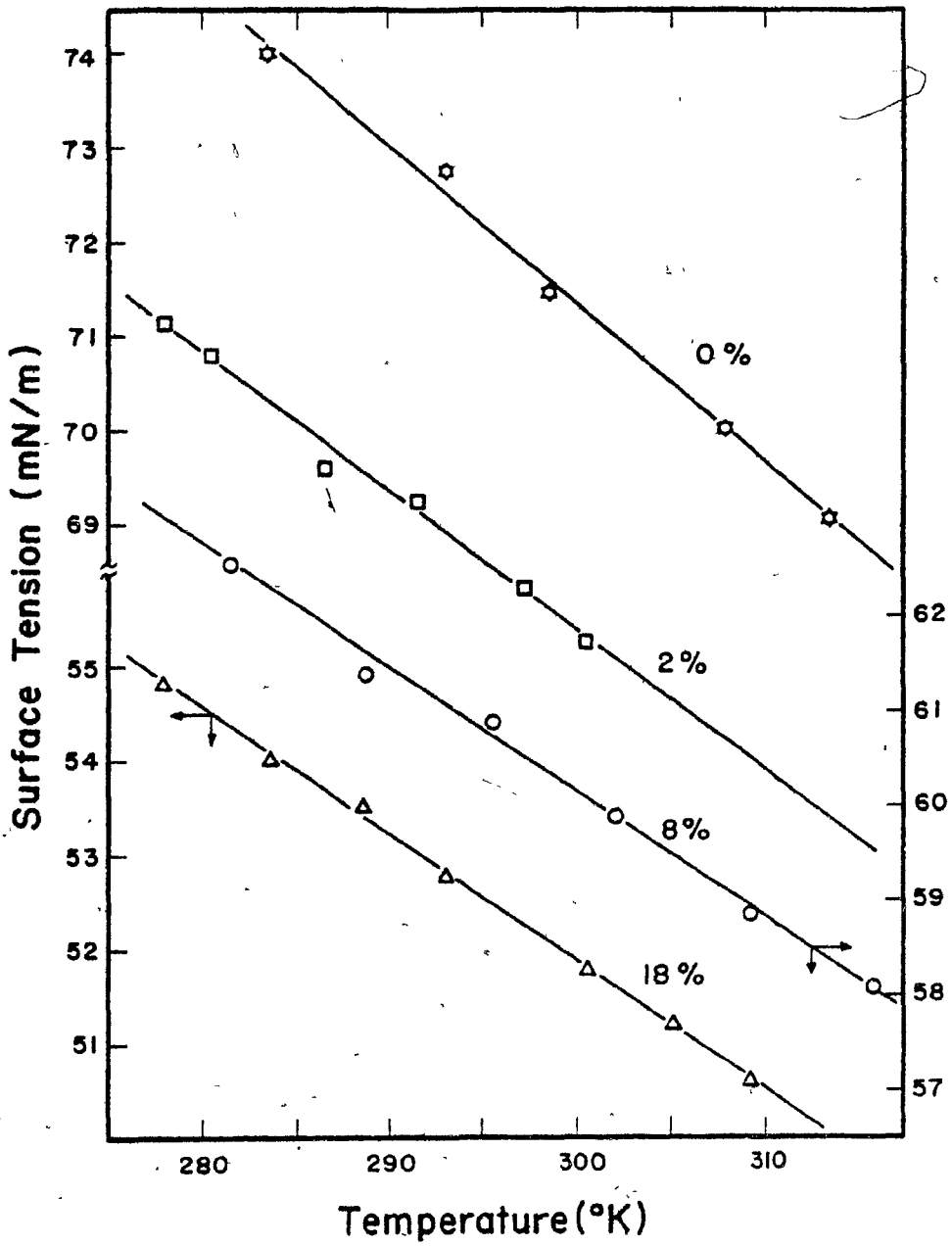


Figure 3.10 Temperature Dependence of Surface Tension for Aqueous Methanol Solutions

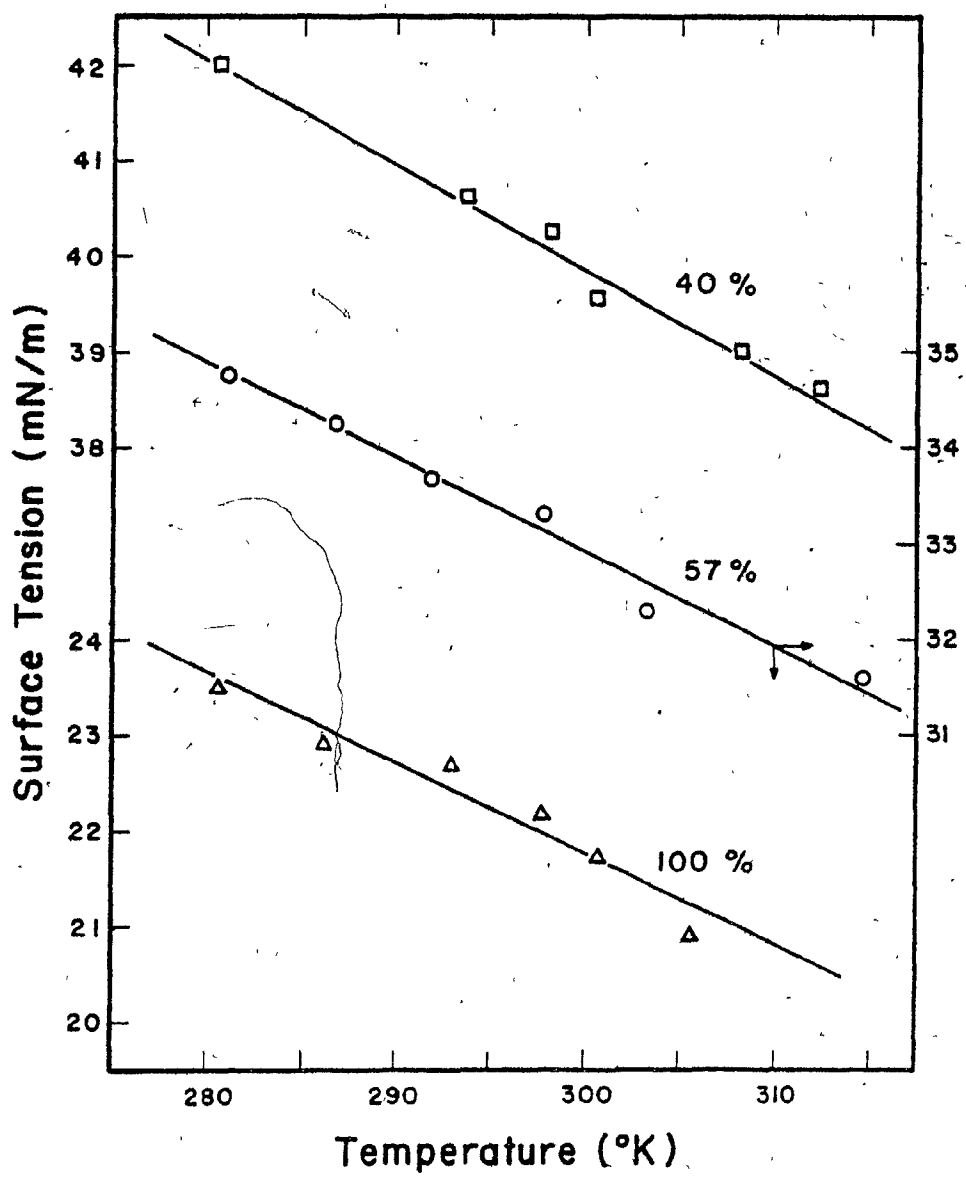
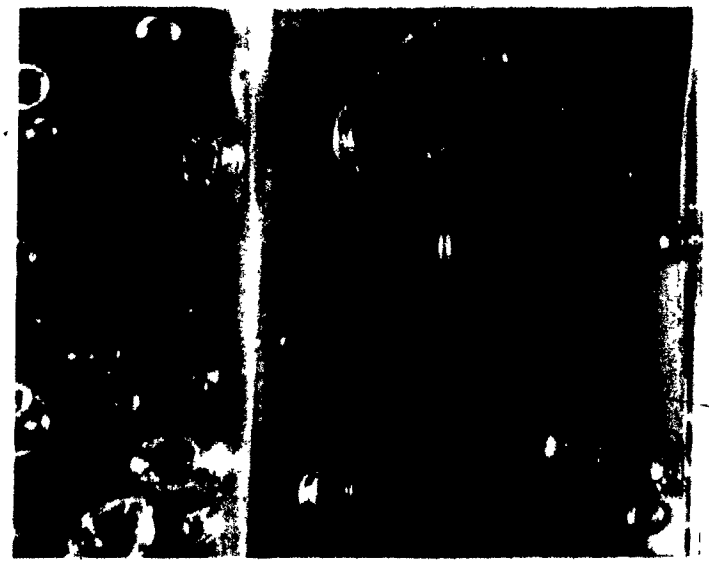


Figure 3.11 Temperature Dependence of Surface Tension for Aqueous Methanol Solutions (Cont'd.)

Figure 3.12 Photographs of Air Bubbles Produced in Aqueous Methanol Solutions - Concentration Range; 0-1.0% (vol.)



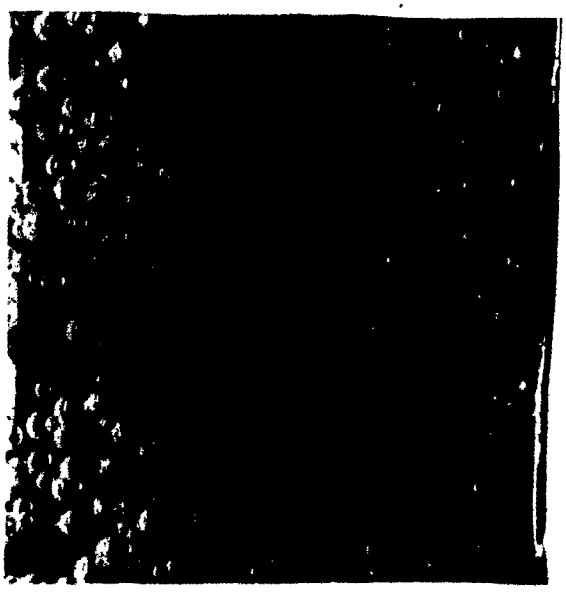
0 %
dist.water
72.5 mN/m



0.2 %
71.7mN/m

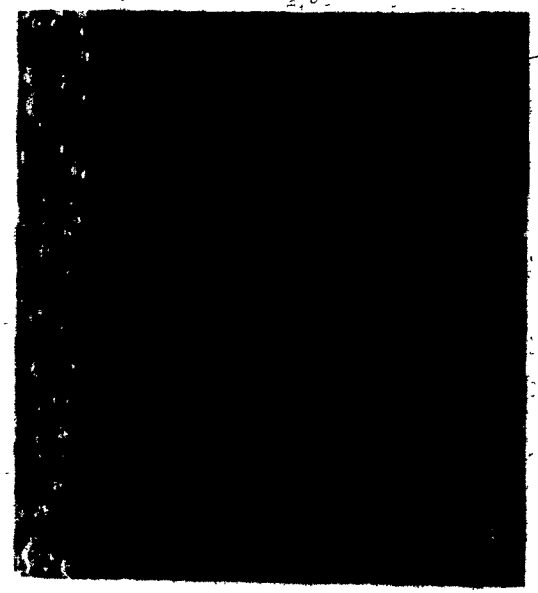


0.5 % — 71.1 mN/m

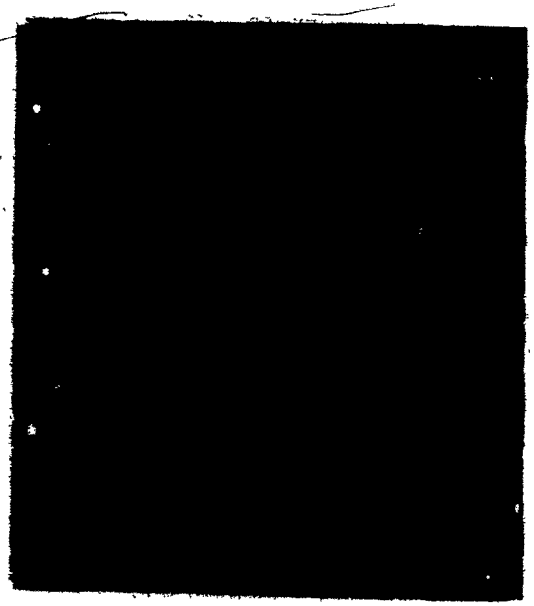


1.0 % — 70.5 mN/m

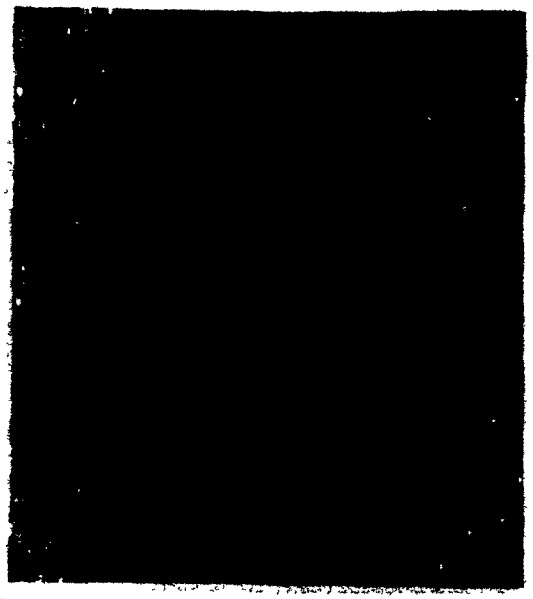
Figure 3.13 Photographs of Air Bubbles Produced in Aqueous Methanol Solutions - Concentration Range; 2-63% (vol.)



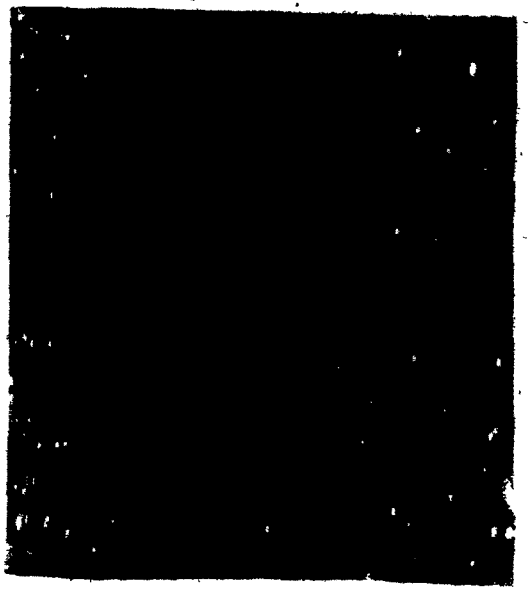
a



b



c



d



e

a – 2 % — 68.6 mN/m

b – 12 % — 55.2 mN/m

c – 27 % — 45.7 mN/m

d – 48 % — 35.5 mN/m

e – 63 % — 31.0 mN/m

Figure 3.14. Photographs of Air Bubbles Produced in Aqueous Methanol Solutions - Concentration Range; 72-100% (vol.)



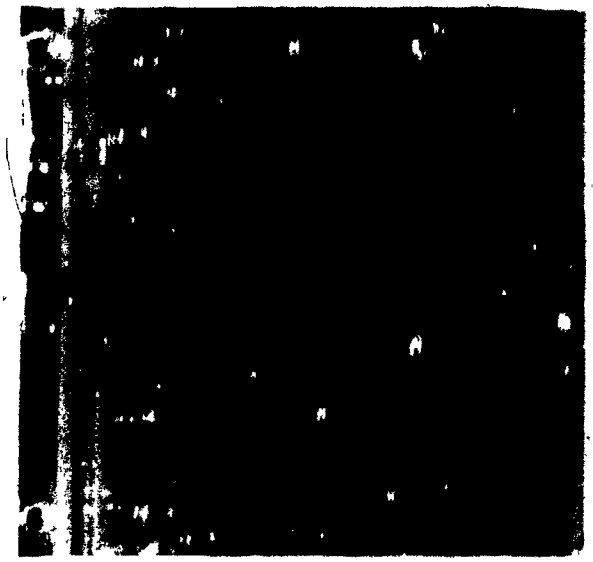
100 %

22.6 mN/m

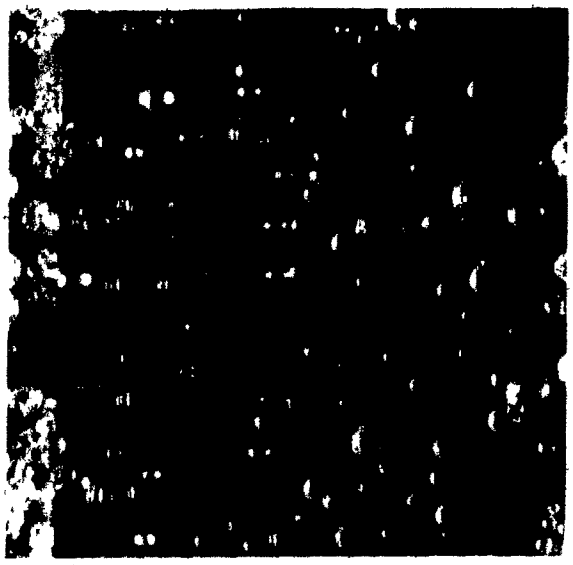


95 %

24.5 mN/m



80 % — 27.7 mN/m



72 % — 28.3 mN/m

sizes of the bubbles vary in a wide range. The bubbles which are smaller than about 1 mm in diameter seem to be perfectly sperical while the larger ones assume non-spherical shapes, e.g. ellipsoidal forms. Presence of small amounts of methanol changes the picture remarkably. This is illustrated in a most dramatic way by a series of photographs in Figure 3.12 which indicates clearly a reduction in size and an increase in the number of bubbles produced with an increase in methanol concentration. As the bubble size is reduced sphericity of the bubbles becomes readily apparent. There appears to be little change in the bubble size distribution with a further increase in methanol concentration from 2% (vol.) to about 48% (vol.). In more concentrated solutions the size of a small number of bubbles starts to increase. This trend can be observed visually in a series of photographs given in Figure 3.14. A reduction in surface tension by increasing the methanol concentration beyond 63% (vol.) is accompanied by a steady decrease in the number of bubbles as well as an increase in the size of the bubbles produced. This phenomenon brought about by an increase in methanol concentration is exactly opposite to those observed in the first series of pictures (Figure 3.12). By comparing these two figures it is interesting to note that the size, shape and the number of air-bubbles produced in the water and methanol are strikingly similar although the surface tension of the former is more than threefold that of the latter.

The distribution of bubble sizes can be expressed in a

more quantitative manner by the use of standardized block diagrams which illustrate the variation of the number of bubbles in each size class produced in solutions of a specified composition. The results obtained for the water-methanol system are shown in Figures 3.15-3.18. As many as 550 bubbles were counted and sized but for the ease of comparison the size distributions in all the solutions are plotted on a 100-bubble basis. The air flow rate was fixed at about 50 ml/min in all cases.

The diameter of the bubbles produced in distilled water (Figure 3.15) ranged from 0.1 to about 4.2 mm. Large bubbles disappear with small additions of methanol. At 1% (vol.) methanol the size distribution assumes a typical shape with a most frequent bubble size class of 0.4-0.6 mm. This average bubble diameter of 0.5 mm is predominant in all solutions in the range of 1 to 72% (vol.) methanol. In more concentrated solutions, there is a shift to the next smaller size class (i.e. 0.3 mm average). A further increase in methanol concentration beyond 63% (vol.) causes larger size bubbles to appear in solutions. The bubbles reach their maximum sizes in methanol containing no added water (Figure 3.18).

In addition to bubble sizes, the number of bubbles are also affected by the methanol concentration. Figure 3.19 shows that the number of bubbles produced per cm^3 increases as a function of the logarithm of the molar concentration (log C_M). The

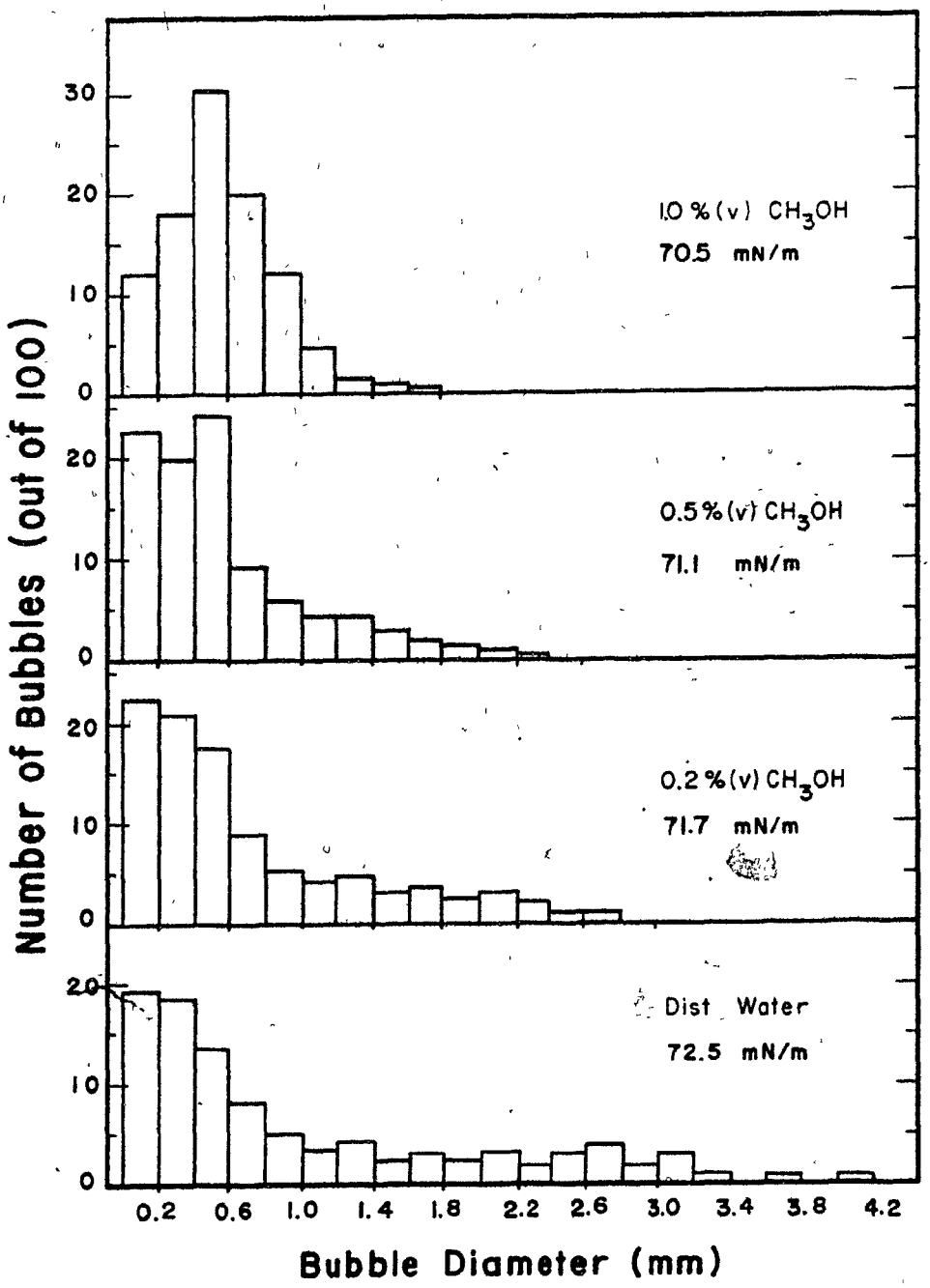


Figure 3.15 Bubble Size Distribution in Aqueous Methanol Solutions - Concentration Range; 0-1% (vol.).

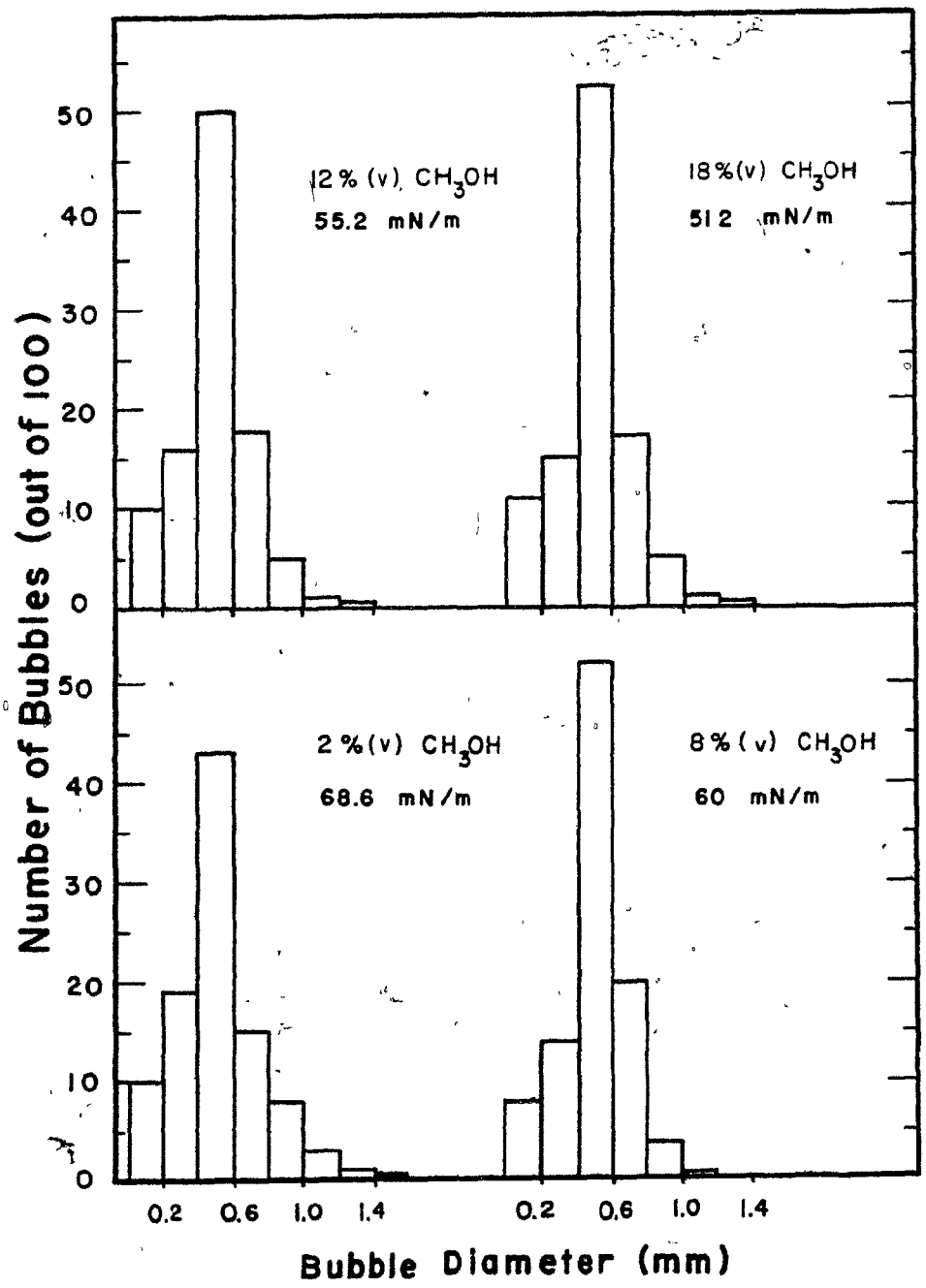


Figure 3.16 Bubble Size Distribution in Aqueous Methanol Solutions - Concentration Range; 2-18% (vol.).

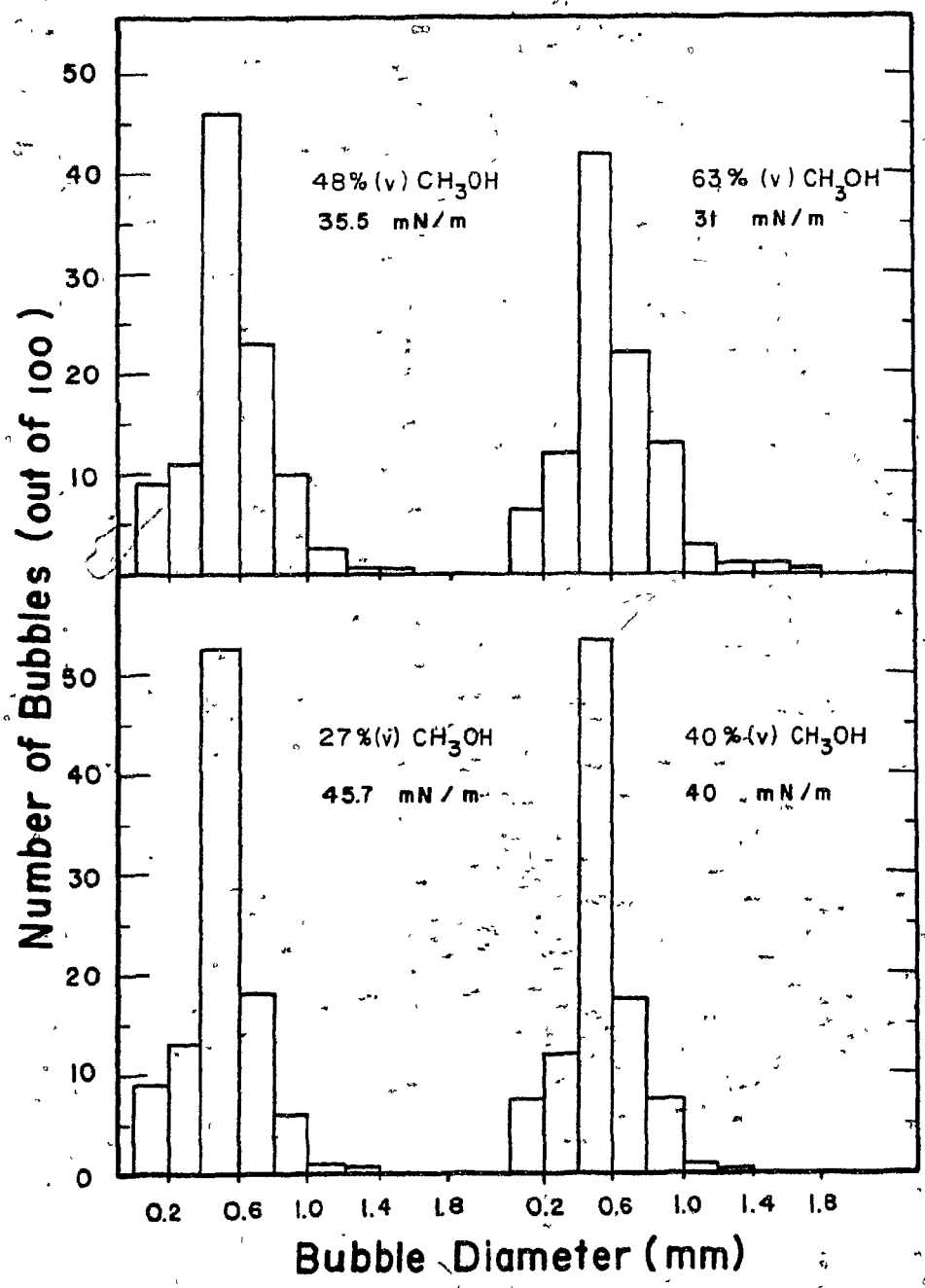


Figure 3.17 Bubble Size Distribution in Aqueous Methanol Solutions - Concentration Range; 27-63% (vol.)

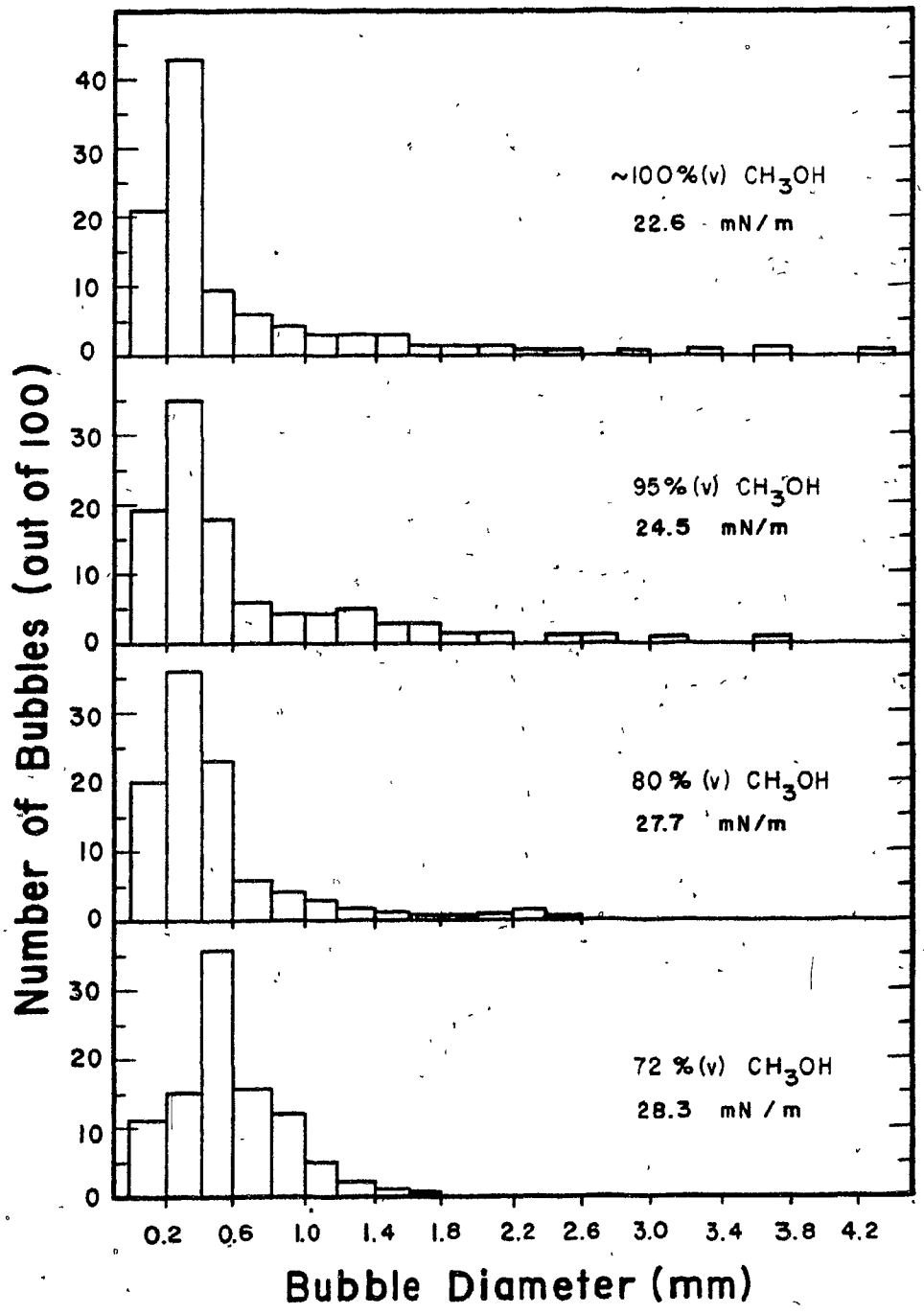


Figure 3.18 Bubble Size Distribution in Aqueous Methanol Solutions - Concentration Range; 72-100% (vol.) .

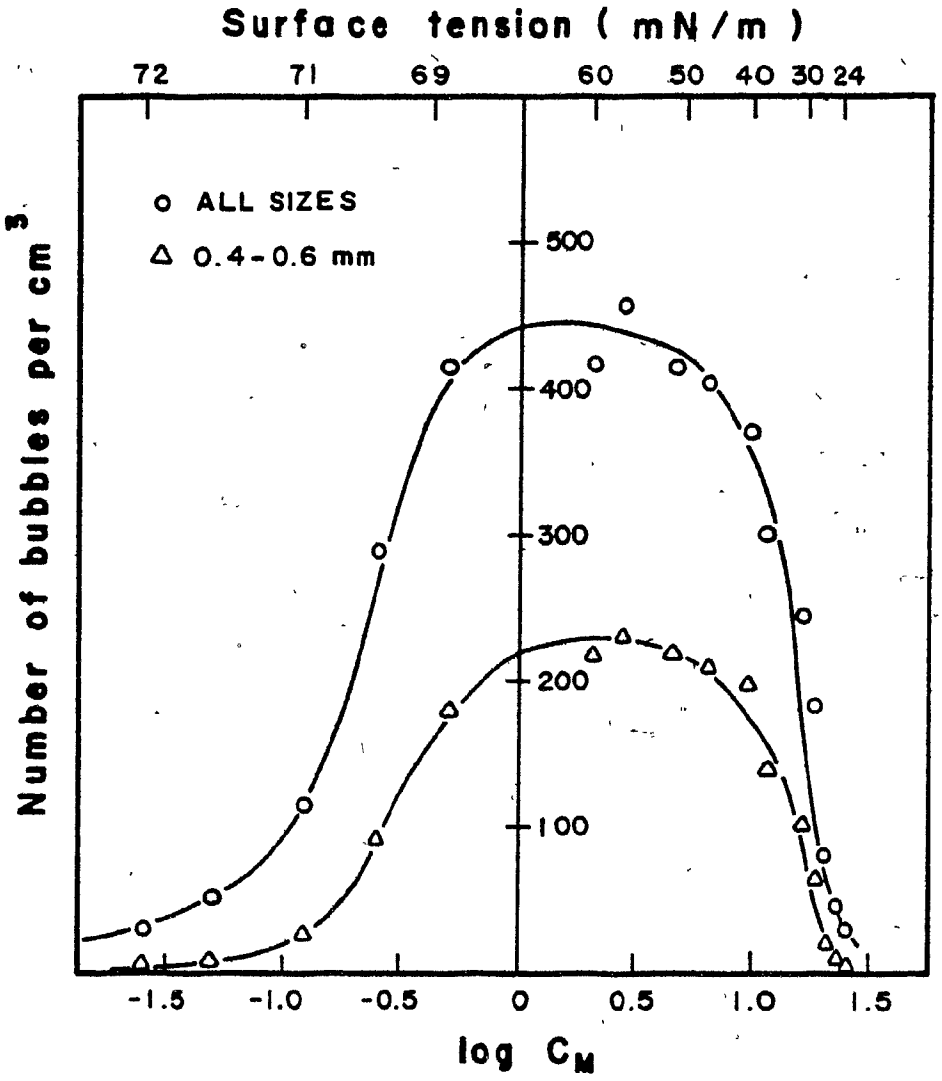


Figure 3.19 Number of Bubbles Produced per cm^3 of Solution vs. log (molar concentration of methanol, C_M) .

number reaches a maximum at about 440 bubbles between the log C_M of -0.2 to 0.7 (i.e. 3 to 20% methanol by volume) then it decreases to small number in methanol itself.

3.4 DISCUSSION

3.4.1. Surface Tension of the Methanol Solutions

In general, the surface tension of an aqueous solution follows two main characteristic patterns with increasing concentration of the solute. The first type exhibits a steady decrease in surface tension; rapidly at low concentrations and more gradually at higher concentrations. In the second case, the surface tension exhibits a continuous increase above that of water. Typically, inorganic electrolyte solutions fall into the second group while a wide range of organic-water solutions fall into the first. The surface tension variation of aqueous methanol solutions (Figure 3.9) is typical of the former category.

How quickly the surface tension falls initially depends, besides concentration, on the structure of the solute molecules, mainly the length of hydrocarbon radical. Methanol with only one methyl group should be expected to be the least effective in depressing the surface tension of water. A comparison with longer-chained alcohol solutions will be made to illustrate this effect. The effect of concentration and the hydrocarbon chain length of a homologous series of heteropolar molecules on the lowering of the solution surface tension was investigated first by Traubé (Adamson, 1976), who presented a rule

stating that the addition of one methylene ($-CH_2-$) group to the hydrocarbon chain in a homologous series would generate the same reduction of surface tension at one-third the concentration. The lowering of the surface tension brought about by a series of homologous compounds can most conveniently be compared by plotting the logarithm of the molar concentration as a function of the solution surface tension. Such a comparison involving the aqueous methanol solutions is made in Figure 3.20 which shows the validity of Traube's rule for methyl, ethyl and butyl alcohol solutions; the $\ln C_M$ vs γ_{lv} curves are spaced approximately by equal concentration intervals [$\ell n(3)$]. For instance, the surface tension of distilled water (72.5 mN/m) may be reduced (to 52.5) by 20 mN/m at equivalent amounts of butyl ($C^B \cong 0.22$ M.), ethyl ($C^E \cong 2.00$ M.) and methyl alcohols ($C^M \cong 6.00$ M.). This is as predicted by Traube's rule since

$$C^M \cong 3 \times C^E \cong 3 \times 3 \times 3 \times C^B \qquad 3.19$$

Traube's rule appears to be valid also for higher homologs of normal aliphatic alcohols from hexyl to decyl alcohols in water (Defay et al., 1966).

A reduction in the surface tension of aqueous alcohol solutions is due to the spontaneous adsorption of alcohol molecules at the solution-gas interface. The work necessary to bring one CH_2 group from the bulk to the solution interface can be estimated using Langmuir's approach (1917). If C^S and C are the surface and bulk concentrations of the organic compound,

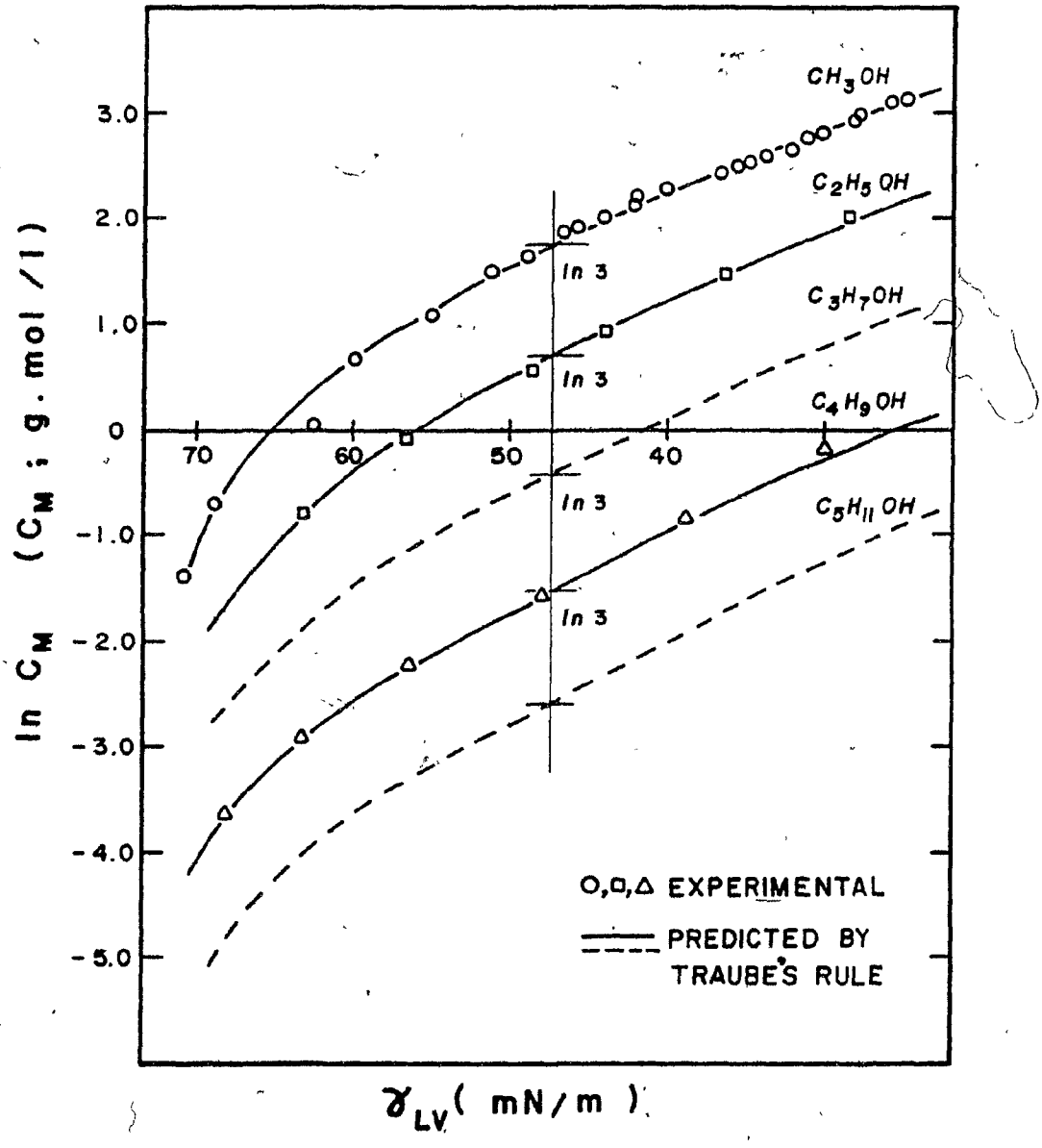


Figure 3.20 Surface Tensions of the Aqueous Solutions of the Homolog Series of Monohydric Alcohols Illustrating the Validity of Traube's Rule

the work (W) necessary to transfer one mole of solute from the bulk solution to the solution-gas interface is given by

$$W = RT \ln \left(\frac{C^S}{C}\right) \qquad 3.20$$

For equal surface concentration of two adjacent n-alcohol molecules in the homologous series, (i.e. the chain length of hydrocarbon radicals; n and n + 1) the difference in work required will be

$$W_{n+1} - W_n = RT \ln \left(\frac{C_n}{C_{n+1}}\right) \qquad 3.21$$

For equal surface concentration ($C_n^S = C_{n+1}^S = C^S$), the surface tensions are assumed to be the same ($\gamma_n = \gamma_{n+1}$); and therefore, in accordance with Traube's rule the concentration ratio, $\frac{C_n}{C_{n+1}}$ will be 3. Using this value in Equation 3.21 at 25°C gives

$$W_{n+1} - W = RT \ln 3 = 2.723 \text{ KJoule/mole} \qquad 3.22$$

Thus, 2.723 KJoules of work is expended to bring one $-CH_2-$ group from the bulk solution to the interface.

A number of equations have been suggested for calculation of surface tensions of solutions. The semiempirical equation proposed by Szyszkowski was found to hold for dilute aqueous solutions of some organic substances (Adamson, 1976).

$$\gamma = \gamma_o [1 - B \log (1 + c/a)] \qquad 3.23$$

Where γ_o is the surface tension of water, c is the molar concentration of the solute, B and a are constants related to the general class of compounds and specific molecule respectively.

It has been found that the surface tension values of aqueous methanol solutions can be represented by Equation 3.23 quite accurately not only for dilute solutions but also concentrated ones up to about 7.5 molar. A comparison can be made by referring to Table 3.3 which lists the experimental and calculated surface tension values. The ratio of these two does not differ significantly from unity. In fact, ignoring the last two values which mark the beginning of the significant deviations, the average of all the ratios tabulated is exactly 1.00.

3.4.2. Thermodynamics of Adsorption at the Methanol Solution Surface

The reason why the surface tension (or surface free energy) of water will be decreased by the addition of methanol can be understood considering the spontaneous adsorption of methanol molecules at the solution-gas interface. This section will be devoted to a quantitative description of this adsorption by making use of the Gibbs equation.

Gibbs' adsorption equation, which is a result of rigorous thermodynamic considerations may be given as follows (Adamson, 1976):

$$d\gamma = -S_s\, dT - \Gamma_1 d\mu_1 - \Gamma_2 d\mu_2 - \Gamma_3 d\mu_3 - \text{etc.} \qquad 3.24$$

where S_s is excess surface entropy, Γ_1, Γ_2, etc., the surface excess of various components, μ_1, μ_2, etc., the chemical potentials of the same components and γ is the surface tension. This

Table 3.3

A Comparison of the Experimental Surface Tension Values of Aqueous Methanol Solutions with those Calculated using the Szyszkowski Equation

(B:0.420, a:1.05)

Methanol (% vol.)	Molarity (g. mol/l	Surface Tension (mN/m) γ_{exp}	$\gamma_{calc.}$	$\frac{\gamma_{exp.}}{\gamma_{calc.}}$
0	0	72.5	72.5	1.00
0.1	0.025	72.1	72.2	~ 1.0
0.2	0.049	71.7	71.9	~ 1.00
0.5	0.123	71.1	71.1	~ 1.00
1.0	0.245	70.5	69.8	1.01
2.0	0.490	68.6	67.5	1.02
4.0	0.977	62.4	63. 8	0.98
8.0	1.950	60.0	58.6	1.02
12.0	2.951	55.2	54.8	1.01
18.0	4.467	51.2	50.6	1.01
21.0	5.129	48.9	49.1	~ 1.00
24.0	5.888	46.6	47.5	0.98
27.0	6.607	45.7	46.2	0.99
30.0	7.413	44.1	44.9	0.98
33.0	8.128	42.1	43.8	0.96
45.0	10.965	36.3	40.3	0.90

equation (at constant pressure) when applied to the methanol-water binary solutions at constant temperature takes the form

$$d\gamma = - \Gamma_M d\mu_M - \Gamma_W d\mu_W \qquad 3.25$$

The surface excess per unit area (Γ) can be defined by a few different ways depending on the selection of a hypothetical dividing surface. According to Gibbs' convention the adsorption of the solvent (i.e., Γ_W for water) is taken as zero. Thus, Equation 3.25 now becomes

$$d\gamma = - \Gamma_M d\mu_M \qquad 3.26$$

Since $\mu_M = RT \ln a_M$, where a_M is the activity of methanol in aqueous solution rearrangement of the preceding equation yields

$$\Gamma_M = - \frac{1}{RT} \left(\frac{d\gamma}{d \ln a_M}\right) \qquad 3.27$$

This is the Gibbs' adsorption equation, of major importance with many applications in the surface chemistry of mineral flotation (Leja, 1982). Since $\frac{d\gamma}{d \ln a}$ is the differential coefficient of the adsorption density function the equation shows that Γ will be positive when the surface tension of water is lowered by the addition of a solute (e.g. methanol), and negative when it is increased (e.g. by inorganic electrolytes).

In Gibbs' convention, in order to assign a definite value to the surface excess Γ of the solute in a binary system, it is necessary to choose a hypothetical geometrical plane surface dividing the two bulk phases, such that the surface excess of

the solvent disappeared (i.e. became zero). In their notable study Guggenheim and Adam (1933) proposed several different conventions and compared the Γ values obtained using each convention with those determined according to Gibbs' convention. Using the ethanol-water binary they demonstrated that contrary to their own values the value of Γ for ethanol according to Gibbs' convention did not eventually become zero but assumed a certain value as the ethanol mole fraction reached 1.0. They also determined how these various conventional sets of Γ were related one to another. These relationships when applied to the system under study may be given as follows:

$$\Gamma_M^{(V)} = \frac{X_W V_W}{\bar{V}} \Gamma_M \qquad 3.28$$

$$\Gamma_M^{(M)} = \frac{X_W \cdot M_W}{\bar{M}} \Gamma_M \qquad 3.29$$

$$\Gamma_M^{(N)} = X_W \cdot \Gamma_M \qquad 3.30$$

where Γ_M is the surface excess of methanol given by the familiar Gibbs equation (i.e. Equation 3.23), $\bar{V}$ is the average molar volume of the solution defined by $\bar{V} = X_M V_M + X_W V_W$, V_W and V_M the molar volumes of water (18.1 cm^3/mole) and methanol (40.7 cm^3/mole) respectively, X_M and X_W are the mole fractions of methanol and water respectively, $\bar{M}$ is the average molar mass of the solution obtained from $\bar{M} = X_M M_M + X_W M_W$, M_W and M_M are the molar masses of water (18.0 g/mole) and methanol (32.0 g/mole). $\Gamma_M^{(V)}$, $\Gamma_M^{(M)}$ and $\Gamma_M^{(N)}$ are the main surface excess values introduced by Guggenheim and Adam (1933). $\Gamma_M^{(V)}$ in what they call convention V may be defined as the excess number of moles of methanol in the

surface region with respect to a region in the bulk with exactly the same volume as the surface region. $\Gamma_M^{(M)}$ is defined similarly but this time (referred to as convention M) the unit of comparison is the mass, not the volume. In the definition of $\Gamma_M^{(N)}$, the basis is the total number of moles (this convention is called convention N) and the surface region will relatively be rich in terms of the number of moles of methanol. Therefore, if Γ_M can be calculated from the Gibbs equation $\Gamma_M^{(V)}$, $\Gamma_M^{(M)}$ and $\Gamma_M^{(N)}$ may also be determined using the relations 3.28, 3.29, and 3.30. In addition to the surface excess values of methanol it is possible to determine also the surface deficiencies of water according to all conventions. The results of calculations are tabulated in Appendix III.

To be able to use the Gibbs' equation the surface tensions and the activities of aqueous methanol solutions are required. The former is known from the measurements carried out in the present work (Appendix III). The latter was determined on the basis of vapor pressure data by Hall et al. (1979). Activity (a) is the product of mole fraction and activity coefficient (f) (see section 3.1.6.). The activity coefficients of methanol and water for the aqueous solutions were calculated from the Margules relation which among other model equations, gave the best fit to the vapor pressure data mentioned above (Gmehling et al., 1982). This equation when written for methanol in aqueous methanol solution is as follows:-

$$\ell n\, f_M = (0.6304 - 0.4134\, X_M)X_W^2 \qquad 3.31$$

For water in the same solution

$$\ell n\, f_W = (0.4237 + 0.4134\, X_W) X_M^2 \qquad 3.32$$

where f_M is the activity coefficient of methanol; f_W - the activity coefficient of water; X_M and X_W - mole fractions of methanol and water respectively. The variations of the activity coefficients calculated from these equations are shown as a function of methanol mole fraction in Figure 3.21. At infinite dilution, the activity coefficients of methanol and water are 1.88 and 1.53 respectively. More recently, Christian et al. (1981) carried out a new set of vapor pressure measurements for dilute methanol solutions up to 10 mole percent using an automated apparatus. Their data resulted in activity coefficients which could be represented by the following equations

$$\ell n\, f_M = (0.487 + 0.020X_M + 3.8X_M^2)\, X_W^2 \qquad 3.33$$

$$\ell n\, f_W = (0.477 - 2.513X_M + 3.8X_M^2)\, X_M^2 \qquad 3.34$$

The activity coefficients of methanol obtained are between 4.5 and 13.3% lower than those calculated using Equation 3.31. The activity coefficients found by Butler et al. (1933) are even lower. Part of the discrepancy may have resulted from some differences in the experimental techniques and equipments.

In Figure 3.22, the adsorption of methanol at the solution-gas interface and the surface tension is shown as a function of the natural logarithm of the activity. As the surface tension

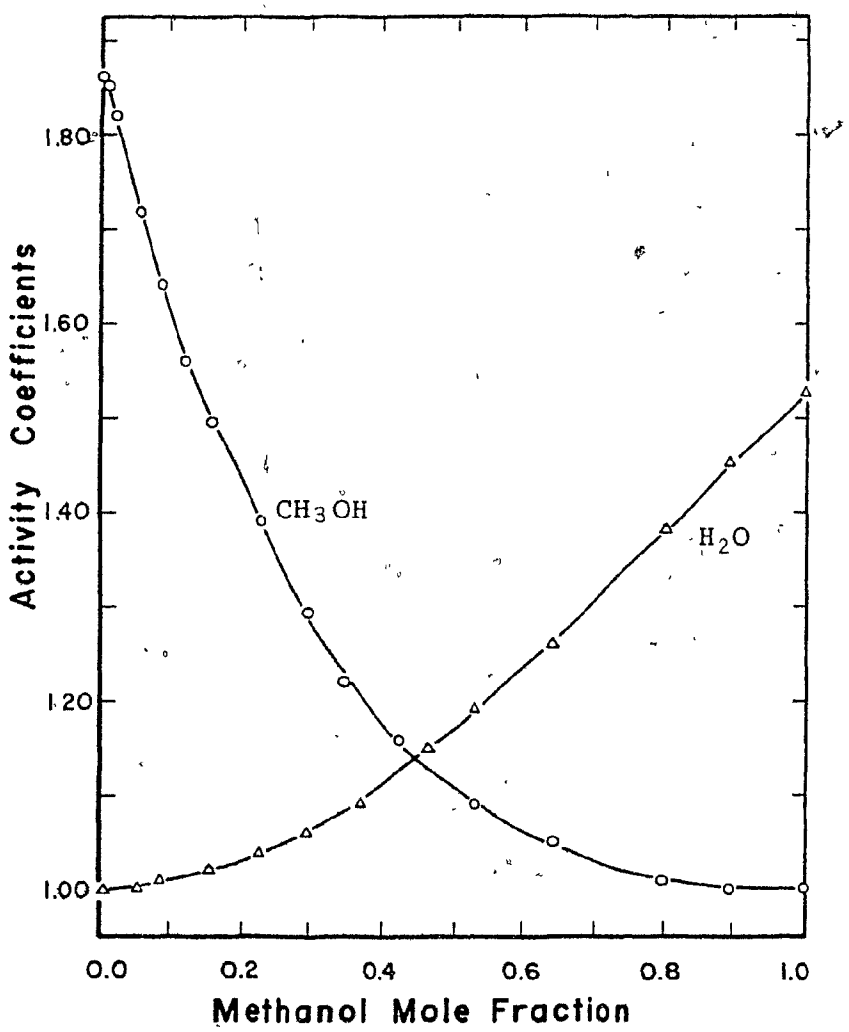


Figure 3.21 Activity Coefficients of Methanol and Water in Aqueous Methanol Solutions .

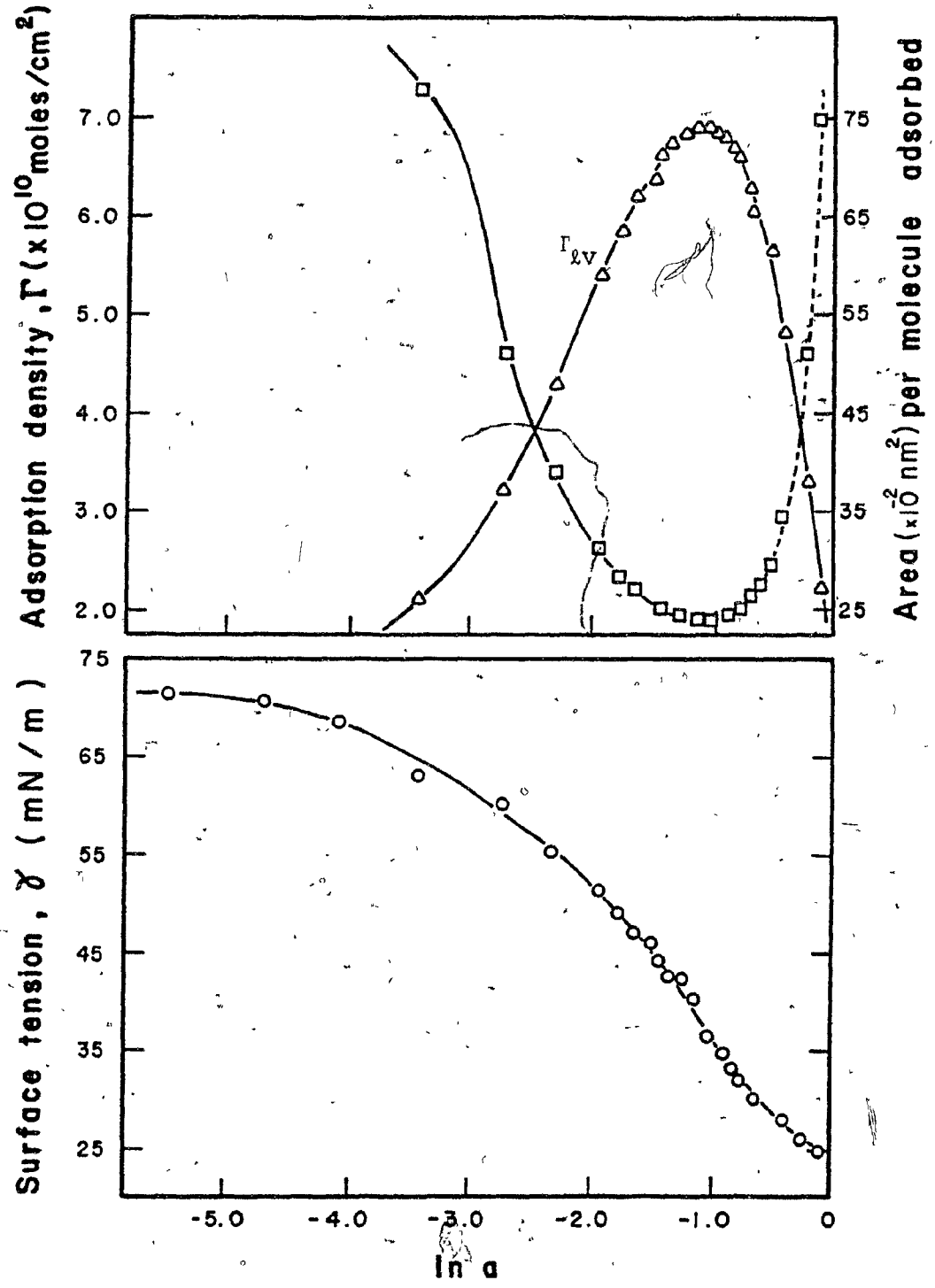


Figure 3.22 Adsorption of Methanol of the Solution-Gas Interface, Area per Adsorbed Molecule and Surface Tension as a Function of ℓn (activity of methanol, a) .

decreases continuously with increasing activity, the adsorption density (i.e. surface excess of methanol increases to reach a maximum value of 6.92×10^{-10} moles/cm^2 at an activity of 0.31 (about 40% methanol by volume). It then decreases as the solutions become more concentrated. Similarly the adsorption at the ethanol solution-gas interface (Guggenheim and Adam 1933) is characterized by a maximum. However, adsorption at the butanol solution-gas interface reaches a plateau at a bulk concentration of about 6.4% by weight (Harkins and Wampler, 1931; De Bruyn and Agar 1962). The maximum Γ value of 6.92×10^{-10} moles/cm^2 for methanol compares with that of 6.45×10^{-10} and 6.03×10^{-10} moles/cm^2 for ethanol and butanol respectively. The surface area occupied by alcohol molecules can be calculated by taking the reciprocal of the adsorption density for each solution composition (see Figure 3.22). At the maximum adsorption density, this area is 0.240 nm^2 as compared to 0.257 and 0.274 nm^2 for ethanol and butanol respectively. These values are reasonable when compared with the area per molecule for normal alcohols in close-packed films of 0.216 nm^2 (De Bruyn and Agar, 1962). From this one can conclude that in addition to butyl and ethyl alcohols, methyl alcohol molecules form at the solution-gas interface a monomolecular adsorption film. This does not happen in dilute solutions prior to the maximum adsorption density being reached. In more concentrated solutions, the area per molecule adsorbed at the interface increases (dashed line in the figure) due to a decrease in adsorption density. This implies a reduction in the number of methanol molecules at the solution surface as the

bulk concentration is further increased. However, the number of methanol molecules present at the solution surface should remain constant (or nearly so) once the bulk concentration corresponding to the maximum adsorption density is exceeded. The areas plotted in this diagram are based on the adsorption densities calculated from Gibbs' equation which gives only relative number of excess (or deficient) molecules at a surface, not the absolute number of molecules.

3.4.3. Bubble Size Distribution

The air bubbles produced in distilled water and methanol are similar in size, shape and number. The sizes range from below 0.1 mm to about 4.2 mm. The large bubbles apparently result from the coalescense due to the collision of two or more bubbles of differing sizes and rising velocities. Another factor that may give rise to the collisions would be the slow-down of bubbles due to the time lost during deflection on the transition zone from cylindrical bottom to the flat body of the cell (Figure 3.8) and on the glass plate placed in the cell. This time delay may be sufficient for some bubbles rising immediately below to reach to and collide with those that are deflected. During the size measurements, the presence of very small bubbles was noted, mostly less than 0.1 mm. This is not surprising since the fritted glass bottom of the cell has a pore size of less than 10 μm. Both in distilled water and methanol the number of these small size bubbles was in general greater than that of large ones. This is somewhat expected

because the probability of collision is known to be proportional to the bubble size. The coalescence between relatively large bubbles is more likely than that of very small ones. This may explain the wide range of bubble sizes observed in the case of distilled water and methanol.

Analogous to the attachment process between a bubble and a particle in flotation, the coalescence process upon collision of two bubbles under dynamic conditions requires the intervening liquid film to thin to a critical thickness before rupture occurs. The time taken for the film to thin and rupture may be regarded as the induction period for coalescence. The presence of large size bubbles in the case of distilled water and methanol indicates that the induction time will be very short when the bubble surfaces are naked, i.e. free of surface active species. The experiments by Deryaguin and Titievskaya (1954) demonstrated that this time was too short to perceive when two bubbles slowly contacted each other.

From the standpoint of solution chemistry, the coalescence process is affected by the nature and concentration of the solute present in water. This effect was investigated as part of a study by Sagert et al. (1976). Using high-speed cinematography they measured the coalescence times between two nitrogen bubbles formed on adjacent nozzles in dilute solutions of homologous n-alcohols (from ethyl to hexyl alcohols). The coalescence times (in the range 1 - 500 ms) were found to be proportional to the concentration of ethanol and

propanol in water. For amyl and hexyl alcohols, they were proportional to about the second power of concentration. The authors developed a model from theoretical considerations involving the excess pressure in the bubble, London forces (effective below a film thickness of 100 nm) and the electrical double layer repulsion forces to calculate the time for stretching a film from infinite thickness to a final thickness. Based on several assumptions, they were able to obtain an estimate of coalescence time as a function of alcohol concentration. A reasonable agreement was reported between the calculated and measured coalescence times. It should be noted that in this particular study the concentration range was very dilute. For instance, the maximum concentration of ethanol used was 0.174 mol/kg or about 1% by volume. Methanol was not included in the experiments by Sagert et al. (1976), but, considering that the dependence of coalescence time on concentration remained the same for short-chained alcohols, one can assume that the coalescence time for methanol will also be proportional to its concentration in aqueous solution.

The above study investigated the coalescence process between two freshly formed bubbles. In an actual process of bubble production, because of the aging of bubble surfaces to some extent and the multiple interactions among the bubbles, the situation must be complex. In general, for a given gas flow rate and a dilute solution, the coalescence process should affect both the size distribution and the number of bubbles produced per unit volume. Since the induction period

for coalescence increases with methanol concentration the number of bubbles surviving the collisions should also increase with the concentration. The number of bubbles present per cm^3 of methanol solution was plotted against concentration in the range 0 - 0.490 g.mol/l (0-2.% by vol.). Figure 3.23 indicates that a linear relationship between bubble production and methanol concentration exists. Hence, for dilute solutions, the number of bubbles per unit volume of solution can be correlated with the coalescence time of bubbles in the same solution.

As indicated earlier, the bubble sizes show a great variation in distilled water. With the introduction of methanol into the water, there is a remarkable reduction in size of the bubbles. The small and very mobile methanol molecules adsorb at the solution-gas interface while the bubbles are being formed and act by preventing coalescence between bubbles growing at adjacent pores of the fritted glass and during their subsequent collisions in the cell. As the concentration of methanol increases, a size class ranging 0.2 to 0.8 mm in diameter emerges as dominant in all the concentrated solutions up to about 75% (by vol.). For example, at 8, 27, and 48% methanol (by vol.), 86, 83 and 80% of the total number of bubbles produced respectively are between 0.2 and 0.8 mm in diameter. Within this size range, the average diameter for the great majority of the bubbles is about 0.5 mm. This size is also characteristic of ethanol solutions. Marrucci and Nicodemo (1966) observed that

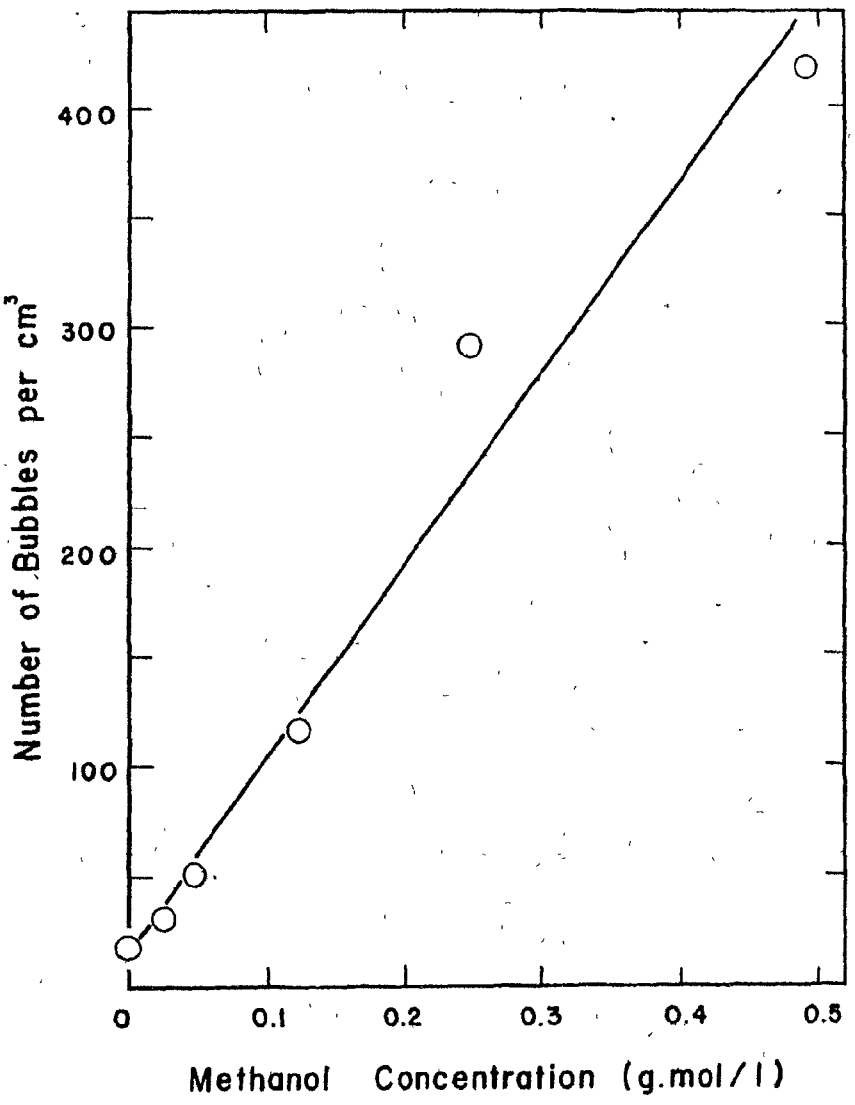


Figure 3.23 Number of Bubbles Produced per cm^3 of Solution as a Function of Methanol Concentration

an ethanol concentration as low as 0.02 gmol/l (~ 0.12% by vol.) is capable of reducing the bubble diameter to about 0.5 mm. A porous plate was used as the gas distributor.

There seems to be no single effect to explain the mechanism that hinders the coalescence. It can be stated, however, that the combined consequences of solute adsorption at the bubble surface are the main causes. The solute may be surface active (e.g. organic compounds) or surface inactive (e.g. inorganic electrolytes). In the latter case, electric double layer repulsion forces may be the main stabilizing factor for bubbles. In the case of methanol solutions, the orientation of the alcohol molecules at the bubble surface creates a film consisting of the -OH groups and associated polar water molecules. This is similar to the film formation on non-polar hydrocarbon droplets (Klassen and Mokrousov, 1963). The orientation process automatically creates an electric double layer. A second important factor which is probably common to both cases, is the viscosity of the film surrounding the bubble. It is generally known that surface viscosity affects the thinning of a liquid film; the greater the surface viscosity, the greater will be the resistance to thinning (Davies and Rideal, 1963). Surface viscosities of methanol solutions are not available. But considering the significant variation shown by bulk viscosities as a function of concentration one may expect the surface viscosities not to remain unaffected. Another factor likely to stabilize the bubble may be due to the Marangoni

effect. During the formation of a bubble in the methanol solution, there exists a methanol mass transfer from solution into the bubble until the gas phase becomes saturated with methanol vapor. This mass transfer is accompanied by local changes in methanol concentration and consequently in surface tension. This point was considered by Marrucci and Nicodemo (1966). They reasoned that if the mass transfer into the bubble has an effect in stabilizing the bubble then the mass transfer in reverse direction should favor destabilization and coalescence of bubbles. This possibility was tested by sending nitrogen gas saturated initially with ethyl alcohol vapor into a pure water. Observing that the coalescence was not favored they have concluded that the Marangoni effect does not play a primary role in the stabilization of the bubbles.

The velocity of ascent of the bubbles was calculated as a function of solution composition using the equation developed for solid spheres by Concha and Almendra (1979). A comparison between the calculated and measured bubble velocities for a given set of solution conditions has shown (Dobby, 1984) that this equation (see Appendix III) successfully predicts the terminal velocities of air bubbles ascending in solution. The average diameter of 0.5 mm was used as the bubble size. The availability of density and viscosity as a function of methanol composition permitted the calculations of such dimensionless parameters as Reynold, Eotvos, Weber and capillary numbers. The definitions as well as the numerical values obtained are given in Appendix III. Both Weber and Eotvos numbers are well

below 1. This suggests (Leja, 1982) that, from a hydrodynamic point of view, the surface tension forces will be dominant in the flotation cell over the whole range of aqueous methanol solution concentrations.

3.4.4. Correlations Between Various Properties

The surface excess values of methanol, Γ_M and the surface deficiencies of water, $-\Gamma_W$, calculated according to the convention V (see section 3.4.2.) for solutions up to the methanol mol fraction of 0.3, are plotted in Figure 3.24. The number of bubbles produced per cm^3 of solution, N_B is given in the same figure. The shape of these two types of curves (N_B and Γ^V) is very similar. Both the number of bubbles and the surface excess (or deficiency) values increase sharply in dilute methanol solutions. After passing through a maximum, each curve falls parallel to the others. This similarity suggests that the number of bubbles (or the interfacial area generated per cm^3) can be correlated with the adsorption densities or some parameter(s) that involve the adsorption densities. There is an apparent lack of correlation between the maximum regions of the curves N_B and $\Gamma^{(V)}$. A better correlation might have been observed if the quantitative relationship between the adsorption densities and the surface viscosity had been known.

Figure 3.25 shows a replot of heat of mixing ($-\Delta H$), adsorption density (Γ) and the bulk viscosity (μ) as a function

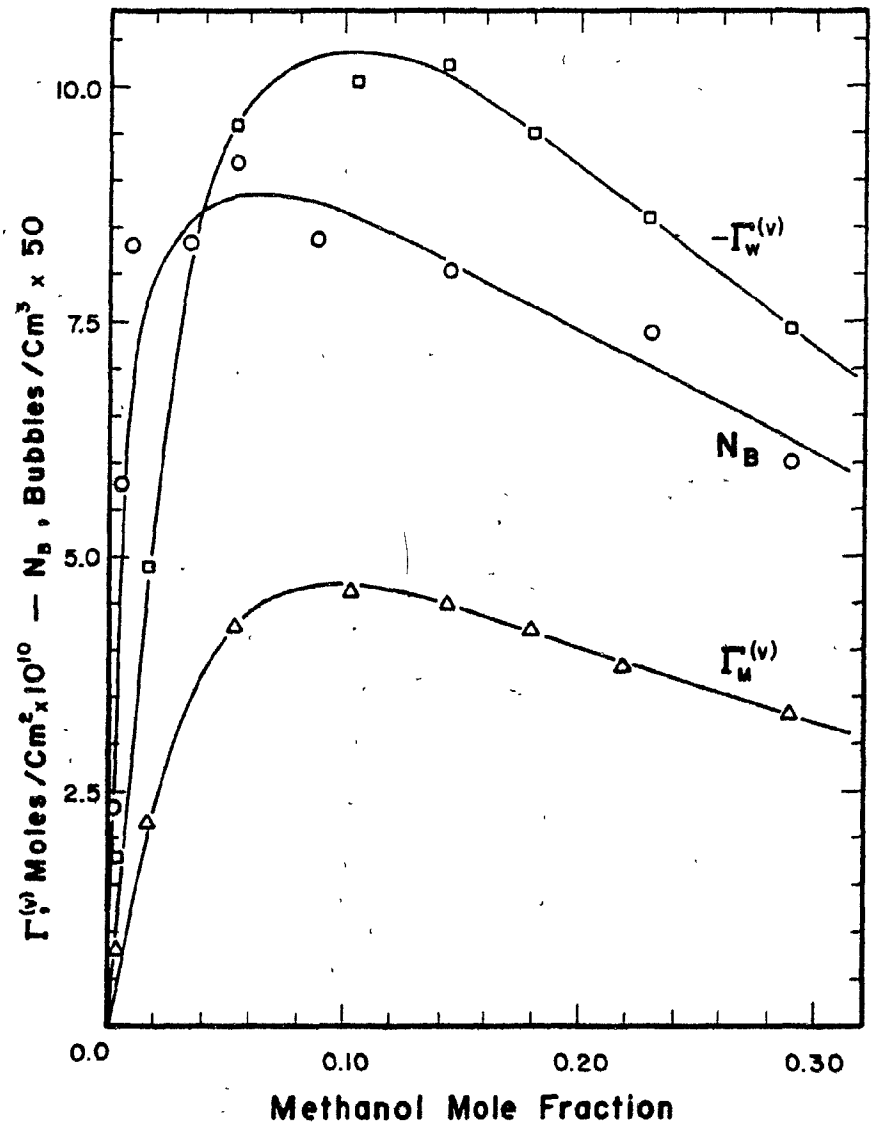


Figure 3.24 Relationship Between the Adsorption Densities at the Solution-Gas Interface and the Number of Bubbles Produced in Aqueous Methanol Solutions .

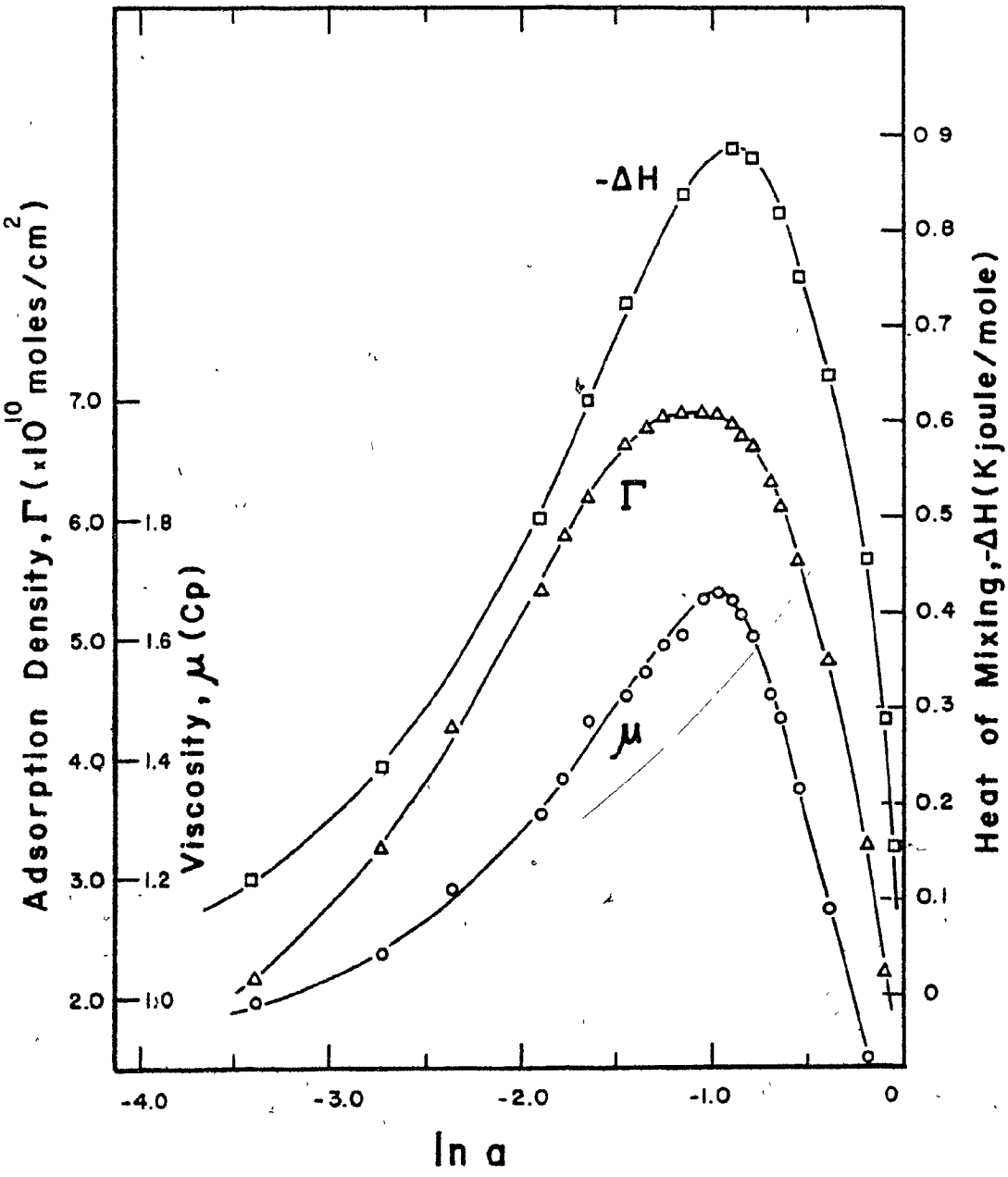


Figure 3.25 Relationship Between Heat of Mixing, Adsorption Density and Viscosity in Aqueous Methanol Solutions .

of logarithm of methanol activity in aqueous methanol solutions. The values of $-\Delta H$ were determined based on the study by Mato and Berrueta (1977) (section 3.1.5.), the Γ values were calculated according to Gibbs' convention (section 3.4.2.) and the μ values were taken from Carr and Riddick (1951) (section 3.1.4.). It is interesting that all three curves correlate well. In the vicinity of methanol activity 0.368 ($\ell n a \cong -1.0$) or ~ 48% methanol by vol. each curve passes through a maximum. It is particularly interesting to note a correlation between a bulk property (μ) and a surface property (Γ).

As indicated in sections 3.12 and 3.13, both methanol and water have highly polar associated molecules. When mixed they are capable of producing co-polymeric formations through intermolecular hydrogen bonding. It is generally accepted that the creation of these bulky structures involves the breakage of some hydrogen bonds followed by the formation of the new ones during rearrangement of the mixed structures. These structural changes are accompanied by evolution of heat due to preferential hydrogen bond formation between alcohol and water molecules. The fact that maximum heat of mixing corresponds to a maximum viscosity suggests that the relative stability of this methanol-water co-polymer formation tends to reach its maximum at this composition. Since the methanol activity of 0.368 is equivalent to a methanol mole fraction of 0.29 ± 0.01 by stoichiometric reasons, it is expected that the ratio of methanol to water in this hydrogen-bonded structure

will be roughly 0.29÷0.71 or 3/7 . Therefore, the correlation between heat of mixing and the bulk viscosity appears to be connected to the structural stability requirements.

The correlation between the bulk viscosity and adsorbtion density can be explained by the following considerations.

No action will occur unless the total free energy is thereby reduced. The spontaneous process will be the increase in the solution surface region of methanol that decreases the surface tension and, hence, diminishes the free energy of the system. This process will be offset by diffusion acting to make the methanol concentration the same in every region of the solution. Diffusion is inversely proportional to the bulk viscosity as described by Stokes-Einstein relation (Atkins, 1978).

$$D = \frac{kT}{6\pi\mu r} \qquad 3.25$$

where D is diffusion coefficient; k, Boltzman constant, and r is the effective radius of the solute molecules. It can be seen that, as the bulk viscosity decreases, the diffusion forces will increase and this will tend to decrease the adsorption density of the solute. Thus, in general, the larger the bulk viscosity of the aqueous methanol solution the greater will be the adsorption density of methanol at the solution-gas interface.

References

Adamson, A.W., (1976). "Physical Chemistry of Surfaces" 3rd Edition, John Wiley and Sons, New York.

Addison, C.C., (1945). The Properties of Freshly Formed Surfaces, Part IV: the Influence of Chain-Length and Structure on the Static and Dynamic Surface Tensions of Aqueous-Alcoholic Solutions, J. Chem. Soc., pp. 98-106.

Addison, C.C. and Elliott, T.A., (1949). The Properties of Freshly Formed Surfaces, Part X: a New Contracting Liquid-Jet Technique for the Study of Soluble Films at Small Surface Ages. J. Chem. Soc., pp. 2789-2805.

Atkins, P.W., (1978). Physical Chemistry, W.H. Freeman and Co., San Francisco.

Butler, J.A.V., Thomson, D.W., and Maclennan, W.H., (1933). The Free Energy of the Normal Aliphatic Alcohols in Aqueous Solution. Part I. The Partial Vapor Pressures of Aqueous Solutions of Methyl, n-Propyl and n-Butyl Alcohols. J. Chem. Soc. Part I, pp. 674-679.

Carr, C. and Riddick, J.A., (1951). Physical Properties of Methanol-Water System. Indust. Eng. Chem., vol. 43, No. 3, pp. 692-696.

Christensen, J.J., Hanks, R.W., and Izatt, R.M., (1982). Handbook of Heats of Mixing, pp. 1437-1442, John Wiley and Sons, New York.

Christian, S.D., Lane, E.H., and Tucker, E.E., (1981). Liquid-Vapor Equilibrium of Dilute Aqueous Solutions of Methanol. J. Solution Chem., vol. 10, No. 3, pp. 181-188.

Concha, F. and Almendra, E.R., (1979). Settling Velocities of Particulate Systems, 1: Settling Velocities of Individual Spherical Particles. Int. J. Miner. Process, vol. 5, No. 4, pp. 349-367.

D'Aprano, A., Donato, I.D., Caponetti, E., and Agrigento, V., (1979). Viscosity Studies of Solutions of Water in n-Aliphatic Alcohols. J. Solution Chem. vol. 8, No. 11, pp. 793-800.

Davies, J.T., and Rideal, E.K., (1963). Interfacial Phenomena, 2nd Edition Academic Press, New York.

De Bruyn, P.L. and Agar, G.E., (1962). Surface Chemistry in Flotation. Chapter 5 in Froth Flotation: 50th Anniversary Volume, D.W. Fuersteneau (Editor), pp. 91-138, AIME, New York.

Defay, R., Prigogine, I and Bellemans, A., (1966). Surface Tension and Adsorption, translated by D.H. Everett, Longmans, Green and Co., London.

Dobby, G.S., 1984. McGill Univ., Dept. Min. Metall. Eng., Private Comm.

Eisenberg, D. and Kauzmann, W., (1969). The Structure and Properties of Water. pp. 222-224, Oxford University Press, New York.

Fletcher, N.H., (1968). Surface Structure of Water and Ice. Phil. Mag., vol. 18, pp. 1287-1300.

Franks, F., (1967). Properties of Aqueous Solutions of Non-Electrolytes. In: Physico-chemical Processes in Mixed Aqueous Solvents. F. Franks (Editor)., pp. 50-70, American Elsevier Publishing Co., New York.

Franks, F. and Ives, D.J.G., (1966). The Structural Properties of Alcohol-Water Mixtures, Chem. Soc. Quart. News, vol. 20., pp. 1-44.

Gmehling, J., Onken, U., and Arlt, W., (1982). Vapor-Liquid Equilibrium Data Collection. Aqueous-Organic Systems. Supplement 1, vol. 1, part 1a, p. 49, Dechema, Frankfurt/Main.

Grainger-Allen, T.J.N., (1970). Bubble Generation in Froth Flotation Machine, c15-22, Trans. I.M.M.

Guggenheim, E.A. and Adam, N.K., (1933). The thermodynamics of Adsorption at the Surface of Solutions. Proc. Roy. Soc., vol. A139, pp. 218-236.

Hall, D.J., Mash, C.J., and Pemberton, R.C., (1979). NPL report Chem. 95 January as reported in Gmehling et al. (1982).

Harkins, W. and Jordan, H.F., (1930). A Method for the Determination of Surface and Interfacial Tension from the Maximum Pull on a Ring, J. Am. Chem. Soc., vol. 52, pp. 1751-1772.

Harkins, W. and Wampler, R.W., (1931). The Activity Coefficients and the Adsorption of Organic Solutes. I. Normal Butyl Alcohol in Aqueous Solution by the Freezing Point Method. J. Am. Chem. Soc., vol. 53, pp.850-859.

Ivash, E.V. and Dennison, D.M., (1953). The Methly Alcohol Molecule and its Microwave Spectrum, The J. Chem. Phys., vol. 21, No. 10, pp. 1804-1817.

De Bruyn, P.L. and Agar, G.E., (1962). Surface Chemistry in Flotation. Chapter 5 in Froth Flotation: 50th Anniversary Volume, D.W. Fuersteneau (Editor), pp. 91-138, AIME, New York.

Defay, R., Prigogine, I and Bellemans, A., (1966). Surface Tension and Adsorption, translated by D.H. Everett, Longmans, Green and Co., London.

Dobby, G.S., 1984. McGill Univ., Dept. Min. Metall. Eng., Private Comm.

Eisenberg, D. and Kauzmann, W., (1969). The Structure and Properties of Water. pp. 222-224, Oxford University Press, New York.

Fletcher, N.H., (1968). Surface Structure of Water and Ice. Phil. Mag., vol. 18, pp. 1287-1300.

Franks, F., (1967). Properties of Aqueous Solutions of Non-Electrolytes. In: Physico-chemical Processes in Mixed Aqueous Solvents. F. Franks (Editor)., pp. 50-70, American Elsevier Publishing Co., New York.

Franks, F. and Ives, D.J.G., (1966). The Structural Properties of Alcohol-Water Mixtures, Chem. Soc. Quart. News, vol. 20., pp. 1-44.

Gmehling, J., Onken, U., and Arlt, W., (1982). Vapor-Liquid Equilibrium Data Collection. Aqueous-Organic Systems. Supplement 1, vol. 1, part 1a, p. 49, Dechema, Frankfurt/Main.

Grainger-Allen, T.J.N., (1970). Bubble Generation in Froth Flotation Machine, c15-22, Trans. I.M.M.

Guggenheim, E.A. and Adam, N.K., (1933). The thermodynamics of Adsorption at the Surface of Solutions. Proc. Roy. Soc., vol. A139, pp. 218-236.

Hall, D.J., Mash, C.J., and Pemberton, R.C., (1979). NPL report Chem. 95 January as reported in Gmehling et al. (1982).

Harkins, W. and Jordan, H.F., (1930). A Method for the Determination of Surface and Interfacial Tension from the Maximum Pull on a Ring, J. Am. Chem. Soc., vol. 52, pp. 1751-1772.

Harkins, W. and Wampler, R.W., (1931). The Activity Coefficients and the Adsorption of Organic Solutes. I. Normal Butyl Alcohol in Aqueous Solution by the Freezing Point Method. J. Am. Chem. Soc., vol. 53, pp.850-859.

Ivash, E.V. and Dennison, D.M., (1953). The Methly Alcohol Molecule and its Microwave Spectrum. The J. Chem. Phys., vol. 21, No. 10, pp. 1804-1817.

Kitchener, J.A., (1964). Foams and Free Films, Chapter 2. In: Recent Progress in Surface Science. J.F. Danielli et al. (Editors). Vol. 1, pp. 50-90.

Klassen, V.I. and Mokrousov, V.A., (1963). An Introduction to the Theory of Flotation. Translated by J. Leja and G.W. Poling, Butterworts, London.

Langmuir, I., (1917). The Constitution and Fundamental Properties of Solids and Liquids. II. Liquids. J. Amer. Chem. Soc., vol. 39, pp. 1848-1905.

Leja, J., (1982). Surface Chemistry of Froth Flotation. Plenum Press, New York.

Luck, W.A.P., (1967). Spectroscopic Studies of the Structure of Associated Liquids, In: Physico-chemical Processes in Mixed Aqueous Solvents. F. Franks (Editor), pp. 11-49. Amer. Elsevier Publishing Co., New York.

Mainhood, J. and Whelan, P.F., (1955). Flotation Frothers for Low-rank Coals. J. Appl. Chem. vol. 5, pp. 133-144.

Marrucci, G. and Nicodemo, L., (1967). Coalescence of Gas Bubbles in Aqueous Solutions of Inorganic Electrolytes. Chem. Eng. Sci., vol. 22, pp. 1257-65.

Mato, F., and Berrueta, J., (1977). Anales de quimica, Madrid, vol. 73, pp. 1495-1499; as reported in Christensen, J.J. et al. (1982).

Meissner, H.P., and Michaels, A.S., (1949). Surface Tensions of Pure Liquids and Liquid Mixtures. Indust. Eng. Chem., vol. 41, No. 12, pp. 2782-2787.

Monick, J.A., (1968). Alcohols: their Chemistry, Properties and Manufacture, Reinhold Book Co., New York.

Nemethy, G. and Scheraga, H.A., (1962). The Structure of Water and Hydrophobic Bonding in Proteins. I. A Model for the Thermodynamic Properties of Liquid Water. The J. Chem. Phys., vol. 36, pp. 3382-3394.

Pauling, L., (1960). The Nature of the Chemical Bond. 3rd Edition. a) p. 261, b) p. 452, c) pp. 474-475. Cornell Univ. Press, New York.

Pratt, L.R. and Chandler, D., (1980). Hydrophobic Interactions and Osmotic Second Virial Coefficients for Methanol in Water. J. Solution Chem., vol. 9, No. 1, pp. 1-17.

Reid, R.C., Prausnitz, J.M., and Sherwood, T.K., (1977). The Properties of Gases and Liquids, 3rd Edition, McGraw-Hill Book Co., New York.

Sagert, N.H., Quinn, M.J., Cribbs, S.C. and Rosinger, E.L.J., (1976). Bubble Coalescence in Aqueous Solutions of n-Alcohols. IN: Foams. R.J. Akers (Editor), Academic Press, New York.

Sun, S.C., (1952). Frothing Characteristics of Pine Oils in Flotation. Trans. AIME, vol. 193, p. 68.

Venkateswarlu, P. and Gordy, W., (1955). Methyl Alcohol. II. Molecular Structure. The J. Chem. Phys., vol. 23, No. 7, pp. 1200-1202.

Vinogradov, S.N. and Linnell, R.H., (1971). Hydrogen Bonding. Van Nostrand Reinhold Co., New York.

Weast, R.C., (1981-82). Editor; Handbook of Chemistry and Physics, CRC Press, West Palm Beach, Forida.

Zuidema, H.H. and Waters, G.W., (1941). Ring Method for the Determination of Interfacial Tension. Indust. Eng. Chem. vol. 13, No. 5, pp. 312-313.

CHAPTER 4

CRITICAL SURFACE TENSION OF WETTING AND OF FLOATABILITY

4. INTRODUCTION

Froth flotation is an important process in mineral separation. The process is complicated by the fact that there are a great number of variables affecting it (Sutherland and Wark, 1955). A difference in the wettability of the minerals to be separated is generally regarded as a prerequisite to the success of the process. Since, according to the concept of critical surface tension of wetting, surface tension of a liquid determines the extent of the wettability of solids by that liquid, surface tension of the flotation medium becomes an important variable by which the wettability of particles may be controlled. Sometimes, there are cases where the problem may involve the separation of two inherently hydrophobic minerals both exhibiting a natural floatability (Mathieu and Bruce, 1974). Theoretically, it is possible to selectively wet one inherently hydrophobic mineral in preference to the other by controlling the surface tension of the flotation medium. There have been several investigations reported on the subject (Hornsby and Leja, 1980; Kelebek and Smith, 1982;

Yarar and Kaoma, 1983). The basic conclusion reached was that selective separation of inherently hydrophobic solids by flotation can be achieved provided that their critical surface tension of wetting, γ_c values differ significantly. However, a more recent study by Hornsby and Leja (1983) has indicated that a difference in γ_c values is not necessarily required for an efficient separation. The concept of critical surface tension of floatability, γ_{cf}, was proposed. Hypothetical adhesion tension vs surface tension diagrams were used to describe the selectivity brought about by surface tension variation.

A detailed experimental investigation of the effect of solution surface tension on the wettability and floatability of inherently hydrophobic minerals will be described. The discussion will also describe selective flotation of inherently hydrophobic minerals.

4.2. EXPERIMENTAL MATERIALS AND PROCEDURE

4.2.1. Reagents

Methanol was the principal reagent used to control the bubble surface tension in the wettability and floatability tests. The properties of aqueous methanol solutions were described in Chapter 3. In addition to methanol, several other reagents were included in the study in order

to compare their wetting behaviour.

One of the wetting agents used is the sodium lignosulphonate, a sulphonation product of lignin, manufactured by Reed Ltd., Quebec City. The exact structure of neither lignin nor lignosulphonates is known. However, the lignosulphonate molecule is thought to be made of randomly-coiled, cross-linked polyaromatic chains (Reed Brochure). A suggested structure of the molecule is shown in Figure 4.1a.

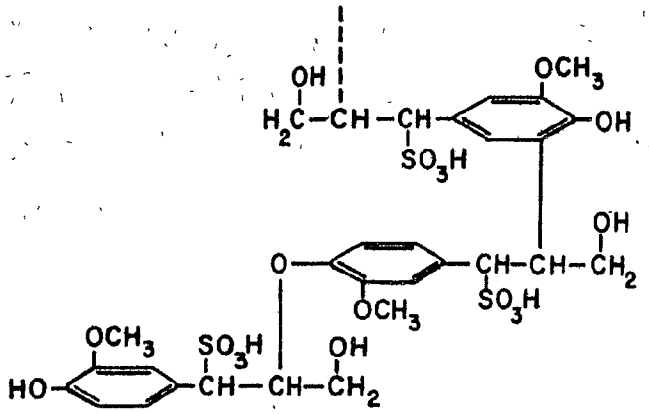


Figure 4.1a. Suggested Structure of Lignosulphonate

The negatively-charged sulphonate groups impart water-solubility to the lignin molecule, but carboxylic and phenolic groups are also involved. This reagent was used in combination with MIBC (10^{-4}M) in the wettability as well as in the separation tests involving talc and molybdenite.

A surfactant commonly known as Syntex (courtesy of Climax Molybdenum Co., Colorado) was used to determine its wetting behaviour on molybdenite. The structural formula of this reagent (Hoover and Malhotra, 1976) may be given as follows:-

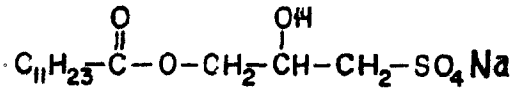


Figure 4.1b. Structure of Syntex

Decyl xanthate was used in order to obtain wettability data using a surfactant which chemisorbs on sulphides.

Surface tension of the aqueous solutions of these reagents are tabulated in Appendix III.

4.2.2. Wettability Tests

Adhesion tensions were determined for a number of inherently hydrophobic minerals using contact angle data obtained in aqueous methanol solutions. The minerals studied include sulphur, molybdenite, talc, graphite, stibnite and coal. However, because of the availability of high purity samples with smooth crystal faces or cleavage planes, sulphur and molybdenite were used as representative hydrophobic solids. Two kinds of samples were prepared for each mineral:- the first one contains no (or

the least possible number of) hydrophilic sites (i.e. high-surface energy locations). For molybdenite, the sample was cleaved along the cleavage plane. In the case of sulphur, the sample was prepared by recrystalization from carbon disulphide. The second type of sample, much more wettable than the first, was prepared from the flotation feed by the disc method. The details of sample preparation may be found in Chapter 2.

Contact angles were measured using the captive bubble method and apparatus (section 2.3.3). In each case, after 20 minutes of contact with the surface, the angles were measured to the nearest degree. In addition to the recrystalized sulphur sample, fracture planes obtained from a natural sulphur crystal from Girgenti, Sicily (courtesy of Redpath Museum, McGill University) were included in contact angle measurements. The angles measured in distilled water were in good agreement with those of the synthetically grown crystal. Subsequent measurements in aqueous methanol solutions were completed using the synthetic sample only. For each sample, between five and nine measurements were taken and averaged. In general, the contact angles measured on the disc samples differed by ± 3°. However, it was observed that as the surface tension of test solution approached γ_c value of the sample, for some regions of the surface contact angles were unmeasurably small while for

others contact angles of about 20° could still be measured. This was attributed to the mosaic nature of the disc samples (i.e. heterogeneity and some degree of surface roughness) and to the difficulty of precise contact angle measurements below 20°. The contact angles measured on the crystal faces remained in a narrower range (i.e. ± 1.5°).

4.2.3. Floatability Tests

The samples used in the floatability tests may be categorized into three main groups. The first group includes polymeric solids, namely polyethylene, PE (Union Carbide), polystyrene, PS (Shell Chem. Co.), polyvinylchloride, PVC (B.F. Goodrich Co.), and polyamide 6, PA6 (Badische Canada Ltd., BASF), which are typical low-surface-energy solids with γ_c values ranging from 31 to about 45 mN/m (Zisman, 1964). The PS sample was received in the pellet form, which was later pulverized. The others were obtained in powder form. Flotation tests with these samples were conducted using the 48 x 150 mesh fraction.

The second group consists of sulphides such as galena, chalcopyrite, orpiment, etc. while the third group includes sulphur and the layer-type minerals like talc and graphite. The sample preparation for these minerals is the same as that reported in Chapter 2.

Immediately prior to flotation tests, the second

group minerals were pretreated to remove hydrophilic surface compounds that may have formed due to oxidation. Treatment of the surfaces of orpiment and stibnite was performed by leaching in a hot 0.1 N sodium hydroxide solution for five minutes, washing with hot distilled water and dilute hydrochloric acid solution (2-4%), finally rinsing thoroughly with distilled water. This treatment was used to dissolve the oxides such as As_2O_3 and Sb_2O_3 from the surfaces, which are otherwise insoluble in water (Bailar et al., 1975a). Similarly, Cu_2O, CuO and $Cu(OH)_2$ are insoluble in water but soluble in ammonia solutions (Bailar et al., 1975b). Therefore, the chalcocite feed sample was pretreated by leaching in ammonia solutions followed by a washing operation similar to the above. Treatment of galena surfaces was carried out using ammonium and sodium chloride solutions (Chapter 5). Preliminary observations proved these pretreatments to be very effective in increasing the floatability of these samples. However, for some minerals such as talc, graphite, and chalcopyrite no pretreatment was necessary as the minerals were highly floatable without any pretreatment.

In addition to low-surface-energy polymers, a high-surface-energy solid was incorporated in the experimental work. Acid purified silica sand (BDH Chem. Co.) was chosen for this purpose. The 80 x 150 mesh fraction was used in the flotation tests.

All flotation tests were carried out at natural pH values of methanol solutions (pH=5.7-6.2) using the flotation cell and following the general procedure described in Chapter 2. Prior to the flotation tests, deslimed feed was washed rigourously with distilled water and methanol solution of desired surface tension before it was transferred to the flotation cell. The flotation time was one minute for the single mineral flotation tests and 30 seconds for the separation of binary mineral mixtures (50:50).

4.3. RESULTS

4.3.1. Wettability Tests

The results of contact angle measurements were plotted in terms of adhesion tension versus solution surface tension. This type of diagram, introduced by Lucassen-Reynders (1963), has been found to linearly represent the contact angle data obtained in both oil and water phases (Smolders, 1967; Bargeman and Van Voorst Vader, 1973). In such a diagram, lines of constant contact angle radiate from the origin, between θ=0° and 180°. The straight line passing through the origin with a slope of 1 (i.e. + 45° line) represents the zero contact angles. Thus intercept of this line with the wettability line of a sample defines a critical surface tension of wetting, γ_c for that sample.

Figure 4.2 illustrates the adhesion tension variation for a disc sample of talc (Quebec), a polished coal sample, and a cleavage plane of graphite. The slope values, β of the wettability lines for these minerals are 0.5, 0.31 and -0.47 respectively. γ_c for the talc and coal samples are the same at 35.5 mN/m whereas γ_c for the graphite sample is 33.4 mN/m. Similarly, Figure 4.3 shows the adhesion tensions of two stibnite samples. The sample obtained by mechanical polishing has a greater β (0.71) and γ_c value (39.5 mN/m) than the sample obtained by fracture (β=0.33, γ_c=32.5 mN/m). As in the case of the results shown in Figure 4.2, the data for these two stibnite specimens were obtained in aqueous methanol solutions. Figure 4.3 also illustrates the adhesion tension variation obtained with mechanically polished stibnite sample using n-decyl xanthate solutions. In contrast to the linearity of the wettability lines obtained with the methanol solutions, the adhesion tension determined using n-decyl xanthate initially decreases with decreasing $\gamma_{\ell v}$ passing through a minimum at 47 mN/m it then increases linearly with further decreases in $\gamma_{\ell v}$. The γ_c value occurs for this system at ~ 37 mN/m.

Two non-linear adhesion tension vs. solution surface tension graphs are shown in Figure 4.4. One was obtained with the polished edge of molybdenite in decyl xanthate solutions while the other was obtained using a molybdenite

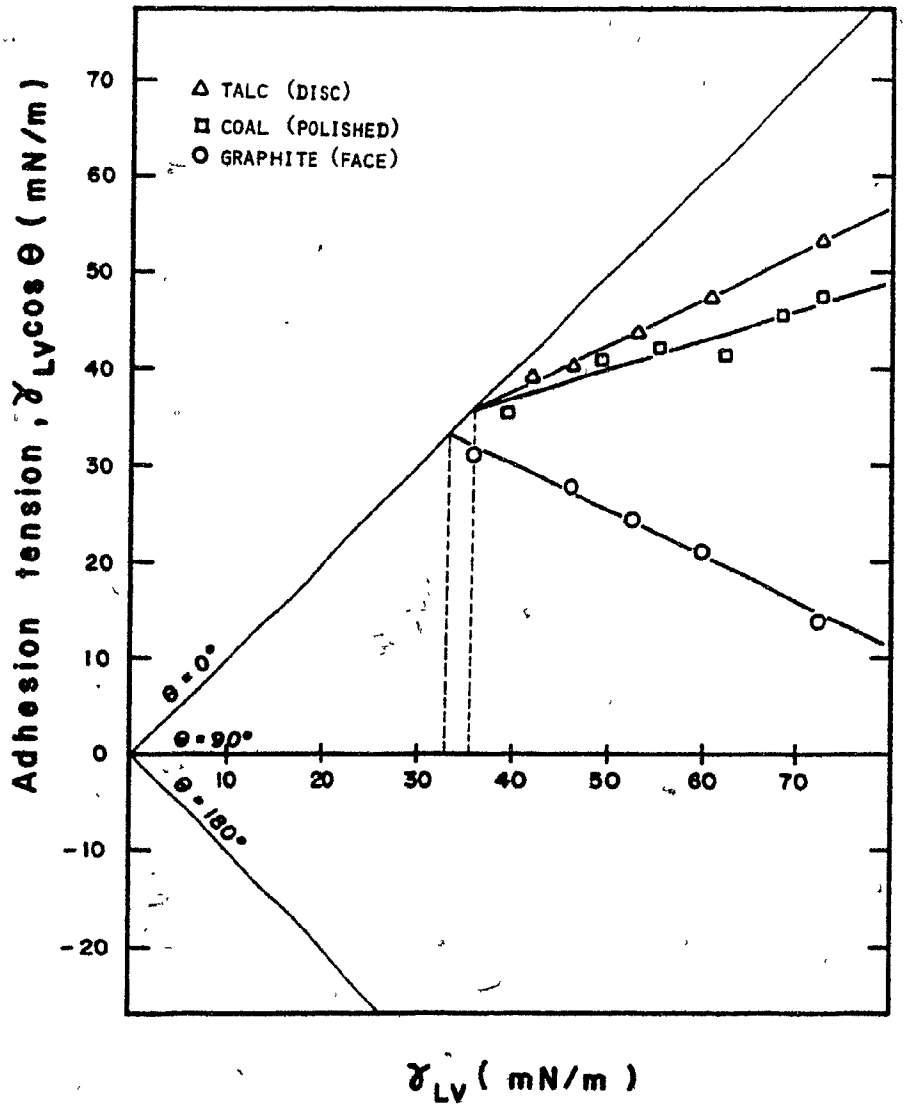


Figure 4.2 Adhesion Tension Diagram for Talc, Coal and Graphite in Aqueous Methanol Solutions

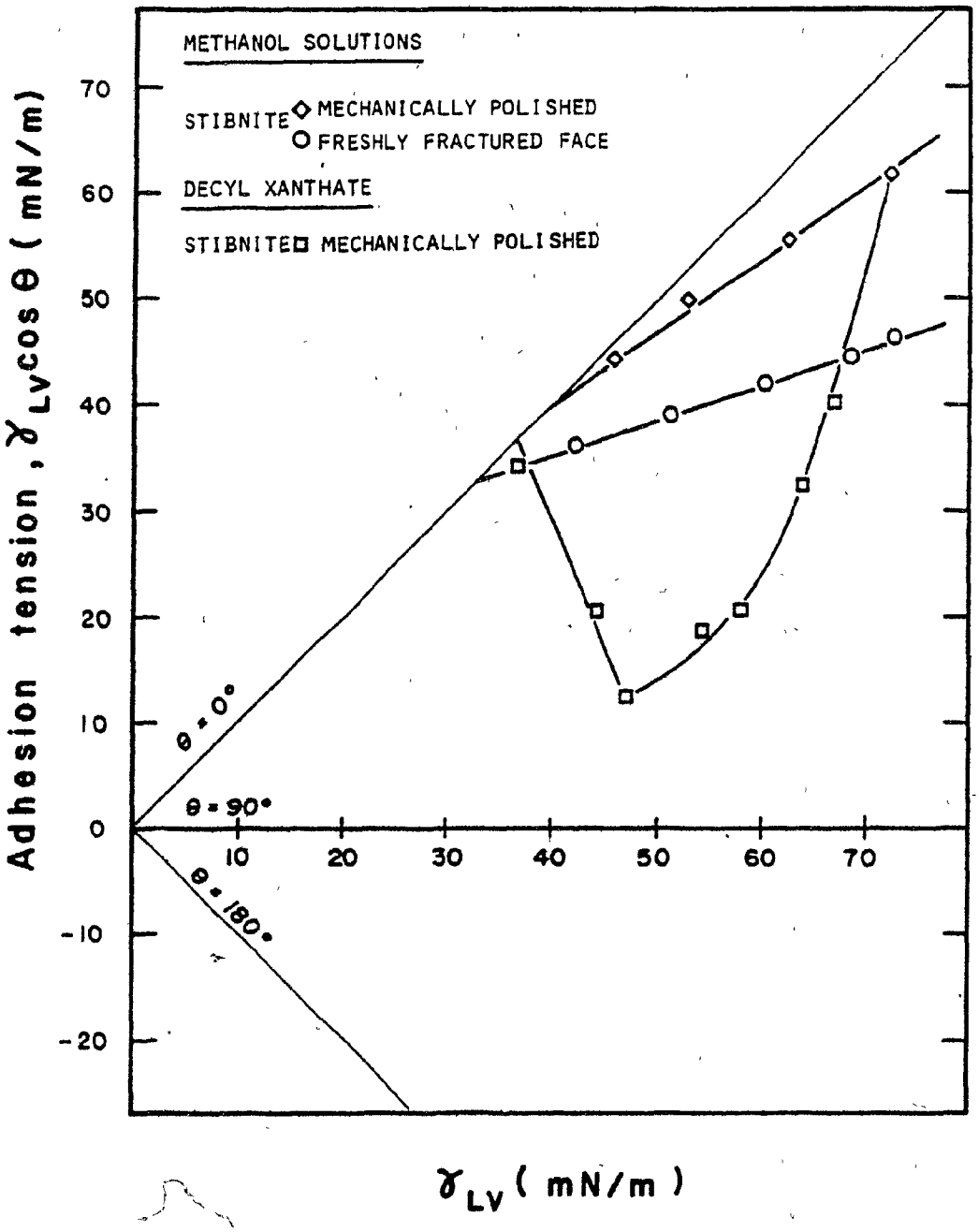


Figure 4.3 Adhesion Tension Diagram for Stibnite in Aqueous Methanol and Decyl Xanthate Solutions

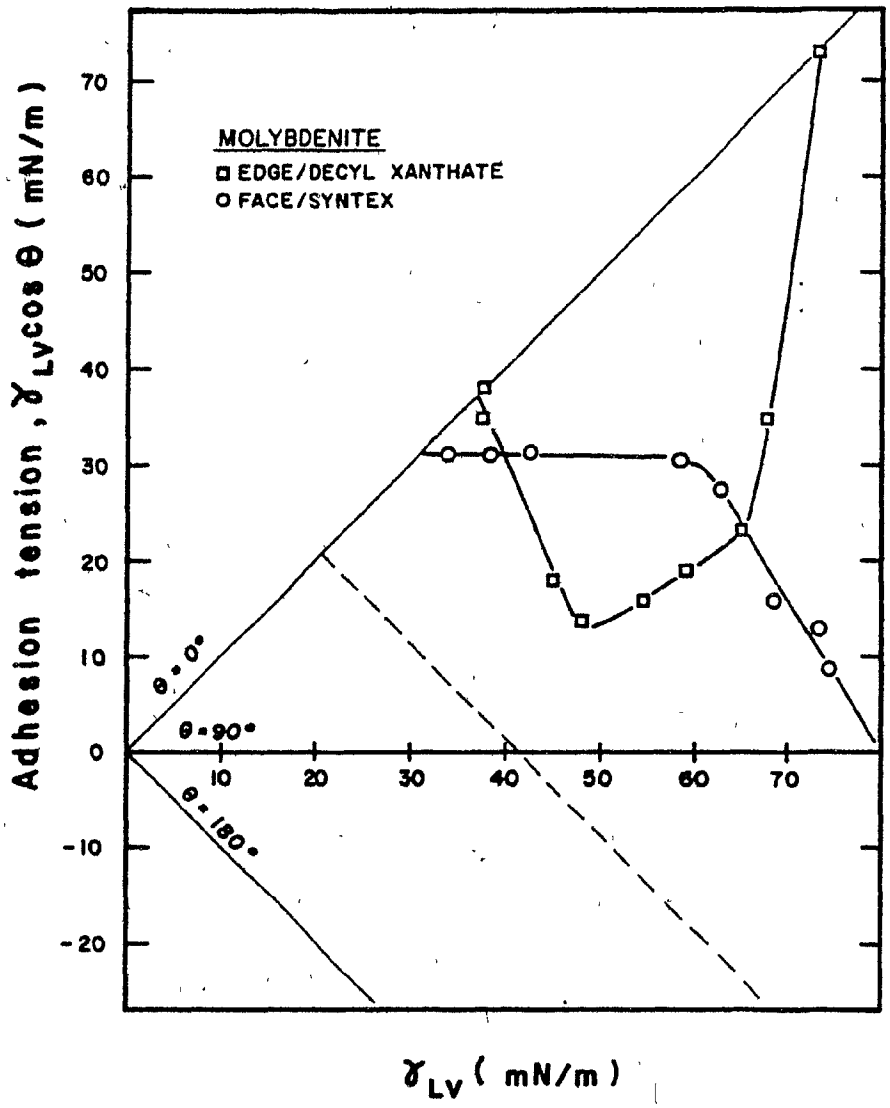


Figure 4.4 Adhesion Tension Diagram for Molybdenite in Aqueous Decyl Xanthate and Syntex Solutions

cleavage plane (face) in Syntex solutions. The edge sample did not give any finite contact angle in Syntex solutions at all surface tension values used. The adhesion tension of the face sample increases linearly with decreasing $\gamma_{\ell v}$ values up to about 60 mN/m then it remains constant at ~ 31 mN/m which represents the γ_c value for this system. Adhesion tension variation of the edge sample is similar to that observed for stibnite (Figure 4.3). The main difference is that the molybdenite edge is completely hydrophilic while the polished stibnite is weakly hydrophobic. However, the γ_c values for both samples are the same (~ 37 mN/m).

A series of straight wettability lines obtained using the molybdenite and sulphur samples and methanol solutions are shown in Figure 4.5. The values of γ_c and β for the disc samples are respectively 41.7 mN/m and 0.34 for the molybdenite, and 33.3 mN/m and 0.05 for the sulphur. The wettability lines for the cleavage plane of the molybdenite and crystal face of the sulphur are nearly parallel to each other. The γ_c and β values of the former are 29.2 mN/m and -0.43 respectively as compared to the respective values of 26.9 mN/m and -0.48 for the latter.

The variation in adhesion tension of molybdenite and talc in the sodium lignosulphonate (Lignosol-XD) and MIBC solutions is shown in Figure 4.6. The MIBC concentration of the solutions was fixed at 10^{-4} M while the Lignosol-XD

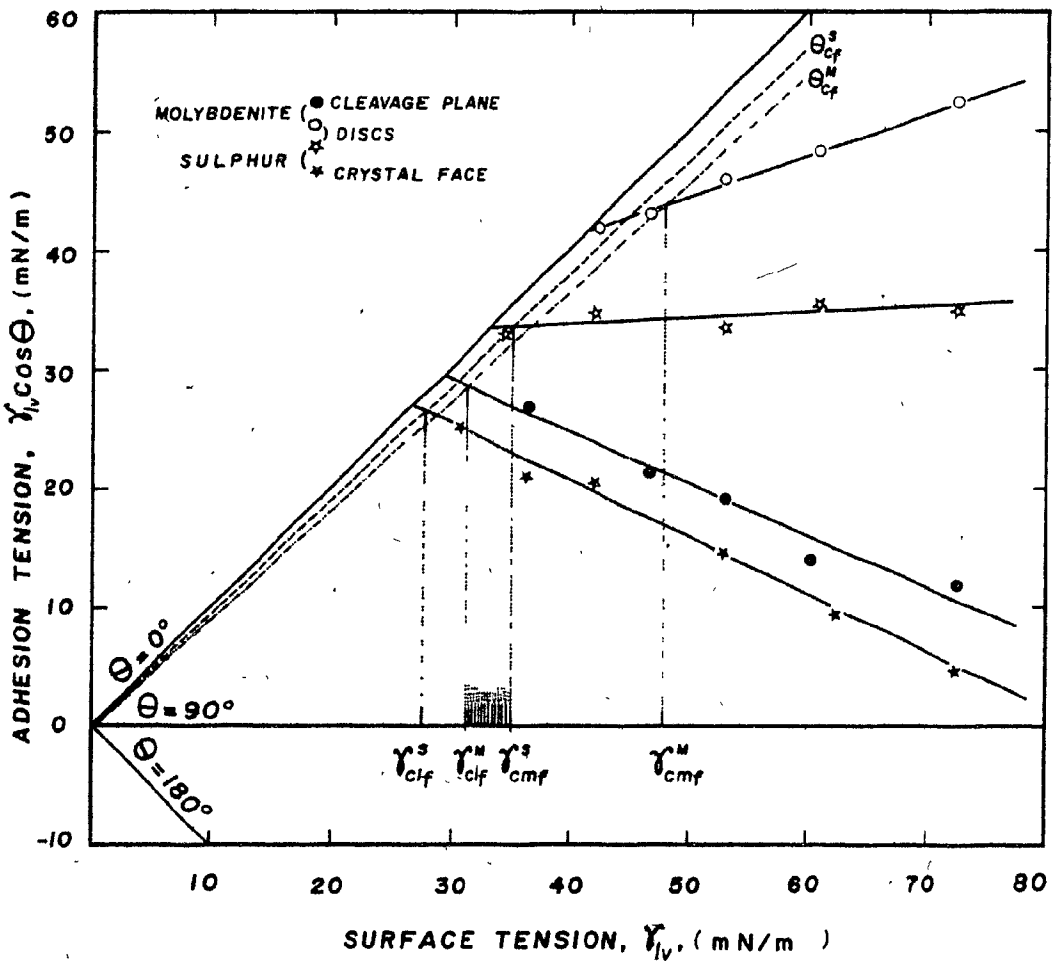


Figure 4.5 Adhesion Tension Diagram Illustrating the Upper and Lower Limits of Critical Surface Tension Range of Wettability and Floatability for Sulphur and Molybdenite

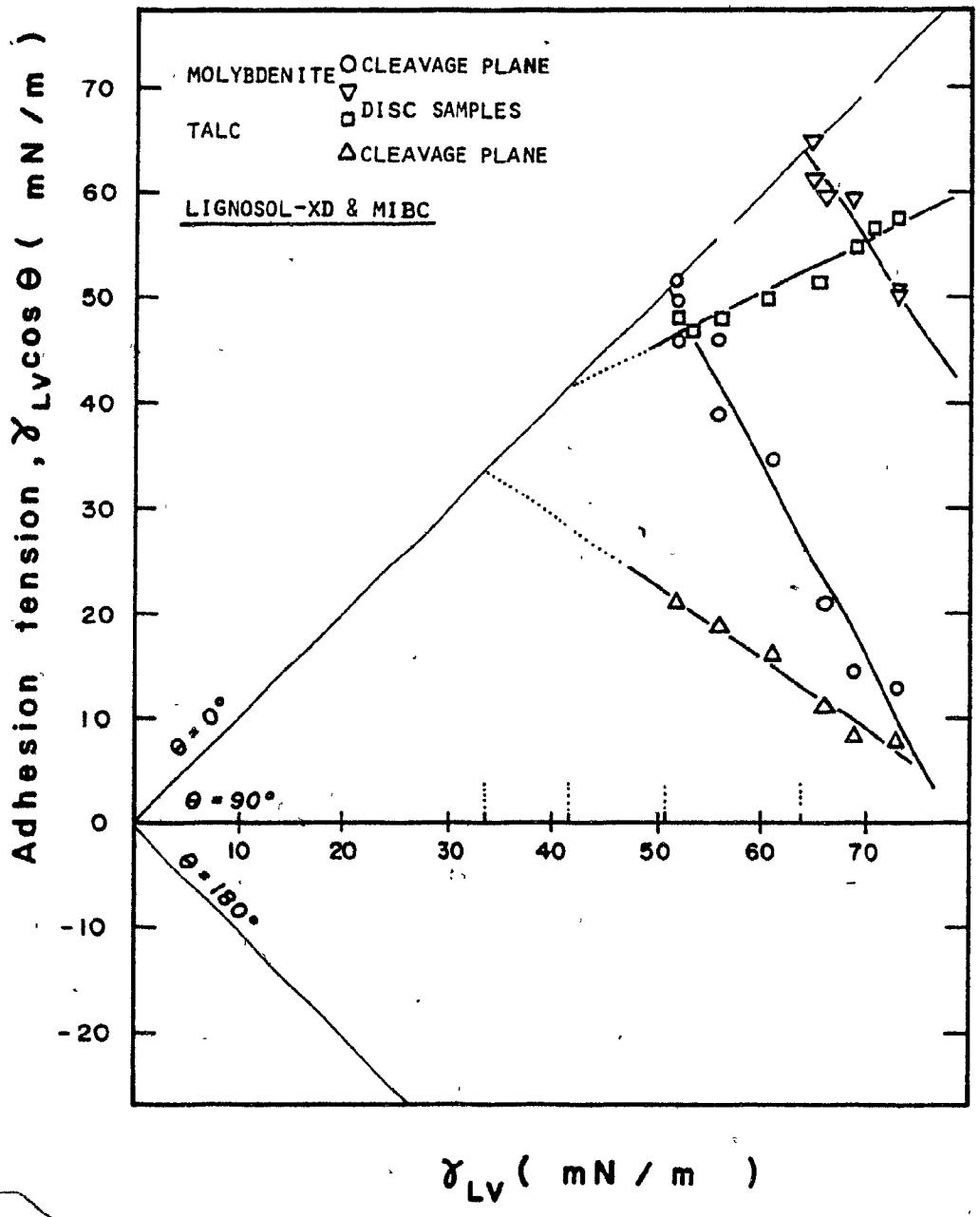


Figure 4.6 Adhesion Tension Diagram for Talc and Molybdenite in Aqueous Lignosulphonate and MIBC Solutions

content was changed in order to obtain solutions of various surface tension. For each mineral, two specimens were tested (a disc and a cleavage plane sample). The reason for studying these two kinds of minerals in the same solution system is to note any wettability differences and relate them to the separability of these two inherently hydrophobic minerals by selective flotation. The disc specimen of talc was prepared from the Quebec talc. Since this sample did not yield cleavage planes of acceptable smoothness, a cleavage plane of talc was obtained from the Oregon sample. The adhesion tension changes linearly in this solution system. The γ_c values are 33.5, 42, 50.7, and 63.7 mN/m for the cleavage plane of talc, the disc sample of talc, the cleavage plane of molybdenite, and the disc sample of molybdenite respectively. The β values, in increasing order, are -1.84, -1.5, -0.69, and 0.5 respectively for the molybdenite cleavage plane the disc sample of molybdenite, the cleavage plane of talc, and the disc sample of talc.

4.3.2. Floatability Tests

The results of flotation tests carried out in aqueous methanol solutions using four types of polymers are shown in Figure 4.7. The flotation recoveries change from 100% to close to 0% over a certain range of surface tension. The lower limit of this critical range is the same (~ 30 mN/m) for PS, PVC, and PA6 (Nylon 6) while it is between 20 and

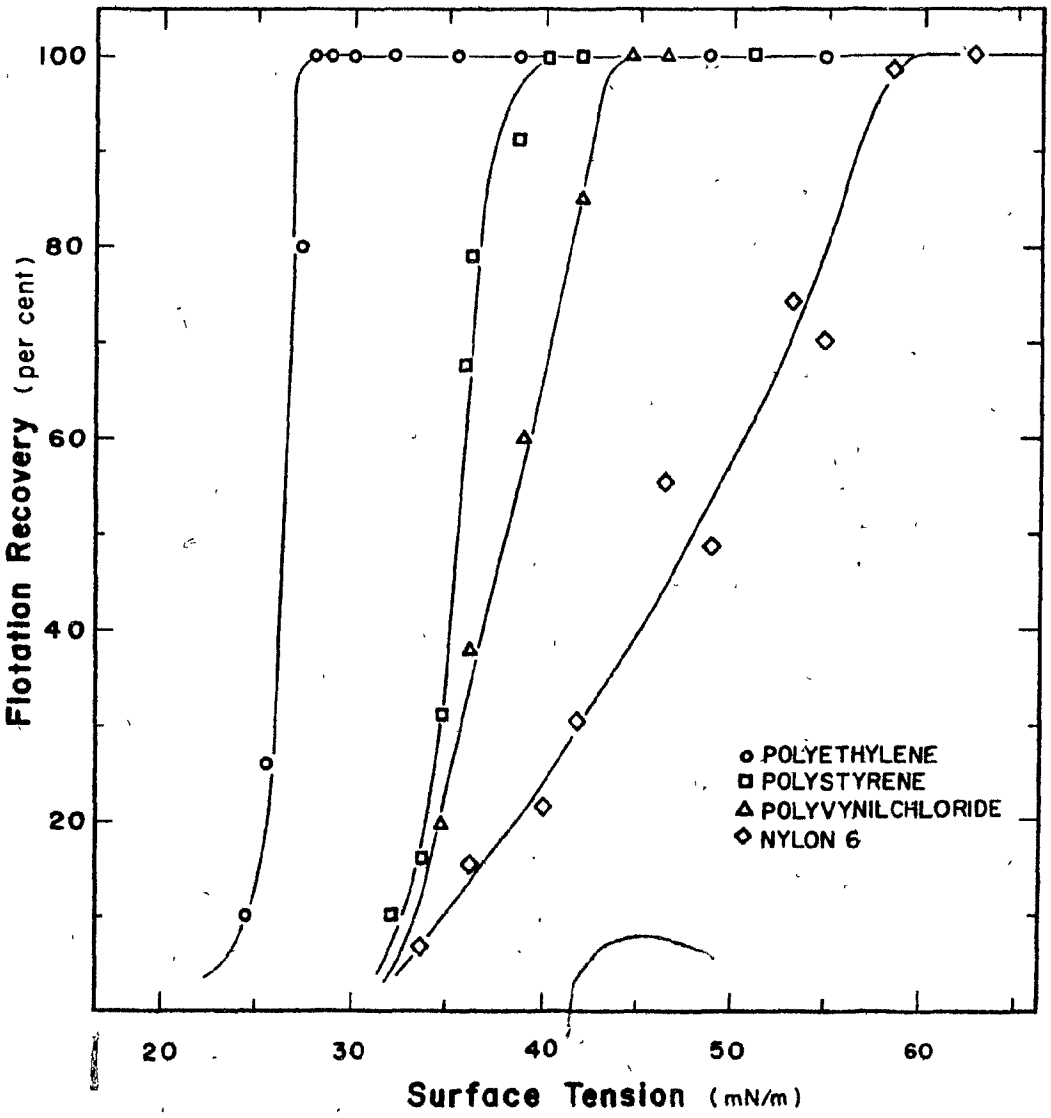


Figure 4.7 Floatability of Various Polymers in Aqueous Methanol Solutions of Various Surface Tension

25 mN/m for PE. The upper limits are approximately 27, 40, 45, and 60 for PE, PS, PVC, and PA6 respectively. The flotation behaviour of these polymers can be contrasted with that of a typical high-surface-energy solid, namely silica. Table 4.1 shows the recoveries

Table 4.1

Flotation of Silica Sand in Methanol Solutions of Various Surface Tension

$\gamma_{\ell v}$ (mN/m)	R(% wt.)
72.5	3.2
68.6	2.8
60.0	1.6
55.2	2.3
51.2	4.7
45.7	4.6
40.5	2.9
34.7	1.6
30.0	1.4
25.5	2.1

obtained with pure silica at different solution surface tensions. The recoveries, R(% wt.) are very low (less than 5%) regardless of the surface tension.

The recoveries obtained in methanol solutions using pretreated sulphide minerals are shown as a function of $\gamma_{\ell v}$ value in Figure 4.8. The curves resemble to those obtained with polymer samples in that the recoveries decrease sharply with decreasing $\gamma_{\ell v}$ values. For the samples of galena and chalcopyrite, the lower limit of the critical range is about

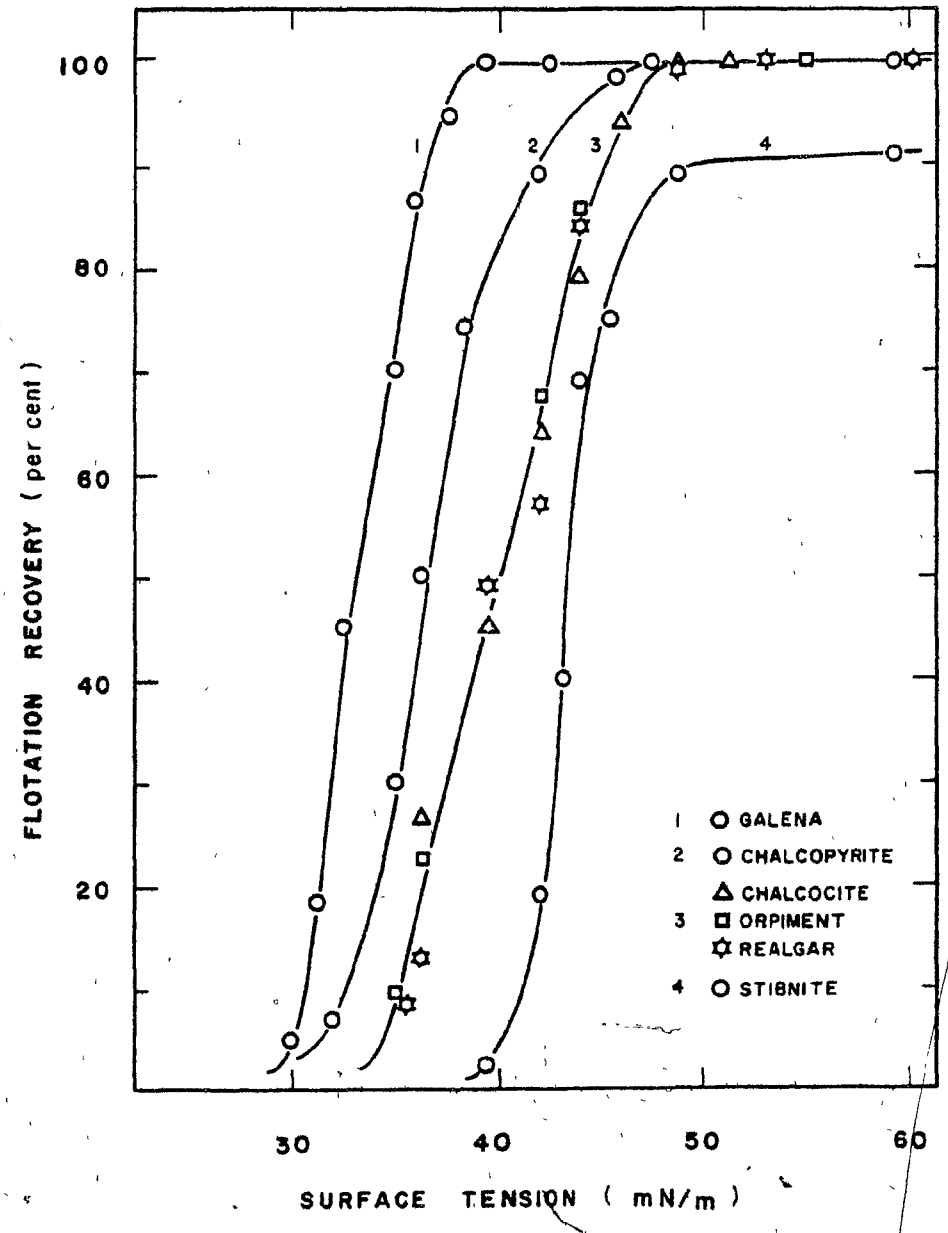


Figure 4.8 Floatability of Pretreated Sulphide Minerals in Aqueous Methanol Solutions of Various Surface Tension

30 mN/m, the same as that observed for PS, PVS, and PA6. For realgar and pretreated chalcocite, and orpiment, the recoveries are represented by the same curve. The lower limit of the critical range is ~ 33 mN/m for these minerals and about 39 mN/m for stibnite. The upper limits of the critical range of floatability are 39 mN/m for galena, 47.5 mN/m for chalcopyrite, chalcocite, orpiment and realgar, and ~ 50 mN/m for stibnite. Among these, only stibnite yielded a maximum recovery significantly less than 100% (~ 90%).

The flotation behaviour of typical inherently hydrophobic minerals (e.g. sulphur, talc, graphite and molybdenite) in methanol solutions is shown as a function for $\gamma_{\ell v}$ in Figure 4.9. The lower limit of the critical range of surface tension for these samples is located in the vicinity of 30 mN/m whereas the upper limit increases from 33.5 mN/m for sulphur to ~ 57.5 mN/m for molybdenite. The recoveries of a number of minerals, including chalcocite, stibnite, orpiment, coal and molybdenite were considerably lower in distilled water than in dilute methanol solutions. The situation is exemplified by the molybdenite sample in Figure 4.9:- The recovery of the molybdenite in distilled water was ~ 43% in the absence of methanol as compared to ~ 95% in the presence of 2% methanol (by vol.).

The results of separation tests on some binary

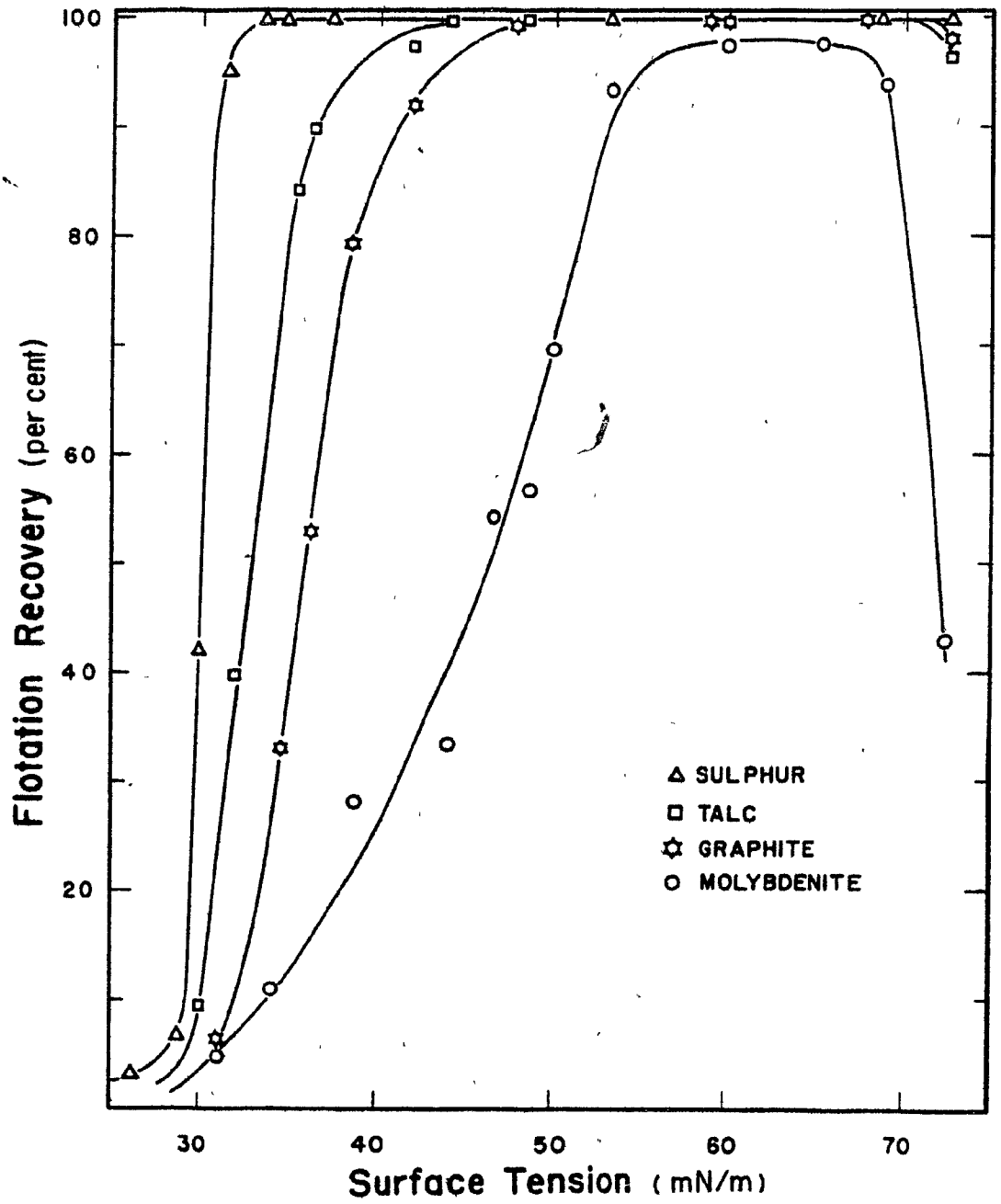


Figure 4.9 Floatability of Sulphur, Talc, Graphite and Molybdenite in Aqueous Methanol Solutions of Various Surface Tension

mixtures of inherently hydrophobic minerals are illustrated in Figure 4.10. The separability of these mineral mixtures was evaluated in terms of separation efficiency (plotted on the ordinate axis). Separation efficiency as described by Schultz (1970) refers to the fraction of the feed material that undergoes complete separation in a concentration process. The figure shows that each curve passes through a maximum at a certain solution surface tension. The methanol solution surface tensions at which the maximum separation is achieved are between 30 and 35 mN/m for the binary mixtures involving sulphur and about 40 mN/m for the mixture of talc and molybdenite. The maximum separation efficiencies obtained with mixtures containing sulphur, range from 63 to 97%. For the mixture of talc and molybdenite, the maximum separation efficiency is 88%.

The separability of talc from molybdenite by selective flotation using solutions of sodium lignosulphonate (lignosol-DX) and MIBC is illustrated in Figure 4.11. In these tests, as in the case of the wettability tests, the MIBC concentration of the lignosol-XD solutions was kept constant at 10^{-4} M. The curve has a maximum separation efficiency of 84% (wt.) in the surface tension range 60 to 65 mN/m. The decrease in the separation efficiency is more pronounced above 65 mN/m than below 60 mN/m.

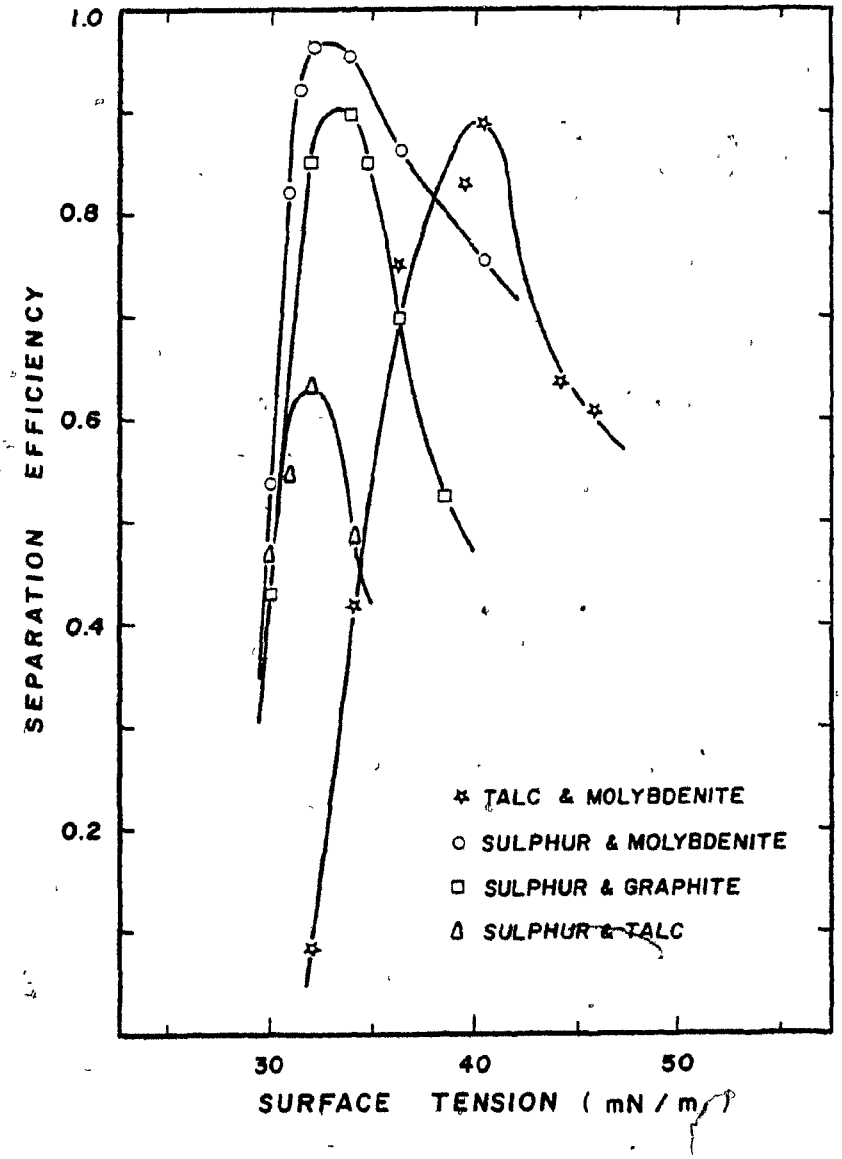


Figure 4.10 Separation Efficiencies for the binary Mixtures (50:50) of Various Inherently Hydrophobic Minerals in Aqueous Methanol Solutions of Various Surface Tension

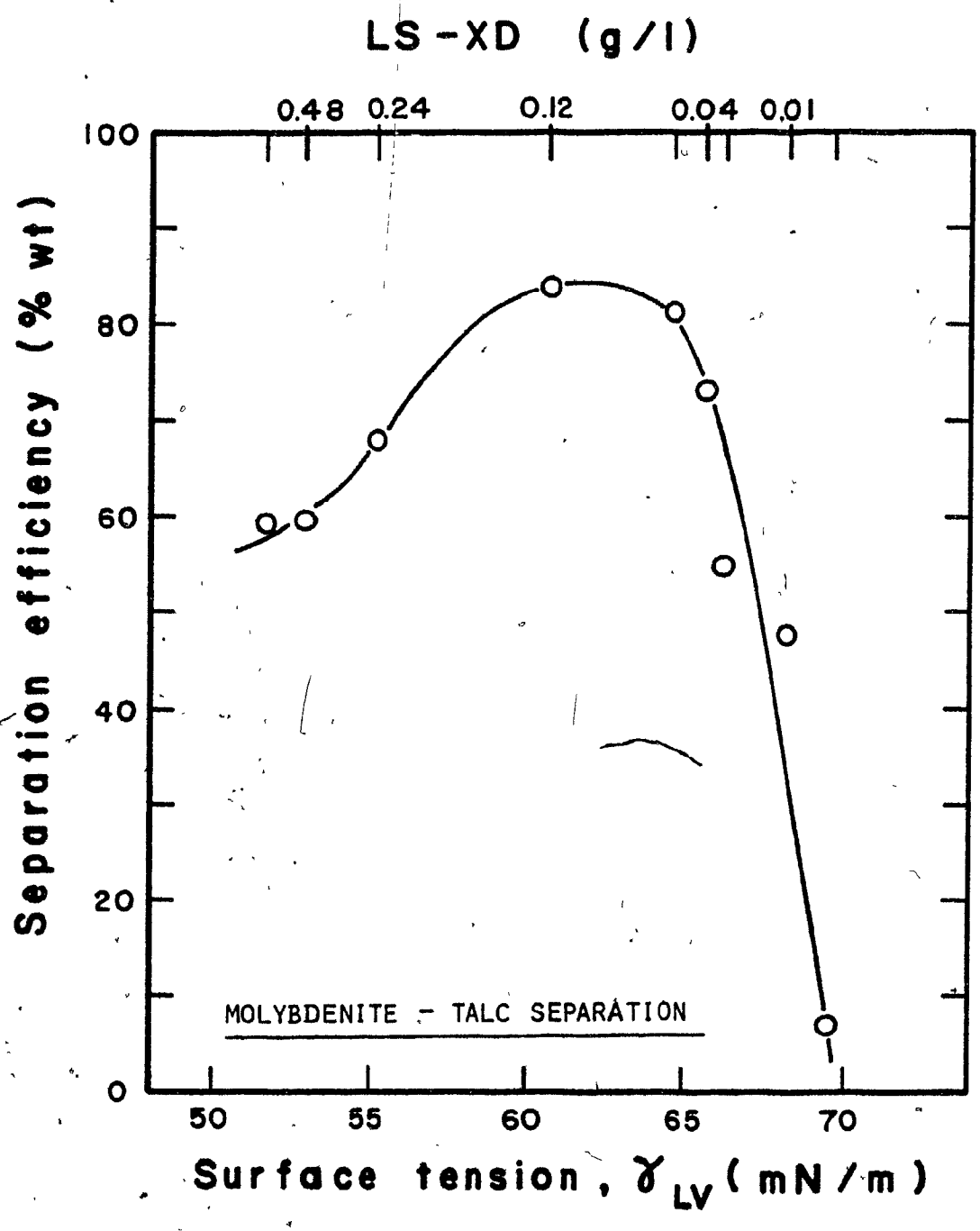


Figure 4.11 Separation Efficiencies for the Binary Mixtures (50:50) of Talc and Molybdenite in Lignosol-XD & MIBC Solutions of Various Surface Tension

4.4. DISCUSSION

4.4.1. Wettability

4.4.1.1. Representation of the Experimental Data

The contact angle and surface tension data may be represented in two different ways. One way is to plot Cos θ against $\gamma_{\ell v}$. If the data are produced using pure liquid droplets, there is a linear relationship between Cos θ and $\gamma_{\ell v}$ (Zisman, 1964). Bernett and Zisman (1959) found that aqueous surfactant solutions produced the same γ_c values for PE and Teflon as those obtained using pure liquids, but the Cos θ vs $\gamma_{\ell v}$ relationship was no longer linear. This non-linearity is also apparent from the contact angles measured on such inherently hydrophobic minerals as graphite, talc and stibnite (Fowkes and Harkins, 1940).

An alternative way of plotting θ and $\gamma_{\ell v}$ data is through the adhesion tension, $\gamma_{\ell v}$ Cos θ vs $\gamma_{\ell v}$, which appears to have been first suggested by Lucassen-Reynders (1963). In Figure 4.12, these two ways of plotting the data are compared using the contact angles measured on sulphur samples in methanol solutions. Because of the linearity of the $\gamma_{\ell v}$ Cos θ vs $\gamma_{\ell v}$ relationship, the contact angle data obtained in the present study are represented by the adhesion tension diagrams. This way, as in the case of the Zisman method, the wettability of a hydrophobic surface may be conveniently

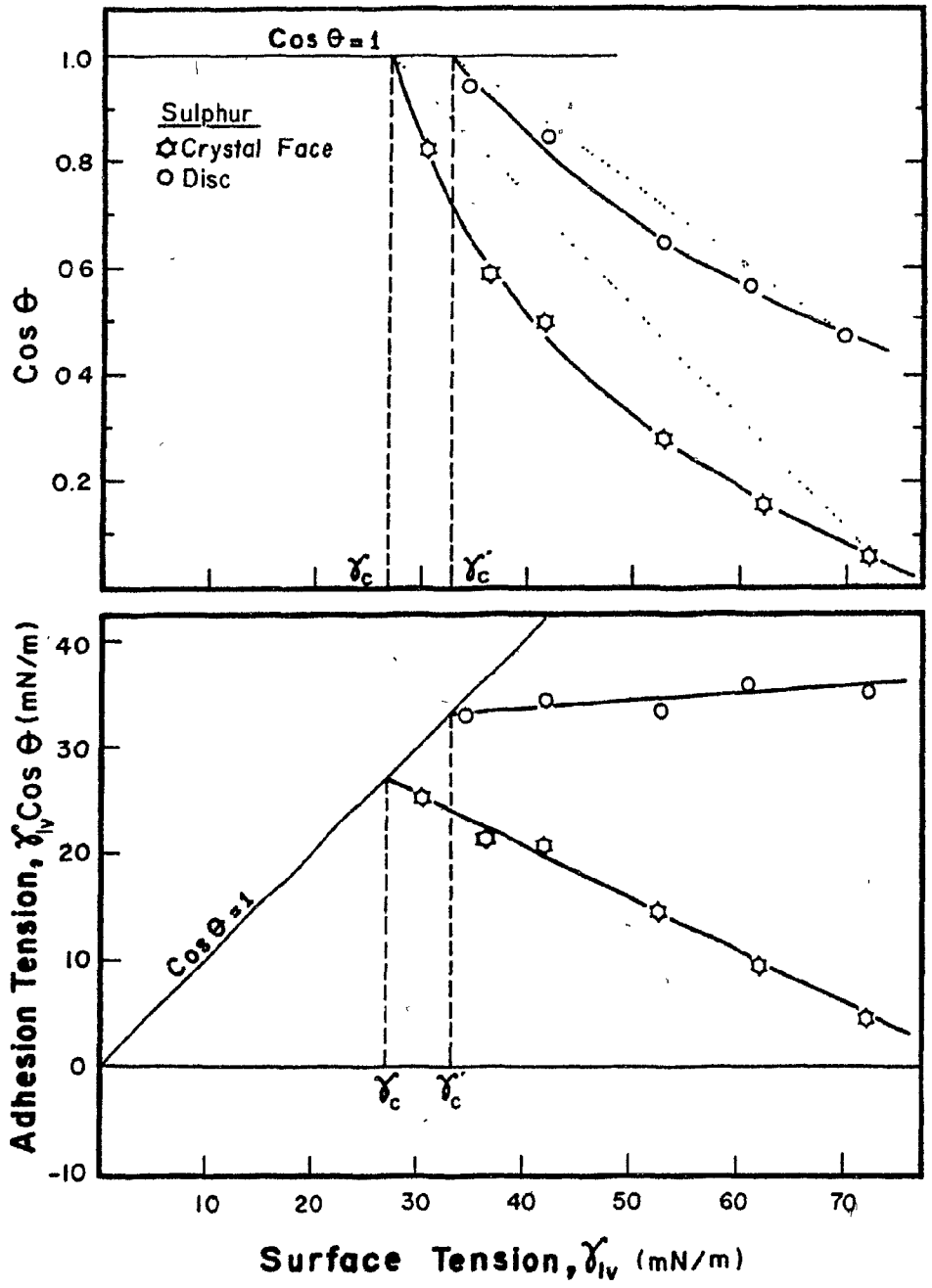


Figure 4.12 Zisman Wettability Diagram (top) and Adhesion Tension Diagram (bottom) for Sulphur in Aqueous Methanol Solutions

characterized by γ_c and the slope of the adhesion tension line, β. The general linear behaviour may be expressed mathematically as follows:-

$$\gamma_{\ell v} \text{ Cos } \theta = \beta \gamma_{\ell v} + (1 - \beta)\gamma_c \qquad 4.1$$

An additional advantage of representing the wettability data as an adhesion tension diagram is that it yields a relationship between the adsorptions at the three interfaces. Several researchers (Lucassen-Reynders, 1963; Somasundaran, 1968) have related the adhesion tension to the adsorption densities of solute at the three interfaces by combining Young's equation (Equation 2.5) with Gibbs' equation (Equation 3.27) based on the assumption of thermodynamic equilibrium. The relationship derived by Lucassen-Reynders is

$$\frac{d(\gamma_{sv}-\gamma_{s\ell})}{d\gamma_{\ell v}} = \frac{d(\gamma_{\ell v} \text{ Cos } \theta)}{d\gamma_{\ell v}} = \frac{\Gamma_{sv} - \Gamma_{s\ell}}{\Gamma_{\ell v}} \qquad 4.2$$

where Γ_{sv}, $\Gamma_{s\ell}$ and $\Gamma_{\ell v}$ are the adsorption densities of the solute at the three interfaces and $d(\gamma_{\ell v} \text{ Cos } \theta)/ d\gamma_{\ell v} = \beta$, the slope of a wettability line on an adhesion tension diagram. The simplest stated explanation for the linearity of a wettability line (i.e. constant β value) is the assumed proportionality of the three adsorptions over the whole concentration range.

4.4.1.2. Adhesion Tension Behaviour

The experimental data obtained in methanol solutions (Figures 4.2, 4.3 and 4.5) fit the linear type of equation (Equation 4.1) very well. The slopes of the wettability lines for the cleavage planes of molybdenite and graphite, and the crystal face of sulphur are negative while those for the polished specimens of coal and stibnite, and the disc samples of talc, sulphur and molybdenite are positive.

Negative slopes are characteristic of a significant non-polarity. Examination of the literature data (Fowkes and Harkins, 1940; Wada, 1950; Fowkes, 1953; Bernett and Zisman, 1959; Furmidge, 1962; Bargeman and van Voorst Vader, 1973) indicates that for various aqueous surfactant solutions the slope β is close to -1 for such non-polar solids as paraffin, Teflon, bee's wax and glyceryl tristearate. Bargeman and van Voorst Vader pointed out that a slope of -1 means $\Gamma_{s\ell} = \Gamma_{sv} + \Gamma_{\ell v}$ (consider Equation 4.2). They also argued that $\Gamma_{sv} = 0$ for non-polar solids which means that $\Pi^v = 0$. Recently, it has been proven by Fowkes et al. (1980) that Π^v is zero for water on Teflon.

The mineral samples studied are not as non-polar as solid paraffin or Teflon. Therefore, the β values of their wettability lines obtained using methanol solutions are less negative and in the case of disc samples they are actually positive. Positive β values not only signify that $\Gamma_{sv} > 0$,

but also $\Gamma_{sv} > \Gamma_{s\ell}$ as can be seen from Equation 4.2. Thus, the more positive the slope is, the greater the adsorption density at the solid/vapour interface, which implies a greater number of polar sites on the solid surface (i.e. a greater polar character). The relative polar character of a sample may be estimated in two ways: (a) by determining the so-called polar component of the surface-free energy of the samples, γ_s^P, using the octane contact angle values in Equation 2.24, and (b) by determining the fraction of hydrophilic sites on the surfaces of the samples, $X_{h\ell}$, using Equation 2.41. The values of slope β are compared with those of γ_s^P and $X_{h\ell}$ in Table 4.2. The β value for paraffin in

Table 4.2

Comparison of β, γ_s^P (average), and $X_{h\ell}$ Values for Various Inherently Hydrophobic Minerals

Sample	β	γ_s^P (mj/m^2)	$X_{h\ell}$
Paraffin	-1.00	0	0
Sulphur C.F.*	-0.48	1.2	-
Molybdenite C.P.†	-0.43	3.1	-
Sulphur disc	0.05	6.7	0.43
Stibnite (2)	0.33	-	0.60
Molybdenite disc	0.34	15.0	0.60
Talc disc	0.50	21.2	0.72
Stibnite (1)	0.71	37.0	0.82
Molybdenite edge	1.00	50.8	1.00
Talc edge	1.00	50.8	1.00

*C.F.: crystal face, †C.P.: cleavage plane

methanol solutions was obtained from the data by Good (1973). It was assumed to contain no polar sites on its surface (hence γ_s^P and $X_{h\ell}$ are zero). Table 4.2 indicates that an increase in the slope values is accompanied by a regular increase in γ_s^P and $X_{h\ell}$, both of which may be considered as an indication of the relative polar character of the samples. The slope of 1 for the edges of molybdenite and talc represents the completely hydrophilic surface for which $\gamma_s^P = 50.8$ mJ/m^2 and $X_{h\ell} = 1.0$.

The non-linear adhesion tension behaviour of stibnite and the molybdenite edges in decyl xanthate solutions is similar (Figures 4.3 and 4.4). The γ_c value is about 37° mN/m for both samples. In these two systems, the surfactant, decyl xanthate, adsorbs on the solid-liquid interface chemically. In contrast to the methanol system, the adhesion tension behaviour of this system is not reversible. At relatively low concentrations (i.e. solutions having $\gamma_{\ell v} > 50$ mN/m), the molecules of decyl xanthate are chemisorbed on the surface with their hydrocarbon radicals directed towards the bulk solution to form a low-surface-energy bydrocarbon coating. In concentrated solutions having $\gamma_{\ell v}$ values lower than 50 mN/m, apparently, additional molecules physically adsorb on top of the chemisorbed layer with reverse orientation, thus, causing the adhesion tension to increase sharply ($\beta \equiv -2.3$). At $\gamma_{\ell v} \equiv 37$ mN/m, the layer of physically adsorbed

decyl xanthate is probably complete and the surface contains many polar groups (from the xanthate) which are directed into the bulk solution. Since the surface is covered with such a polar layer (i.e. wetting film) the bubbles do not form a finite contact angle with it.

The adhesion tension variation of the molybdenite cleavage plane-Syntex system may be described with two straight lines. The slope of the first wettability line which holds for the solution surface tension range between 72.5 and 60 mN/m is -1.4. The negative value of this slope, according to Equation 4.2, may be interpreted as $\Gamma_{s\ell} > \Gamma_{sv}$. At $\gamma_{\ell v} < 60$ mN/m, the slope assumes a value of nearly zero, which means $\Gamma_{s\ell} \cong \Gamma_{sv}$. The configuration of the molecular orientation of the Syntex at the surface causing this type of behaviour is not clear. In the low concentration region (i.e. $72.5 > \gamma_{\ell v} > 60$ mN/m), the surfactant molecules are likely to lie prone to the surface through hydrophobic bonding between hydrocarbon group and hydrophobic molybdenite surface. In more concentrated solutions, additional molecules are adsorbed both at the bubble and molybdenite surface. At $\gamma_{\ell v} = 31$ mN/m ($\equiv \gamma_c$), the surfaces become saturated with polar groups so that no contact can be established between the bubble and molybdenite surface.

4.4.1.3. Selective Wetting Between Inherently Hydrophobic Minerals

The adhesion tension diagram may conveniently be used

to describe a surface tension range within which selective wetting occurs between two inherently hydrophobic minerals. Referring to Figure 4.2, graphite has a γ_c value of about 33.4 mN/m as compared to 35.5 mN/m, (the γ_c values), for both coal and talc samples. In solutions for which 33.4 mN/m $< \gamma_{\ell v} <$ 35.5 mN/m, coal and talc samples will be completely wetted, whereas the graphite surface will still form a finite contact angle with the bubble. Therefore, this narrow range of surface tension constitutes a selective wetting region between graphite and the other two minerals. There is no selective wetting region between coal and talc since their γ_c values are the same.

The selective wetting region between two hydrophobic minerals depends not only on the sample preparation technique but also the type of surfactant used. Samples prepared from the same mineral may have different γ_c values and thus a different selective wetting region if the sample preparation technique is different. In the present study, two kinds of sample were prepared from talc, molybdenite and sulphur. The cleavage planes (or crystal faces) and disc samples (Figure 4.13) represent the least wettable (or the most non-polar), and the most wettable (or the least non-polar) surfaces respectively. The purpose was to determine experimentally the lower and upper limits of the wettability band for each mineral. The samples prepared differently (e.g. by polishing, fracture, etc.) are most likely to have their

wettability lines within these limits. The wettability bands for sulphur and molybdenite samples in methanol solutions may be noted from Figure 4.5. For sulphur, this band is described by the two wettability lines having β and γ_c values of respectively 0.05 and 33.3 mN/m for the disc and -0.48 and 26.9 mN/m for the crystal face. For molybdenite, the wettability band is broader. Similarly, it may be described by the upper wettability line having β of -0.43 and γ_c of 41.7 mN/m, and by the lower wettability line with β of 0.35 and γ_c of 29.2 mN/m. The range of polarity corresponding to these wettability bands of sulphur and molybdenite expressed in terms of γ_s^p, is 1.1-8.0 mJ/m^2 and 2.8-16.5 mJ/m^2 respectively (Figure 4.13). It may be also noted that the selective wetting region is narrower for cleavage planes than for disc specimens of these minerals.

The wettability lines (Figure 4.6) for molybdenite obtained using Lignosol-XD and MIBC solutions have much greater γ_c and lower β values than those obtained using methanol solutions. For instance, γ_c and β values for the cleavage plane are 50.7 mN/m and -1.84 respectively in the lignosol solution as compared to 26.9 mN/m (γ_c) and -0.43 (β) in methanol solutions. This may be interpreted as the wettability by the lignosol solutions being much greater than that by methanol solutions. Apparently,

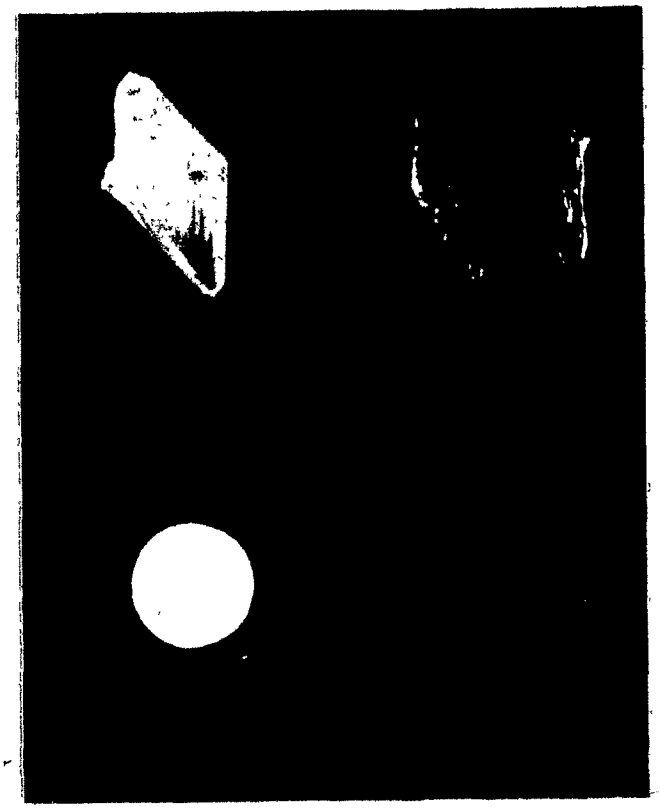


Figure 4.13 Crystal and Disc Samples of Sulphur (left) and Molybdenite (right) with Their γ_s^p Values Indicated

(γ_s^p is in mJ/m^2)

the molybdenite surface has a stronger tendency to form hydrophobic bonding with the hydrophobic part of the lignosulphonate molecule than with the methyl group of a methanol molecule. Due to the high adsorption density of former molecules at the molybdenite-solution interface, the surface is expected to acquire a γ_c value in relatively low concentration (hence, high $\gamma_{\ell v}$) solutions.

The wettability of the talc cleavage plane by the lignosol solution (γ_c = 33.5 mN/m) is much less than that of molybdenite cleavage plane. Selective wetting region between the two is characterized by a relatively broad surface tension range from 33.5 to 50.7 mN/m. In the case of disc samples of the two minerals, the wettability difference is even greater; the selective wetting region is characterized by a broader range of solution surface tension (i.e. 42 to 63.7 mN/m).

4.4.1.4. Mechanism of Wetting

With the exception of the most non-polar solids such as Teflon and paraffin, the γ_c determined in aqueous alcohol solutions is always less than γ_c determined using pure liquids. Latter γ_c value is in general between 40 and 45 mN/m for various minerals (Chapter 2) and coals (Parekh and Aplan, 1978). γ_c obtained using short chain n-alcohol solutions appears to occur at a solution surface tension just below 30 mN/m. For example, in aqueous solutions of

methanol, ethanol, propanol and butanol, polycarbonate and polypropylene were found to have γ_c values of 26 and 28 mN/m respectively (Wolfram, 1966). Similarly, γ_c of 26 - 30 mN/m were obtained for polystyrene, polyvinyl chloride, nylon 6-6 and cellulose using ethanol solutions (Dann, 1970; Murphy et al., 1972; Ottewil and Vincent, 1972; Van Voorst Vader, 1977). The contact angle and surface tension data by Fowkes and Harkins (1940) indicate that in butanol solutions, the γ_c values for the cleavage planes of talc, graphite and stibnite are 29, 28 and 26 mN/m respectively. In the present study, using methanol solutions the γ_c values for the cleavage planes of molybdenite, graphite and sulphur were also found to be about 30 mN/m. Recently, Hornsby (1981) and Hornsby and Leja (1983) pointed out that a limiting maximum value for γ_c in aqueous alcohol solutions was 30 mN/m. However, no explanation of this observation was suggested.

In order to explain this and the mechanism of wetting in general, the relative adsorption densities of methanol must be considered. The adsorption densities at the solution-gas interface, $\Gamma_{\ell v}$, have been determined (Chapter 3). For the purpose of the present discussion, they are reconsidered here along with the viscosity variation of the solutions (Figure 4.14). $\Gamma_{s\ell}$ and Γ_{sv} are not known. However, from the linearity of the adhesion tension data and from Equation 4.2, it is assumed that $\Gamma_{\ell v}$, $\Gamma_{s\ell}$

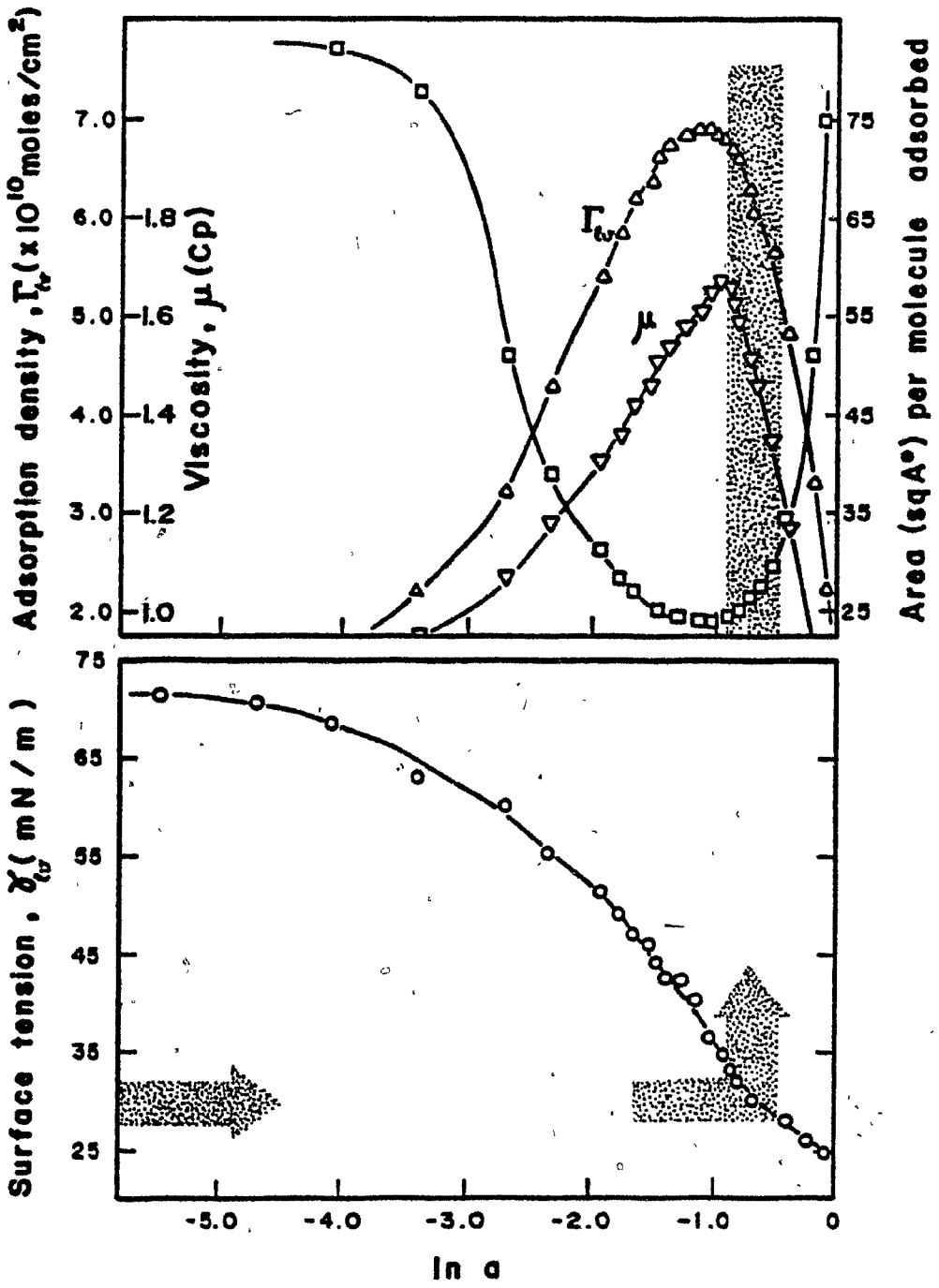


Figure 4.14 Surface Tension, Adsorption Density and Viscosity Variation in Aqueous Methanol Solutions

and $\Gamma_{s\ell}$ remain proportional to each other over the whole concentration range (Lucassen-Reynders, 1963). From Figure 4.14, it may be noted that the solution surface tension of $\simeq$ 30 mN/m corresponds about to maximum absorption density and minimum area per adsorbed methanol molecules. This indicates that in solutions with $\gamma_{\ell v} \simeq 30$ mN/m, the solution-gas interface (e.g. bubble surface) is covered with a closely packed layer of methanol molecules with their polar groups oriented towards the bulk solution. Because of the proportionality of the adsorption at three interface, $\Gamma_{s\ell}$ for methanol may be expected to assume a maximum value (or nearly so) in solutions with similar surface tension. Methanol molecules will be adsorbed on highly hydrophobic solid surfaces through their methyl groups (i.e. hydrophobic bonding) and the polar -OH groups will be directed towards the bulk solution. This type of orientation at both interfaces favours hydrogen bonding between water and methanol molecules. Relatively high viscosities corresponding to this range of surface tension (Figure 4.14) indicates that appreciable hydrogen-bonding has taken place between water and methanol molecules (Chapter 3). The hydrogen-bonding between adsorbed methanol molecules and bulk water is expected to increase the stability and thickness of the wetting film. This is supported by the experimental observation that the induction period increases regularly as the solution surface tension decreases and approaches γ_c. For

example, it was noted that in distilled water, the induction time for bubble-molybdenite (cleavage plane) attachment was too short to perceive. However, in aqueous methanol solutions, it was 5-10 seconds at 52.9 mN/m and 15-20 seconds at 36.3 mN/m. In solutions for which $\gamma_{\ell v} \leq \gamma_c$ (~ 30 mN/m), the wetting films are expected to be infinitely stable, hence no finite contact angle should be formed even after very long bubble-solid contact time. In less concentrated solutions (i.e. $\gamma_{\ell v} > 30$ mN/m), contact angle formation will be possible due to relatively lower surface pressures of methanol at both the solid-solution and solution-gas interfaces leading to the formation of less stable wetting films.

Considering the above, the mechanism of wetting by methanol solutions may be schematically illustrated in Figure 4.15. In distilled water, the intervening wetting film between bubble and the hydrophobic solid surface (e.g. cleavage plane of molybdenite) is unstable. In methanol solutions, the stability of the wetting film increases as the adsorption density of methanol at the solid-solution and solution-gas interface increases. The wetting film attains its greatest stability in solutions with $\gamma_{\ell v} \leq \gamma_c \equiv 30$ mN/m since both interfaces are covered with polar layers (Figure 4.15c).

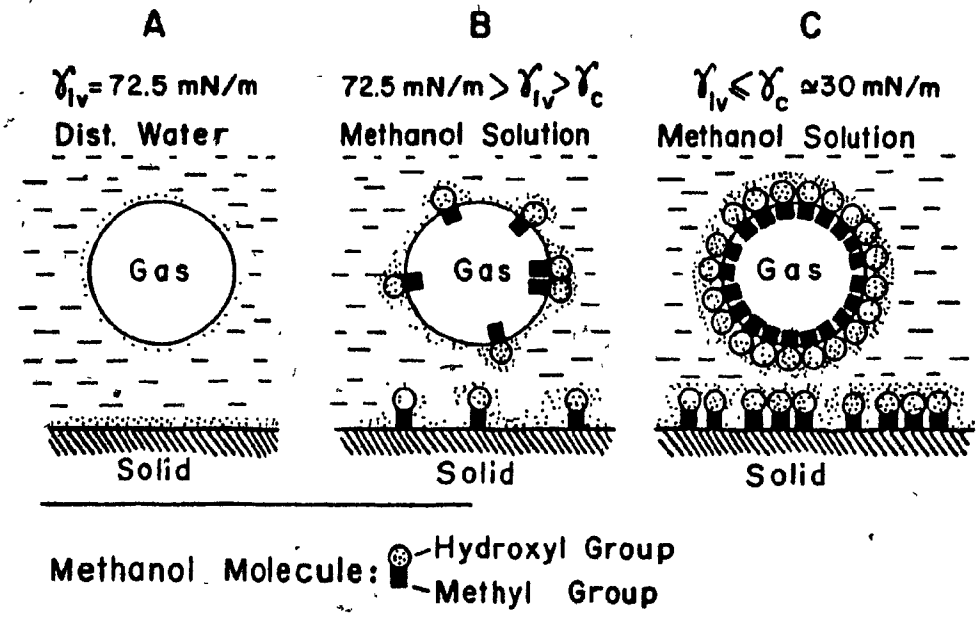


Figure 4.15 Schematic Representation of the Wetting Mechanism in Aqueous Methanol Solutions

This wetting mechanism, although proposed here for methanol solutions, should be valid for solutions of other short chained alcohols. Examination of the adsorption isotherm of ethanol (Guggenheim and Adam, 1933) and of butanol (Harkins and Wampler, 1931) reveals that the adsorption densities of these alcohols at the solution-gas interface reach their maximum values at about 30 mN/m.

4.4.2. Floatability

4.4.2.1. Typical Flotation Behaviour

Flotation behaviour of polymers and the minerals studied (excluding silica) in aqueous methanol solutions of decreasing surface tension show characteristic similarities (Figures 4.7-4.9). In general, for all samples, the flotation rate was notably lower in the absence of methanol (i.e. $\gamma_{\ell v}$ = 72.5 mN/m) than in the presence of a small concentration of it (e.g. $\gamma_{\ell v}$ = 68.6 mN/m). A similar observation has been noted with molybdenite samples of different stoichiometric compositions (Kaoma and Yarar, 1982). The increase in recovery due to introduction of small amount of methanol into water was attributed to the adsorption of methanol at the solid-liquid interface with the methyl group oriented towards the aqueous phase. The implication was that methanol had a collecting power. The author, although disagreeing on the suggested mode of orientation, agrees that methanol adsorbs at the solid-liquid interface. Considering the range

of concentrations being dealt with and the volatile character of methanol, it should adsorb not only at the solid-liquid interface but also at the solid-gas interface. The linearity of the adhesion tension vs. solution surface tension relationship (Lucassen-Reynders, 1963) suggests that the relative adsorption densities of methanol at three interfaces remains proportional over a large concentration range. The enhanced recoveries in an aqueous methanol solution of low concentration may be explained alternatively as follows. It should be noted that there is a significant difference in the number and size of bubbles in the absence and presence of methanol (Chapter 3). For a given flowrate, the former case (i.e. $\gamma_{\ell v}$ = 72.5 mN/m) produces a small number of bubbles with drastically varying sizes, distorted shapes and violent oscillations. As noted by Fuerstenau and Wayman (1958), such a situation may cause a repulsion between bubbles and particles. Therefore, the particles which are not strongly hydrophobic (e.g. nylon 6, molybdenite, etc.,) may not be captured by the bubbles as opposed to the strongly hydrophobic particles (e.g. polyethylene, sulphur, etc.,). However, the latter case produces a greater number of bubbles with small variations in size rising at a slower rate and with a homogeneous distribution in the cell. Such a situation will greatly increase the probability of bubble-particle collisions during flotation.

Another contributing factor to the enhanced recoveries

is a probable decrease in induction period due to the presence of methanol. As shown by Lekki and Laskowski (1971), a frother can reduce the induction periods significantly.

As the concentration of methanol is increased and $\gamma_{\ell v}$ is decreased, high recoveries are maintained up to a certain point beyond which sharp decreases do occur. These floatable/non-floatable transitions may be attributed to the formation of stable wetting films which causes the induction periods to increase and eventually to become longer than the usual bubble-particle contact times.

The fact that the γ_c values as obtained by the Zisman approach are comparable with those of well-known low-surface energy solids (e.g. nylons, nitrated hydrocarbons (Zisman, 1964)) and apparent similarity displayed by the floatability curves of both polymers and mineral samples may lead one to conclude that all the sulphide minerals are inherently floatable (an old controversial topic that has started to attract a renewed attention recently. See Chapter 1). However, such a conclusion is not without a doubt; the sulphur extraction tests with the pretreated galena, dry ground chalcopyrite and realgar showed presence of elemental sulphur on the surfaces of these minerals. It is likely, but, not precisely known that this observed flotation behaviour of common sulphides is owing to the presence of liberated sulphur on their surfaces.

4.4.2.2. Reproducibility

Reproducibility of the tests within the critical surface tension range of floatability and above it is illustrated in Table 4.3 for a sulphide and non-sulphide mineral sample. In general, it is seen that standard deviations for the sulphide sample (i.e. chalcopyrite) are higher than those for talc and that within the critical range, standard deviations are considerably higher than those above it, where recoveries close to 100% are obtained. This is not surprising, because, within the critical range partial wettabilities of the particles are such that the floatabilities are most sensitive to small changes in other flotation variables besides surface tension. This is reflected as fluctuations in the recoveries. Above the critical range, the particles are relatively non-wettable by the flotation medium so that the effect of other variables causing fluctuations is overcome by this relatively non-wettable condition of surface. In general, the variables affecting the reproducibility include changes in composition, particle size, slimes, pre-washing the flotation feed prior to tests, and time of exposure of surfaces to air or, to a smaller extent, water, which may cause oxidation to various extents. This is especially important for sulphides, considering different states of oxidation of sulphur. For example, if the sulphide mineral surface is oxidized so that elemental sulphur is liberated, then γ_c may be expected to change to a lower value.

Table 4.3

Reproducibility of Flotation Tests in the Critical Surface Tension Range of Floatability and Above for Talc and Chalcopyrite Samples

$\gamma_{\ell v}$ (mN/m)	R(% wt.)	SD	CI	n
30.0*	9.4	1.50	5.9 - 12.9	4
	-	-	-	-
32.0	38.8	2.25	33.5 - 44.1	4
	6.8	2.45	1.0 - 12.6	4
35.0	85.2	2.14	80.2 - 90.2	4
	-	-	-	-
38.5	-	-	-	-
	74.1	5.2	61.9 - 86.3	4
42.1	-	-	-	-
	85.5	5.72	72.0 - 99.0	4
45.7	99.8	0.21	99.3 - 100	4
	98.6	0.73	96.9 - 100	4
72.5	96.0	0.78	94.2 - 97.8	4
(dist.water)	95.6	0.87	93.6 - 97.6	4

$\gamma_{\ell v}$ (mN/m) Surface tension at the solution-gas interface
R (% wt.) Recovery on a weight per cent basis, mean value
SD Standard Deviation
CI Confidence Interval at 95% level
n Number of tests
* The figures on the first line refer to talc, those on the second one to chalcopyrite

Ultimately, the surface may assume a γ_c value close to that of sulphur ($\gamma_c \cong 27$ mN/m). However, if oxidation continues

to a further stage, then γ_c may be changed to a higher value. Then, the surface may be converted to an oxide-like surface with a flotation response similar to that of silica sand (Table 4.1).

4.4.2.3. Critical Surface Tension Range of Floatability

It has been established that, for a number of inherently hydrophobic minerals and polymers, there exists a certain range of solution surface tension below which the solid particles remain non-floatable and above which they are almost 100 per cent floatable. Upper limit of this range (referred to as critical surface tension of maximum floatability, γ_{cmf}) marks a transition to highest recovery as opposed to lower limit (critical surface tension of least floatability, $\gamma_{c\ell f}$) corresponding to a solution surface tension at which the sample is virtually non-floatable. Within the critical surface tension range, various degrees of wetting of particles are reflected in terms of correspondingly different recoveries. Apparently, the size of this critical range is an indication of heterogeneity of the solid; the wider the range is the more heterogeneous the solid. The heterogeneity may be an intrinsic property of the solid and/or it may be caused by partial oxidation of solid surfaces. For example, for molybdenite consisting of hydrophilic edges and partially oxidized faces, the critical surface tension range of floatability was found to be 28 to 57.5 mN/m whereas it was only about 27 to 33 mN/m for sulphur. The γ_{cmf} value for the graphite sample is

about 47.5 mN/m. Its $\gamma_{c\ell f}$ value however, is above the same as that of sulphur (Figure 4.9).

According to the concept of critical surface tension of floatability (Hornsby and Leja, 1983), the solid particles can be non-floatable even when their surfaces are not completely wetted (i.e. $\gamma_{cf} > \gamma_c$ in same aqueous surfactant solutions). However, experimentally, cases where $\gamma_c \geq \gamma_{c\ell f}$ are encountered. For instance, the $\gamma_{c\ell f}$ values for sulphur, molybdenite, graphite and coal samples are about 27-29 mN/m and the γ_c values obtained from the adhesion tension diagrams (Figures 4.2 and 4.5) for the same samples (faces for the first three and polished specimen for the coal) are 27, 29, 33.4 and 35.5 mN/m respectively. Considering that aqueous methanol solutions establish surface tension equilibrium in a few milliseconds (Addison, 1945; Addison and Elliott, 1949) some correlation may be sought between γ_c and $\gamma_{c\ell f}$. There appears to be a remarkable correlation in the case of sulphur and molybdenite for which γ_c and $\gamma_{c\ell f}$ values are the same. A case where $\gamma_c > \gamma_{c\ell f}$ (e.g. graphite and coal samples) is contrary to what is expected as it means that flotation can be possible at a surface tension $\gamma_{\ell v}$ below the γ_c value of a particular sample (possibility of particles being recovered under extreme hydrodynamic conditions, i.e., not via attachment of air bubbles, is precluded due to absence of such conditions). However, it can be realized that γ_c as obtained from the wettability diagram does not always have to correlate with $\gamma_{c\ell f}$. The

value of γ_c depends specifically on the technique of surface preparation. In flotation, however, wettability of different particle surfaces may be very different depending on the surface anisotropy, heterogeneity and different extents of oxidation. Therefore, the γ_c value may not necessarily correspond to a limiting value such as $\gamma_{c\ell f}$. It may be an intermediate $\gamma_{\ell v}$ value between $\gamma_{c\ell f}$ and γ_{cmf} representing a group of heavily wetted particles. $\gamma_{c\ell f}$ value in effect expresses a γ_{cf} value for the least wettable solid particles in flotation, specifically particles which are predominated by well preserved cleavage planes or crystal faces.

Similarly, γ_{cmf} value expresses a γ_{cf} value for the most wettable solid particles. These particles are likely to be those that have undergone relatively more oxidation than the others. Therefore, an inherently hydrophobic flotation feed consists essentially of particles with distinct γ_{cf} values ranging from $\gamma_{c\ell f}$ to γ_{cmf}. In the critical surface tension range, the floatability of particles has been found to be very sensitive to small changes in a number of variables that may affect any flotation process. Recently, Hornsby and Leja (1983) reported that small degrees of oxidation affecting floatability of coal could be detected through the use of surface tension of floatability curves. Due to its sensitivity, it is anticipated that the technique may find other applications in investigations related to the surface chemistry of minerals particularly those with inherent hydrophobic characteristics.

Critical range of floatability may schematically be illustrated by making use of the adhesion tension diagram. The wettability lines for the cleavage plane of molybdenite and the crystal face of sulphur and their γ_c values may be used to designate a lower limit for the critical surface tension range of floatability, namely $\gamma_{c\ell f}$. Disc samples, due to their mosaic nature have large hydrophilic-to-hydrophobic ratios. The hydrophilic sites produced by the rupture of interatomic bonds followed by possible oxidation give rise to the polarity of the surface. As the non-polar character of the surface diminishes, the slope of wettability lines continuously increases (Figure 4.5 and Table 4.2). In their classical work, Gaudin et al. (1957) proposed a threshold density of ionic bonds on inherently hydrophobic surfaces for a transition from floatability to non-floatability. Disc samples can be assumed to represent the particles in flotation with that threshold value. Their wettability lines may then be used to designate an upper limit for the critical surface tension range of floatability, namely γ_{cmf}. This can be done by assuming a locus for the critical contact angle of each mineral. Because of its greater density, a larger critical contact angle value was assumed for molybdenite (i.e. $\theta^{M}_{cf} > \theta^{S}_{cf}$). Intercepts of the wettability lines at these critical angles corresponds to the upper limits (disc samples) and lower limits (faces) of the critical surface tension range of floatabilities (Figure 4.5).

The values of $\gamma_{c\ell f}$ and γ_{cmf} obtained from the wettability diagram are compared with those obtained from the floatability curves in Table 4.4. The agreement between the results given in the table suggest that the assumptions made are fair.

Table 4.4

Comparison of $\gamma_{c\ell f}$ and γ_{cmf} Values of Floatability and Wettability Tests

Critical range (mN/m)	$\gamma^S_{c\ell f}$	γ^S_{cmf}	$\gamma^M_{c\ell f}$	γ^M_{cmf}
Wettability diagram	27.5	35	31	48
Floatability curves	27	33	28-29*	57.5-49.5*

*Average of three values reported for molybdenite samples of differing stoichiometric composition (Kaoma and Yarar, 1982)

4.4.2.4. Selective Flotation and Efficiency of Separation

Based on the concept of critical surface tension of wetting (Zisman, 1964), there have been several attempts (Hornsby and Leja, 1980; Kelebek and Smith, 1982; Yarar and Kaoma, 1983) to exploit the differences in wettabilities of inherently hydrophobic solids in order to effect their separation. These investigations, rather preliminary in nature, have led to a basic conclusion that selective separation of inherently hydrophobic solids by flotation can be achieved provided that their γ_c values differ significantly. As shown previously by Finch and Smith (1975) through flotation tests with collector treated high-surface-energy minerals and by Hornsby and Leja (1980)

through test tube experiments with low-surface-energy solids, the selectivity between two inherently hydrophobic solids (with γ_c^{S1} and γ_c^{S2}) will be caused on the following condition:-

$$\gamma_c^{S2} > \gamma_{\ell v} > \gamma_c^{S1} \qquad 4.3$$

The second solid, S_2 due to its complete wetting, will be depressed in a solution with a surface tension $\gamma_{\ell v}$, while S_1, being only partially wetted, will be able to float in the same solution. A significant difference between γ_c values makes a separation much easier but it is not essential for an efficient selective flotation. For instance, in the case of sulphur and molybdenite the γ_c values of the faces obtained in aqueous methanol solutions were very close (i.e. 27 and 29 mN/m respectively). This closeness was also reflected in their $\gamma_{c\ell f}$ values. The results shown in Figure 4.10 indicate that highly efficient separations are achievable when γ_c and $\gamma_{c\ell f}$ values are very close.

Selectivity in flotation was evaluated in terms of the separation efficiency proposed by Schulz (1970). It was determined as the difference in the recovery, in the concentrate, of partially wetted mineral sample and the one that undergoes relatively more wetting at a certain surface tension. For the general case:-

$$E_s(\gamma_{\ell v}) = R^{S1}(\gamma_{\ell v}) - R^{S2}(\gamma_{\ell v}) \qquad 4.4$$

where E_s is the separation efficiency, R^{S1} and R^{S2} are the fractional recoveries of solid 1 and solid 2 at a surface tension $\gamma_{\ell v}$.

In each curve, the separation efficiency reaches a maximum level at certain $\gamma_{\ell v}$ value. This value, as might be expected, is between γ_{cmf}^{S1} and $\gamma_{c\ell f}^{S2}$. As $\gamma_{\ell v}$ decreases beyond the γ_{cmf}^{S1} value, overall R^{S1} will decrease due to inability of some particles (say with $\gamma_{cf}^{'S1}$) to float at this lowered surface tension (say $\gamma_{\ell v}'$) for $\gamma_{\ell v}' \leq \gamma_{cf}^{'S1}$. Since solid 2 is arbitrarily chosen as the more wettable one, a greater number of its particles are already non-floatable at a relatively higher $\gamma_{\ell v}$ value. Thus, as $\gamma_{\ell v}$ approaches $\gamma_{c\ell f}^{S2}$, R^{S2} will decrease but the overall drop in R^{S2} will not be as great as that of R^{S1}. As a consequence, the E_s value will also decrease. With $\gamma_{\ell v}$ increasing above γ_{cmf}^{S1} high R^{S1} values will be maintained, but R^{S2} will also start to increase due to dewetting, causing E_s to decrease correspondingly. Therefore, solid 1 can selectively be floated from the mixture leaving most of the solid 2 depressed in the cell. The effective separation interval is from $\gamma_{c\ell f}^{S2}$ to γ_{cmf}^{S1}. This is depicted in wettability diagram for the samples of sulphur and molybdenite (Figure 4.5) where the interval is shaded with vertical lines. In this case, the maximum separation efficiency for the mixtures of sulphur and molybdenite is expected to be between 31 and 35 mN/m. As seen from Figure 4.10 this is indeed the case, i.e., the surface

tension of the solution corresponding to maximum separation efficiency is about 32.5 mN/m.

It was speculated that the value of surface tension corresponding to the maximum separation efficiency for a binary mixture of inherently hydrophobic solids should be predictable using the functional expressions of the individual surface tension of floatability curves. The functional relationship between the recoveries and surface tension was obtained by second degree polynomial regression using the data points in selected intervals (Figure 4.16). The equations represent the experimental data closely in the intervals marked on each curve (shown by dotted line) beyond which deviations are displayed (solid and dotted plus dashed lines for the experimental and calculated data respectively). Figure 4.17 shows a plot of the recoveries observed versus the recoveries estimated from the equations for inherently hydrophobic solids. Coefficients and standard errors of estimate (S.E.E.) are given in Table 4.5.

Table 4.5

Results of Polynomial Regression of Second Degree for the Surface Tension of Floatability Curves of the Samples

Samples	Coefficients			S.E.E.
	a	b	c	
Sulphur	-0.0733	4.7692	-76.6116	0.0431
Talc	-0.0079	0.6404	-12.0323	0.0382
Graphite	0.0137	-0.8023	11.7837	0.0329
Molybdenite	0.0016	-0.0960	1.4802	0.0203

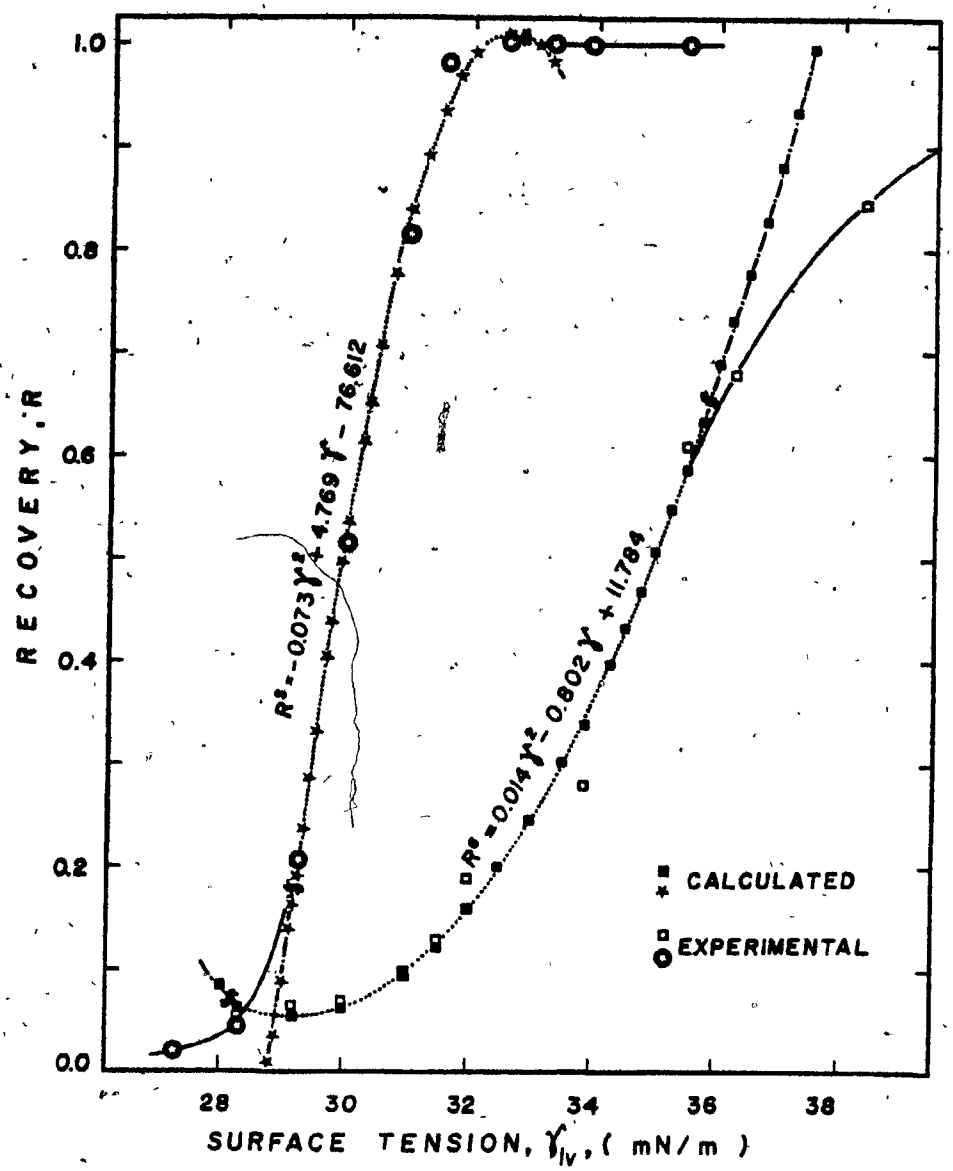


Figure 4.16 Floatability vs. Surface Tension Curves for Sulphur and Graphite Samples and Their Functional Expressions; R^S and R^G respectively

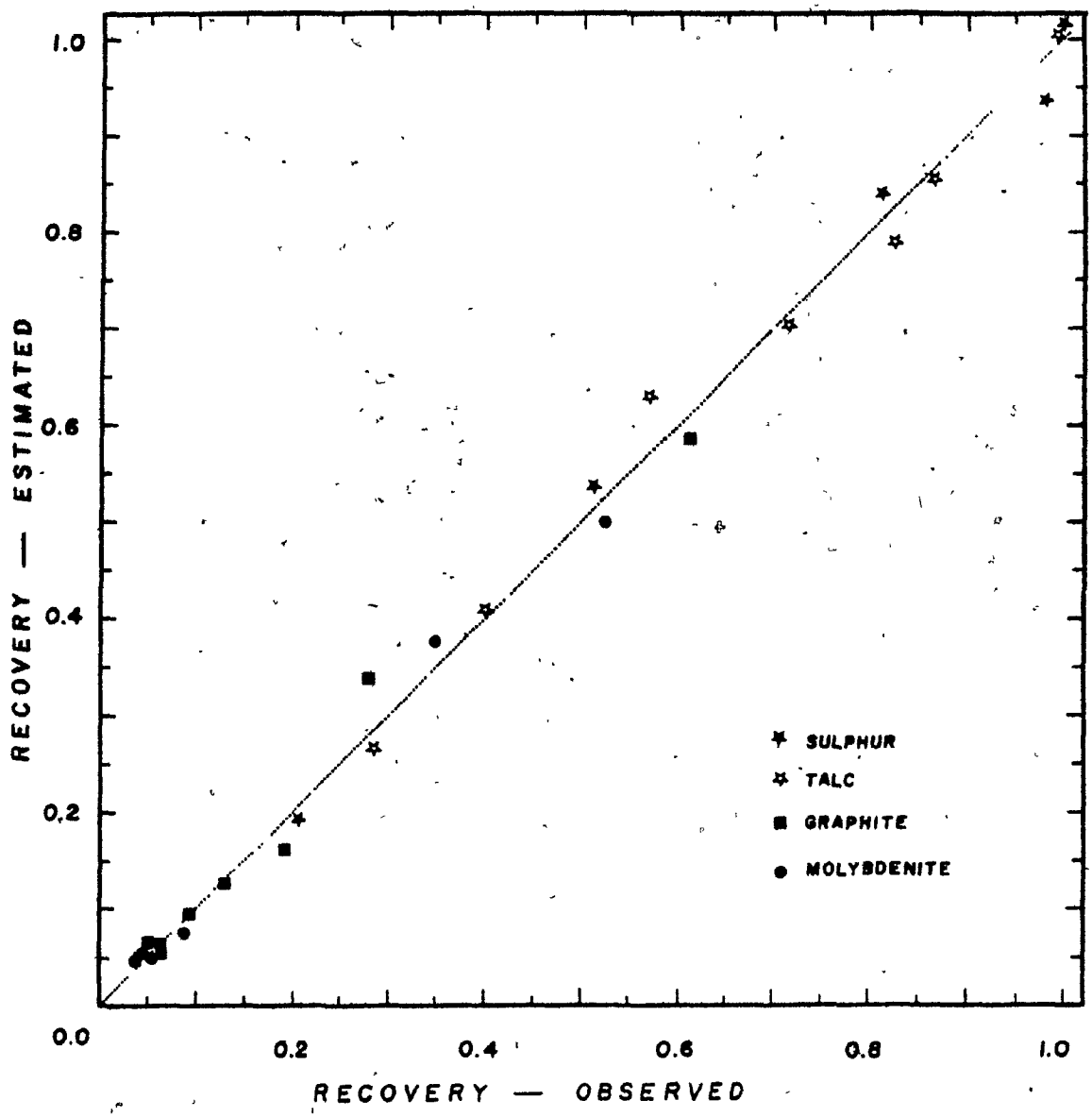


Figure 4.17 Comparison of Observed and Estimated Values for the Fractional Recoveries of the Inherently Hydrophobic Mineral Samples Within Their Critical Surface Tension Range of Floatability

For some samples (e.g. molybdenite), higher order equations (e.g. third degree) were slightly better fit. However, for simplicity and homogeneity, second order equations were adopted to serve the purpose.

For an inherently hydrophobic solid i, the fractional recovery, R^{Si} may be expressed as follows:-

$$R^{Si} = a_i \gamma_{lv}^2 + b_i \gamma_{lv} + c_i \qquad 4.5$$

where a_i, b_i and c_i are the coefficients of the equation. In the case of two inherently hydrophobic solids, the equations become:-

$$R^{S1} = a_1 \gamma_{lv}^2 + b_1 \gamma_{lv} + c_1 \qquad 4.6$$

$$R^{S2} = a_2 \gamma_{lv}^2 + b_2 \gamma_{lv} + c_2 \qquad 4.7$$

Combining the equations 4.4, 4.6 and 4.7

$$E_s = (a_1 - a_2)\gamma_{lv}^2 + (b_1 - b_2)\gamma_{lv} + c_1 - c_2 \qquad 4.8$$

For a maximum separation efficiency, Equation 4.8 should be differentiated and the result set to zero;

$$\frac{\partial E_s}{\partial \gamma_{lv}} = 2(a_1 - a_2)\gamma_{lv} + (b_1 - b_2) = 0 \qquad 4.9$$

From which:-

$$\gamma_{lv}(max) = \frac{b_2 - b_1}{2(a_1 - a_2)} \qquad 4.10$$

Equation 4.10 thus obtained may be used to calculate the

solution surface tension at which maximum separation efficiency for each binary mixture can be expected. Table 4.6 compares predicted and experimental $\gamma_{\ell v}$(max.) and E_s(max.) results. Experimental and predicted $\gamma_{\ell v}$(max.) values for all binary mixtures agree within ± 0.6 mN/m. However, the agreement between the experimental and predicted values of E_s(max.) is relatively poor. As noted previously, the recoveries within the critical range fluctuate due to the effect of variables other than surface tension. The standard deviations are as high as 5-6 per cent. Therefore, the lack of agreement between the experimental and predicted E_s(max.) values may be expected.

Table 4.6

Comparison Between Experimental and Predicted Results of the Separation

Samples	Experimental		Predicted	
	$\gamma_{\ell v}$(max.)	E_s(max.)	$\gamma_{\ell v}$(max.)	E_s(max.)
Talc & Molybdenite	40.0	0.88	38.8	0.76
Sulphur & Molybdenite	32.5	0.97	32.5	0.92
Sulphur & Graphite	33.0	0.90	32.0	0.81
Sulphur & Talc	32.0	0.63	31.6	0.59

The mechanism of the separation of talc from molybdenite using lignosulphonate solutions is essentially similar to that using methanol solutions. The main difference between

the action of these two reagents is that the former adsorbs on the molybdenite surfaces to a greater extent than the latter. This may be inferred from the increase in $-\beta$ values of their respective wettability lines (Figure 4.6). The $-\beta$ values for talc do not show a comparable increase. In fact, the β values for disc samples of talc using the solutions of both lignosol-XD and methanol are the same (0.5). In neutral solutions (pH = 7.2±0.2) which were used in the selective flotation tests, the lignosulphonate adsorption by talc appears to be negligible in the concentration range 0-0.12 g/ℓ. The recoveries within this range (i.e. $\gamma_{\ell v}$ = 60.3 - 72.5 mN/m) are over 96% for talc, but for molybdenite they decrease from 93% to 12.6%. Thus, the separation efficiency continuously increases as $\gamma_{\ell v}$ decreases from 72.5 mN/m to 60.4 mN/m. In more concentrated solutions, γ_{cf} values of some talc particles are reached due to decreasing $\gamma_{\ell v}$ values. Since the low recoveries of molybdenite are maintained, the separation efficiencies decrease due to decreasing talc recoveries in the same solutions (Figure 4.11). High separation efficiencies obtained demonstrate that lignosulphonate is a selective wetting reagent for molybdenite. The adsorbability of lignosol-XD by molybdenite can be compared with that of talc in Figure 4.18 which shows the zeta coefficients determined as a function of pH. The term zeta coefficient, $\Delta\zeta$ introduced by Gaudin and Sun (1946) is an expression showing the difference between the zeta potential of mineral particles in

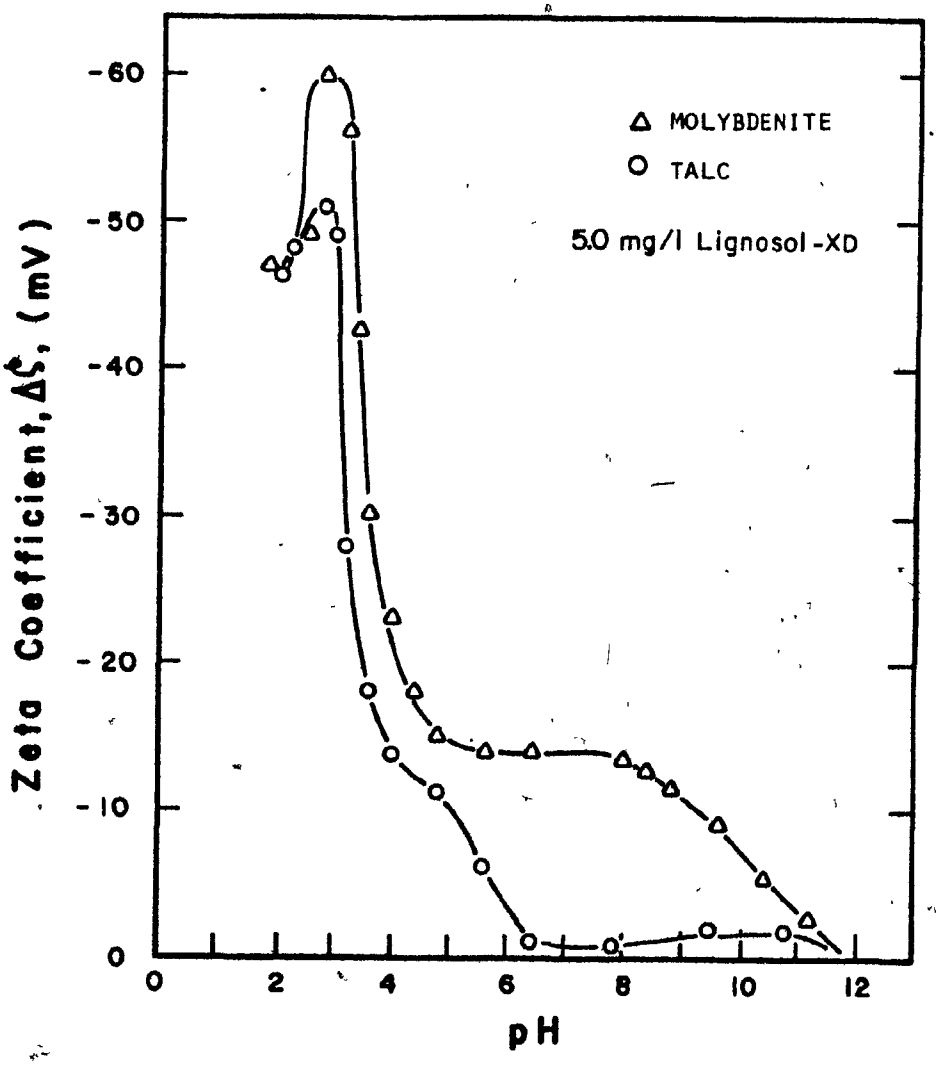


Figure 4.18 Zeta Coefficients for Molybdenite and Talc at pH=7.2 Due to Lignosol-XD

a chemical solution, ζ_{cs} and that in distilled water, ζ_{dw} at the same pH value:-

$$\Delta\zeta = \zeta_{cs} - \zeta_{dw} \qquad 4.11$$

The zeta coefficient curves for molybdenite and talc indicate the amount of the lignosulphonate adsorption. Due to the presence of negatively charged sulphonate groups in the adsorbate, the negative charge on the particles increases, hence $\Delta\zeta$ becomes relatively more negative. Above pH ≈ 6.0 the $\Delta\zeta$ value for talc is about zero and about -14 mV for molybdenite within the pH range 5 to 8. This indicates the selective adsorption of lignosulphonate on molybdenite as compared to negligible adsorption on talc and explains the selective flotation of talc from molybdenite-talc mixtures. In strongly alkaline solutions (pH $\geq$ 11), since both talc and molybdenite have large negative zeta potentials, they cannot adsorb the negatively charged lignosulphonate species. In strongly acidic solutions, these mineral particles due to their positive surface charge (see Figures 2.8 and 2.13) do adsorb appreciable amount of lignosulphonate through a simple mechanism of Coulombic attraction.

4.4.2.5. Estimation of Induction Periods During Flotation

The time taken for the rupture of the wetting film between bubbles and hydrophobic particles is known as the induction period (Sutherland and Wark, 1955). It is regarded as an important factor in the theory of flotation. Eigeles

and Volova (1960) used a specially-designed equipment (contact apparatus) to determine the induction period during the attachment of a captive bubble with a movable bed of particles in solutions. They found that in collector solutions, the induction period could be as short as 5 milliseconds. However, it is an extremely difficult parameter to experimentally determine for actual flotation conditions.

Sutherland (1948) was first to theoretically examine the process of collisions between bubbles and particles and to propose an equation which relates the induction period to the flotation rate constants. Sutherland's equation is

$$K = 3 \Pi \phi Rr v N \text{Sech}^2 \left(\frac{3 v\lambda}{4R}\right) \qquad 4.12$$

where K is the flotation rate constant (S^{-1}); ϕ- fruitfulness factor; R - bubble radius (cm); r - particle radius (cm); v - velocity of ascent of bubbles (cm/s); N - number of bubbles per cm^3 of solution; and λ - induction period(s). Fruitfulness factor, ϕ, denotes the proportion of particles retained in the froth. When there is no drop-back of particles from the froth layer, ϕ is equal one. Recently, Jowett (1980) used this equation to determine the relationship between the induction time and particle size. He assumed R and N to be 0.1 cm and 200 bubbles/cm^3 respectively.

More recently, based on an analysis of the bubble-particle collision and attachment, and on some recent

developments in hydrodynamics and flotation theory, Dobby and Finch (1984) presented a new flotation model which makes use of induction periods to explain the peak in size-by-size recovery data that is often observed (Trahar, 1981). Dobby and Finch did not use a condensed single equation such as Equation 4.12 relating K to λ. In their approach, λ is estimated through a computer program after several steps of initial calculation (Dobby, 1984).

The availability of all the necessary variables in Equation 4.12 allows the estimation of induction periods as a function of the surface tension of methanol solutions. The average R and N values were determined photographically (Chapter 3). The values of v were calculated using the equation proposed by Concha and Almendra (1979) (Appendix III). K was determined as a function of $\gamma_{\ell v}$ from the first order flotation rate equation. $\emptyset$ was taken as 1 since no deflector was used in the flotation cell. The results of calculations tabulated in Appendix IV are shown in Figure 4.19. The induction periods estimated using the flotation model by Dobby are also included in the figure for comparison. λ obtained from both models increases as the surface tension of the flotation medium decreases to approach γ_c of the samples. (i.e. 27-30 mN/m). Within the critical range of floatability, the λ values (according to Sutherland's equation) range from 13 to 27 ms for sulphur and talc, and from 17 to 36 ms for molybdenite. Thus, in the vicinity of their critical surface

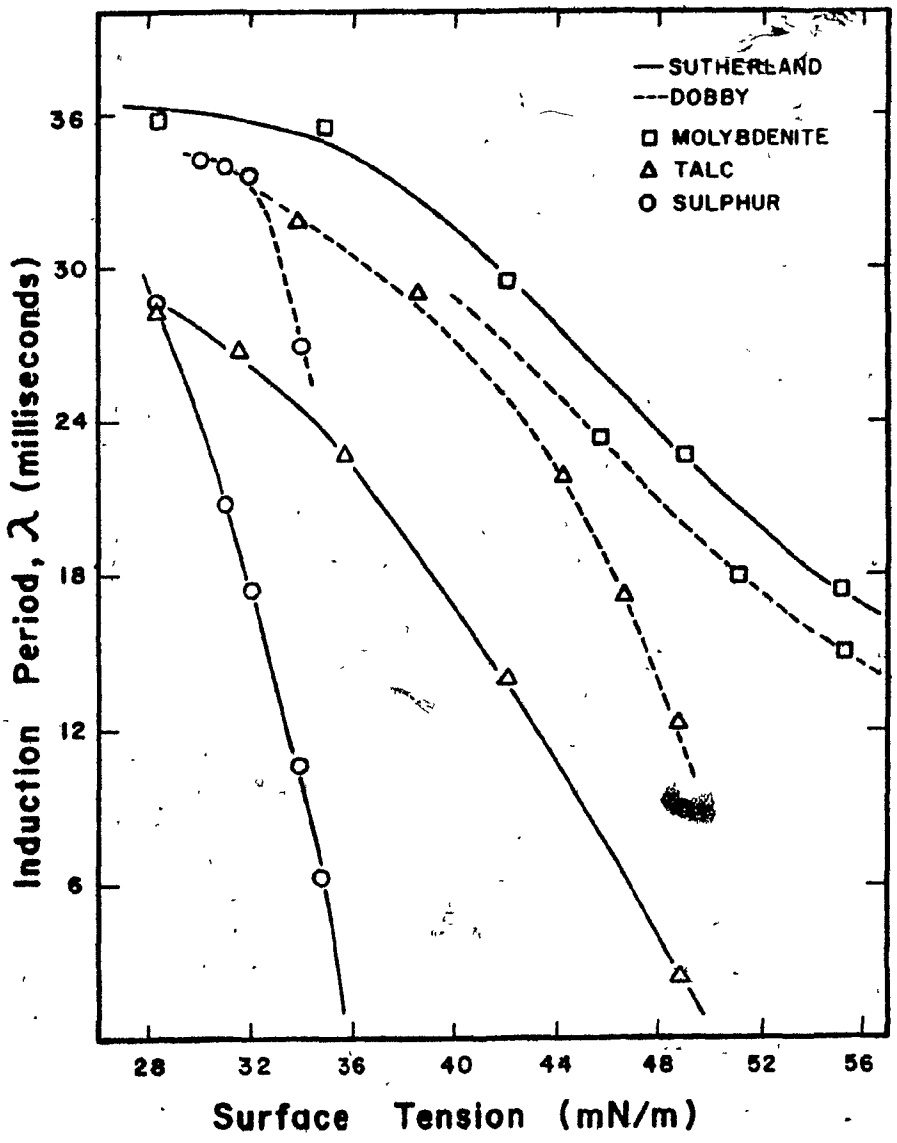


Figure 4.19 Induction Periods as a Function of Surface Tension of Aqueous Methanol Solutions

tension of floatability, the lifetime of the intervening wetting films between the particles and bubbles may be said to be about 28 ms for sulphur and talc, and 36 ms for molybdenite. Corresponding λ values according to Dobby's model range from 31 to 35 ms for sulphur, and from 24 to 35 ms for talc.

Since the actual induction periods under dynamic conditions of flotation are not known, it is difficult to discuss the validity of the numerial values of λ. Nevertheless, the size of these λ values may be examined in reference to Figure 4.10 which shows the selective flotation of sulphur and talc from their binary mixtures with molybdenite as a function of $\gamma_{\ell v}$. At $\gamma_{\ell v}$ values of 32.5 mN/m and of 40 mN/m, the separation efficiencies are maximum. This requires an appreciable difference between the λ values of individual minerals. The λ values calculated using Sutherland's equation are indeed very different; at 32.5 mN/m they are 15 ms for sulphur and 33.5 ms for molybdenite, and at 40 mN/m, 16.5 ms for talc and 32 ms for molybdenite. The λ values obtained using Dobby's model do not appear to show comparable differences. For example, in the case of talc-molybdenite separation, at 40 mN/m a λ value of 27.5 ms for talc is very close to 28.7 ms, the extrapolated λ value for molybdenite.

4.5 REFERENCES

Addison, C.C. (1945). The Properties of Freshly Formed Surfaces, Part IV: The Influence of Chain Length and Structure on the Static and Dynamic Surface Tensions of Aqueous-Alcoholic Solutions. J. Chem. Soc. pp. 98-105.

Addison, C.C. and Elliott, T.A. (1949). The Properties of Freshly Formed Surfaces, Part X: A New Contracting Liquid-Jet Technique for the Study of Soluble Films at Small Surface Ages. J. Chem. Soc., pp. 2789-2805.

Bailar, J.D., Emeleus, H.J., Nyholm, R. and Dickenson, A.F.T. (Editors). (1975). Comprehensive Inorganic Chemistry, Pergamon Press, a) Vol. 2, pp. 607-609, b) Vol. 3, pp. 28-29.

Bargeman, D. and Van Voorst Vader, F. (1973). Effect of Surfactants on Contact Angles at Non-Polar Solids. J. Colloid Interface Sci., Vol. 42, pp. 467-472.

Bernett, M.K. and Zisman, W.A. (1959). Relation of Wettability by Aqueous Solutions to the Surface Constitution of Low-Energy Solids, J. Phys. Chem., Vol. 63, pp. 1241-1246.

Concha, F. and Almendra, E.F. (1979). Settling Velocities of Particulate Systems, 1: Settling Velocities of Individual Spherical Systems. Int. J. Miner. Process., Vol. 5, No. 4, pp. 349-367.

Dann, J.R. (1970). Forces Involved in the Adhesion Process. I. Critical Surface Tension of Polymeric Solids as Determined with Polar Liquids, J. Coll. Interface Sci., Vol. 32, No. 2, pp. 302-320.

Dobby, G.S. (1984). A Fundamental Flotation Model and Flotation Column Scale-Up., Ph.D. Thesis, Dept. Min. Metall. Eng., McGill Univ.

Dobby, G.S. and Finch, J.A. (1984). A Model of Particle Capture in Froth Flotation: Symp. on Challenges in Mineral Sciences, (J.A. Finch; Editor), Ann. Conf. Met., Quebec City, August 16-19.

Eigeles, M.A. and Volova, M.L. (1960). Kinetic Investigation of Effect of Contact Time, Temperatures and Surface Condition on the Adhesion of Bubbles to Mineral Surfaces. In: 5th Int. Miner. Process. Congr., London, IMM, pp. 271-284.

Finch, J.A. and Smith, G.W. (1975). Bubble-Solid Attachment as a Function of Bubble Surface Tension. Can. Metall. Quart. Vol. 14, No. 1, pp. 45-51.

Fowkes, F.M. (1953). Role of Surface Active Agents in Wetting, J. Phys. Chem. Vol. 57, pp. 98-103.

Fowkes, F.M. and Harkins, W.D. (1940). The State of Monolayers Adsorbed at the Interface Solid-Aqueous Solution. J. Amer. Chem. Soc. Vol. 62, pp. 3377-3386.

Fowkes, F.M. McCarthy, D.C., and Mostafa, M.A. (1980). Contact Angles and the Equilibrium Spreading Pressures of Liquids on Hydrophobic Solids. J. Coll. Interface Sci., Vol. 78, No. 1, pp. 200-206.

Fuerstenau, D.W. and Wayman, C.H. (1958). Effect of Chemical Reagents on the Motion of Single Air Bubbles in Water, Trans. AIME., Vol. 211, pp. 694-699.

Furmidge, C.G.L. (1962). Studies at Phase Interface. I. The Sliding of Liquid Drops on Solid Surfaces and a Theory for Spray Retention. J. Coll. Sci., Vol. 17, pp. 309-324.

Gaudin, A.M., Miaw, H.L. and Spedden, H.R. (1957). Native Floatability and Crystal Structure. In: Proc. 2nd Int. Congr. Surf. Activity. Vol. III, Electrical Phenomena and Solid/Liquid Interface, (J.H. Schulman: Editor), Butterworths, London, pp. 202-219.

Gaudin, A.M. and Sun, S.C. (1946). Correlation Between Mineral Behaviour in Cataphoresis and in Flotation. Trans. AIME., Vol. 169, pp. 347-362.

Good, W.R. (1973). A Comparison of Contact Angle Interpretations, J. Coll. Interface Sci., Vol. 44, No. 1, pp. 63-71.

Guggenheim, E.A. and Adam, N.K. (1933). The Thermodynamics of Adsorption at the Surface of Solutions. Proc. Roy. Soc., Vol. A139, pp. 218-236.

Harkins, W. and Wampler, R.W. (1931). The Activity Coefficients and the Adsorption of Organic Solutes. I. Normal Butyl Alcohol in Aqueous Solution by the Freezing Point Method. J. Amer. Chem. Soc., Vol. 53, pp. 850-859.

Hornsby, D.T.B. (1981). The Floatability of Coal and Other Inherently Hydrophobic Solids in Relation to the Surface Tension of Aqueous Methanol Solutions. Ph.D. Thesis, Dept. Min. Miner. Process Eng., Univ. British Columbia, Vancouver.

Hornsby, D.T. and Leja, J. (1980). Critical Surface Tension and the Selective Separation of Inherently Hydrophobic Solids. Colloids and Surfaces, Vol. 1, pp. 425-429.

Hornsby, D.T. and Leja, J. (1983). Critical Surface Tension of Floatability. Colloids and Surfaces. Vol. 7, No. 4, pp. 339-348.

Jowett, A. (1980). Formation and Disruption of Particle-Bubble Aggregates in Flotation. In: Fine Particles Processing. Vol. 1 (P. Somasundaran: Editor), AIME., New York, pp. 720-754.

Kaoma, J. and Yarar, B. (1982). Correlation of the Critical Surface Tension of Wetting and Non-Stoichiometric Composition of Molybdenum Sulphide. In: Proc. Climax 4th Int. Conf. Chem. Uses Molybdenum. (H.F. Barry and P.C.H. Mitchell: Editors), pp. 117-122.

Kelebek, S. and Smith, G.W. (1982). Critical Surface Tension of Wetting of Inherently Floatable Solids. Paper presented at the 21st Ann. C.I.M. Conf. Met., August 29 - September 1, Toronto.

Lekki, J. and Laskowski, J. (1971). On the Dynamic Effect of Frother-Collector Joint Action in Flotation. Trans. IMM, Vol. 80, pp. C174-180.

Lucassen-Reynders, A.H. (1963). Contact Angles and Adsorption on Solids. J. Phys. Chem., Vol. 67, pp. 969-972.

Mathieu, G.I. and Bruce, R.W. (1974). Getting the Talc out of Molybdenite Ores. Can. Min. J., Vol. 95, No. 6, pp. 75-77.

Murphy, W.J., Roberts, M.W. and Ross, J.R.H. (1972). Contact Angle Studies of Some Low Energy Polymer Surfaces. J. Chem. Soc. Faraday Trans. I., Vol. 68, pp. 1190-1199.

Ottevill, R.H. and Vincent, B. (1972). Colloid and Surface Chemistry of Polymer Lattices. Part 1. Adsorption and Wetting Behaviour of n-Alkanols. J. Chem. Soc., Faraday Trans. I., Vol. 68, pp. 1533-1543.

Parekh, B.K. and Aplan, F.F. (1978). Critical Surface Tension of Wetting of Coal. In: Recent Developments in Separation Science, (N.N. Li: Editor), Vol. IV, pp. 107-113.

Schulz, F.N. (1970). Separation Efficiency. Trans. AIME., Vol. 247, pp. 81-87.

Smolders, C.A. (1967). Wetting of Polymers: Contact Angles of Aqueous Surfactant Solutions on Polar Polymers in Oil. In: Wetting, SCI Monograph, No. 25, Soc. Chem. Ind., London, pp. 319-326.

Somasundaran, P. (1968). The Relationship Between Adsorption at Different Interfaces and Flotation Behaviour, Trans. SME/AIME. Vol. 241, pp. 105-108.

Sutherland, K.L. (1948). Physical Chemistry of Flotation. XI: Kinetics of the Flotation Process. J. Phys. Coll. Chem., Vol. 52, pp. 394-425.

Sutherland, K.L. and Wark, I.W. (1955). Principles of Flotation. Australasian IMM, Melbourne.

Trahar, W.J. (1981). A Rational Interpretation of the Role of Particle Size in Flotation. Int. J. Miner. Process., Vol. 8, pp. 289-327.

Van Voorst Vader, F. (1977). Effects of Surfactants on Wettability Chem.-Ing.-Tech., Vol. 49, No. 6, pp. 488-493.

Wada, M. (1950). Fundamental Studies on Interfacial Tensions in Flotation . III. Tilting-Plate Method of Determining Contact Angle and Wetting Tension of Aqueous Solutions of Frothers for Paraffin-Wax. Sci. Rept. Research Inst., Tohoku Univ. A2, pp. 102-126.

Wolfram, E. (1966). New Data on the Wettability of Polymers. Kolloid-Zeit. Polymere. Vol. 211, No. 1-2, pp. 84-94.

Yarar, B. and Kaoma, J. (1983). The Critical Surface Tension of Wetting of Sulphide Minerals. Paper presented at the 112th Ann. Metting AIME. March 6-10, Atlanta.

Zisman, W.A. (1964). Relation of Equilibrium Contact Angle to Liquid and Solid Constitution. In: Contact Angle, Wettability and Adhesion, Advances in Chemistry Series, Vol. 43, pp. 1-51.

CHAPTER 5

EFFECT OF ELEMENTAL SULPHUR FORMATION ON THE FLOTATION RATE OF GALENA AND CHALCOPYRITE

5.1 INTRODUCTION

Galena and chalcopyrite used in the present study were found to be naturally floatable. Their natural floatability and its pH dependence have been discussed in Chapter 2. Liberated sulphur at the surface appears to play a role in rendering these sulphide minerals floatable. Finkelstein et al. (1975) reported that the effect of sulphur on natural floatability is not consistent. In a detailed study, the amount of surface sulphur was determined on a number of sulphide minerals after various treatments. The relationship between the amount of liberated sulphur and the natural floatability of these minerals was examined. No correlation between sulphur coverage of the surface and observed recoveries was found in tests where the coverage was estimated to be zero up to several monolayers. The elemental sulphur consistently rendered the sulphide mineral highly floatable only when its concentration at the surface is very high. The recoveries of galena and chalcophyite were 100% when the sulphur concentration at their surfaces was greater than 20 hypothetical monolayers. For sulphur concentrations corresponding to less than 3 monolayers, the recoveries ranged

irregularly from 5 to 70%.

All allotropic forms of elemental sulphur are known to be strongly hydrophobic. Their γ_c values are in the vicinity of 30 mN/m (Olsen et al. 1967). Inherent floatability of these sulphur allotropes was confirmed by Finkelstein et al. If the surfaces are effectively covered even with a single monolayer (or less) of sulphur, high recoveries for both galena and chalcopyrite should be expected in a consistent manner. The irregularities observed by Finkelstein et al. may have been caused by the coexistence of hydrophilic oxidation products with the hydrophobic one (i.e. sulphur).

In a more recent study by Heyes and Trahar (1977), chalcopyrite was found to be naturally floatable under oxidizing pulp conditions. The mechanism of this natural floatability was not explained. Attempts to detect sulphur in leach solutions after extraction of floated minerals with acetone was unsuccessful. In spite of this, Trahar (1983) is of the opinion that the observed natural floatability is due to elemental sulphur formation. Luttrell and Yoon (1983) confirmed the natural floatability of chalcopyrite in oxidizing pulps and were able to detect extracted elemental sulphur using ethanol as a solvent. The preliminary test results obtained in the present study also indicated that ethanol could be used successfully to quantitatively determine the liberated sulphur on the sulphide minerals.

In this chapter, the relationship between the amount of liberated sulphur and the natural floatability of galena and chalcopyrite will be re-examined. As demonstrated in the preceding chapter, the natural floatabilities of inherently hydrophobic minerals may be differentiated through their surface tension of floatability curves. The purpose of the experimental work to be described is twofold: - a) to determine the effect of solution surface tension on the flotation rate of galena, chalcopyrite and sulphur within their critical surface tension range of floatabilities, and b) to relate the flotation rate data to the amount of liberated sulphur on galena and chalcopyrite which was quantitatively determined in ethanol leach solutions using UV spectrophotometry. Sulphur was used as a reference mineral to compare its flotation rate with those of galena and chalcopyrite.

5.2 FLOTATION RATE

Flotation kinetics are influenced by many factors, some chemical and others physical in nature (Sutherland and Wark, 1955). The surface tension of the flotation medium may be regarded as an important variable controlling the wettability and floatability of the minerals (Chapter 4).

Flotation rate equation can either be developed from assumptions or facts established about the mechanism of the process, or, more commonly, determined empirically by curve

fitting to recovery-time data or by analogy with similar rate process (Arbiter and Harris, 1962). Sutherland (1948) using the first method of approach developed a relationship between a rate constant and collision hydrodynamics (Equation 4.12). Use of Sutherland's equation for the determination of the flotation rate constant is not practical as some of its variables are difficult or impossible to measure (e.g. induction period, λ). Moreover, some of the assumptions made in the derivation of Sutherland's equation do not appear to be realistic (Laplante, 1980; Dobby, 1984).

Rate equations for the flotation of the samples were obtained empirically from the recovery-time data. The general rate equation may be written as follows:-

$$\frac{dR}{dt} = K\ (1-R)^n \qquad 5.1$$

where K denotes the rate constant; R is the fractional recovery at time t and n is a positive number indicating the order of the equation. Integrating Equation 5.1 for a first order flotation rate (i.e. n=1) yields

$$\ell n\left(\frac{1}{1-R}\right) = Kt \qquad 5.2$$

In the case of second order flotation rate (i.e. n=2), the integrated equation may be arranged as follows (Arbiter, 1951):-

$$\frac{t}{R} = \frac{1}{K} + t \qquad 5.3$$

If the first order equation is valid, a plot of $\ln(\frac{1}{1-R})$ versus t should give a straight line with a slope K. If the rate equation is second order then a plot of t/R against t should result in a straight line. In this case, the reciprocal of the intercept will yield the second order flotation rate constant, K.

5.3 EXPERIMENTAL MATERIALS AND PROCEDURES

5.3.1. Mineral Samples

Freshly broken pure galena crystals (Kansas) were used. Visible impurities were segregated and discarded. During the visual examination of the impurities under a microscope, the presence of tiny yellowish crystals were noted. Qualitative tests later indicated these to be elemental sulphur. Like galena, the chalcopyrite (Quebec) was very pure (Chapter 2); a notable impurity was quartz.

5.3.2. Infrared Spectra

Infrared spectra of galena, chalcopyrite and sulphur were taken to identify the oxidation products formed on the surfaces. Finely ground mineral samples were intimately mixed and re-ground with KBr. Then, the mixture was pressed into a pellet under a load of 20 tonnes for about 10 minutes. The die compartment of the hydraulic press was evacuated through a mechanical pump before and during pressing. The spectra were scanned in the wave number range from 300 to 4000 (cm^{-1}) immediately after pellet preparation using

Nicolet 7000 series IR equipment (Nicolet Instrument Corporation, USA). When the per cent transmittance was too low, the thickness and the mineral content of the pellet was reduced to a suitable level.

5.3.3. Pretreatment of Galena

Preliminary tests indicated that, unlike the chalcopyrite sample, the galena was not always highly floatable. The reason for this was thought to be the formation of water insoluble $PbSO_4$ at the surface. It was decided that the negative effect of this hydrophilic surface compound and possible others be minimized or eliminated. Before each flotation test, the freshly prepared feed sample was subjected to a pretreatment with an ammonium chloride leach solution which was used by Gaudin and Wilkinson (1933) to clean the galena surface. The solution was prepared in the following way:- An excess quantity of NH_4Cl was added into a 250 ml beaker containing distilled water. The mixture temperature of 5°C was raised to room temperature (~ 22°C). The suspension was mixed for 30 minutes at this temperature after which the salt was removed by filtration. The natural pH (~ 4.35) of the filtrate was adjusted to 1.45 by the addition of hydrochloric acid. This stock solution was diluted with three times its volume of distilled water (pH became ~ 2.7). According to Gaudin and Wilkinson, a greater concentration of NH_4Cl and HCl results in undue metathesis of the hydrochloric acid with galena, and in precipitation of salts on the mineral.

Surface pretreatment of the particles was carried out as follows: A predetermined weight (0.550-0.650 g) of galena (100x200 mesh) was added in a 25 ml beaker containing hot cleaning solution (~ 15 ml) and mixed with a teflon coated magnet for 5 minutes at mildly boiling temperatures. The beaker was removed from the hot plate, the slime size particles produced during stirring were decanted off then, the sample was washed continuously (on a coarse porosity filter paper in a funnel) first with hot, later, with cold distilled water and finally with a methanol solution of the desired surface tension. With this pretreatment, galena was rendered very floatable.

Another leaching solution tested was a hot, saturated solution of NaCl containing no HCl. The pretreatment procedure was the same. The pretreatment with this solution was also found to be very effective in rendering galena readily floatable.

5.3.4. Extraction and Determination of Sulphur

Since the samples of galena and chalcopyrite were floatable without collector or frother, the involvement of elemental sulphur was a distinct possibility. Apart from the natural floatability, two experimental observations supported this possibility:- a) the IEP of pH=2.1 for chalcopyrite was the same as that of elemental sulphur, and b) the γ_c value of 31 mN/m for galena obtained by Zisman method was practically

the same as that of elemental sulphur. To experimentally prove the existence of elemental sulphur at the surfaces of galena and chalcopyrite, the samples were subjected to the sulphur extraction tests using ethanol. About 10 g of mineral was placed in each of a number of 100 ml flasks which were filled with absolute ethanol (Consolidated Alcohols Ltd.) and tightly stoppered. Agitation was provided by mounting the flasks vertically on the metallic bar of the agitation apparatus which was rotated by a motor on its longitudinal axis at 36 r.p.m. After agitation for a predetermined time, the flasks were removed from the apparatus and a clear ethanol extract was obtained by filtration and/or centrifuging.

The quantitative determination of sulphur in the ethanol extract was carried out by using the Model 124D double beam UV spectrophotometer (Perkin Elmer). The spectrum had two characteristic absorption bands at 262 mμ and 275 mμ with similar peak intensities. The analysis was carried out using the band at 275 mμ (Friedman and Kerker, 1953; Bass, 1953). The UV spectra and the calibration curve are given in Appendix V.

5.3.5. Flotation Tests

Flotation tests were performed using the micro-flotation cell and the general procedure described in Chapter 2. Only freshly prepared samples and solutions were used. The tests were conducted using methanol solutions having various surface tensions without any pH adjustment. The natural pH of

the solutions ranged from pH=5.4 to 6.7. Gas flow to the cell was stopped abruptly at various times ranging from a few seconds to 60 seconds. The precise flotation time and the recovery obtained within that time were recorded. The recovery-time data gathered were used to determine the flotation rate equations.

5.4 RESULTS

5.4.1 Infrared Spectra

The infrared spectra of galena and chalcopyrite are shown in Figures 5.1 and 5.2 respectively. Each figure includes the spectra of sulphur in the same frequency range as that of the sulphide mineral for comparison between the absorption bands. Major oxidation products (i.e. elemental sulphur and various sulphoxyl ions) are shown on the spectra at their expected absorption frequencies. The assignment of the absorption bands is based on the characteristic frequency data for sulphur and sulphoxyl ions (Miller and Wilkins, 1952; Miller et al., 1960; Kazuo, 1971). The strong absorption band appearing at 465 cm^{-1} - 470 cm^{-1} is due to stretching frequency of -S-S- bonds (Neff and Walnut, 1961). In the vicinity of this absorption band, the spectra of both galena and chalcopyrite is similar to that of sulphur. At other frequencies, it is apparent that all three spectra have comparable features. This suggests that oxidation produces similar sulphoxyl ions at the surfaces of these minerals.

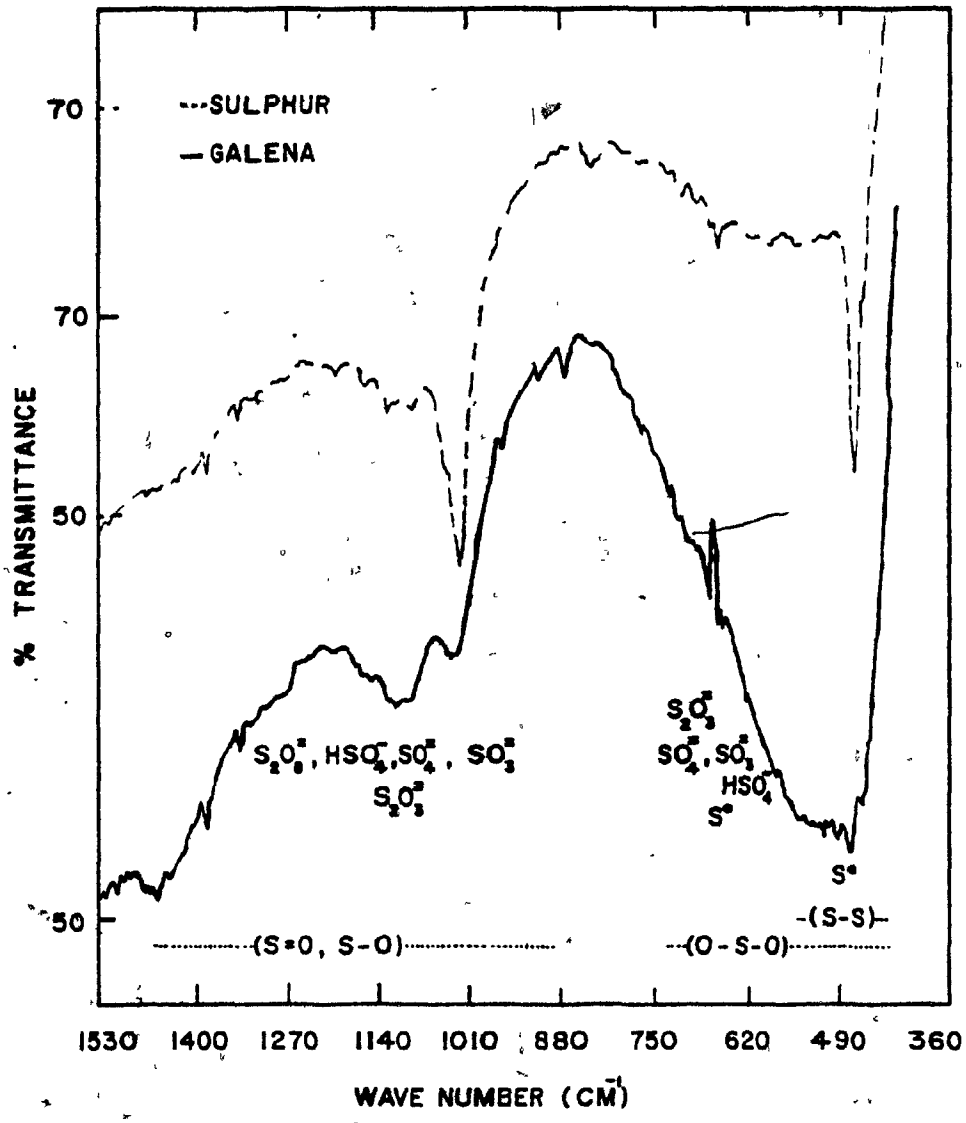


Figure 5.1 Infrared Spectra of Sulphur and Galena

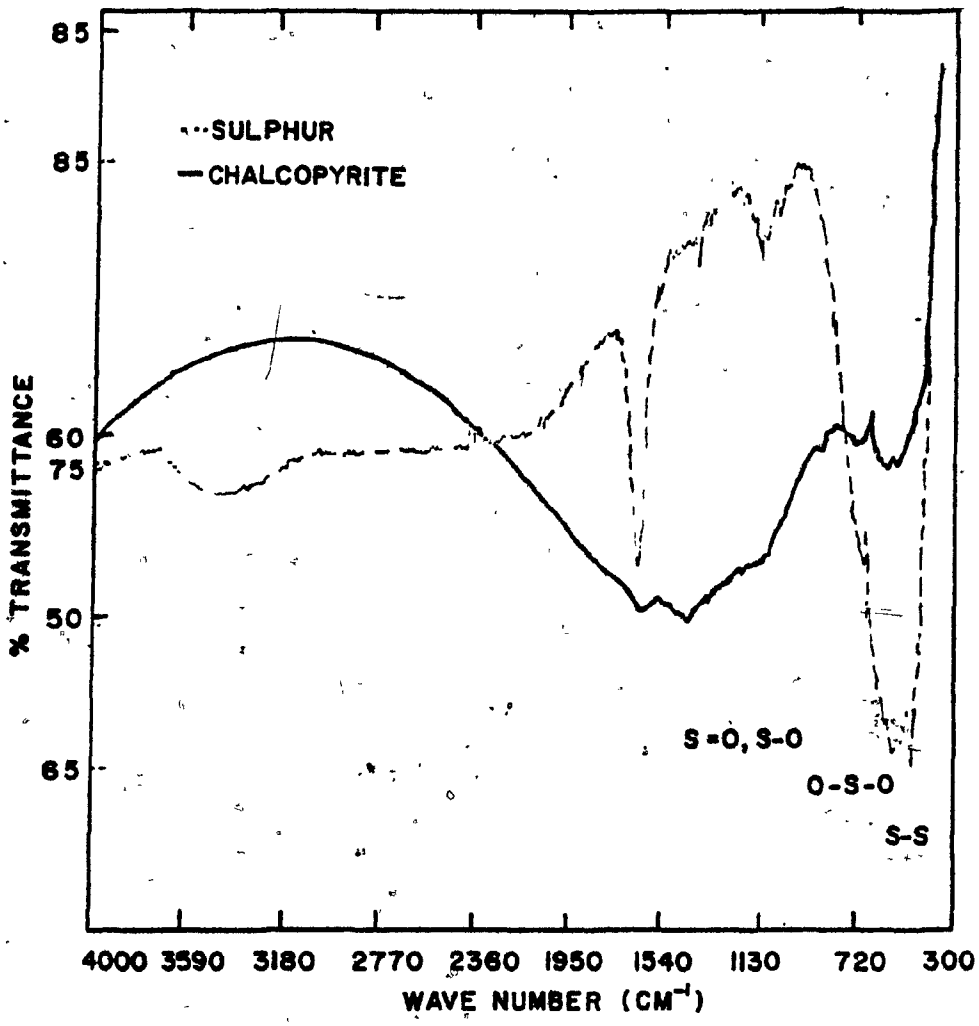


Figure 5.2 Infrared Spectra of Sulphur and Chalcopyrite

5.4.2. Sulphur Extraction Tests

The amount of elemental sulphur extracted from galena, chalcopyrite and realgar is shown in Figure 5.3. The galena sample (PbS-1) ground in 5% sodium sulphide solution (i.e. a reducing environment) had a relatively small amount of liberated sulphur at its surface. The sample (PbS-2) which had been freshly ground in the open air showed nearly twice as much extracted sulphur as that ground in the sodium sulphide solution. The samples ground dry and subsequently pretreated with acidified ammonium chloride solution (PbS-3) and with neutral saturated sodium chloride solution (PbS-4) contained even larger amounts of sulphur extracted from their surfaces (> 1.5 mg/10 g. sample). The amount of liberated sulphur extracted from dry ground chalcopyrite (0.73 mg/10 g sample) was similar to that extracted from dry ground galena (0.67 mg/10 g sample). Grinding realgar in the open air produced more liberated sulphur at its surface (1.18 mg/10 g sample) than at the chalcopyrite and galena surfaces.

From Figure 5.3 it may be noted that the amount of elemental sulphur extracted into ethanol reaches a maximum value in one hour of agitation time. It then decreases with increasing agitation time. This is common to all samples except chalcopyrite for which there is only one data point.

5.4.3. Flotation Tests

Floatability of sulphur (80x150 mesh), chalcopyrite

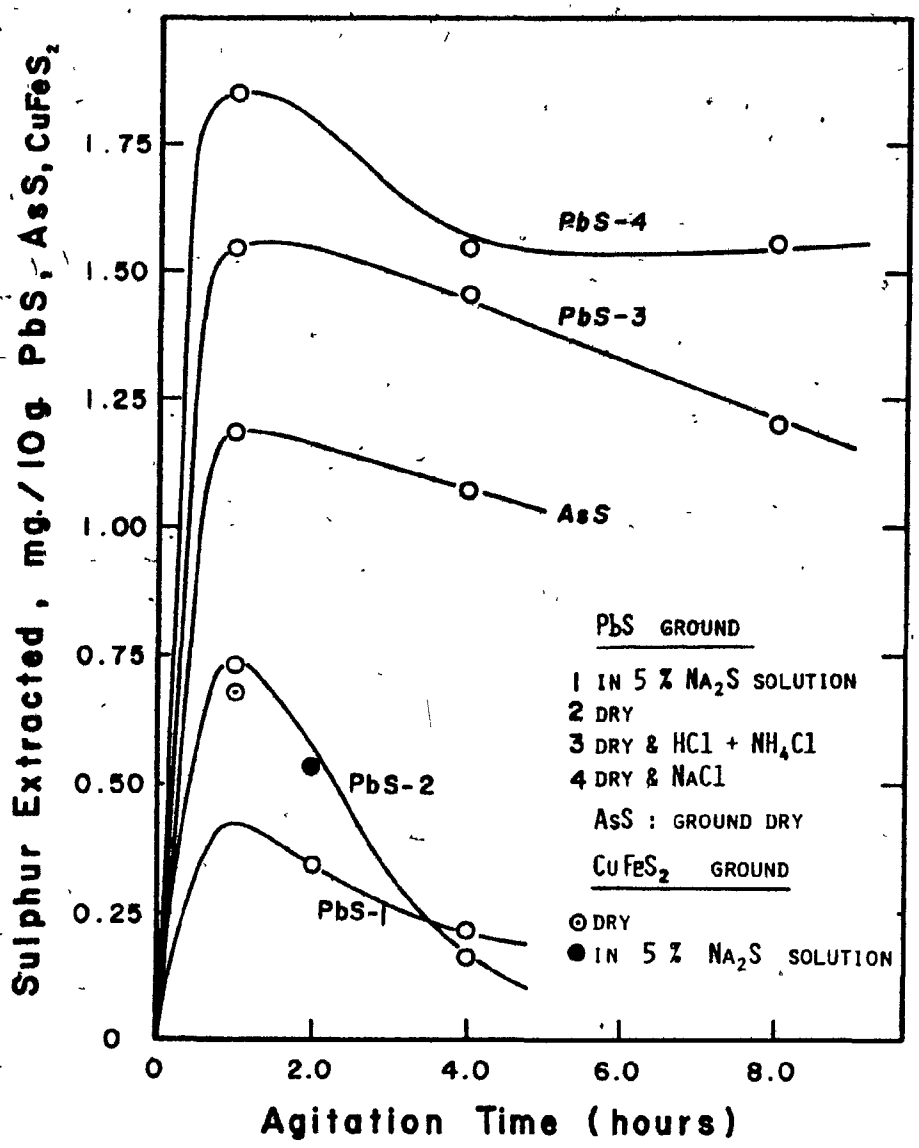


Figure 5.3 Amount of Liberated Sulphur Extracted from Sulphide Minerals

(100x200 mesh) and galena (100x200 mesh) were determined in aqueous methanol solutions of various surface tensions. Chalcopyrite sample was prepared freshly by dry grinding before each flotation test. Galena sample (dry ground) was pretreated using acidified ammonium chloride solutions immediately prior to flotation tests. The recoveries obtained are given in Tables 5.1-5.3 as a function of flotation time.

Table 5.1

Flotation of Sulphur in Aqueous Methanol Solutions of Various Surface Tensions as a Function of Time

$\gamma_{\ell v}$ = 29.2 mN/m		$\gamma_{\ell v}$ = 30 mN/m		$\gamma_{\ell v}$ = 31 mN/m		$\gamma_{\ell v}$ = 31.5 mN/m	
t(sec.)	R(%)	t(sec.)	R%	t(sec.)	R%	t(sec.)	R%
5	4.4	5	8.3	8	18.8	5	23.3
25	12.6	25	22.0	25	51.4	10	39.3
40	16.8	40	41.0	40	67.4	25	62.3
60	26.8	60	49.2	60	81.6	40	86.7
-	-	-	-	-	-	60	95.5

Table 5.2

Flotation of Chalcopyrite in Aqueous Methanol Solutions of Various Surface Tensions as a Function of Time

$\gamma_{\ell v}$ = 35 mN/m		$\gamma_{\ell v}$ = 36.3 mN/m		$\gamma_{\ell v}$ = 39.5 mN/m		$\gamma_{\ell v}$=42 mN/m	
t(sec.)	R(%)	t(sec.)	R(%)	t(sec.)	R(%)	t(sec.)	R(%)
5	2.4	5	5.2	15	37.1	10	65.7
15	4.2	15	16.1	40	73.3	15	78.6
30	8.2	25	25.0	50	78.4	25	91.0
45	9.9	40	34.7	60	87.5	35	97.5
60	19.1	60	49.9	-	-	45	99.0

Table 5.3

Flotation of Pretreated Galena* in Aqueous Methanol Solutions of Various Surface Tensions as a Function of Time

$\gamma_{\ell v}$ = 32 mN/m		$\gamma_{\ell v}$ = 35 mN/m		$\gamma_{\ell v}$ = 36.3 mN/m		$\gamma_{\ell v}$ = 38.3 mN/m		$\gamma_{\ell v}$ = 39.5 mN/m	
t(sec.)	R(%)	t(sec.)	R%	t(sec.)	R%	t(sec.)	R%	t(sec.)	R%
10	10.2	8	11.3	4	8.4	10	37.4	5	46.4
20	16.9	20	37.7	8	18.8	15	50.8	8	60.0
30	21.0	25	47.2	15	39.3	30	74.3	15	87.4
45	38.0	35	56.9	30	68.5	40	80.4	25	96.3
-	-	40	62.2	40	70.1	60	94.6	35	99.4
-	-	50	69.6	60	87.0	-	-	-	-

*Sample dry ground then pretreated using acidified ammonium chloride solution

5.5 DISCUSSION

5.5.1. Formation of Elemental Sulphur on Chalcopyrite and Galena

In recent years, there has been a renewed interest in the fundamental surface chemistry and natural floatability of common sulphides. Two of the most studied sulphides are chalcopyrite and galena. The results obtained in the present work are in agreement with the basic finding that these minerals can float without requiring any flotation reagents unless the flotation is carried out in a reducing medium. There are conflicting reports about the cause of the observed natural floatability. According to Fuerstenau and Sabacky (1981), the sulphide minerals are inherently floatable due to their original surface chemistry. The lack of hydrogen bonding between sulphide ions and water molecules which determines the extent of wettability of sulphide minerals was reported as the possible reason for the natural floatability. On the other hand, the results obtained by Heyes and Trahar (1977), Trahar (1983), and Luttrell and Yoon (1983), strongly suggest that the observed natural floatability of chalcopyrite is brought about by superficial oxidation. Thus, according to these studies the natural floatability of chalcopyrite is an acquired property. Although Heyes and Trahar (1977) could not prove its existence on chalcopyrite analytically, elemental sulphur was believed to be the hydrophobic entity responsible for flotation (Trahar, 1983).

On the basis of their electrochemical studies, Gardner and Woods (1979a) suggested the following oxidation reactions for the formation of elemental sulphur on chalcopyrite:-

$$CuFeS_2 + 3/2O_2 + 3H_2O \rightleftharpoons CuS + 2Fe(OH)_3 + 2\ S^0 \qquad 5.4$$

$$CuFeS_2 + 1/2\ O_2 + 2H^+ \rightleftharpoons CuS + S^0 + Fe^{2+} + H_2O \qquad 5.5$$

The first reaction takes place in alkaline solutions while the second one represents the sulphur liberation in acid solutions.

Surface oxidation of galena leading to the formation of elemental sulphur was represented by the following reaction (Eadington and Prosser, 1969):-

$$PbS + H_2O + 1/2\ O_2 \rightleftharpoons Pb^{2+} + S^0 + 2OH^- \qquad 5.6$$

It should be noted that these reactions represent only the formation of metastable surface oxidation products. The equilibrium surface oxidation product containing sulphur is sulphate (Garrel and Christ, 1965). As pointed out by Trahar (1983), the rate of formation of sulphate is presumably low except at high positive electrochemical potentials whereas elemental sulphur is readily formed (Pourbaix, 1976). Recent electrochemical studies (Ho and Conway, 1978; Gardner and Woods, 1979b) agree on the formation of elemental sulphur as a result of surface oxidation of galena. The details of the oxidation mechanism given by Eadington and Prosser (1969) were strongly opposed by Gutierrez (1981) on theoretical grounds

and assumptions involved. However, he does not seem to specifically oppose the formation of elemental sulphur, nor does he propose a new oxidation mechanism. The results of sulphur extraction tests obtained in the present study prove the existence of appreciable quantities of elemental sulphur on various galena samples. Similarly, the presence of elemental sulphur on chalcopyrite have been shown conclusively using various analytical techniques including ESCA (Buckley and Woods, 1981), mass spectrometry, ESCA and UV technique (Luttrell and Yoon, 1983). Among these techniques, the UV technique has a distinct advantage over the others since the samples do not need to be dried for analysis. Drying the samples is likely to affect the surface composition of the samples. The results of the present UV analysis confirmed the presence of elemental sulphur on the chalcopyrite sample and support the observations by Luttrell and Yoon (1983).

5.5.2. Effect of Surface Tension on the Kinetics of Flotation

In this section, flotation characteristics of the samples in methanol solutions are examined. The effect of solution surface tension on the flotation kinetics of elemental sulphur is compared with that of chalcopyrite and galena samples whose liberated sulphur contents were determined.

The recovery-time data obtained with these samples (Tables 5.1-5.3) were plotted according to the criterion of Equation 5.2 ($\ell n\ [1/(1-R)]$ versus time) in Figures 5.4-5.6.

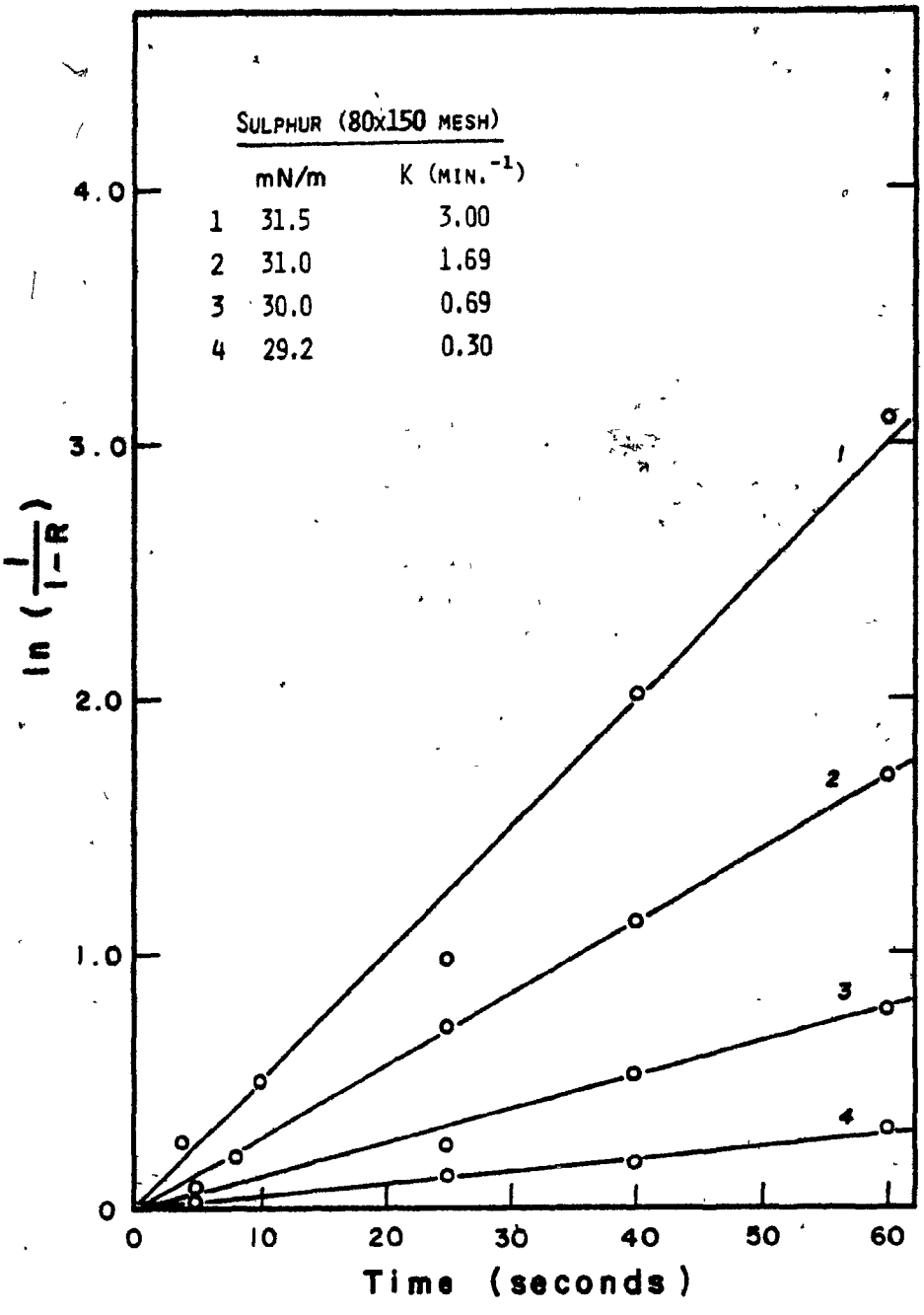


Figure 5.4 Graphical Representation of the First Order Rate Data for the Flotation of Sulphur in Aqueous Methanol Solutions

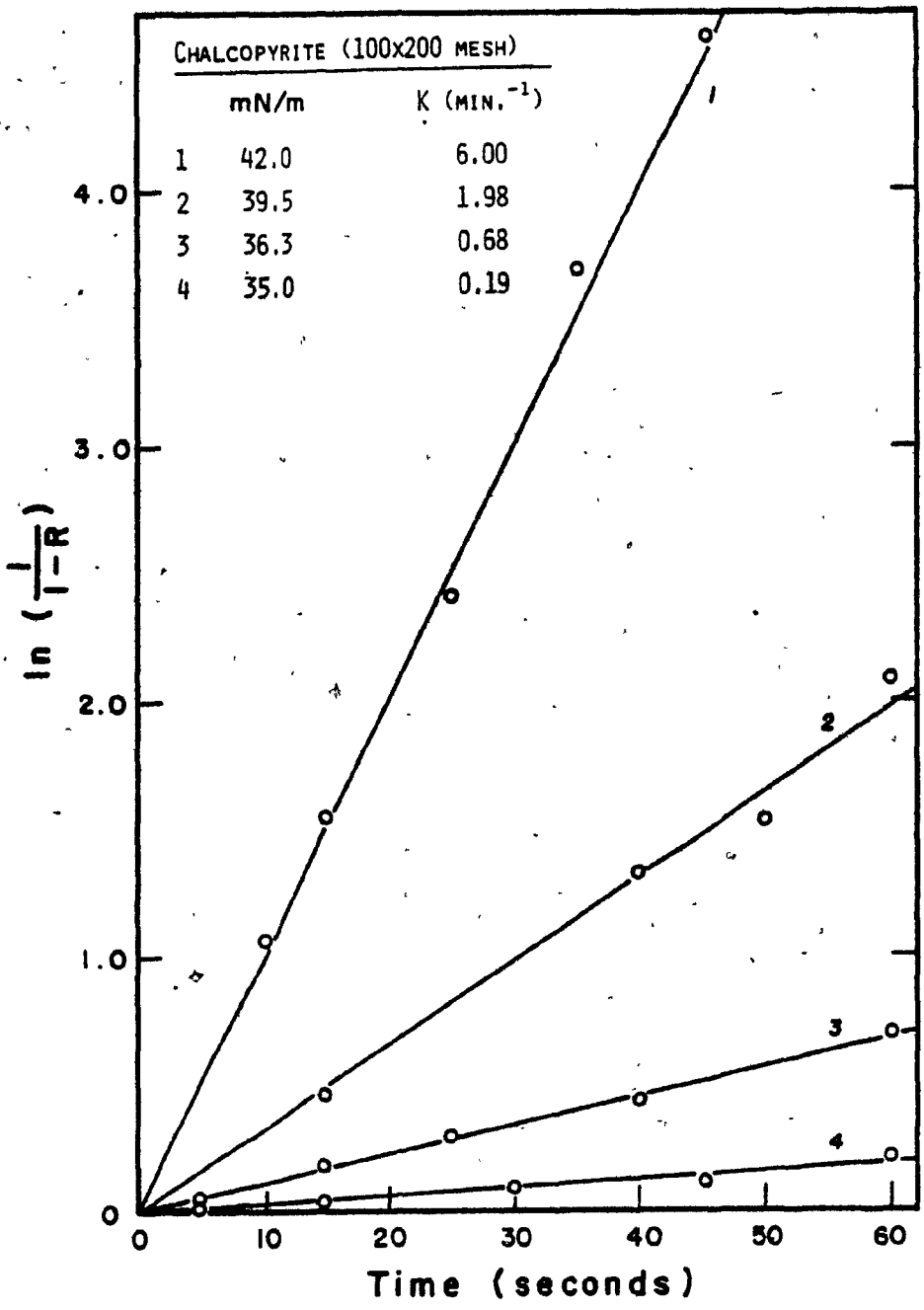


Figure 5.5 Graphical Representation of the First Order Rate Data for the Flotation of Chalcopyrite in Aqueous Methanol Solutions

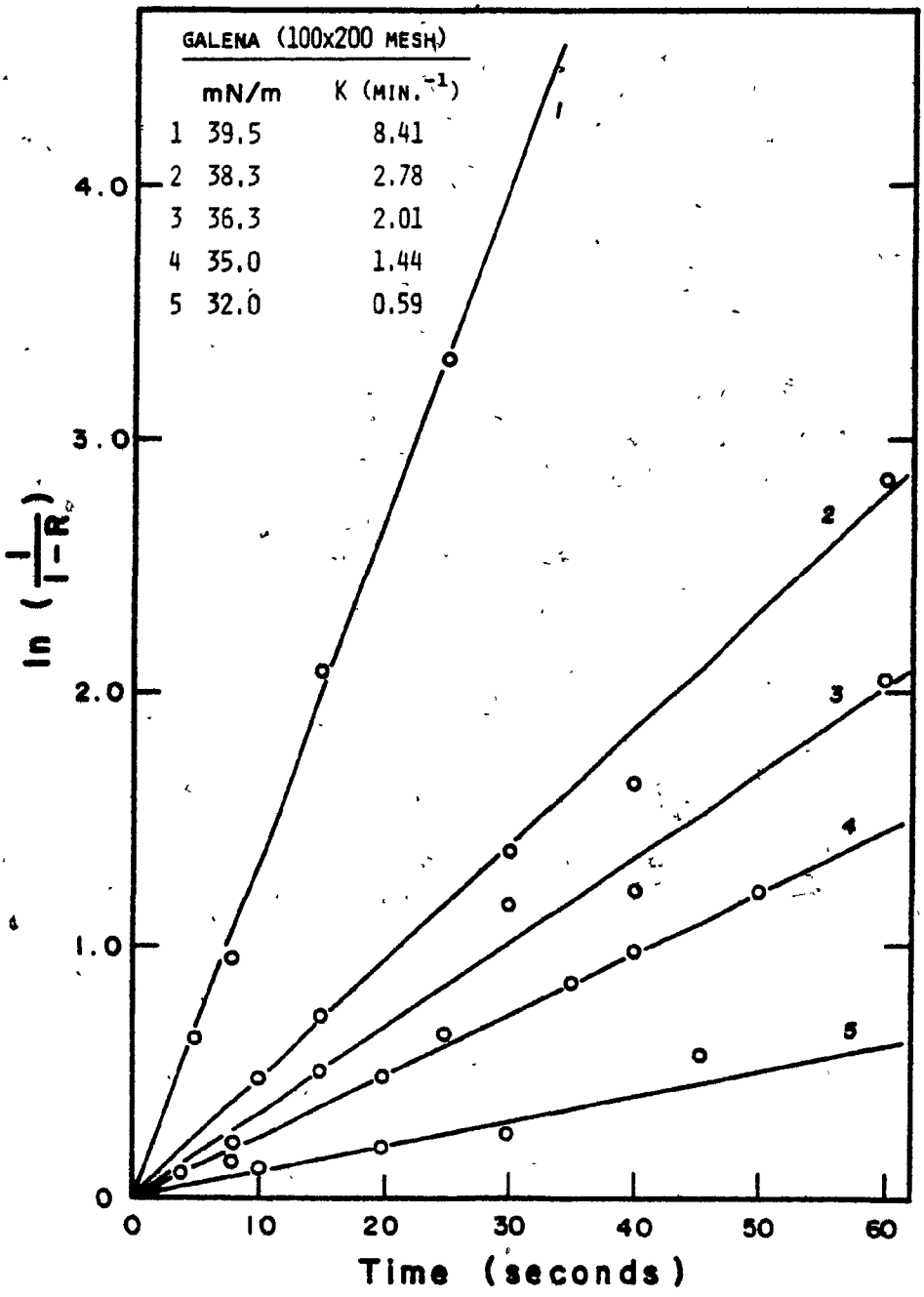


Figure 5.6 Graphical Representation of the First Order Rate Data for the Flotation of Galena in Aqueous Methanol Solutions

They exhibit a reasonably well defined linear behaviour required by the first order equation. It may also be noted that the data plotted this way obey the boundary condition of passing through the origin. The results give additional experimental support to the earlier studies (Morris, 1952; Imaizumi and Inoue, 1965) indicating that flotation process can be better represented by the first order rate equation which is now widely accepted (Thorne et al., 1976; Klimpel, 1980; Agar and Barrett, 1983).

The first order flotation rate constants (K) are shown on Figures 5.4-5.6 as a function of surface tension ($\gamma_{\ell v}$). When the ℓn K values are plotted against $\gamma_{\ell v}$ for each sample, a straight line is obtained (Figure 5.7). The linear behaviour may be described by the following equations:-

$$\ell n\, K_S = 0.984\ \gamma_{\ell v} - 29.923 \qquad 5.7$$

$$\ell n\, K_G = 0.316\ \gamma_{\ell v} - 10.721 \qquad 5.8$$

$$\ell n\, K_C = 0.358\ \gamma_{\ell v} - 13.319 \qquad 5.9$$

where K_S, K_G, and K_C are the first order rate constants for sulphur, galena and chalcopyrite respectively. The latter two minerals have surfaces containing elemental sulphur. It should be noted that these equations are valid specifically for the critical surface tension range of floatabilities of these samples (Chapter 4). At a certain $\gamma_{\ell v}$ value above the critical range, the flotation rate becomes too fast to determine. Its

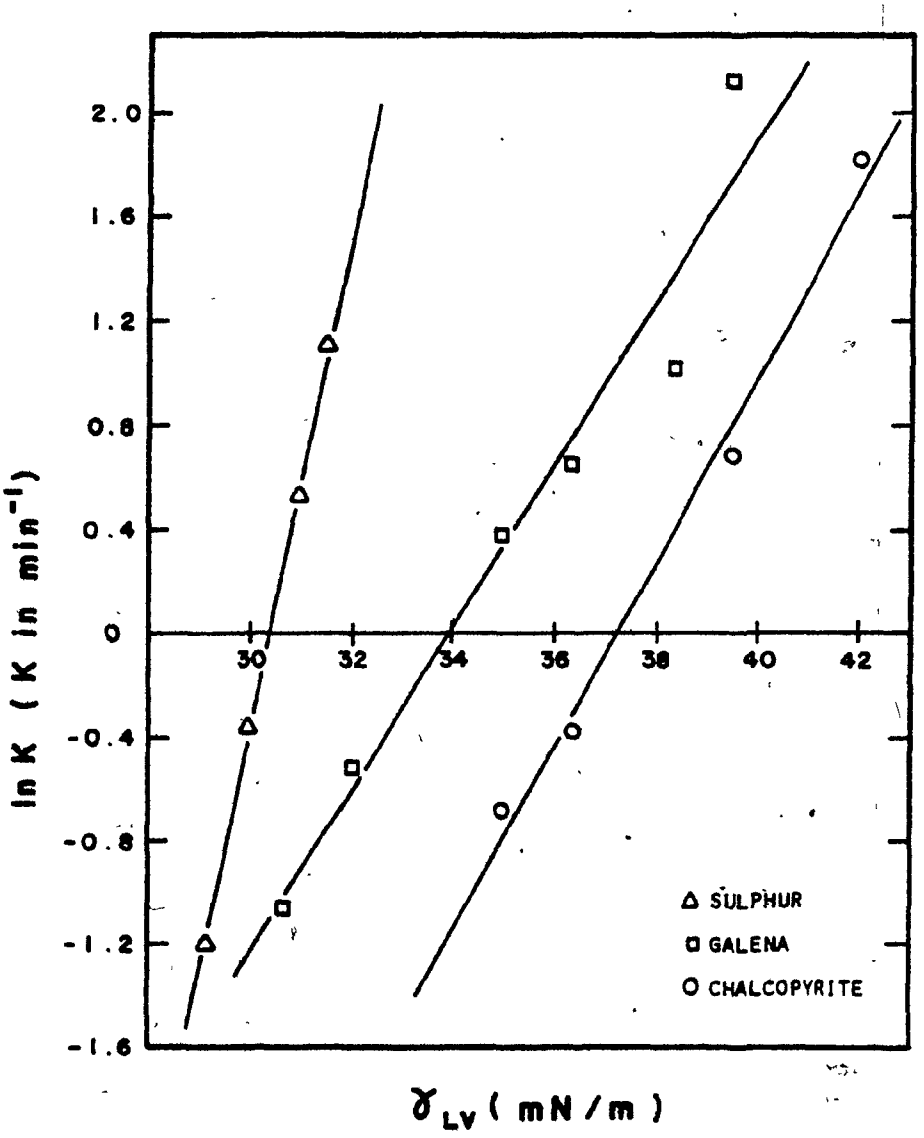


Figure 5.7 Variation of ℓn K as a Function of $\gamma_{\ell V}$ within the Critical Surface Tension Range of Floatability of Sulphur, Chalcopyrite and Galena

dependence on $\gamma_{\ell v}$ may not be described by the same empirical relationships as those given in Equations 5.7-5.9.

5.5.3 Correlation Between the Amount of Liberated Sulphur and Flotation Rate of Chalcopyrite and Galena

Previously, Finkelstein et al. (1975) have confirmed the idea that sulphide minerals can be rendered floatable by the formation of elemental sulphur on their surfaces. But no co-relation could be established between the amount of surface sulphur and the floatability of these minerals. Instances of high floatability at low surface coverages and low floatability in the presence of multilayers of sulphur were observed. In order to establish a correlation, the quantities of elemental sulphur in terms of hypothetical monolayers have been compared with the floatability of these minerals measured in terms of per cent recoveries obtained in water.

Both from the theoretical and practical viewpoints, the floatability of mineral particles in flotation may be best characterized by the flotation rate constant. Since the rate constants were determined for various test solutions having different $\gamma_{\ell v}$ values (note that Finkelstein et al. used only one type of solution, namely water), a better estimate of the speculated correlation can be made. It is more practical for comparison purposes to express the amount of liberated sulphur in terms of equivalent monolayers. The monolayer was assumed to be close-packed (Finkelstein et al., 1975). The packing area of sulphur was taken to be 8.62 $\mathring{A}^2$/atom.

For the estimation of sulphur layers on chalcopyrite and galena, the specific surface areas of these minerals are required. For chalcopyrite, Heyes and Trahar (1977) found that the surface area of size fractions determined by BET method could be described by the following empirical relation:-

$$A = 18.8\ d^{-1.23} \qquad 5.10$$

where A is the specific surface area in m^2/g, and d is average particle size in μm. The surface area of the chalcopyrite sample used was estimated from Equation 5.10. The inspection of the published BET surface areas of size fractions of galena reveals that the surface area-size relationship for galena can be described by a similar form of empirical equation:-

$$\log A_G = -1.022 \log d + 4.626 \qquad 5.11$$

A_G is the specific surface area of galena in cm^2/g, d is in μm. The literature data from which Equation 5.11 was obtained are flotted in Figure 5.8. The results of calculations (Appendix V) are given in Table 5.4. Concentration of sulphur monolayers on realgar was included in the table. Its specific surface area is based on a value given by Finkelstein et al. (1975).

On freshly ground chalcopyrite and galena samples used by Fineklstein et al., the sulphur concentration was 2 and 0.3 monolayer(s) respectively as compared to 1.8 monolayers on

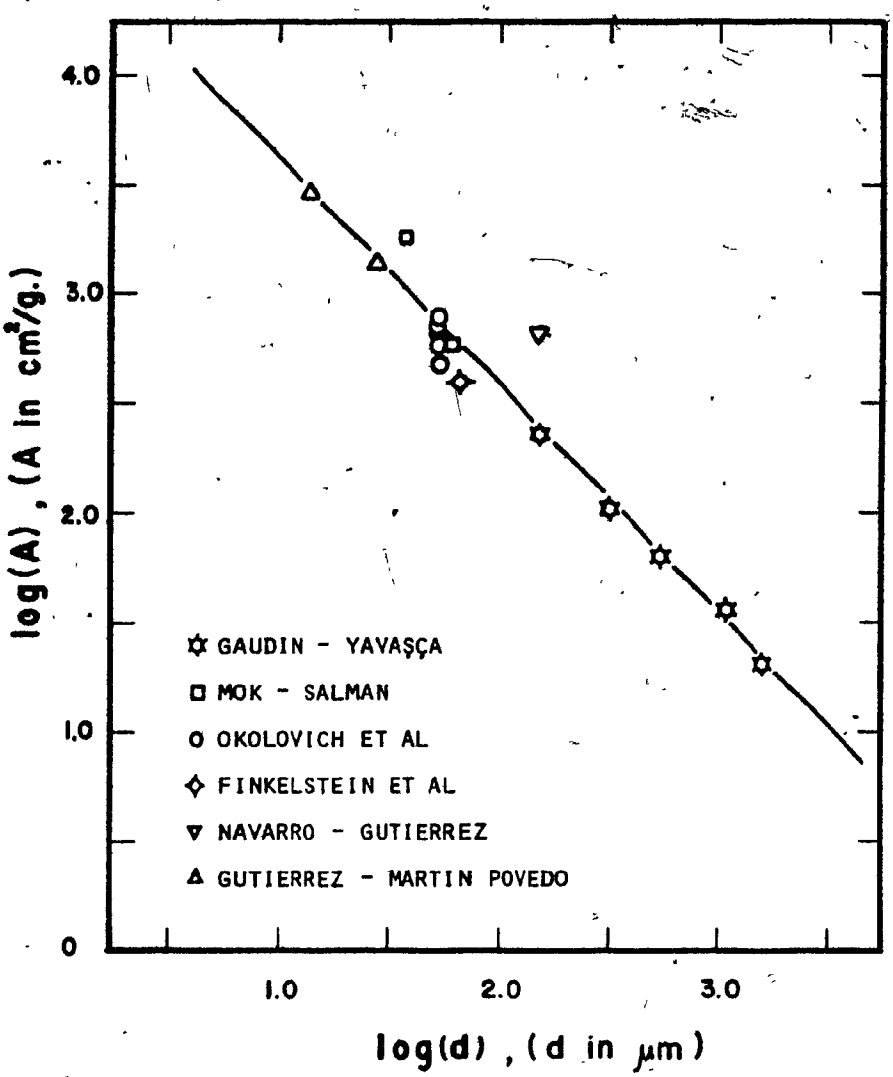


Figure 5.8 Relationship between the Specific Surface Area and Particle Size of Galena

Table 5.4

Amount of Elemental Sulphur
Formed on Sulphide Minerals

Samples*	Description	S^{o} found MG./10 G.	Equivalent† Monolayers
Galena 1	Freshly ground (dry)	0.730	3.1-3.6
Galena 2	Ground in 5% Na_2S	0.420	1.8-2.1
Galena 3	#1: NaCl leached	1.850	7.8-9.1
Galena 4	#1: NH_4Cl + HCl leached	1.542	6.5-7.6
Chalcopyrite	Freshly ground (dry)	0.674	1.8
Realgar	Freshly ground (dry)	1.183	1.6

*Particle size: 100x200 mesh
Specific surface areas used: galena: 0.03631 ± 0.00269 $M^2/G.$
Chalcopyrite: 0.0614 $M^2/G.$, realgar: 0.1220 $M^2/G.$
†Close packing assumed, based on elemental sulphur area of 8.62 sq A°/atom and 1 hour extraction.

chalcopyrite and ~ 3.4 monolayers on galena found in the present study. The values for chalcopyrite is in good agreement while those for galena are very different. The natural floatabilities of both of their samples determined using the same type of cell (Partridge and Smith, 1971) were very low (≤ 15%) as compared to high recoveries (> 95%) obtained in the present study. These discrepancies may be related to different histories of the samples, varying degrees of oxidation and differences in experimental procedures. For example, in the present study washing the freshly ground samples immediately prior to flotation tests was found to be very effective in increasing the recovery (section 2.5.2.2, Table 2.2). The prewashing is

thought to increase the hydrophobic-to-hydrophilic ratio of the particles by decreasing the concentration of soluble hydrophilic surface species on the surface. Finkelstein et al. recognized the deleterious effects of hydrophilic oxidation products and attempted to leach out the hydrophilic surface species by various treatments. However, they noted that 'hot aqueous solutions of ammonium acetate, and sodium chloride removed not only the hydrophilic products but also the sulphur - probably by mechanical action.', They did not specify the treatment procedure nor did they appear to have determined the sulphur concentration of the samples after the treatment. Contrarily, the results obtained in the present work indicate that the sulphur concentration on galena was increased appreciably (Table 5.4) by treatment with acidified ammonium chloride, and neutral sodium chloride solutions. Table 5.5 shows

Table 5.5

Correlation Between the Quantity of Liberated Sulphur and Flotation Rate Constants of Chalcopyrite and Galena

Liberated Sulphur	Chalcopyrite	Galena	Sulphur
mg/10 g	0.67	1.54	-
Monolayers	1.8	6.5-7.6	-
Surface Tension*	Flotation Rate Constants (min^{-1})		
30	0.08	0.29	0.67
31	0.11	0.40	1.17
32	0.16	0.54	4.48
33	0.22	0.75	12.79

*mN/m

the correlation between the surface concentration of sulphur on chalcopyrite and galena, and the flotation rate constants. The rate constants of the chalcopyrite sample are lower at all surface tension values than those of galena which has a larger amount of liberated sulphur on its surface. The rate constants of sulphur itself are much higher than those of both galena and chalcopyrite sample.

5.6 REFERENCES

Agar, G.E. and Barrett, J.J. (1983). The Use of Flotation Rate Data to Evaluate Reagents. CIM Bulletin, Vol. 76, No. 851, pp. 157-162.

Arbiter, N. (1951). Flotation Rates and Flotation Efficiency. Trans. AIME., Vol. 190, pp. 791-796.

Arbiter, N. and Harris, C.C. (1962). Flotation Kinetics. In: Froth Flotation 50th Anniversary Volume, (D.W. Fuerstenau: Editor), AIME., New York, pp. 215-246.

Bass, A.M. (1953). The Optical Absorption of Sulfur. J. Chem. Phys., Vol. 21, No. 1, pp. 80-82.

Buckley, A. and Woods, R. (1981). Investigation of the Surface Oxidation of Sulfide Minerals via ESCA and Electrochemical Techniques. Engineering Foundation Conference on Interfacial Phenomena in Mineral Processing August 2-7, Rindge, New Hampshire.

Dobby, G.S. (1984). A Fundamental Flotation Model and Flotation Column Scale-Up. Ph.D. Thesis, Dept. Min. Metall. Eng., McGill University.

Eadington, P. and Prosser, A.P. (1969). Oxidation of Lead Sulphide in Aqueous Suspensions. Trans. IMM., Vol. 78, pp. C74-C82.

Finkelstein, N.P., Allison, S.A., Lovell, V.M. and Stewart, B. V. (1925). Natural and Induced Hydrophobicity in Sulphide Mineral Systems. Symposium Series, Amer. Inst. Chem. Eng., Vol. 71, No. 150, pp. 165-175.

Friedman, H.L. and Kerker, M. (1953). Ultra-violet Absorption of Aqueous Sulfur Solutions. J. Coll. Sci., Vol. 8, pp. 80-85.

Fuerstenau, M.C. and Sabacky, B.J. (1981). On the Natural Floatability of Sulfides. Int. J. Miner. Process., Vol. 8, pp. 79-84.

Gardner, J.R. and Woods, R. (1979a). An Electrochemical Investigation of the Natural Floatability of Chalcopyrite. Int. J. Miner. Process., Vol. 6, pp. 1-16.

Gardner, J.R. and Woods, R. (1979b). A Study of the Surface Oxidation of Galena Using Cyclic Voltammetry. J. Electroanalytical Chem., Vol. 100, pp. 447-459.

Garrels, R.M. and Christ, C.L. (1965). Solutions, Minerals and Equilibria. Harper and Row, New York, N.Y.

Gaudin, A.M. and Wilkinson, W.D. (1933). Surface Actions of Some Sulfur-Bearing Organic Compounds on Some Finely-Ground Sulfide Minerals. J. Phys. Chem., Vol. 37, pp. 833-845.

Gaudin, A.M. and Yavasca, S. (1946). Principles of Comminution-Size and Surface Distribution. Trans. AIME., Vol. 169, pp. 88-94.

Gutierrez, C. (1981). Existence of an Induction Period in the Oxidation of Galena and Lead Sulfide in Water. Min. Eng., AIME., Vol. 33, No. 2, pp. 192-194.

Gutierrez, C. and Martin-Poveda, F. (1981). Flotation of Galena. Influence of Grain Size, of Pulp Deoxygenation, and of Cleaning with Ammonium Acetate. Int. Miner. Process., Vol. 8, pp. 111-123.

Heyes, G.W. and Trahar, W.J. (1977). The Natural Floatability of Chalcopyrite. Int. J. Miner. Process., Vol. 4, pp. 317-344.

Ho, F.C. and Conway, B.E. (1978). Electrochemical Behaviour of the Surface of Lead Sulfide Crystals as Revealed by Potentiodynamic, Reflectance, and Rotating-Electrode Studies. J. Coll. Interface Sci., Vol. 65, No. 1, pp. 19-35.

Imaizumi, T. and Inoue, T. (1965). Kinetic Consideration of Froth Flotation. In: Miner. Process. (A. Roberts: Editor), Proceed. Sixth Int. Miner. Process. Congr., Cannes, France, Pergamon Press, New York, pp. 581-589.

Kazuo, N. (1971). Infrared and Raman Spectra of Inorganic and Coordination Compounds. 3rd Edition, John Wiley & Sons, New York, p. 173.

Klimpel, R.R. (1980). Selection of Chemical Reagents for Flotation. AIME/SME Preprint No. 80-34.

Laplante, A.R. (1980). Effect of Air-Flow-Rate on the Kinetics of Flotation. Ph.D. Thesis, Univ. of Toronto, Dept. Metall. Materials Sci.

Luttrell, G.H. and Yoon, R.H. (1983). Surface Chemistry of Collectorless Flotation of Chalcopyrite, AIME/SME, Preprint No. 83-193.

Miller, F.A., Carlson, G.L., Bentley, F.F., and Jones, W.H. (1960). Infrared Spectra of Inorganic Ions in the Cesium Bromode Region (700-300 cm^{-1}). Spectrochimica Acta, Vol. 16, pp. 135-235.

Miller, F.A. and Wilkins, C.H. (1952). Infrared Spectra and Characteristic Frequencies of Inorganic Ions, Analytical Chem., Vol. 24, No. 8, pp. 1253-1294.

Mok, J. and Salman, T. (1964). Contact Angle and Adsorption Studies. Can. Min. J., Vol. 85, No. 11, pp. 70-73.

Morris, T.M. (1952). Measurement and Evaluation of the Rate of Flotation as a Function of Particle Size, Trans. AIME, Vol. 191, pp. 794-798.

Navarro, A. and Gutierrez, C. (1981). Influence of the Semiconducting Character of a Bed of Galena Particles on its Potential During Flotation, J. Coll. Interface Sci., Vol. 81, No. 2, pp. 390-395.

Neff, V.D. and Walnut, T.H. (1961). Effect of Temperature on the Intensity and Structure of Bands in the Infrared Spectrum of Rhombic Sulfur. J. Chem. Phys., Vol. 35, No. 5, pp. 1723-1729.

Okalovich, A.M., Konevskikh, N.N. and Figurkova, L.I. (1968). Specific Surface of minerals. In: Flotation Agents and Effects (V.A. Glembotskii et al.: Editors). (Isr. Program Sci. Transl. 1970).

Olsen, D.A., Moravec, R.W., and Osterhaas, A.J. (1967). The Critical Surface Tension Values of Group VIA Elements, J. Phys. Chem., Vol. 71, pp. 4464-4466.

Partridge, A.C. and Smith, G.W. (1971). Small-Sample Flotation Testing: a New Cell, Trans. IMM, Vol. 80, pp. C199-200.

Pourbaix, M. (1976). Contribution to Discussion. Applications Techniques de la Science Electrochimique à la Protection Centre la Corrosion. Rapports Tech. CEBELCOR 129, RT 234, pp. 167-169, quoted by Trahar (1983).

Sutherland, K. L. (1948). Physical Chemistry of Flotation XI: Kinetics of the Flotation Process, J. Phys. Chem., Vol. 52, pp. 394-425.

Sutherland, K.L. and Wark, I.W. (1955). Principles of Flotation, Australasian IMM, Melbourne.

Thorne, G.C., Manlapig, E.V., Hall, J.S., and Lynch, A.J. (1976). Modelling of Industrial Sulphide Flotation Circuits, Ch. 26 in Flotation - A.M. Gaudin Memorial Volume, (M.C. Fuerstenau: Editor), AIME.

Trahar, W.J. (1983). A Laboratory Study of the Influence of Sodium Sulphide and Oxygen on the Collectorless Flotation of Chalcophrite, Int. J. Miner. Process, vol. 11, pp. 57-74.

CHAPTER 6

GALENA-XANTHATE SYSTEM

6.1 INTRODUCTION

Chapter 4 was concerned with the use of surfactants to increase the wettability of inherently hydrophobic, low-energy solids in aqueous solutions. The inherently hydrophobic minerals constitute only a small group among the vast majority of minerals that are of industrial interest. In conventional froth flotation systems, surface active reagents are used to induce hydrophobicity to desired components of the flotation feed, that is, to increase their dewettability so that they can be selectively floated. Therefore, the concept of critical surface tension of wetting is directly applicable to describe the hydrophilic-hydrophobic transition of minerals in flotation and has begun to be employed (Parekh and Aplan, 1974; Finch and Smith, 1975; 1979; Hornsby and Leja, 1980). The study of Parekh and Aplan reported the results of wettability of various surfactant coated minerals. However, the results were obtained using pure liquid droplets and no attempt was made to relate the findings to the flotation behavior of the samples. Finch and Smith (1975) were the first investigators to discuss the flotation behavior in terms of critical surface tension of wetting. However, in their

experiments the wettability was judged by the quantity of particles picked up by a captive bubble and by flotation tests only. They did not measure contact angles as a function of solution surface tension to determine the critical surface tension of wetting.

It is known that xanthates are chemisorbed by sulphide minerals and the resulting hydrophobicity level of the surface is determined by the length of the hydrocarbon chain. This chapter has been devoted to a systematic study of wettability and floatability of galena pretreated with n-alkyl xanthates of increasing hydrocarbon chain as a function of solution surface tension.

6.2 EXPERIMENTAL MATERIALS AND PROCEDURES

6.2.1. Reagents

Potassium n-alkyl xanthates were prepared by the addition of a specified amount of carbon disulphide to a solution of potassium hydroxide in normal alcohol solutions. The general reaction to produce potassium n-alkyl xanthates is as follows:-

$$R\text{-}OH + CS_2 + KOH \longrightarrow ROCSSK + H_2O \qquad 6.1$$

where R denotes a normal alkyl hydrocarbon chain. Alkyl groups of increasing chain length (from methyl to dodecyl) were used. The products were dissolved in acetone and reprecipitated by petroleum ether at least twice to obtain high purity samples. The method of preparation and purification was similar to that

described by Rao (1971).

Lead xanthates were precipitated by mixing the saturated solutions of potassium alkyl xanthate and lead chloride, filtered washed with distilled water and dried in a desiccator under oxygen-free nitrogen gas at low pressure. All the xanthates were used within two weeks after their preparation. All reagents used in the preparation and purification of xanthates were reagent grade.

Other reagents used include potassium bromide (spectrophotomotric-grade, J.T. Baker Co.) for the preparation of infrared pellets, octane (synthetic, boiling point range; 124-126°C, Anachemia) for the contact angle measurements, and methanol (reagent grade, Am. Chemicals Ltd.) for controlling the solution surface tensions.

6.2.2. Galena Sample

The galena used was from Kansas. It was obtained through Wards Natural Science Establishment, Rochester, New York, and was very crystalline. Visible impurities which appeared at the exterior part of some block pieces were segregated by cleavage. The resulting clean sample assayed 99.6% PbS (section 2.3.1.).

6.2.3. Infrared Spectra

The nature of surface compound produced when the galena sample was treated with xanthate solution was studied using

infrared spectrophotometry. Fine particles (-3μm) of the galena sample were prepared by wet grinding in a hand mortar and sedimentation in distilled water. About 100 mg. of this fine powder was placed in a freshly prepared xanthate solution and agitated for five minutes in a test tube. Then the suspension was left stand for 30 minutes after which it was filtered using a membrane filter paper of 0.2 μm pore size (Sartorius) under suction with a water pump and dried in a desiccator at low pressure. 1.1 ± 0.1 mg. of this sample was ground with about 350 mg. of KBr and subsequently the mixture was pressed in an evacuated die into a pellet employing a hydraulic press. Infrared spectra were scanned on a Perkin-Elmer Model 237B spectrophotometer immediately after the preparation of pellets.

Dihexyl and didodecyl dixanthogens were prepared by oxidation of respective potassium xanthates with iodine and extraction by petroleum ether (Rao, 1971). Two drops of this extract were added on to 350 mg. of finely ground KBr powder in an evacuable container and the ether was evaporated under low pressure generated through a water pump. The resulting mixtures were made into pellet and their spectra determined.

6.2.4. Surface Tension Measurements

Surface tension of aqueous methanol and potassium decyl xanthate solutions were determined using the Fisher Autotensiomat which operates on the principles of the du Nouy ring method. The solutions were prepared using single distilled

water immediately prior to measurements. The platinum-iridium rings were of 4.00 and 6.00 cm. mean circumference. The surface tension values were determined only for freshly formed solution surfaces (see Chapter 3 for details).

6.2.5. Contact Angle Measurements

Pieces of galena with approximate dimensions 0.7 cm. x 0.7 cm. x 1.5 cm. were obtained by cleavage, ground using a series of emery papers under distilled water and polished with aqueous slurries of alumina in successively decreasing particle sizes. The polished specimens were stored under distilled water until required for treatment with the solutions of potassium xanthate. Each specimen was kept in contact with the solution containing about 25 mg. xanthate per 100 cm^3 for 30 minutes. Subsequently it was taken out from the solution slowly with the polished face approximately vertical to the solution surface during which a speedy retraction of the liquid film from the galena surface was observed. Then, the sample was immediately transferred into an all glass contact angle cell containing distilled water. The distilled water was changed repeatedly while keeping the xanthated galena sample in contact with a steady stream of distilled water. This was continued until there was no difference in the surface tensions of distilled water before and after washing the sample.

The contact angles of the air bubbles were measured in distilled water, then in aqueous methanol solutions of increasing concentration. After the measurement at a certain tension

value the solution over the sample was withdrawn by a suction system while the sample was continuously showered by a new solution of reduced surface tension eventually to fill the cell. The apparatus used was based on the original design due to Taggart et al. (1930). (section 2.3.3.2) The bubble holder consisted of a 1.0 mm diameter glass capillary tube. The contact angles were measured with the air bubbles of 1.5 ± 0.2 mm in diameter. The stage upon which the cell rests was tapped lightly (Sutherland and Wark, 1955) to achieve an equilibrium value of contact angle and to be comparable, all bubbles were kept in contact with the surfaces for about twenty minutes, prior to the angles being read to the nearest degree by means of a built-in protractor. Five to seven pairs of readings for each surface tension value were averaged.

The octane contact angles were measured in the same manner as described for the air bubbles. The octane and water phases were previously saturated with each other. The surface tension values were verified by measurements. The water used in these tests was doubly distilled which was found to have approximately the same surface tension value as the single distilled water. For these experiments 250 cm^3 of octane was washed with 600 cm^3 of double distilled water by mixing the two in a one-litre stoppered flask and separating most of the octane phase without disturbing the oil-water interface to mix with about the same amount of fresh water in a new flask. This procedure (repeated four times) helped the two phases saturate

with each other and the elimination of any surface active trace impurities that might have adsorbed at the oil-water interface. The octane contact angles were measured using these two phases.

6.2.6. Flotation Tests

Flotation tests were performed using a microflotation cell of 100 cm^3 capacity, which was similar in form to that described by Partridge and Smith (1971). The cell contents were mixed by means of a glass coated magnetic bar (1.6 cm in length) and magnetic stirrer.

In general, lead xanthates produced by precipitation from potassium xanthates were so light that the evaluation of their floatability was difficult when used in their natural state. This has been experienced previously by Finkelstein et al. (1975). Following their procedure, lead xanthate precipitates were first pressed into pellets from which the 65x200 mesh size fraction was obtained by grinding and screening. This flotation feed was washed first with ether then with the flotation test solution several times before it was used to determine the floatability.

In a second series of experiments, natural galena (100 x 200 mesh) was treated with xanthate solutions, washed with plenty of distilled water, then floated as a function of solution surface tension with and without prior ether washing.

Each flotation feed was prepared in batches 0.5 g immediately before the tests. The conditioning time was five minutes. Stirring was started at the last minute so as not to produce slimes (especially in the case of compacted particles). Flotation was continued for one minute at an air flow rate of 50 cm^3/min.

6.3 RESULTS

6.3.1. Infrared Spectra

Figure 6.1 shows the infrared spectra of lead methyl xanthate, dimethyl dixanthagen and the galena sample which was previously treated with potassium methyl xanthate solution. The corresponding spectra for hexyl and dodecyl compounds are shown in Figures 6.2 and 6.3 respectively. The location of major bands are marked on the figures. Several bands between 1020 and 1065 cm^{-1} are assigned to the stretching mode of C=O. The principal band within this range is common to all three spectra. The bands in the immediate vicinity of 1100, 1120 and 1200 cm^{-1} are attributed to the stretching vibration of the C-O-C group. The bands at 1252 and 1255 cm^{-1} are due to the stretching mode of the C-O-C group in dixanthogen molecule. Therefore, one characteristic feature of the dixanthogen spectra is the shift of the stretching mode (observed for lead xanthates at about 1200 cm^{-1}) to 1250 - 1260 cm^{-1}. A second difference between the spectra of dialkyl dixanthogen and those of lead xanthates is the reduction in the intensity of the band at about 1120 cm^{-1} for the former. The bands between 1475 and

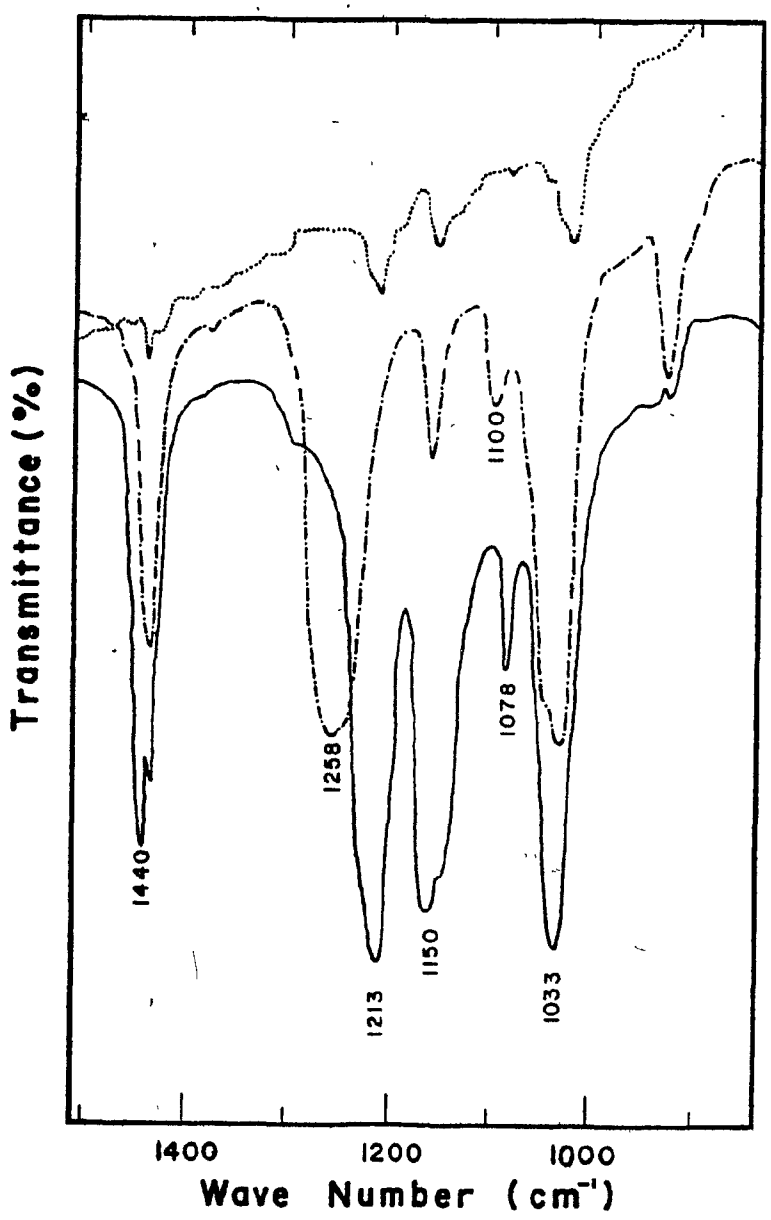


Figure 6.1 Infrared Spectra of Lead Methyl Xanthate (dotted line), Dimethyl Dixanthogen (dashed line) and the Galena Sample Treated with Potassium Methyl Xanthate Solution at Natural pH

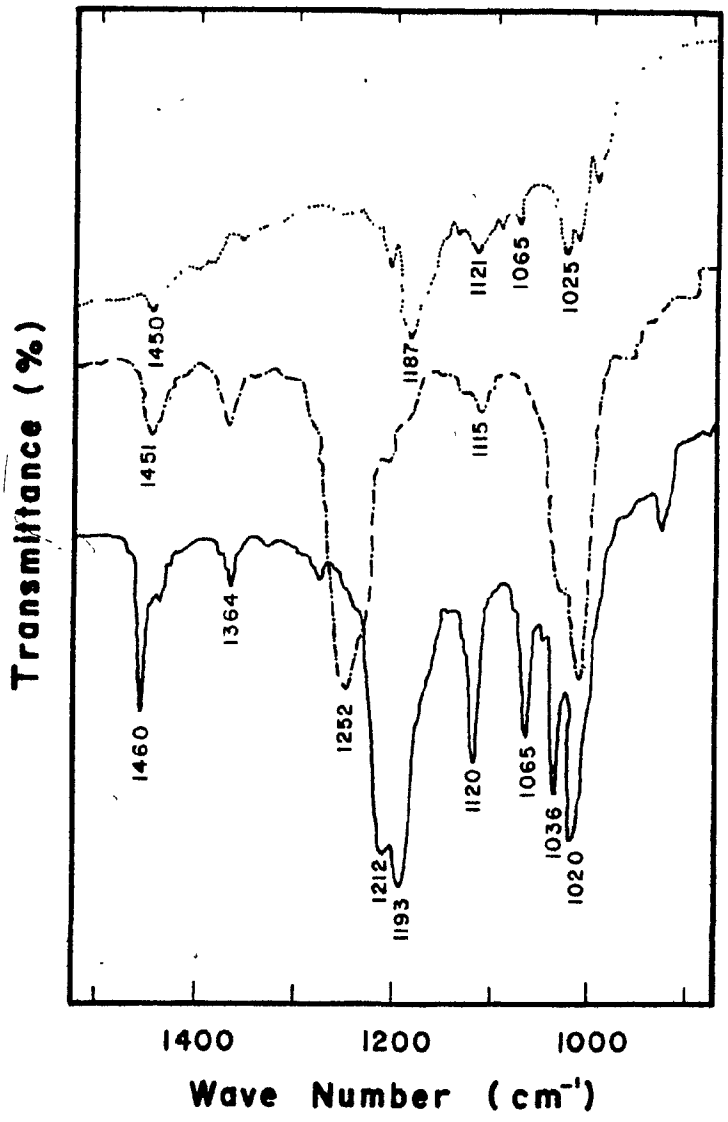


Figure 6.2 Infrared Spectra of Lead Hexyl Xanthate (dotted line), Dihexyl Dixanthogen (dashed line), and the Galena Sample Treated with Potassium Hexyl Xanthate Solution at Natural pH

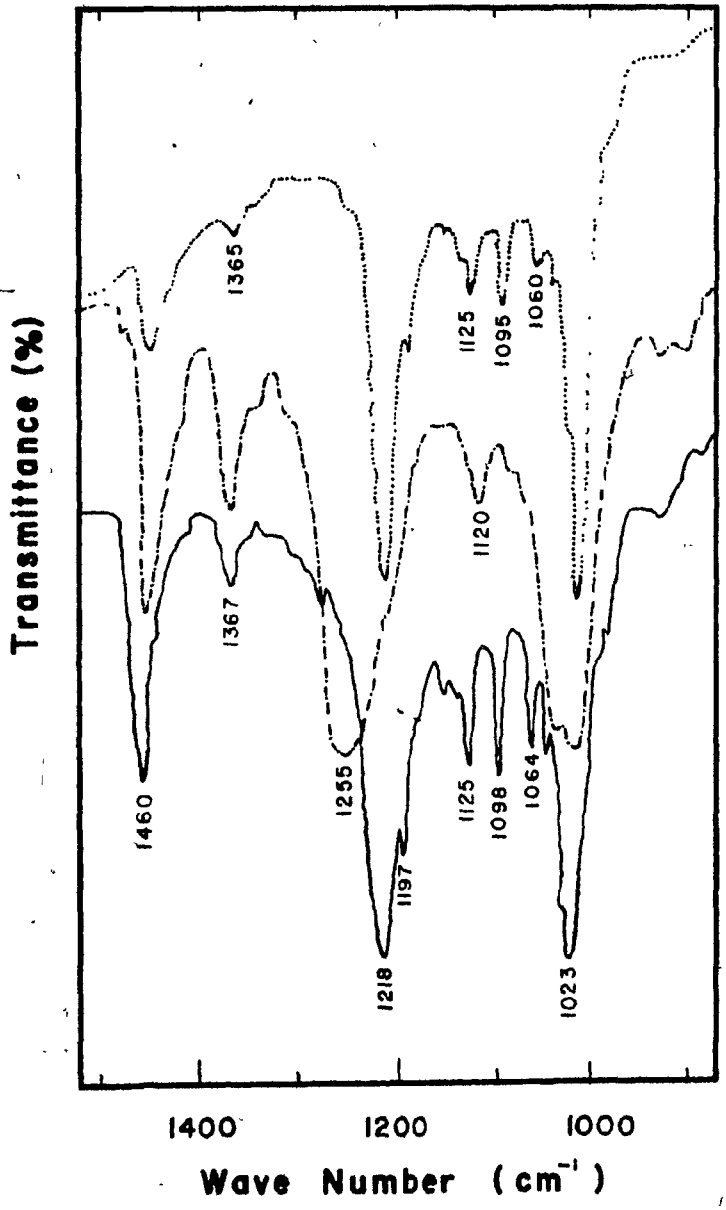


Figure 6.3 Infrared Spectra of Lead Dodecyl Xanthate (dotted line), Didodecyl Dixanthogen (dashed line), and the Galena Sample Treated with Potassium Dodecyl Solution at Natural pH

1300 cm^{-1} are assigned to the C-H bending mode (Kendall, 1966). The band near 1460 cm^{-1} is attributed specifically to the presence of CH_3- and/or -CH_2- groupings which induce a hydrophobic character to a molecule or surface compound. These structural assignments are in general agreement with those obtained by Leja et al. (1963), Goold and Finkelstein (1969) and more recent studies reviewed by Giesekke (1983).

6.3.2. Contact Angle Measurements

Contact angles of air bubbles and octane droplets on xanthated galena surface in distilled water are shown as a function of hydrocarbon chain length in Figure 6.4. The contact angles measured with the bubbles in the pioneer work by Wark and Cox (1934) are included in the figure. Their measurements were carried out with bubbles about 5 mm in diameter in solutions containing 25 mg. per liter of the xanthate. The contact angles rise rapidly at first and then more slowly as the number of carbon atoms in the aliphatic hydrocarbon group increases. For methyl to butyl xanthates, the values of the contact angles are the same as those obtained by Wark and Cox. However, a difference in contact angle values measured by these authors and the present study becomes apparent for longer chain xanthates.

Contact angles of the octane droplets in distilled water are much larger than those of air bubbles. The difference between the two becomes increasingly more pronounced as the chain length increases.

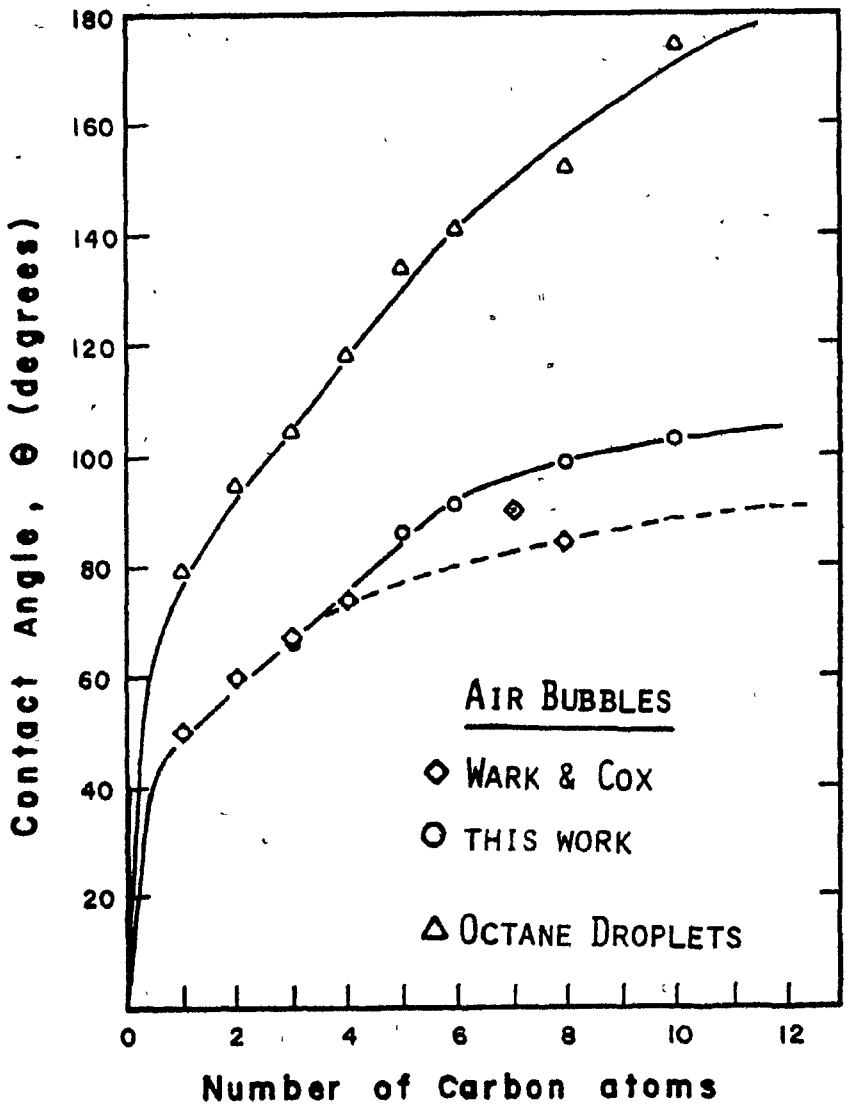


Figure 6.4 Contact Angles of Air Bubbles and Octane Droplets on Xanthated Galena as a Function of the number of Carbon Atoms in the Hydrocarbon Group

The values of contact angles measured on xanthated galena in aqueous methanol solutions (Appendix VI) were used to calculate the adhesion tension, γ_{LV} Cosθ. Figure 6.5 shows the relationship between adhesion tension and surface tension of the methanol solutions, γ_{LV}. For each hydrocarbon chain length, adhesion tension changes linearly with a slope β in the range 72.5 to about 42 mN/m. At about 42 mN/m, there is an apparent change in the direction of the wettability lines. They assume a different slope, β' so as to converge in a narrow range of critical surface tension values, γ_c. The variation of the values of β, β' and γ_c obtained by regression is shown with respect to the chain length of the hydrocarbon radical in Table 6.1. In general, the slopes and γ_c values decrease with an increase in the chain length. It can be noted that the γ_c values for all samples studied are located in the range 26 to 30 mN/m.

Figure 6.6 shows the adhesion tension diagram for the system of the galena-decyl xanthate. The surface tension values are those of decyl xanthate solutions (Appendix III). The dependence of adhesion tension upon solution surface tension is very different from that observed for xanthated galena surface in aqueous methanol solutions. Initially, the adhesion tension decreases sharply with a small decrease in the surface tension of decyl xanthate solution. Passing through a minimum it then increases with a further decrease in surface tension. This increase is not linear in the surface tension range of 67 to 47.5 mN/m. Linearity is apparently exhibited for surface tensions less than 47.5 mN/m. The

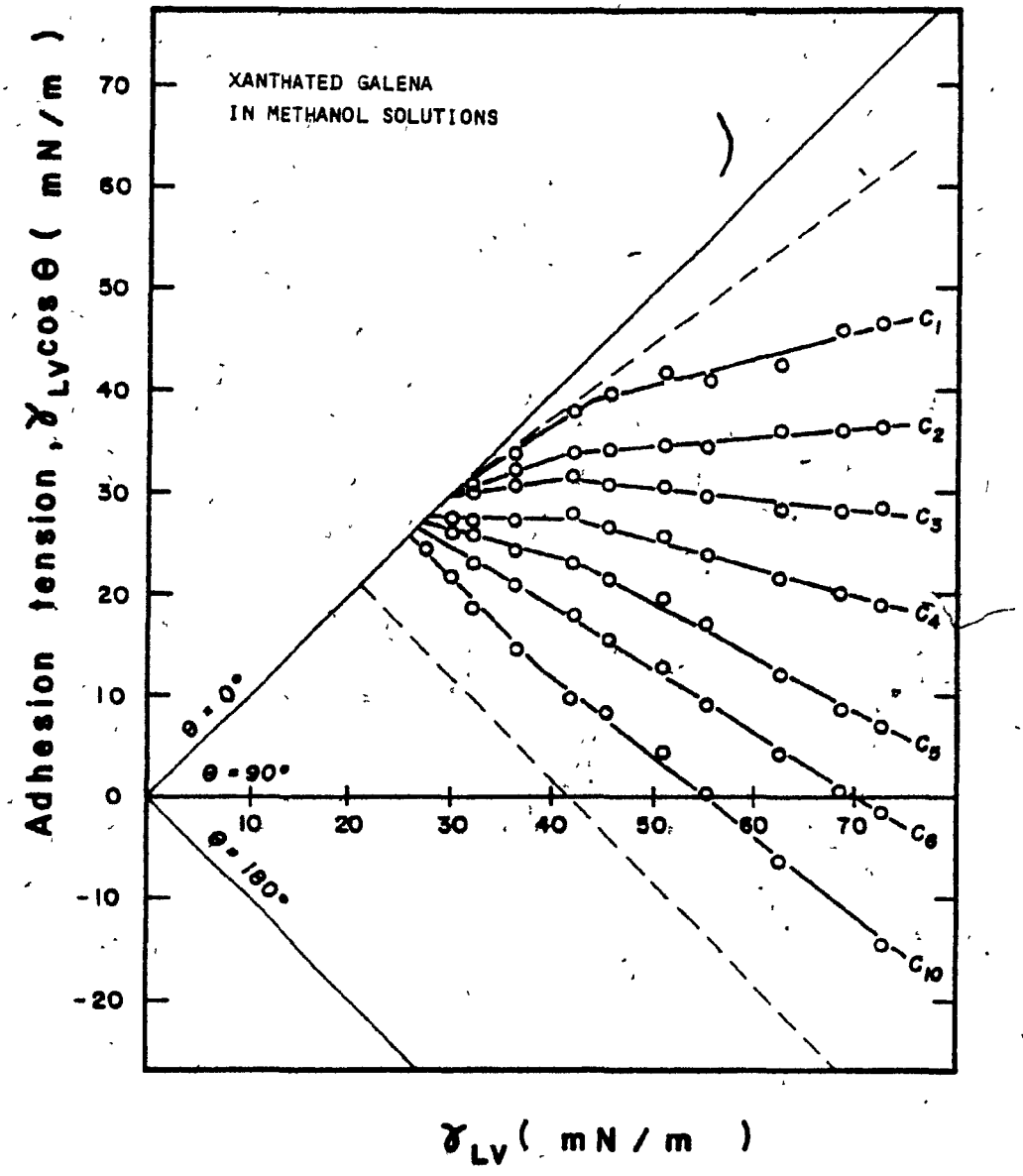


Figure 6.5 Adhesion Tension Diagram for Galena Pre-treated with n-Alkyl Xanthates of Increasing Hydrocarbon Chain Length in Aqueous Methanol Solutions

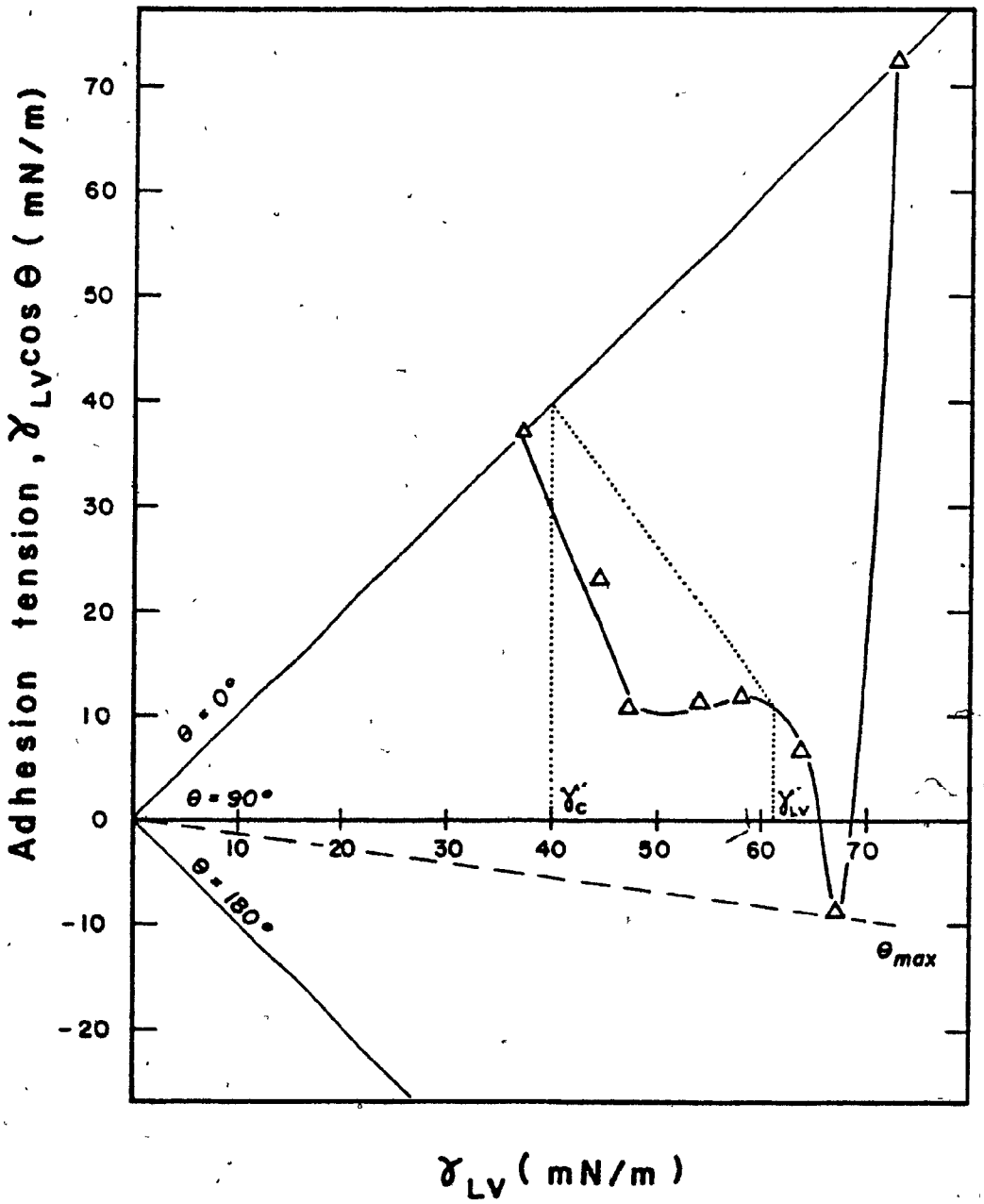


Figure 6.6 Adhesion Tension Diagram for Galena in Aqueous Potassium Decyl-Xanthate Solutions

Table 6.1

The Values of Critical Surface Tension of Wetting and Slopes of Wettability Lines for Xanthates of Various Chain Length Adsorbed on Galena

Alkyl Group of Adsorbed Xanthate	γ_c (mN/m)	β	β'
Methyl -	29.8	+0.26	+0.62
Ethyl -	30.0	+0.09	+0.33
Propyl -	29.0	-0.10	+0.26
Butyl -	26.9	-0.31	+0.07
Pentyl -	26.8	-0.64	-0.64
Hexyl -	27.0	-0.64	-0.64
Decyl -	26.1	-0.84	-1.19

critical surface tension of wetting value for this system occurs at about 37 mN/m.

6.3.3. Flotation Tests

Flotation recoveries of lead methyl, hexyl and dodecyl xanthates are shown as a function of solution surface tension in Figure 6.7. In distilled water, the floatability of lead methyl xanthate is relatively low (~ 30%) as compared to that of the latter two (100%). The recovery of lead methyl xanthate increases to ~ 100% in dilute methanol solutions (i.e. 2% by vol.). The recoveries start to drop when the surface tension is decreased below a certain value for each xanthate studied. For the methyl, hexyl and dodecyl xanthates, these values are 60, 46 and 30 mN/m respectively. In this range, the recoveries decrease almost linearly with a decrease in solution surface tension. The lowest recoveries correspond to the surface tension values between 22.6 and 30 mN/m.

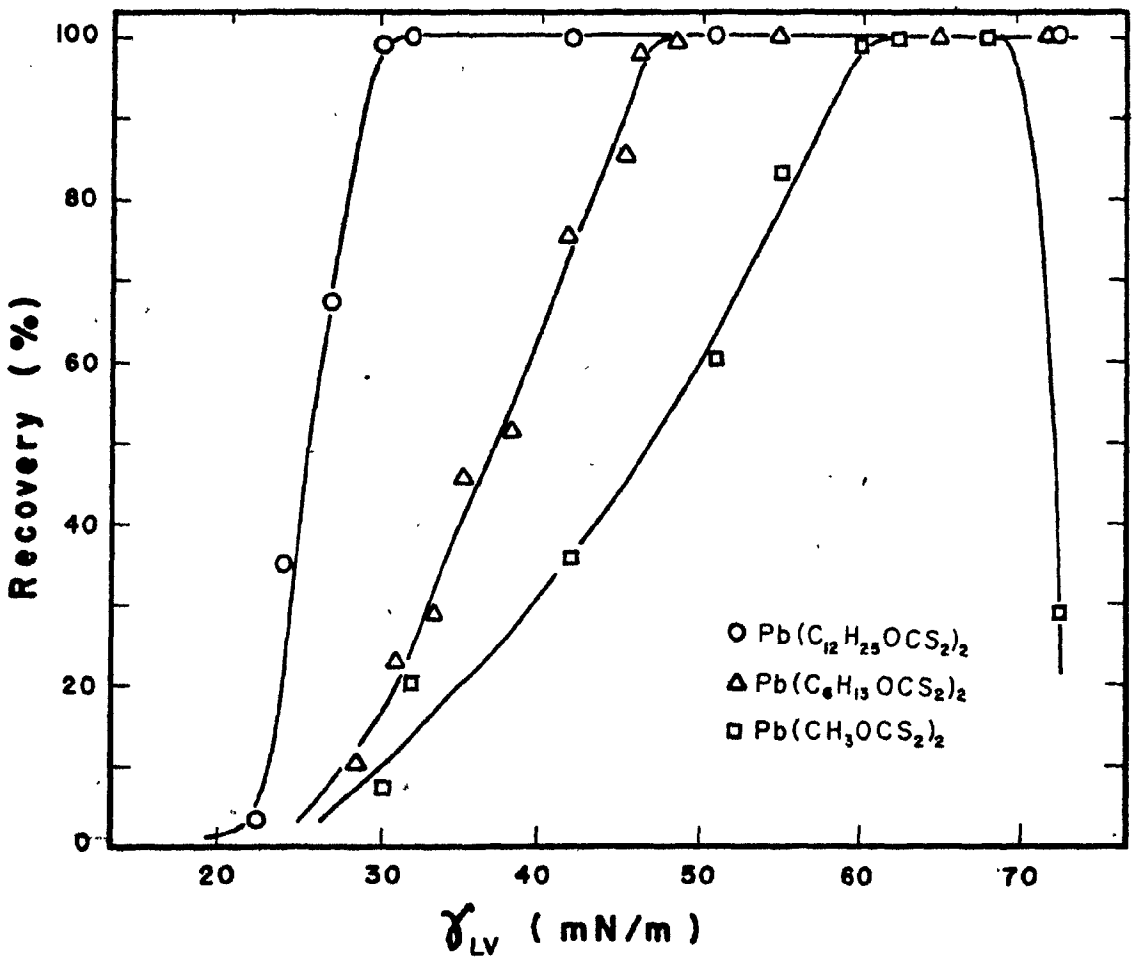


Figure 6.7 Flotation of Bulk Lead Alkyl Xanthates in Methanol Solutions as a Function of Surface Tension

The recoveries obtained for galena pretreated with potassium xanthates of the same alkyl group as those of the bulk xanthates are shown in Figure 6.8. The shape of these recovery curves is similar. However, several differences can be noted. First, the recovery of methyl xanthated galena is not as low as in the case of bulk methyl xanthate. Secondly, the recoveries start to decrease at a much lower surface tension value than observed for the bulk xanthates. For example, in the case of methyl and hexyl xanthates the values of surface tension shift from 60 and 46 to about 43 and 32 mN/m respectively. There is relatively little change for dodecyl xanthate, a shift from 30 to 28 mN/m. This figure shows also the effect of washing the xanthated samples with ether prior to flotation on the recoveries. Similar recoveries are obtained at higher surface tension values when the feed is prewashed with ether. The recovery curves approach each other in the surface tension range 22.5 to 30 mN/m where they exhibit lowest recoveries as in the case of bulk lead xanthates.

6.4 DISCUSSION

6.4.1. Adsorption of Alkyl Xanthates on Galena

The chemical nature of the interaction between galena and xanthates has been known for about 50 years. This was proved conclusively by calorimetric measurements of Mellgren (1966) who showed that the heat of adsorption of xanthate corresponds to the heat of reaction between xanthate and a lead

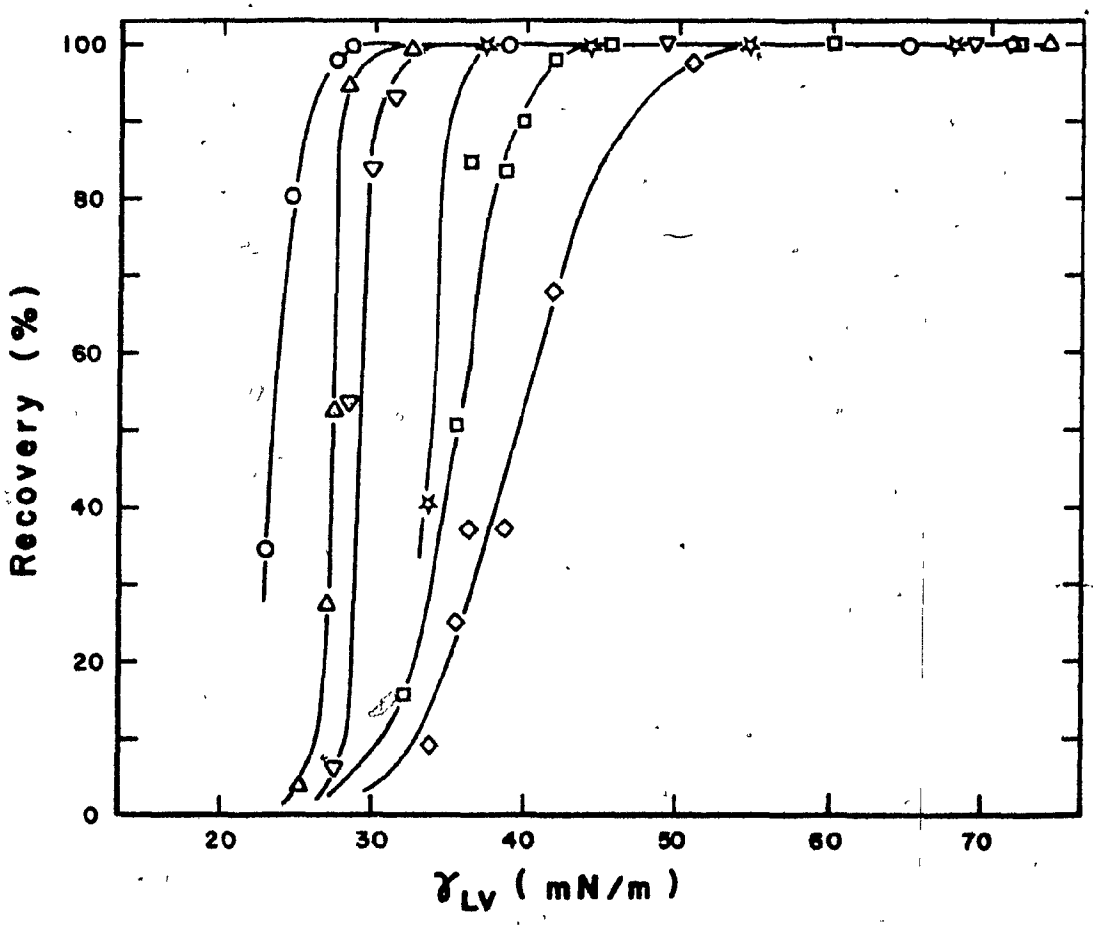


Figure 6.8 Flotation of Xanthated Galena in Methanol Solutions as a Function of Surface Tension

Methyl Xanthated (□ unwashed, ◇ prewashed with ether)
Hexyl Xanthated (△ unwashed, ▽ prewashed with ether)
Dodecyl Xanthated (○)

Decyl Xanthate Solutions (☆)

salt. However, the chemistry of this process and the nature of the interaction products have been a controversial subject over the years. Several mechanisms have been proposed to explain these interactions. The first is the chemical theory of Taggart et al. (1934) which indicates that the reactions rendering the mineral surface hydrophobic are chemical reactions of well recognized types, i.e. the reactions taking place in bulk solution to produce a new phase such as a precipitate. This view was opposed by Wark and Sutherland (1955) who proposed the ion-exchange theory which is shared also by Gaudin (1957). According to this theory, the hydrophobicity is brought about by an ion-adsorption mechanism. Exchange takes place between the xanthate and sulphoxy-ions of the galena surface (oxidation product(s) of sulphide ion). The exchange of sulphide ion itself is thermodynamically unfavorable. The ion-exchange mechanism thus recognizes the active role of oxygen. However, it does not seem to be the only possible mechanism. According to the semiconductor theory of Plaksin and Shafaeev (1963), the adsorption of oxygen converts galena from an n-type (electron-donating) to a p-type semiconductor (electron-accepting) by taking electrons from the valence band, thus creating electron vacancies (holes) which are known as anodic sites. An electron donating ionic species such as xanthate adsorbs on these anodic sites, whereby producing a surface lead xanthate compound ($\overline{Pb}$-SSCOR). The existence of the lead xanthate was shown by Leja et al. (1963) using infrared spectrophotometry and by

Hagihara et al. (1964) using an electron diffraction technique. The former reported the formation of a chemisorbed monolayer of xanthate plus physically adsorbed multilayers of lead xanthate and the latter reported only a monomolecular film of xanthate. The representation of this monomolecular xanthate film on galena is shown in Figure 6.9.

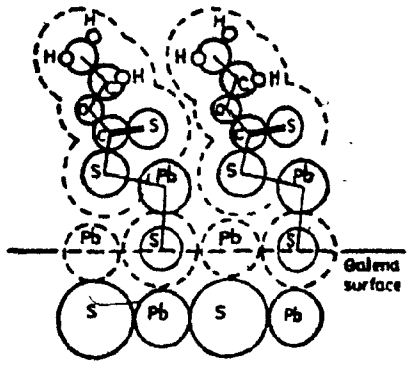


Figure 6.9 Representation of a Chemisorbed Monomolecular Film of Xanthate on Galena

Whether the hydrophobicity is induced by this lead xanthate or a dixanthogen or any other species such as sulphur has been the subject of a number of research papers. Mellgren (1966) reported that lead ethyl xanthate was not floatable. Based on electrochemical studies, Woods (1972) suggested that the hydrophobic layer on the surface is produced by two independent simultaneous chemical processes. The anodic reaction produces dixanthogen, an oxidation product of xanthate, and the cathodic

reaction involves the reduction of oxygen. Later, these conclusions found strong opposition. Natural floatability of heavy metal xanthates was demonstrated by Finkelstein et al. (1975) and Poling (1976) by taking certain experimental precautions. Finkelstein et al. used a flotation feed prepared from recrystalized xanthates, and compacted precipitates in their micro-flotation tests. Poling reached the same conclusion on the basis of vacuum flotation results. The results of the flotation tests obtained in the present study support these conclusions (section 6.5.7).

As demonstrated previously (Leja et al., 1963; Poling, 1963; Poling and Leja, 1963) distinct differences occur between the spectra of dixanthogens and metal xanthates. Therefore, the nature of the adsorption or reaction products on galena treated with xanthates can be deduced from infrared spectra. A comparison of the spectra given in Figures 6.1.3 shows that the bulk lead xanthates and the adsorbed xanthate have similar structures. On the other hand, the spectra of dialkyl dixanthogens are different (see the structural assignments given in section 6.4.1). The results support the findings of Greenler (1962), Poling and Leja (1963) and others reviewed recently by Giesekke (1983). A common conclusion from these studies is that the infrared spectroscopy furnishes evidence for the formation of lead alkyl xanthate and no dialkyl dixanthogen when galena is treated with aqueous solution of potassium alkyl xanthates. There is also electrochemical evidence in favor of the above conclusion. The rest

potential, E_h of a galena electrode in ethyl xanthate solutions containing dissolved oxygen is much lower than the potential required for the formation of diethyl dixanthogen. The findings of Woods (1972) who first suggested the formation of dixanthogen as the hydrophobic species were reviewed critically by Finkelstein and Poling (1977). Based on the results of electrochemical studies carried out by independent researchers, they expressed doubts concerning the validity of Woods' conclusion. Finkelstein and Poling (1977) in their extensive review state:

> *"The controversy regarding the surface product that is responsible for rendering galena floatable when it is treated with xanthate under flotation conditions is now fully resolved. It can be accepted that dixanthogen cannot be formed when galena is treated with solutions of xanthate in the presence of dissolved oxygen, but that lead xanthate or surface modifications of lead xanthate are formed, and that these are fully capable of rendering the surface sufficiently hydrophobic."*

It is important that the adsorbed xanthate coating be free from any physically bound dixanthogen. Otherwise it can act as a source of contamination in the contact angle measurements especially with octane droplets by diffusing into the octane phase and thus changing the oil-water interfacial tension. Finkelstein and Poling (1977) emphasize that dixanthogen present for example by deliberate addition to the galena-xanthate system only chemisorbs after the surface has been covered with surface lead xanthate. Thus, it appears that contamination of the oil-water interface by an oily substance such as dixanthogen is not likely.

6.4.2. Contact Angles

Pioneer work by Wark and his associates on the contact angle measurements has shown that when xanthate is adsorbed on the surface of galena the hydrocarbon groups are oriented. The polar thiocarbonate groups are chemically bound to the surface and the hydrocarbon groups packed closely are disposed outward. With this type of orientation they form a hydrophobic coating on the surface thus acting as a barrier to the hydrophilic forces of the surface. The contact angle obtained on such a surface depends on the length of the hydrocarbon chain. Figure 6.4 shows the dependency of contact angle on the number of carbon atoms of normal xanthates adsorbed on the galena sample studied. For contact angles of air bubbles, a comparison between the measurements by Wark and Cox (1934) and this work shows that up to four carbon atoms in the hydrocarbon chain, there is an excellent agreement between the contact angles. For n-amyl and n-hexyl xanthates a comparison cannot be made since Wark and Cox do not have data points for these xanthates. For n-octyl xanthate, the value of contact angle reported by Sutherland and Wark (1955) seems to be significantly lower than that measured in the present work and surprisingly, it is lower than even the value of contact angle measured for heptyl xanthate reported by Siedler (Sutherland and Wark, 1955). Likely reasons for these discrepancies may be (a) Differences in the bubble sizes; (b) Impurities (e.g. dixanthogen); (c) Failure to recognize the establishment of a maximum

contact angle; and (d) Differences in the surface tension of the liquid phase.

Wark and Cox in their original experiments used air-bubbles of 5 mm. in diameter, about three times as large as those used in the present work. Sutherland and Wark stated that contact angle was independent of the bubble size. However, Leja and Poling (1960) found that the angles were independent of the bubble size in the range 4.5 to about 2.2 mm. in diameter. Contact angles showed some increase for smaller bubbles. Present study shows that the angles observed for methyl to butyl xanthates are the same as those measured by Wark and Cox in spite of the significant difference in the bubble sizes. Hence, the difference in contact angles for long-chained xanthate solutions cannot be attributed to the size effect.

In both studies xanthates were purified prior to making up the solutions and only freshly prepared solutions were used. Therefore, the presence of dixanthogen is not likely unless the potential of the solution is raised deliberately to the level where the production of dixanthogen from xanthate may start.

The technique of contact angle measurement was similar to that used by Wark and Cox. The time allowed for chemisorbtion of xanthate was sufficient for the contact angles to reach a maximum value. The vibration of bubbles attached to the sample by light tapping as suggested by Wark and Cox was found to be effective in bringing the contact angle to an apparent equilibrium value.

The major difference between the experimental procedure of this study and that of previous studies by Wark and Cox, and Siedler (Sutherland and Wark 1955) is the liquid phase in which contact angles were measured. Since the present study deals with the effect of surface tension on the wettability a datum-point was desired at about 72.5 mN/m. Thus, contact angles on xanthated galena were measured after washing the sample repeatedly with distilled water until no xanthate residue remained in the liquid phase. The surface tension value of the distilled water containing the washed sample which had been pretreated with potassium decyl xanthate was verified by measurement. Traditionally, contact angles have been measured in xanthate solutions.

It is generally known that xanthates in common use do not show any significant surface activity at the solution-gas interface. However, in accordance with Traube's rule, the surface tension of xanthate solutions (at equivalent concentration) is expected to decrease as the hydrocarbon chain length increases. Traube's rule states that the surface activity at the solution-gas interface is approximately tripled for each additional methylene group ($-CH_2-$) in the molecule. (section 3.3.1) Therefore, the previously noted discrepancy may be explained by considering the differences in the interfacial tensions. Equilibrium contact angles established in xanthate solution and in distilled water are related to three interfacial tensions by the Young equation:-

$$\text{Cos}\theta^{xs} = \frac{\gamma_{sv}^{xs} - \gamma_{sl}^{xs}}{\gamma_{lv}^{xs}} \qquad 6.2$$

$$\text{Cos}\theta^{dw} = \frac{\gamma_{sv}^{dw} - \gamma_{sl}^{dw}}{\gamma_{lv}^{dw}} \qquad 6.3$$

where the superscripts xs and dw refer to xanthate solution and distilled water respectively. The relations between these interfacial tensions may be written as

$$\gamma_{sv}^{dw} = a \times \gamma_{sv}^{xs} \; ; \; \gamma_{sl}^{xs} = b \times \gamma_{sl}^{dw} \; ; \; \gamma_{lv}^{dw} = c \times \gamma_{lv}^{xs} \qquad 6.4$$

For the galena-xanthate system, in general, $c > b \geq a \geq 1$. Since xanthate is not a volatile substance, the factor a may be assumed to be very close to unity. Similarly, b may be taken as unity when the adsorption of xanthate is limited to a chemisorbed monolayer in xanthate solutions. When additional xanthate molecules may be adsorbed physically on top of this monolayer such that the polar groups of some of the xanthate molecules are oriented toward the bulk solution the factor b is probably more than unity. For short-chained xanthates the factor c may be regarded as unity. However, as the hydrocarbon chain length increases it should increase beyond unity. For the galena surface coated with a long-chained xanthate (assuming that a and b are unity), combining Equations 6.2, 6.3 and 6.4 yield the following:-

$$\frac{\text{Cos}\theta^{dw}}{\text{Cos}\theta^{xs}} = \frac{1}{c} < 1 \qquad 6.5$$

$$\text{Cos}\theta^{xs} > \text{Cos}\theta^{dw} \text{ and } \theta^{xs} < \theta^{dw} \qquad 6.6$$

In the case of short-chained xanthates; $c \cong 1$ and thus $_{\theta}{}^{xs} \cong {}_{\theta}{}^{dw}$.

6.4.3. Adhesion Tensions in Aqueous Methanol Solutions

The use of adhesion tension diagram to express the wettability of low-energy solid surfaces is relatively new. Lucassen-Reynders (1963) appears to be the first researcher to show the advantage of representing the wettability in terms of adhesion tension by combining Young's equation with the Gibbs' equation. This way, the wettability of a low-energy solid surface by aqueous surfactant solutions can be related to the relative adsorption densities of surfactant species at the three interfaces. This approach has been utilized by Somasundaran (1968) to show the relationship between adsorption at different interfaces (i.e. solid-gas, solid-liquid and liquid-gas). The adhesion tensions for the quartz-dodecylammonium acetate system were determined indirectly from the capillary rise of the solutions in glass tubes based on the assumption that the surfaces of glass and quartz behave in a similar manner. Therefore, this approach, not requiring the measurement of contact angles is limited in its application to that particular system.

In the present work, adhesion tension was determined from the contact angle and the surface tension data for the system of xanthated galena-aqueous methanol solutions (Figure 6.5). It was found that the plot of adhesion tension vs. surface tension could not be represented by a single line. At

about 40-42 mN/m there is an apparent change in the slope of the wettability line. The reason for this change is not precisely known. Nevertheless, several relevant points can still be made. It should be noted that this range of surface tensions corresponds to the maximum adsorption density of methanol at the solution-gas interface (see Figure 3.22). As shown by Lucassen-Reynders the slope of the wettability line, β is related to the adsorption densities as follows:-

$$\frac{d(\gamma_{\ell v}\ \mathrm{Cos}\theta)}{d\gamma_{\ell v}} = \beta = \frac{\Gamma_{sv} - \Gamma_{s\ell}}{\Gamma_{\ell v}} \qquad 6.7$$

A linear relationship between adhesion tension and surface tension (i.e. constant slope) is most simply explained by assuming that the relative adsorption densities at three interfaces (i.e. Γ_{sv}, $\Gamma_{s\ell}$ and $\Gamma_{\ell v}$) remain proportional to each other. Therefore, the change of slopes should reflect a required change in the relative adsorption densities. For the slope to increase, the rate of decrease in Γ_{sv} and $\Gamma_{s\ell}$ should be slower than the rate of decrease in $\Gamma_{\ell v}$ and this new proportionality should be maintained for more concentrated solutions. However, due to the absence of adsorption data at the solid-gas and solid-liquid interfaces, the actual relationship between the adsorption densities cannot be obtained to independently check the validity of these statements.

Alternatively, the change in the slope values may have resulted from the dissolution of some chemisorbed xanthate from the surface of galena due to an increase in solvent power of

methanol solutions with concentration. A decrease in the hydrophobicity level of the resulting surface may be responsible for a change in proportionality of the adsorption densities at the three interfaces. This explanation seems to be more reasonable than the preceding one. The adhesion tension variation of such inherently hydrophobic minerals as molybdenite, sulphur and graphite, which contains no dissolvable hydrocarbonaceous surface coating, does not show a change in slope (see Chapter 4). Furthermore, the contact angles measured in distilled water at the end of experiments, which showed considerable hysteresis in some cases, were relatively lower than those at the beginning. The reproducibility of the contact angles measured in distilled water were initially $\pm$ 1.5°. After the experiments had been completed, the methanol solution was transferred from the cell and the sample washed repeatedly with distilled water without any exposure to air. The variation of the contact angles in distilled water has been examined. In general, a poorer reproducibility was observed. For example, in the case of propyl xanthated surface the contact angles measured at six different locations were 64/61, 61/65, 66/67, 57/55, 48/45, 61/50 as compared to the 7 pairs of initial angles in distilled water which remained constant at 67 $\pm$ 1°. This indicates some degree of hydrophobicity loss which should have been due to dissolution of some xanthate from the surface. However, it is important to note that these differences were not observed for every sample for which the variation of contact angles was examined, for example, samples

coated with ethyl and hexyl xanthates (see Appendix VI).

The γ_c values for all xanthate coatings are located between 26 and 30 mN/m (Table 6.1). This range corresponds nearly to the range of the γ_c values obtained for such inherently hydrophobic minerals as molybdenite and sulphur (cleavage or crystal faces). The mechanism of wetting by methanol solution is expected to be similar in both cases (Chapter 4).

In the range of critical surface tension of wetting, the adsorption density of methanol at the xanthated galena-solution interface should be relatively high but probably not as high as that at the solution-gas interface which is closely packed (as indicated by Figure 3.22). At both of these interfaces the -OH groups of methanol molecules are directed towards the solution. The thickness of the wetting film at these interfaces may further increase through the hydrogen bonding between methanol and water molecules. Relatively high bulk viscosities in this particular concentration range support hydrogen bond formation (Chapter 3). The increase in the thickness of the wetting film may also be inferred from the observed increases in induction time with decreasing surface tension during contact angle measurements on molybdenite and graphite surfaces (Chapter 4).

Adsorption and wetting behavior on galena coated with xanthates in aqueous methanol solutions should be viewed as approximating that of paraffin as the hydrocarbon chain length

increases. This is the case indeed; as the hydrocarbon chain length increases the slopes of the wettability line steadily decrease and become similar to the slope of the wettability line for paraffin as indicated by the dashed line with a slope of -1 in Figure 6.5. Conversely, the increase in slopes of the wettability line with a decrease in the hydrocarbon chain length of the xanthates shows an increase in the hydrophilicity level of the surface (i.e. polarity of the xanthated surface).

6.4.4 Polarity Level of Xanthated Galena Surfaces

The degree of polarity of the surfaces can be estimated from the contact angle measurements with octane droplets. The polar component of the surface free energy, γ_s^p of xanthated galena surfaces may be determined using the equation suggested by Bagnall and Green (1979) (Chapter 2). The results (Figure 6.10) show that the polarity of the xanthated galena decreases as the hydrocarbon chain length increases. The decrease is most significant when the naked galena surface is coated with methyl xanthate. For xanthates with longer hydrocarbon chains, there is appreciably less decrease. The polar component approaches zero asymptotically as the number of carbon atoms increases beyond 6. The polar component of zero may be said to represent paraffin wax containing no hydrophilic sites while the polar component of 50.8 mj/m^2 corresponds to a completely hydrophilic surface. Using the polar component scale between 0 to 50.8 mj/m^2, for each xanthate coating a relative hydrophobicity level (by %) may be assigned as done with the

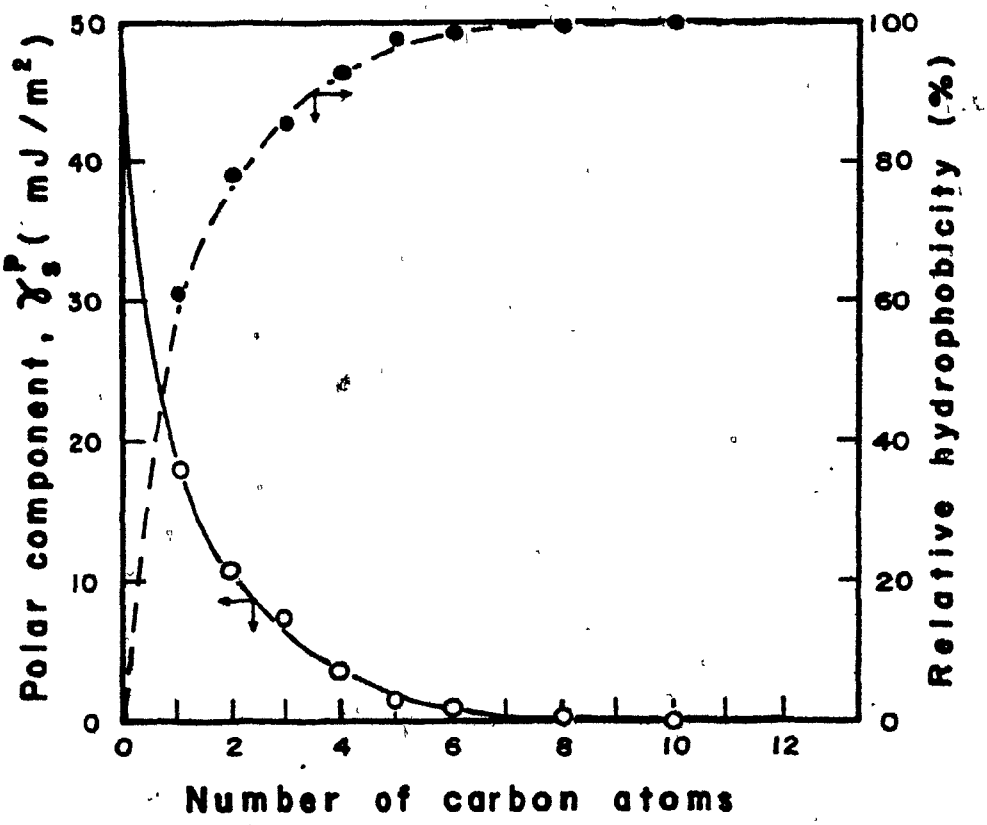


Figure 6.10 Polar Component of the Surface-Free Energy of Xanthated Galena as a Function of the Number of Carbon Atoms in the Hydrocarbon Group

inherently hydrophobic minerals (Chapter 2). This is shown by the dashed line in the same figure. According to this diagram, a polished galena surface (aged at least for 30 minutes) having no hydrophobicity will have about 77% relative hydrophobicity when treated with ethyl xanthate as compared to about 97% when treated with amyl xanthate. Therefore, both the polar components and the slopes of the wettability lines characterize the hydrophobicity level of xanthated galena surfaces. When the polarity change is expressed by $\ell n \gamma_s^p$ with respect to the number of carbon atoms a linear relationship is obtained up to 8 carbon atoms in the hydrocarbon chain of the xanthate (Figure 6.11). The relative hydrophobicity changes may be expressed in a similar fashion.

6.4.5 Adhesion Tensions of Air Bubbles and Octane Droplets in Water

Since contact angle values of air bubbles and octane droplets are available for xanthated galena samples with various hydrophobicity levels depending upon the hydrocarbon chain length, the relationship between these two kinds of contact angles can be examined. When the adhesion tensions of the bubbles and the droplets in distilled water are plotted as a function of the number of carbon atoms, N_c, two straight lines approximately parallel to each other are obtained (Figure 6.12). These lines are mathematically expressed by the following two equations:-

$$\gamma_{AW} \cos\theta_{AW} = -9.83\ N_c + 56.77 \qquad 6.8$$

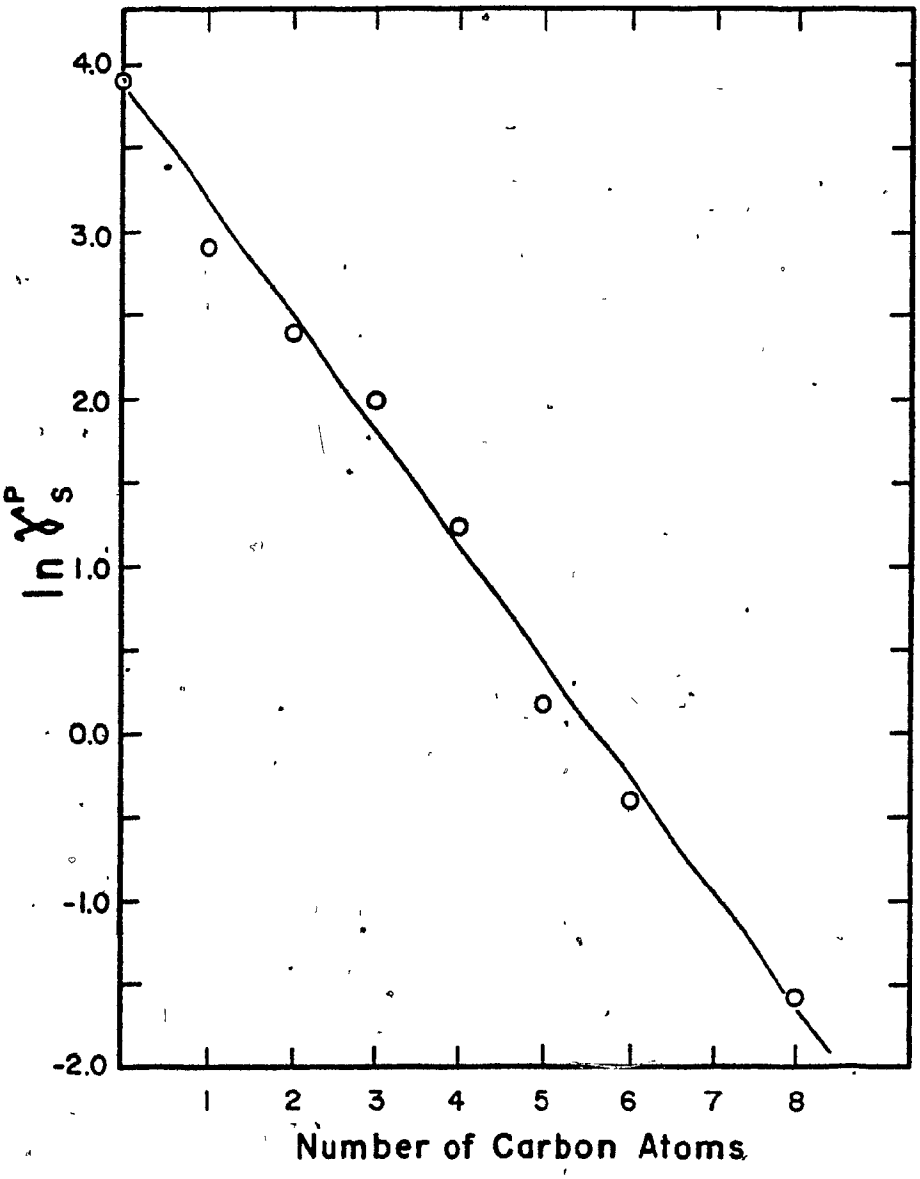


Figure 6.11 The Linear Relationship Between $\ell n\ \gamma_s^P$ and the Number of Carbon Atoms for Xanthated Galena

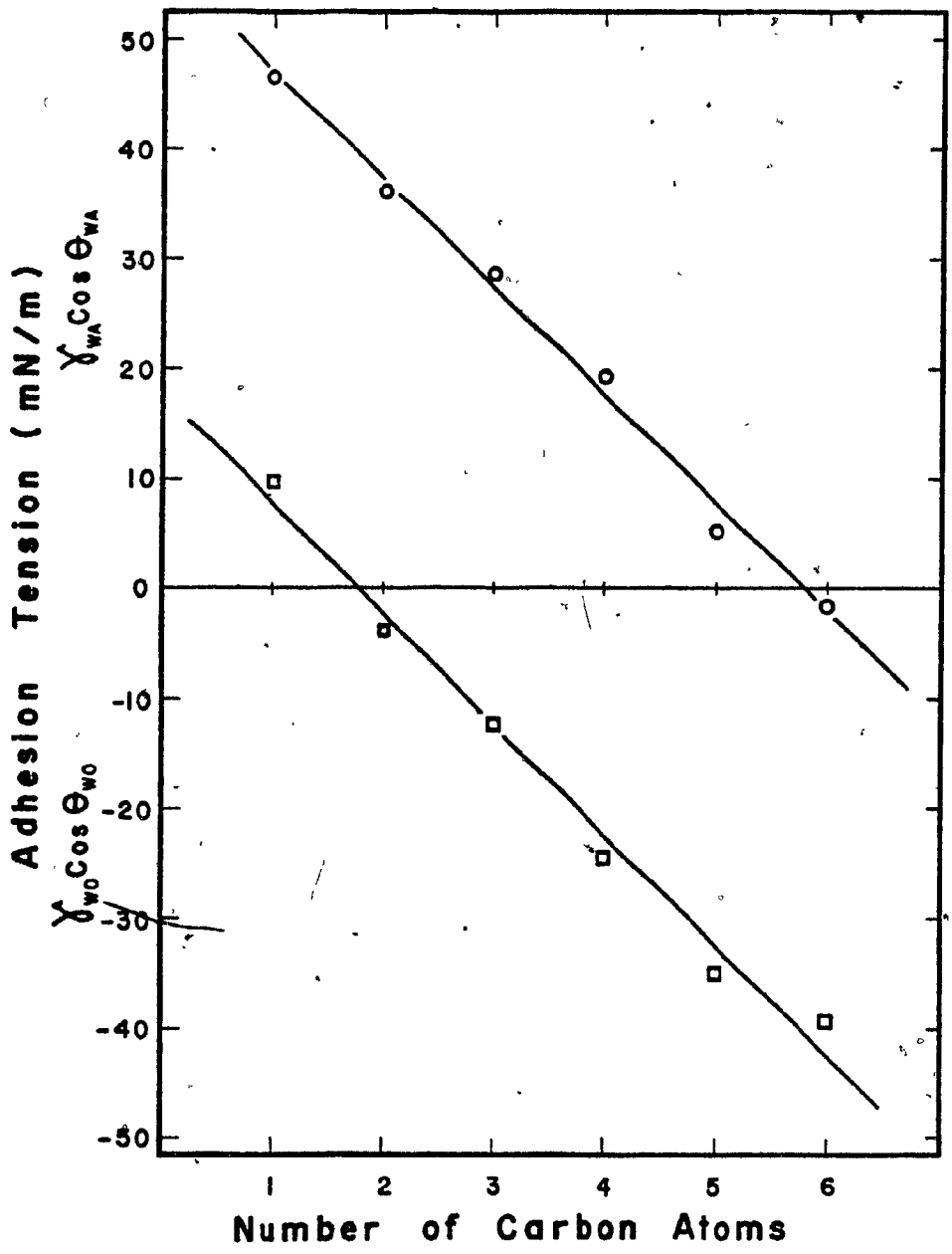


Figure 6.12 Adhesion Tension of Air Bubbles (o) and Octane Droplets (□) for Xanthated Galena in Distilled Water as a Function of the Number of Carbon Atoms

$$\gamma_{OW} \cos \theta_{OW} = -10.05\ N_C + 17.59 \qquad 6.9$$

where θ_{AW} and θ_{OW} are the contact angles of the air bubbles and the octane droplets on xanthated galena surface respectively. It should be noted that the validity of these equations is limited to hydrocarbon chains containing up to 6 carbon atoms. Eliminating of N_C from the equations and using the numerical values of interfacial tensions yields the following equation relating θ_{AW} to θ_{OW}:-

$$\cos\theta_{OW} = 1.462\ \cos\theta_{AW} - 0.797 \qquad 6.10$$

This empirical equation was found to be valid for a number of minerals which possess inherent hydrophobicity. These are listed in Table 6.2. For each mineral there is a good agreement between the observed and calculated contact angles of

Table 6.2

Comparison Between Observed and Predicted Contact Angle of Octane Droplets on Inherently Hydrophobic Minerals in Water. (θ in degrees)

Sample	$\theta_{AW}^{obs.}$	$\theta_{OW}^{pre.}$	$\theta_{OW}^{obs.}$
Sulphur	87	136	135
Molybdenite	80	123	120
Graphite	59	92.5	90
Coal	49	81	78
Orpiment	44	75	75.5
Realgar	42	73	72

octane droplets. This simply shows the common nature of the surface forces that render a surface hydrophobic. Since the measurement of the octane contact angle on a hydrophobic surface is always more laborious than the measurement of contact angles with air-bubbles, such an equation can be useful in predicting the octane contact angle on an unknown hydrophobic surface from which the polar component of surface free energy of that surface may be estimated.

6.4.6 Wettability of the Galena-Decyl Xanthate System

Adhesion tension vs. surface tension relationship of the galena-decyl xanthate system (Figure 6.6) is very different from that obtained with aqueous methanol solutions. This diagram illustrates a double reversal of wetting. Initially in distilled water, the galena surface is completely hydrophilic, giving a zero contact angles, that is, the polished galena sample is a high-surface energy solid in distilled water. It is converted to a low-surface energy solid with the introduction of a small quantity of decyl xanthate reducing solution surface tension to about 67 mN/m. In this stage the surface reaches its maximum hydrophobicity by a first layer of chemisorbed decyl xanthate molecules. Adhesion tension is minimum at this maximum hydrophobicity. With a further decrease in solution surface tension it starts to increase, that is, the solid surface is made relatively less hydrophobic in more concentrated decyl xanthate solutions. In accordance with the concept of critical surface tension of wetting, this can be attributed to an increase in the wetting power of the

solution with a decrease in its surface tension. In this stage additional xanthates are adsorbed physically on top of the chemisorbed monolayer with their polar groups directed towards the bulk solution. As the surface tension continues to decrease with increasing decyl xanthate concentration, the density of these polar groups at the galena surface also increases. Thus, the wettability of the surface increases. For solution surface tensions $\leq \gamma_c$ (37 mN/m), the surface becomes completely wetted. In other words, it behaves like a high-surface energy solid again, relative to the solution surface tension.

This diagram illustrates the danger of using excessive amounts of xanthate (especially with a long hydrocarbon chain). It will not only be wasted but will also be detrimental to the flotation of the sulphide mineral involved. Flotation rate should increase as the difference between the operating surface tension of flotation medium and the critical surface tension of wetting of the mineral being floated increases. For example, performing flotation at $\gamma'_{\ell v} \approx$ 60 mN/m (or higher) is both theoretically and economically more desirable than at a lower surface tension value, say $\gamma''_{\ell v} \approx$ 50 mN/m since the difference $\gamma'_{\ell v} - \gamma'_c$ will be relatively larger.

6.4.7 Flotation Tests

The shape of the flotation curves of bulk lead alkyl xanthates and xanthated galena sample is similar to that of the inherently hydrophobic minerals (Chapter 4): There is a range of solution surface tension for each sample above which the

sample is 100 per cent floatable and below which it remains non-floatable. Apparently, the size of this critical range is related to the hydrophobicity and heterogeneity of the sample: The wider the range is the less hydrophobic and more heterogeneous the sample. In the case of lead methyl xanthate which has the least relative hydrophobicity, the critical range is the largest (i.e. 60-25 mN/m). For the more hydrophobic lead hexyl and lead dodecyl xanthates, the critical ranges are comparatively narrower (i.e. 47-25 and 30-22.5 mN/m respectively).

The hydrophobicity of lead methyl xanthate is so low that in distilled water the flotation recovery does not exceed 30% (by wt.). However, as the surface tension is decreased by introducing some methanol ~ 2% (by vol.) the recovery increase is to 100%. This behavior was observed also for some inherently hydrophobic minerals (e.g. molybdenite). A similar explanation given earlier (Chapter 4) should apply: In distilled water collision probability between particles and bubbles will be low since the number of bubbles is relatively small. Also the probability of attachment will be low due to violent hydrodynamic conditions generated by these bubbles which have a large size distribution (Chapter 3). In dilute methanol solutions (e.g. 1-2% by vol.), however, due to the production of a great number of small bubbles with a narrow size range the conditions are more favorable for high probability of the bubble-particle collisions and attachment. Aside from this, in dilute methanol solutions the induction time is expected to decrease. This

should increase the rate of flotation of lead methyl xanthate particles. As the surface tension is further decreased, critical surface tension of wetting for some particles is approached so that they are not floatable at this reduced surface tension (i.e. $\gamma_{\ell_v} \leq \gamma_{cf}$). Therefore, the recoveries start to decrease at a surface tension specific to each hydrophobic sample. These surface tensions constitute the upper limit of critical range for each sample. Lower limit of the critical range is observed between 30 to 23 mN/m where minimum recoveries are obtained. This range is nearly the same as the critical surface tension of wetting (Figure 6.5). That is, the results of wettability and floatability tests are in good agreement. It should be noted that the samples used in these tests are prepared in radically different fashions. The wettability tests were performed on a polished galena sample having a chemisorbed xanthate. Thus, the surface is homogeneously coated having a certain degree of hydrophobicity depending upon the hydrocarbon chain length. The particles of bulk lead xanthates faced the following operations during their preparation:-

(a) Pressing of the precipitates to obtain a dense, compacted mass

(b) Crushing, grinding and screening

(c) Washing of the particles with ether prior to flotation.

Each of these operations is expected to reduce the hydrophobicity of the particles: Pressing, crushing and grinding will cause the rupture of some covalent bonds. Later, the particle

surfaces will be oxidized at or near these broken bonds. Thus, hydrophilic sites will be produced. The particles will become more heterogeneous. Washing with ether will not only remove any oxidation by-product that may be hydrophobic in nature (e.g. dixanthogen) but also dissolve some of the surface xanthate on the particles. This will further decrease the density of hydrophobic sites on the particle surface. The particles in the flotation tests will have a range of wettabilities depending upon the density of hydrophobic sites at their surfaces. A single γ_c value determined by wettability test, therefore, represents only the least wettable particles in the flotation feed,not all the flotation feed. The critical range is widest in the case of the least hydrophobic sample. Lead methyl xanthate having only the methyl groups at the surface will presumably have the least resistance to surface alterations towards a lower hydrophobicity and more heterogeneity. As the hydrocarbon nature of the solid increases, the production of hydrophilic sites will relatively be more difficult. This may explain the continuously narrower range of surface tension of floatabilities observed for lead xanthates as the hydrocarbon chain length increases in order from methyl to hexyl and dodecyl.

In the case of xanthated galena particles, the critical surface tension range of floatabilities is comparatively narrower (Figure 6.8). For example, for galena pre-treated with hexyl xanthate, the γ_{cmf} value is about 30 mN/m as compared with 47 mN/m for compacted bulk lead hexyl xanthate

while the γ_{clf} values for both are the same. This may be explained by the same reasoning as applied previously: Galena particles were ground and sized and then treated with xanthate. The xanthated flotation feed was not subjected to any operation that would create hydrophilic sites. Consequently, the galena particles should have had relatively more homogeneous hydrophobic coating at their surfaces. Therefore, most of the particles are affected by the wetting action of aqueous solutions over a relatively narrow range of surface tension.

The washing of the xanthated particles with ether prior to flotation apparently reduced their hydrophobicity level. This resulted in a shift of the floatability curves towards higher surface tension values.

A comparison between the flotation behavior (Figure 6.8) and wettability (Figure 6.6) of galena coated with decyl xanthate shows that at the γ_c value ($\sim$ 37 mN/m) the recovery of galena is 100%. This is in sharp contradiction with the behavior of xanthated galena samples in methanol solutions where the recoveries are minimum in the vicinity of the γ_c value established in methanol solutions. This may be related to a difference in the time-dependent decrease in solution surface tension. Short-chain alcohols establish the solution surface tension equilibrium in the order of a few milliseconds (Addison, 1945; Addison and Elliott, 1949). Therefore, in the case of methanol solutions bubble surface tension both in contact angle and flotation tests is expected to be very close in value (for

the same composition). However, in the case of decyl xanthate with a hydrocarbon chain of 10 carbon atoms, the establishment of solution surface tension equilibrium will take a longer time. A previous research in this laboratory (Finch and Smith, 1972) demonstrated the time-dependent decrease in surface tension of alkaline solutions of dodecylammonium acetate (with a hydrocarbon chain of 12 carbon atoms). The time scale in the contact angle measurements is usually long enough for the surface tensions to decrease to an equilibrium value (or nearly so) while the time scale in the flotation process is not. This implies that a 100% recovery with decyl xanthate solutions may have been obtained not at a surface tension value of 37 mN/m but at a relatively higher value.

6.5 REFERENCES

Addison, C.C., (1945). The Properties of Freshly Formed Surfaces, part IV: The Influence of Chain Length and Structure on the Static and Dynamic Surface Tensions of Aqueous-Alcoholic Solutions. J. Chem. Soc., pp. 98-106.

Adolison, C.C. and Elliott, T.A., (1949). The Properties of Freshly Formed Surfaces, part X: A New Contracting Liquid-Jet Technique for the Study of Soluble Films at Small Surface Ages. J. Chem. Soc., pp. 2789-2805.

Bagnall, R.D. and Green, G.F., (1979). Some Observations on Octane Contact Angles in Aqueous Media. J. Coll. Interface Sci., vol. 67, No. 2, pp. 387-388.

Finch, J.A. and Smith, G.W., (1972). Dynamic Surface Tension of Alkaline Dodecylamine Acetate Solutions in Oxide Flotation. Trans. Inst. Min. Metall., vol. 81, pp. 6213-218.

Finch, J.A. and Smith, G.W., (1975). Bubble-Solid Attachment as a Function of Bubble Surface Tension, Can. Metall. Quart., vol. 14, No. 1, pp. 45-51.

Finch, J.A. and Smith, G.W., (1979). Contact Angles and Wetting. Minerals Sci. Engng., vol. 11, No. 1, pp. 36-63.

Finkelstein, N.P., Allison, S.A., Lovell, V.M. and Stewart, B.V., (1975). Natural and Induced Hydrophobicity in Sulfide Mineral Systems. Amer. Ins. Chem. Eng. Symp. Ser., vol. 71, No. 150, pp. 165-175.

Finkelstein, N.P. and Poling, G.W., (1977). The Role of Dithiolates in the Flotation of Sulphide Minerals. Minerals Sci. Engng., vol. 9, No. 4, pp. 177-197.

Gaudin , A.M., (1957). Flotation. 2nd Ed. McGraw Hill Book Co. Inc., New York, p. 573.

Giesekke, E.W., (1983). A Review of Spectroscopic Techniques Applied to the Study of Interactions Between Minerals and Reagents in Flotation Systems. Intern. J. Miner. Process., vol. 11, pp. 19-56.

Goold, L.A. and Finkelstein, N.A., (1969). An Infrared Investigation of the Potassium Alkyl Xanthate and Alkyl Trimethyl Ammonium Bromide Mixed-Collector System, Randburg, NIM report: 498, p. 18.

Greenler, R.G., (1962). An Infrared Investigation of Xanthate Adsorption by Lead Sulfide. J. Phys. Chem., vol. 66, pp. 879-883.

Hagihára, H. and Sakurai, T., (1967). Proc. 4th Int. Congr. on Surface Activity Substances, vol. 3, Gordon and Breach, New York, p. 361.

Hornsby, D.T. and Leja, J., (1980). Critical Surface Tension and the Selective Separation of Inherently Hydrophobic Solids. Colloids and Surfaces, vol. 1, pp. 425-429.

Kendall, D.N., (1966). Applied Infrared Spectroscopy, Reinhold Publishing Co., New York, pp.

Leja, J., Little, L.H. and Poling, G.W., (1963). Xanthate Adsorption Studies Using Infra-red Spectroscopy. Trans. Inst. Min. Metall., vol. 72, pp. 407-423.

Leja, J. and Poling, G.W., (1960). On the Interpretation of Contact Angle. Proc. Intern. Miner. Process. Congr., London, Inst. Min. Metall., pp. 325-341.

Lucassen-Reynders, A.H., (1963). Contact Angles and Adsorption on Solids, J. Phys. Chem., vol. 67, pp. 969-972.

Mellgren, O., (1966). Heat of Adsorption and Surface Reaction of Potassium Ethyl Xanthate on Galena. Trans. AIME., vol. 235, pp. 46-60.

Parekh, B.K. and Aplan, F.F., (1974). Wetting Properties of Minerals Coated with Surfactants, Proc. Chem. Inst. Canada, Flocculation and Dispersion Symp., Toronto, pp. 21-35.

Partridge, A.C. and Smith, G.W., (1971). Small-Sample Flotation Testing: a New Cell, Trans. Inst. Min. Metall., vol. 80, pp. C199-200.

Plaksin, I.N. and Shafaeev, R.Sh., (1963). Influence of Surfave Properties of Sulphide Minerals on Adsorption of Flotation Reagents. Trans. Inst. Min. Metall., vol. 72, p. 715.

Poling, G.W., (1963). Infrared Studies of Adsorbed Xanthates. Ph.D. Thesis, University of Alberta, Edmonton.

Poling, G.W., (1976). Reactions Between Thiol Reagents and Sulphide Minerals. Flotation, A.M. Gaudin Memorial Volumes, M.C. Fuerstenau (Ed.), Trans. AIME, vol. 2, pp. 334-363.

Poling, G.W. and Leja. J., (1963). Infrared Study of Xanthate Adsorption on Vacuum Deposited Films of Lead Sulphide and Metallic Copper Under Conditions of Controlled Oxidation, J. Phys. Chem., vol. 67, pp. 2121-6.

Rao, S.R., (1971). Xanthates and Related Compounds, New York, Marcel Dekker, p. 504.

Somasundaran, P., (1968). The Relationship Between Adsorption at Different Interfaces and Flotation Behavior, Trans. AIME, vol. 241, pp. 105-108.

Sutherland, K.L. and Wark, I.W., (1955). Principles of Flotation, Australasian Inst. Min. Metall., Melbourne, p. 489.

Taggart, A.F., del Giudice, G.R.M. and Ziehl, O.A., (1934). The Case for the Chemical Theory of Flotation, Trans. AIME, vol. 112, pp. 348-381.

Taggart, A.F., Taylor, T.C. and Ince, C.R., (1930). Experiments with Flotation Reagents, Trans. AIME, vol. 87, pp. 285-386.

Wark, I.W. and Cox, A.B., (1934). Principles of Flotation I. An Experimental Study of the Effect of Xanthates on Contact Angles at Mineral Surfaces, Trans. AIME, vol. 112, pp. 184-244.

Woods, R., (1972). Electrochemistry of Sulphide Flotation, Proc. Australas. Inst. Min. Metall., vol. 241, pp. 53-61.

CHAPTER 7

CONCLUSIONS, CLAIMS TO ORIGINAL RESEARCH AND SUGGESTIONS FOR FURTHER WORK

7.1 CONCLUSIONS

7.1.1. Fundamental Surface Properties of Minerals Studied

7.1.1.1. Layer-Type Minerals

a) Contact angle, electrokinetic properties and natural flotation behaviour of the layer-type inherently hydrophobic minerals have been determined. A correlation has been found between these pH-dependent properties. Previous attempts to correlate contact angles with zeta potentials or flotation recoveries were unsuccessful due to the low hydrophilic-to-hydrophobic ratios of the samples used. As this ratio increases beyond 1 the correlation becomes more apparent.

7.1.1.2. Sulphide Minerals

a) Surface properties and flotation response of common sulphides such as chalcopyrite and galena depend critically on the experimental conditions such as sample preparation, aging in the air or in solution, and various pretreatments.

b) Chalcopyrite sample used has an IEP at pH ≈ 2.1 which is the same as the IEP value of elemental sulphur. The IEP

value of freshly ground (wet) galena is located between pH=6 and pH=8. Oxidation tends to decrease both the IEP value and the magnitude of the zeta potentials.

c) Some specimens of chalcopyrite, galena and chalcocite freshly prepared, avoiding long periods of polishing and washing rigourously with distilled water immediately prior to tests gave finite contact angles which were persistent and pH-dependent. At low pH of 2.3 the induction period decreased appreciably and an increase in the magnitude of the angles was noted.

d) Chalcopyrite and galena have been found to float in the absence of flotation reagents. Washing the freshly ground samples rigourously with distilled water immediately prior to tests is very effective increasing the recovery. The pre-washing is thought to increase the hydrophobic-to-hydrophilic ratio of the particles by decreasing the concentration of soluble hydrophilic surface species on the surface.

e) The preceding two conclusions support the natural floatability of common sulphides. The presence of elemental sulphur on chalcopyrite, galena and realgar has been established. The question whether or not the observed floatability is due totally to the liberation of elemental sulphur on these sulphides, however, remains uncertain.

7.1.1.3. Polar Characteristics

a) The degree of polarity of the inherently hydrophobic minerals can be characterized by the polar component of the surface free energy (γ_s^P) determined from contact angles of octane. γ_s^P appears to be a more practical parameter than γ_c since it involves only one contact angle determination. The average γ_s^P value for crystal face of sulphur is very low (i.e. 1.1 mj/m^2). Common sulphides such as chalcopyrite and galena have very large γ_s^P values (i.e. 42.5 to 50.8 mj/m^2). Liberation of sulphur on common sulphides should lower their γ_s^P values.

7.1.1.4. Critical Surface Tension of Wetting

a) Of the ten minerals studied eight have γ_c values (determined by Zisman's method) ranging from ~ 40 to 46 mN/m. The γ_c value of graphite found by Parekh and Aplan has been confirmed. Galena has the lowest γ_c value of 31 mN/m. The other exception is molybdenite with a γ_c value of ~ 50 mN/m. The value of the slope b varies from 0.57×10^{-2} for talc to 4.65×1010^{-2} for molybdenite.

b) The significance of the Zisman parameters in flotation studies is doubtful. γ_c and b values are difficult to relate to the flotation behaviour of minerals as they do not actually represent the wetting behaviour of an aqueous solution (i.e. flotation medium).

7.1.1.5. Surface Pressures

a) Surface pressure of water vapour (π^v) on a coal and two samples of molybdenite has been determined from literature adsorption data. Using π^v = 14 mN/m, the dispersion component of the surface-free energy of molybdenite (γ_s^d) has been found to be 113 mj/m^2 as compared to 109 mj/m^2, the value reported by Fowkes for graphite.

7.1.2. Methanol-Water System

a) Surface tension of aqueous methanol solutions determined using the du Noüy ring method can be represented by Szyszkowski's equation accurately not only for dilute solutions but also concentrated ones up to about 30% (by vol.).

b) Relative adsorption density of methanol at the aqueous solution-gas interface reaches a maximum value when the methanol concentration of the solutions is 40-48% (by vol.). At maximum adsorption density, methanol molecules form a monomolecular adsorption film at the interface, the area per molecule adsorbed being about 0.24 nm^2.

c) The bulk viscosity and the heat of mixing values of aqueous methanol solutions show typical maxima for solution composition at which the relative adsorption density of methanol at the solution-gas interface is maximum.

d) The diameter of the air bubbles produced in distilled water varies in a wide range from 0.1 to about 4.2 mm. Large

bubbles disappear with small additions of methanol. The most frequent bubble size class of 0.4-0.6 mm is predominant in all solutions in the range of 1 to 72% methanol (by vol.).

7.1.3. Critical Surface Tension of Wetting and of Floatability

a) γ_c and β values of a number of inherently hydrophobic minerals determined in aqueous methanol solution are much lower than those determined using Zisman's method (see Conclusion 7.1.1.4). γ_c values of strongly hydrophobic minerals are close to 30 mN/m. For less hydrophobic disc samples of polished specimens γ_c and β values are greater.

b) The floatability of inherently hydrophobic minerals have been investigated using aqueous methanol solutions of various surface tension. For an inherently hydrophobic mineral there exists a certain range of surface tension below which the mineral remains non-floatable and above which it is almost 100 per cent floatable.

c) Upper and lower limits of the critical surface tension range may be estimated from an adhesion tension versus surface tension diagram. The particles with well preserved cleavage or crystal faces determine the lower limit, $\gamma_{c\ell f}$ and those with some threshold degree of ionic character determine the upper limit, γ_{cmf}.

7.1.4. Selective Flotation

a) Inherently floatable solids can efficiently be separated from each other by controlling the solution surface tension. The mechanism of separation may be explained in terms of the critical surface tension of wetting and of floatability.

b) Quadratic equations are found to be sufficient to express most of the critical range of floatability as a function of surface tension of methanol solution. These equations can be used to predict the surface tension value at which maximum separation efficiency can be achieved for two inherently hydrophobic solids whose $\gamma_{c\ell f}$ values are very close.

c) Talc can be separated from molybdenite by flotation using sodium lignosulphonate which acts as a selective wetting agent for molybdenite. Selectivity can be identified from their adhesion tension diagrams and zeta coefficients in neutral solution.

7.1.5. Induction Periods

a) Induction periods were estimated for molybdenite, talc, sulphur and graphite using Sutherland's equation and the recent model proposed by Dobby and Finch. Induction periods obtained from Sutherland's equation appear to account for the selective flotation of these minerals from one another.

7.1.6. Kinetics of Flotation

a) Flotation rate in aqueous methanol solutions is best

described by a first order rate equation. The dependence of the flotation rate constant on the solution surface tension can be described by the following empirical equation:-

$$\ell n\ K = a\ \gamma_{\ell v} - b$$

where K is the first order rate constant, $\gamma_{\ell v}$ is the surface tension within the critical surface tension range, and a and b are the empirical constants.

7.1.7. Presence of Elemental Sulphur on Sulphide Minerals

a) Freshly ground chalcopyrite, galena and realgar have shown various quantities of liberated sulphur on their surfaces. The pretreatment of the galena sample with acidified ammonium chloride or neutral saturated sodium chloride solution rendered the mineral readily floatable. As shown by the UV analysis, the pretreated galena samples contain large concentration of elemental sulphur (6.5-9 equivalent monolayers) on their surfaces.

7.1.8. Correlation Between Sulphur Content and Flotation Rate

a) The concentration of liberated sulphur of chalcopyrite and galena can be correlated with the flotation rate of the samples within the critical surface tension range. The larger the concentration of surface sulphur, the faster the sample floats.

7.1.9. Behaviour of Xanthated Galena

a) Both γ_c and β values decrease for xanthated galena in aqueous

methanol solutions as the hydrocarbon chain length increases (from methyl to decyl). The decrease is much more pronounced in the case of the latter than the former. The greater the slope β the less non-polar the xanthate coating on galena (the greater the γ_s^p).

b) As in the case of strongly hydrophobic minerals, minimum recoveries are obtained in the vicinity of the critical surface tension of wetting values (i.e. 26-30 mN/m). Increasingly higher solution surface tension values are required for the floatability of particles as the chain length of xanthate decreases.

c) The relationship between the contact angles of air bubbles (θ_{AW}) and octane droplets (θ_{OW}) may be described by the following empirical equation

$$\text{Cos } \theta_{OW} = 1.462\ \theta_{AW} - 0.797$$

7.2. CLAIMS TO ORIGINAL RESEARCH

a) A correlation between the contact angle, zeta potential and flotation behaviour of various inherently floatable minerals has been demonstrated using a new sample preparation technique for contact angle measurements developed in the present study.

b) Elemental sulphur obtained from galena and a lead/zinc ore has been used in the electrokinetic study.

c) The effect of various pretreatments on the electrokinetic properties of galena has been determined.

d) The pH dependence of the natural floatability of chalcopyrite and galena has been determined.

e) An experimental evidence supporting the natural floatability of chalcopyrite, galena and chalcocite has been obtained using the captive bubble contact angle method.

f) The hydrophilic-to-hydrophobic ratios of the naturally floatable minerals have been estimated using Cassie's equation.

g) Polar characteristics of the minerals have been evaluated from the so-called polar component of their surface-free energy estimated using the octane contact angles measured.

h) Zisman method has been extended to determine the critical surface tension of wetting, γ_c of a number of minerals that show or that are claimed to show natural floatability.

i) Surface pressure of water vapour on coal and molybdenite has been determined from the literature adsorption data, from which the dispersion component of the surface-free energy, γ_s^d of molybdenite has been estimated to be 113 mj/m^2.

j) Relative adsorption density (or surface excess) of methanol and the surface deficiency of water at the solution-gas

interface have been determined according to conventions by Gibbs, and Guggenheim and Adam.

k) Bubble size distribution in aqueous methanol solutions has been photographically determined as a function of methanol concentration (or bubble surface tension) using a specially constructed cell.

ℓ) The number of air bubbles produced in aqueous methanol solutions has been shown to be related to the surface excess of methanol or surface deficiency of water at the solution-gas interface.

m) A correlation has been noted between the bulk viscosity of the aqueous methanol solutions and the adsorption density of methanol, and the heat of mixing of methanol with water.

n) The wettability bands for sulphur and molybdenite in aqueous methanol solutions have been determined using specially prepared samples (i.e. crystal faces and disc samples).

o) Mechanism of wetting and a maximum limiting value of ~ 30 mN/m for γ_c of a number of inherently hydrophobic solids in aqueous solutions of short-chained alcohols have been explained.

p) Extensive use of the adhesion tension diagrams has been made to determine the critical surface tension range within which preferential wetting occurs between the inherently hydrophobic minerals.

q) The relation between the slope of the wettability line and the polar character of the minerals has been shown.

r) Selective flotation of inherently hydrophobic minerals in aqueous methanol solutions has been achieved. The efficiency of the process has been evaluated using the separation efficiency of Schulz.

s) The surface chemistry of the selective flotation of talc from molybdenite using sodium lignosulphonate has been investigated.

t) Induction periods have been estimated from Sutherland's euqation and a recent model by Dobby and Finch. They show a value of 32 ± 4 ms in the vicinity of the surface tension of least floatability.

u) The flotation rates of chalcopyrite and galena obtained using aqueous methanol solutions of various surface tension have been correlated with the quantity of liberated sulphur on the surfaces of these minerals.

v) The wettability and floatability of galena pretreated with xanthates of increasing hydrocarbon chain (from methyl to decyl) have been investigated as a function of solution surface tension.

w) An empirical relation between the contact angles of air bubbles and octane droplets on a hydrophobic solid has been found.

7.3 SUGGESTIONS FOR FURTHER WORK

a) Wettability tests may be conducted using mineral powders. Both receding and advancing contact angles may be determined as a function of solution surface tension to obtain wettability lines for each type. In such a study, the effect of variables such as pH, particle size and oxidation on the wettability and floatability within the critical surface tension range may also be evaluated.

b) Surfactants with long hydrocarbon chain length may be tested similar to the use of methanol. Since their surface activity is expected to be much greater than methanol, lower concentration range may be sufficient to find selective wettability regions for possible separation of inherently hydrophobic solids. The mixtures of surfactants may also be tested.

c) The effect of various reagents (e.g. depressants) on inherently hydrophobic minerals such as molybdenite, graphite and coal may be evaluated using adhesion tension diagrams. This may help these reagents be classified according to the γ_c and β values obtained.

d) Conditions leading to elemental sulphur formation on sulphide minerals may be investigated.

f) Problems associated with detection of elemental sulphur in an organic leach solution (e.g. acetone) have created some confusion about its existence on sulphide minerals. This matter may be investigated systematically by incorporating in a study various allotropic forms of sulphur, poly-sulphides and solvents.

APPENDIX I

Analysis of Mineral Samples and Calibration Curves

Talc (Quebec)

Ignition Loss:

One gram samples of talc (-80x270 mesh) were dried at 115°C and ignited in porcelain crucibles at 900°C.

Table A.I.1

Results of Ignition Tests

Before Ignition wt. g.	After Ignition wt. g.	Ignition Loss %(wt.)
1.0305	0.9803	4.9
1.0410	0.9901	4.9
1.0680	1.0129	5.1
1.0587	1.0061	5.0
1.0554	1.0015	5.1

Average per cent ignition loss is 5.0 ± 0.2, roughly 0.2% greater than the expected value of 4.8% (Mchardy, 1972).

Acid Leaching Loss:

One gram samples were boiled in conctrated by hydrochloric and nitric acids.

Table A.I.2

Results of Acid-Leaching Tests

Before Leaching wt. g.	After Leaching wt. g.	Acid Soluble Matter, %(wt.)
1.0431	1.0058	3.5
1.0302	1.9959	3.3
1.0510	1.0102	3.9
1.0373	1.0004	3.6

Average per cent soluble matter is 3.6 ± 0.3%.

Sulphide Minerals

The samples of sulphide minerals were assayed for their metal content using an atomic absorption spectrophotometer (a.a.s) (Model 357, Inst. Lab. Inc.). In general, the methods outlined by Donaldson (1973) were employed for the dissolution of the samples (in duplicates).

For each metal to be assayed, a series of standard solutions were prepared by dilution with distilled water of the 1000 ppm reference solution (Fisher Sci. Co.). The absorbance readings obtained under the specified conditions of the a.a.s. (Table A.I.3) were used for the construction of calibration curves given in Figures A.I.1 to A.I.3.

Table A.I.3

Operating Conditions of the Atomic Absorption Spectrophotometer

Metal Assayed	Wavelength (nm)	Current (mA)	Bandpass (nm)	Cathode Lamp (Company)	Flame gases
As	193.7	4	1	Visimax	Air/C_2H_2
Cu	324.7	10	1	Westinghouse	Air/C_2H_2
Fe	248.3	10	0.3	Westinghouse	Air/C_2H_2
Mo	313.3	12	0.5	Corning	NO_2/C_2H_2
Ph	217.0	5	1	Corning	Air/C_2H_2
Sb	217.6	7	1	Cathodeon	Air/C_2H_2

References

Donaldson, E.M. (Compiler) (1973). "Methods for the Analysis of Ores, Rock and Related Materials" Mines Branch Monograph 881, Ottawa.

McHardy, J.C. (1972). Surface Chemistry of Talc Flotation. M.Sc. Thesis, Dept Min. Metall. Eng., McGill University, Montreal.

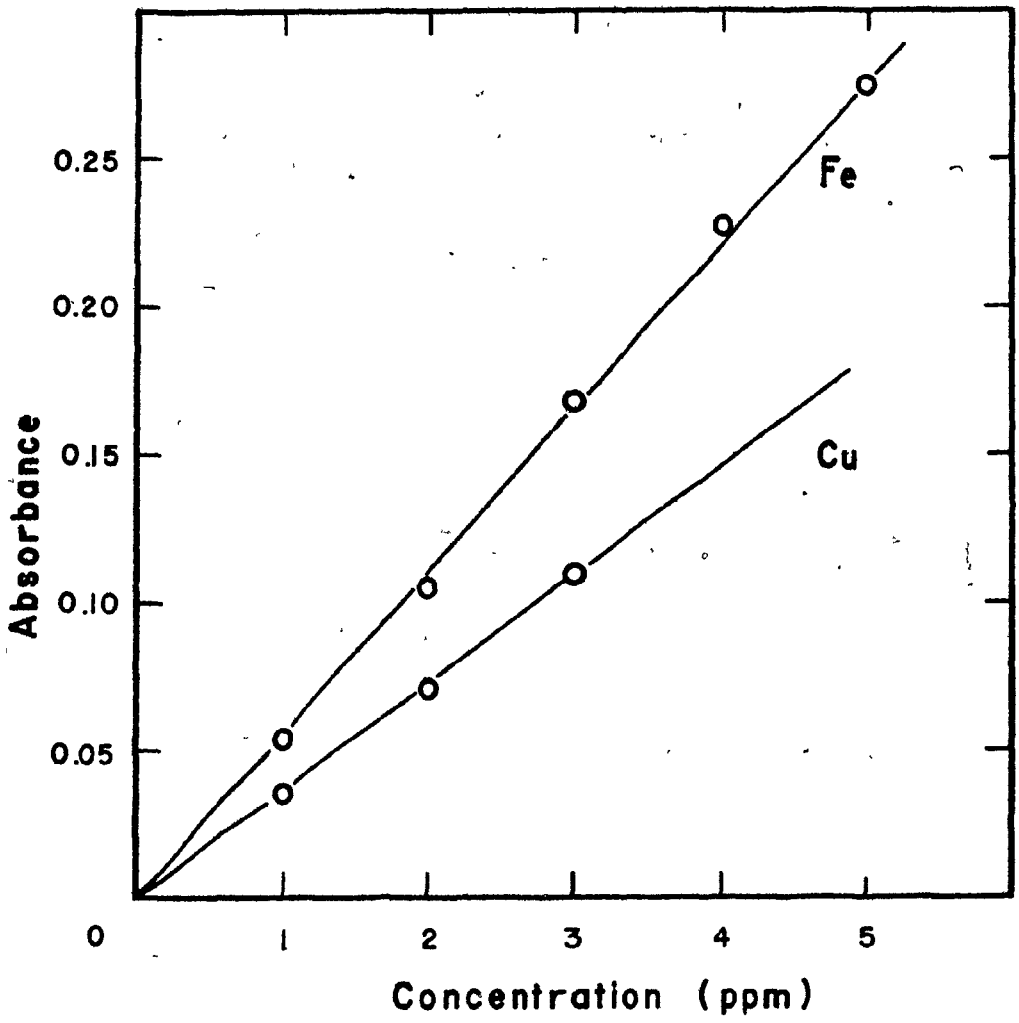


Figure A.I.1 Calibration Curves for the Determination of Iron and Copper by Atomic Absorption

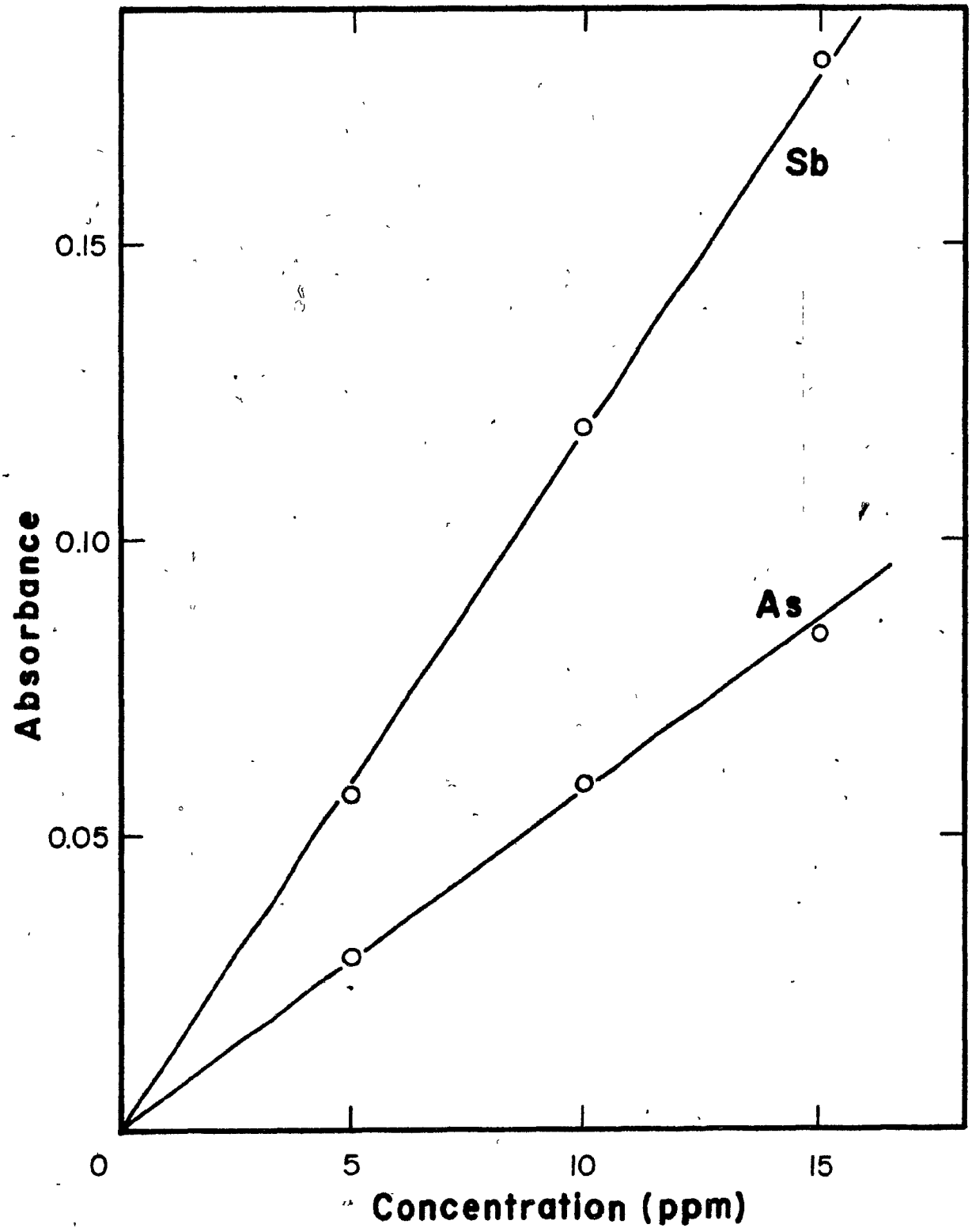


Figure A.I.2 Calibration Curves for the Determination of Antimony and Arsenic by Atomic Absorption

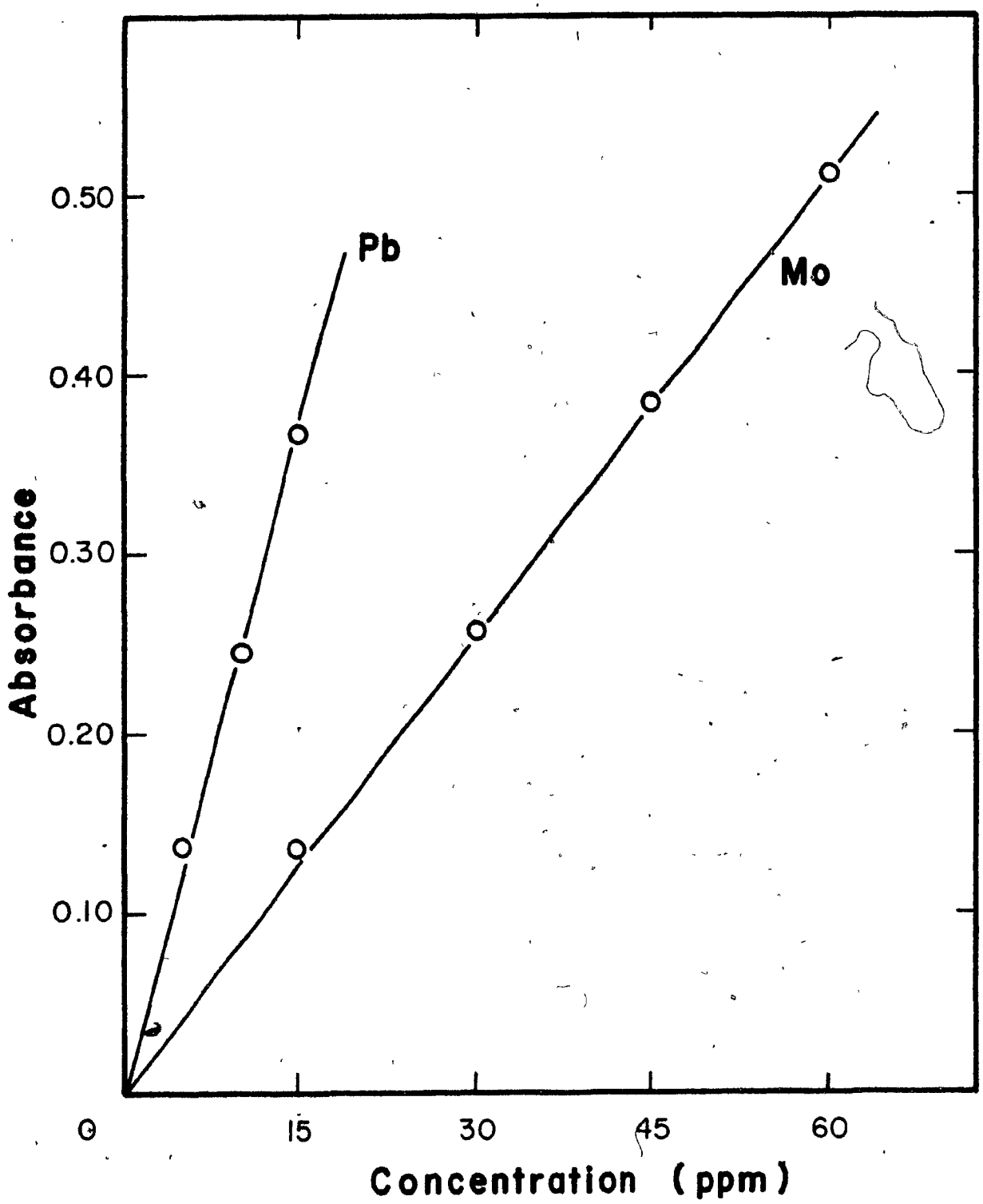


Figure A.I.3 Calibration Curves for the Determination of Lead and Molybdenum by Atomic Absorption

APPENDIX II

Table A.II.1

Results of Electrophoretic Measurements for Talc (Quebec) and Molybdenite

pH	E (Volt)	$\mu \times 10^{-4}$ cm/sec/Volt/cm	ζ (mV)
		Talc	
1.31	20	1.12	14.41
2.45	40	1.43	18.31
2.65	40	1.81	23.21
3.10	60	-0.72	- 9.25
3.60	40	-0.90	-11.57
4.00	40	-1.73	-22.18
6.35	50	-2.11	-28.44
7.90	40	-2.50	-37.13
11.35	30	-3.66	-49.98
		Molybdenite	
1.65	20	1.63	20.91
2.48	30	1.66	21.42
2.75	40	1.87	24.02
3.10	40	1.43	18.38
3.67	40	-1.32	-17.01
3.85	40	-0.09	-12.58
4.60	50	-2.44	-31.34
5.03	50	-2.27	-29.17
5.20	50	-2.49	-31.97
5.40	40	2.58	-33.10
6.02	40	-2.40	-30.85
6.40	40	-2.56	-32.90
7.18	40	-2.42	-31.11
8.40	40	-2.59	-33.33
9.81	40	-3.09	-39.77
11.4	30	-3.76	-48.30

Table A.II.2

Results of Electrophoretic Measurements for Chalcopyrite and Sulphur

pH	E (Volt)	$\mu \times 10^{-4}$ cm/sec/Volt/cm	ζ (mV)
	Chalcopyrite		
1.55	20	1.02	13.11
2.17	30	0.78	10.03
2.26	30	-0.77	- 9.95
3.10	40	-1.32	-17.00
4.35	40	-1.64	-21.05
6.05	60	-1.95	-25.02
8.10	60	-2.68	-34.50
3.95	40	-2.99	-38.44
11.60	30	-3.85	-49.50
	Sulphur from Galena		
2.1	30	-.24	3.04
2.15	30	-0.25	-3.25
3.20	40	-0.70	-9.04
4.10	40	-1.32	-17.0
6.80	50	-1.71	-21.92
8.55	40	-4.16	-53.5
10.0	40	-5.05	-64.9
	Sulphur from Pb/Zn Conc.		
2.05	30	0.44	5.62
3.65	40	-1.05	-13.50
5.15	40	-2.30	-29.55
6.95	40	-3.78	-48.56
7.85	40	-4.09	-52.51
9.20	40	-3.99	-51.28
10.45	30	-4.39	-56.38

Table A.II.3

Results of Electrophoretic Measurements for Galena

pH	E (Volt)	$\mu \times 10^{-4}$ cm/sec/Volt/cm	ζ (mV)
	Ground in Dist. Water		
2.20	30	1.44	18.56
3.25	40	2.83	36.41
4.83	40	3.23	41.49
5.80	40	2.23	28.66
6.36	50	0.92	11.79
6.45	50	-0.74	-9.56
7.3	80	0.70	8.99
7.3	80	-0.68	-8.72
8.4	40	-1.56	-20.03
8.78	70	-1.58	-20.25
9.54	30	-2.84	-36.49
10.60	30	-3.13	-40.19
11.26	30	-2.88	-37.05
	Ground Dry (fresh)		
2.33	40	1.22	15.71
2.90	60	1.39	17.90
4.55	70	1.97	25.35
5.30	80	0.55	7.02
5.30	80	-0.52	-6.71
7.93	70	-1.82	-23.35
	Ground Dry & Pretreated		
2.4	40	0.75	9.68
3.2	80	0.93	11.91
4.25	80	0.82	10.54
4.95	80	-0.74	-9.51
5.45	70	-0.99	-12.71
7.30	70	-1.31	-16.85
8.50	70	-1.98	-25.47
9.35	70	-2.48	-31.84
10.60	40	-3.31	-42.53
11.35	40	-4.16	-53.43
	Ground Dry & Aged for 4-5 Months		
1.95	30	0.42	5.46
1.90	40	-0.59	-7.61
3.35	70	-0.89	-11.48
5.60	70	-1.03	-13.26
8.40	70	-2.42	-31.09
9.60	70	-2.28	-29.29
10.65	40	-2.44	-31.40

TABLE A.II.4

Contact Angles Measured on Disc Samples of Talc

Disc 1 (-100x150 mesh)		Disc 2 (-200 mesh)	
pH	θ	pH	θ
6.1±0.2	46.5±2	5.6	39.0±1
7.5±0.1	44.5±2	4.5	39.0±1
8.4±0.1	40.0±1	3.75	38.0±2
9.75	35.0±1	2.7	39.0±2
10.6	32.5±2	1.75	38.0±2
12.0	27.0±2	2.75	37.0±1
13.0	17.0±2	3.7±0.1	35.0±2
11.9	18.0±1	4.8±0.1	33.0±1
10.3±0.1	19.0±2	5.75	33.0±2
9.6	20.0±1	7.2	32.0±2
8.5	20.0±1	8.3	29.0±1
7.7±0.1	23.0±2	9.4	25.0±2
6.7±0.1	28.0±2	10.4	18.0±2
5.9±0.1	30.0±2	11.2	nil
3.95	33.0±2	10.35	15>θ>0
2.5	36.0±3	9.35	17.0±3
1.5	37.5±1.5	8.25	21.0±2
0.8	38.0±2	7.40	23.0±3
-	-	5.70	23.0±2
-	-	4.9 0.1	25.0±2
-	-	3.75	28.0±1
-	-	2.70	32,0±2
-	-	1.7	35.5±1
-	-	1.25	35.0±1

Contact angle, θ in degrees.

Table A.II.5

Contact Angles Measured on Disc Samples of Molybdenite

Disc 1 (-100x150 mesh)		Disc 2 (-200 mesh)	
pH	θ	pH	θ
5.7	54.0±3	5.4	48.0±2
6.0 0.2	48.0±2	4.9	47.5±1.5
7.85	44.5±1.5	3.1	46.0±2
8.60	41.0±3	1.75	44.0±2
9.55	33.5±1.5	2.6	42.0±2
10.60	19.5±1.5	3.65	40.5±1.5
9.50	33.5±1.5	4.8	38.5±1.5
8.65	40.0±3	5.8	38.0±2
7.0 0.1	42.0±2	7.25	36.0±2
5.75	45.0±2	8.75	nil
4.6	46.0±2	10.40	nil
3.7	47.0±2	11.20	nil
2.55	47.0±2	10.35	nil
-	-	8.45	nil
-	-	5.8	nil
-	-	3.0	15>θ>0
-	-	2.20	15>θ>0
-	-	1.25	37.0 2

Contact angle in degrees.

Table A.II.6

Contact Angles Measured on Disc samples (-200 mesh) of Stibnite and Graphite

Stibnite		Graphite	
pH	θ	pH	θ
6.25	34.0±1	6.05	26.0±1
5.05	36.0±1	7.1	25.0±1
2.90	44.0±2	9.32	18.0±1
2.10	43.0±3	10.75	15.0±1
1.40	42.5±1.5	11.35	15>θ>0
3.85	42.0±2	8.45	16.0±1
5.50	36.0±2	7.85	19.0±1
6.25	34.0±2	6.90	23.5±1.5
7.20	33.0±2	5.05	26.5±1.5
8.25	31.5±1.5	4.05	30.0±2
9.50	28.0±1	2.85	31.5±1.5
10.90	25.0±2	1.67	32.5±1.5
		1.12	32.5±1.5

Table A.II.7

Contact Angles of Various Liquid Droplets on Mineral Samples

Mineral	Water	Glycerin	Forma-mide	Methylene Iodide	1-Bromo Naphthane
Talc	34±2	29±2	23±3	22.5±1.5	14±2
Realgar	57±2	51.5±1.5	42±1	31.5±1.5	13±2
Orpiment	48±1	44±2	37±2	27.5±1.5	-
Cinnabar	75±3	52±2	36±1	33.5±1.5	14±2
Graphite	59±2	44.5±1.5	40±2	21±2	-
Stibnite	76±3	67.0 ±2	60±2	39±2	14±2
Galena	47±3	34.5±1.5	32±2	28±1	26.5±1.5
Pyrite	72±2	68±2	45±1	38±1	23.5±1.5
Chalcocite	81±3	73.5±2	48±2	37±1	12+2
Chalcopyrite	65±2	58±2	44±2	36±1	15±1
Molybdenite	80±1	68.5±3	59±2	7±2	-

Table A.II.8

Flotation of Molybdenite as a Function of pH in the Absence and in the Presence of MIBC(10^{-4}M)

No Frother		Frother	
pH	%R	pH	%R
1.7	39.6	3.0	99.6
2.6	41.8	7.1	95.0
3.4	36.2	7.6	83.7
5.2	35.6	9.3	89.2
7.2	25.2	11.1	54.0
9.1	16.5	12.2	36.3
11.1	14.6	-	-

Table A.II.9a

Natural Flotation Response of Galena as a Function of pH [Sample prepared anf floated in distilled water presaturated with various gases]

N_2-Saturated		Air-Saturated		O_2-Saturated	
pH	%R	pH	%R	pH	%R
1.85	49.6	2.0	76.7	2.6	32.8
2.95	48.5	3.6	86.5	4.45	76.7
4.3	61.3	6.5	87.4	6.7	87.1
6.15	82.5	8.6	84.1	8.45	76.2
6.8	81.7	10.1	77.2	10.5	69.5
8.4	59.4	10.4	84.8	11.5	51.7
9.6	64.1	11.5	79.0	-	-
10.4	74.1	-	-	-	-
10.6	66.7	-	-	-	-
11.65	62.5	-	-	-	-

Table A.II.9b

Natural Flotation Response of Chalcopyrite as a Function of pH [Sample dry ground and floated in O_2-Saturated solutions]

pH: 1.85	2.9	3.65	4.35	5.4	6.5	8.75	10.1
%R: 91.2	91.5	70.2	39.8	3.2	40.4	40.6	27.5

APPENDIX III

Table A.III.1

Thermodynamic Excess Functions of Mixing Between Water and Methanol (25°C)

X_m	$\ell n f_m$	$\ell n f_w$	ΔH^{XS} (J/mole)	ΔG^{XS} (J/mole)	$T\Delta S^{XS}$ (J/mole)
0.0022	0.6295	0.6×10^{-5}	-15.81	3.45	-19.25
0.0090	0.6155	0.68×10^{-4}	-63.44	13.90	-77.34
0.0371	0.5703	1.13×10^{-3}	-241.44	55.15	-296.59
0.0887	0.4931	0.0063	-497.15	122.61	-619.75
0.1228	0.4460	0.0118	-622.39	161.43	-783.81
0.1596	0.3986	0.0196	-724.52	198.53	-923.05
0.2281	0.3194	0.0386	-840.23	254.46	-1094.69
0.3157	0.2341	0.0705	-885.33	302.79	-1188.12
0.3701	0.1894	0.0937	-874.66	320.07	-1194.73
0.4625	0.1269	0.1382	-817.24	329.63	-1146.87
0.5325	0.0896	0.1750	-755.89	321.06	-1076.94
0.6394	0.0476	0.2342	-649.46	284.80	-934.26
0.7995	0.0121	0.3238	-455.37	184.92	-640.29
0.8939	0.0029	0.3736	-288.71	104.69	-393.40
0.9500	0.9×10^{-4}	0.4010	-153.38	49.91	-203.29
0.9750	0.2×10^{-4}	0.4126	-81.08	25.62	-106.70
0.9850	0.1×10^{-4}	0.4171	-49.76	15.53	-65.29
0.9977	0.1×10^{-5}	0.4227	-7.85	2.41	-10.27

A - Estimation of the Methanol Content of the Air Bubbles Produced in Aqueous Methanol Solutions

Methanol is a highly volatile substance. The air bubbles produced in its aqueous solutions are expected to contain an appreciable amount of methanol vapor, M, in addition to some water vapor, W. Assuming that the ideal gas equation is obeyed, the equilibrium concentration of methanol vapor inside the bubbles can be estimated. The general form of the equation of state for a gas is as follows:-

$$PV = nRT \qquad 1$$

where P is pressure of a gas consisting of a number of moles, n, and occupying a volume V. The partial pressure of nitrogen, oxygen, methanol (M), and water (W) may be expressed using Equation 1. However, there exists an excess pressure, ΔP, inside a bubble with radius r_b. This is expressed as:-

$$\Delta P = \frac{2\gamma}{r_b} \qquad 2$$

The partial pressures are

$$P_{N_2} = n_{N_2} \frac{RT}{V} \qquad 3$$

$$P_{O_2} = n_{O_2} \frac{RT}{V} \qquad 4$$

$$P_M = n_M \frac{RT}{V} \qquad 5$$

$$P_W = n_W \frac{RT}{V} \qquad 6$$

According to Dalton's Law, the total pressure, P_T, of

a gas mixture is equal to the sum of the partial pressures of the components. Thus, the addition of Eq. 3 to 6 termwise yields

$$P_T = P_{N_2} + P_{O_2} + P_M + P_W = (n_{N_2} + n_{O_2} + n_M + {}_W)\left(\frac{RT}{V}\right) \qquad 7$$

Δp will decrease as the solutions become more concentrated, due to a reduction in surface tension, γ. It will be negligibly small except for very small bubbles. From Eq. 2 to 7

$$\frac{P_{N_2}}{n_{N_2}} = \frac{P_{O_2}}{n_{O_2}} = \frac{P_M}{n_M} = \frac{P_W}{n_W} = \frac{P_T}{n_{N_2}+n_{O_2}+N_M+n_W} \qquad 8$$

from which the mole fraction of methanol inside the bubble may be obtained

$$\frac{n_M}{n_{N_2}+n_{O_2}+n_M+n_W} = \frac{P_M}{P_T} \qquad 9$$

Eq. 9 is equivalent to the volume fraction of methanol. Thus, the volume percentage of methanol vapor inside the bubble can be estimated provided that the partial pressure of methanol is known. The total pressure, P_T of the bubble may be taken as 760 mm Hg. The partial pressure of methanol may be obtained by the following equation (Chapter III). The vapor pressure

$$P_M = \alpha_M . P_M^o$$

of pure methanol, P_M^o is about 127 mmHg (at 25°C). The activities, α_M are known as a function of methanol concentration of solutions. The results are tabulated in Table A.III.2.

Table A.III.2

Concentration of Methanol Vapor Inside Air Bubbles Produced in Methanol Solutions

% Methanol (vol) in solution	α_M	P_M (mmHg)	% Methanol (vol) in air bubble
2	0.017	2.12	0.28
12	0.098	12.42	1.63
21	0.169	21.41	2.82
30	0.238	30.20	3.97
36	0.284	36.01	4.74
45	0.352	44.73	5.89
54	0.423	53.70	7.07
63	0.498	63.27	8.33
72	0.583	73.98	9.73
80	0.671	85.16	11.21
90	0.809	102.77	13.52
95	0.897	113.86	14.98
100	1.000	127.00	16.71

B - Surface Tension Measurements

Method

Surface tension measurements were done using the du Noüy ring method as described in section 3.2.2. Since it involves the detachment of a platinum ring from a solution surface it is considered to be among the dynamic methods which also include the drop weight and the Wilhelmy slide methods. (Adamson, 1976). The method requires the use of a correction factor, F, which was proposed empirically by Harkins and Jordan (1930) and in a different form by Zuidema and Waters (1941). The correction factor by the latter researchers is given by the following equations:-

$$(F - a)^2 = \frac{4b}{(\pi r_r)^2} \times \frac{P}{\rho_\ell - \rho_g} + K$$

$$F = 0.725 + \sqrt{\frac{0.01452\ P}{C^2(\rho_\ell - \rho_g)} - \frac{1.679\ r_w}{r_r} + 0.04534}$$

where:

F = correction factor
r_r = radius of the ring (cm)
r_w = radius of the wire of the ring (cm)
P = apparent value measured (mN/m)
ρ_ℓ = density of the liquid phase (g./cm^3)
ρ_g = density of the gas phase (g./cm^3)
C = circumference of the ring (cm)
$K = 0.04534 - 1.679\ r/R$
$a = 0.725$
$b = 0.0009075$

The a, b, and the numerical part of K are the same for all

rings. For the platinum ring used, for methanol solutions the wire radius (r_w) was 0.0135 cm and the ring radius (r_r) 0.6380 cm. Thus $r_w/r_r = 0.02116$ and C = 4.00867 cm. The densities of the aqueous methanol solutions are available as a function of methanol composition (Carr and Riddick, 1951). The gas phase was partially saturated with methanol vapor. For the methanol concentration range 0 - 100% (v) the density of the gas phase remains approximately within the range 0.0012-0.0014 g/cm^3. Therefore, the expression $P/(\rho_\ell - \rho_g)$ can correctly be evaluated. The variation of F as a function of $(P/(\rho_\ell - \ell_g)$ is shown in Figure A.III.1. The correction factors calculated using the equation are listed as a function of the methanol concentration of aqueous solutions in Table A.III.4. Actual surface tension values were calculated by multiplying the apparent surface tension values (obtained by measurement) with the corresponding correction factors.

$$\gamma = \bar{P} \times F$$

These are also listed in the same table (last column).

Equipment

The apparent surface tension values were measured using the Fisher Autotensiomat. The equipment is seen in Figure A.III.2. It consists of three basic parts and is fully automated. There are:

(a) - main part (on the right in the figure) which houses the sample container, the ring assembly and the mechanical detachment arrangements.

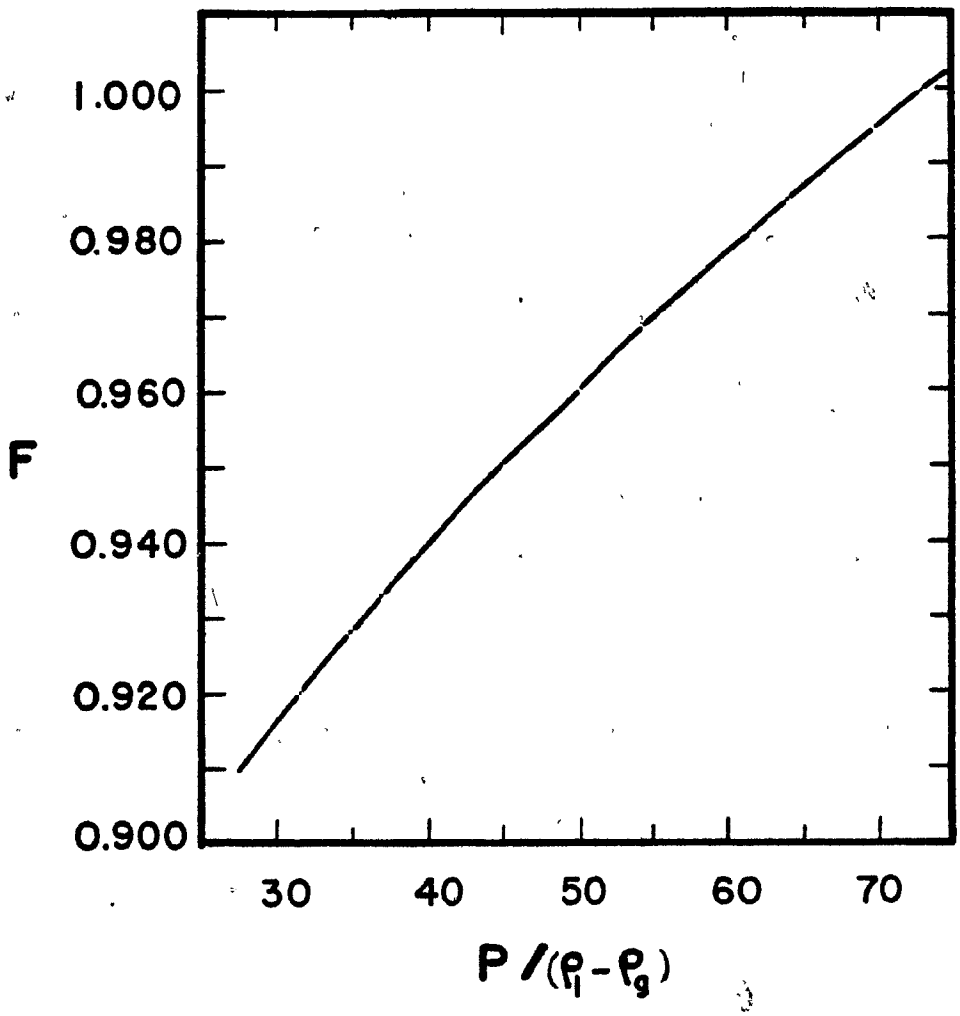
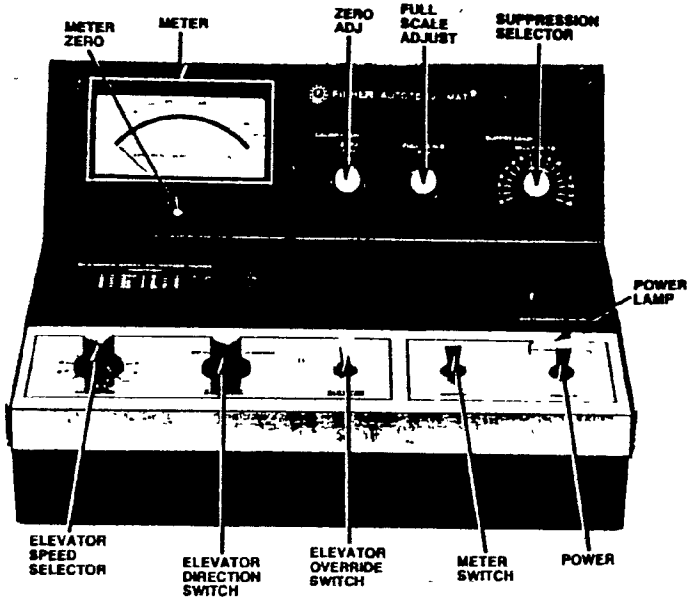


Figure A.III.1 Correction Factor Chart for Surface Tension Determination



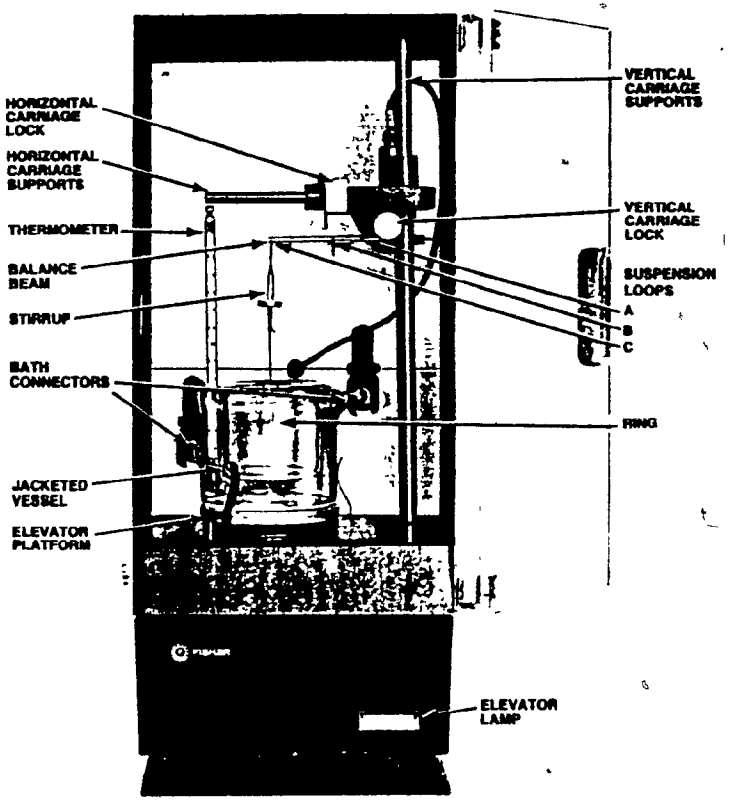


Figure A.III.2 Fisher Autotensiomat for the Measurements of Solution Surface Tension

(b) - control panel and the panel meter (on the left in the figure) which contains control, calibration and adjustment units as well as a scale meter for direct readout.

(c) - an accessory recorder (not seen in the figure) which records the graphic display of changes in surface tension patterns and thus permits the observation and the examination of force profiles from beginning to the end of the detachment process during the continuous pull of the ring.

All three parts are connected to each other. Before starting the measurements calibration of the instrument is required. This is done by loading the ring with known analytical balance weights supplied with the instrument and observing the corresponding apparent surface tension indicated. To obtain apparent surface tension values, one can use either the panel meter or the recorder, but not both of them simultaneously.

Experimental Procedure

Before starting the measurements, the ring and the sample container were thoroughly cleaned. The ring was cleaned initially by rinsing with spectro-grade acetone, allowed to dry and then by flaming to red heat in the oxidizing portion of a gas flame. All the glassware was cleaned with the freshly prepared dichromate-sulphuric acid mixture, followed by a thorough rinsing in distilled water. The instrument was calibrated by suspending the pre-cleaned platinum ring from the

beam of a transducer-balance assembly and adjusting the controls for obtaining apparent surface tension readings. After calibration, the ring was immersed in the solution to a depth of about 1 cm. Then the elevator platform was brought down at a controlled and constant rate of descent causing the ring to be pulled from the solution. A force proportional to the surface tension was in turn exerted on the balance beam and converted to an analog signal. The surface tension forces were continuously recorded on a chart recorder during the detachment process of the ring. The maximum of each recorded curve gave the apparent surface tension of the corresponding solution.

Other Solutions

In addition to methanol solutions decyl xanthate, lignosulphonate, and syntex solutions were used in order to determine the effect of their wetting power on various samples (Chapter 4). The surface tension of these solutions was measured using the same method and the instrument. All the solutions were freshly prepared. The measurements were done at the freshly formed solution surface. A fresh surface was obtained immediately before pulling the ring out of the bulk solution by adding a new solution to the cell so as to cause overflowing. The effect of surface aging on the surface tension was not determined. Because of the accidental loss of the previous ring during initial flaming, these measurements

were completed using a platinum ring of 6.0050 cm mean circumference and of the r_w/r_r ratio of 0.01859. Before starting the measurements special care was exercised to make sure that the ring was horizontal when hooked by the stirrup. A departure from the horizontal plane was found to produce erroneous results (Adamson, 1976). The results of measurements are tabulated in Tables A.III.6-9.

C - Standard Deviations and Confidence Intervals for the Surface Tension Determinations

The standard deviation (SD) of the apparent (uncorrected) surface tension (P) measurements was calculated using the familiar equation:-

$$SD = \sqrt{\frac{\sum_{i=1}^{n} (P_i - \bar{P})^2}{n - 1}}$$

where $\bar{P}$ is the arithmetic average or mean value of n surface tension measurements at a certain solution composition. For the aqueous solutions of methanol, n varied from 3 to 5.

The confidence interval, CI at a 95% level was calculated using the relationship:-

$$CI = \bar{P} \pm \frac{(t_{n-1,0.05})(SD)}{\sqrt{n}}$$

where t is the critical value corresponding to $v = n-1$ degrees of freedom and $\alpha = 0.05$ for 95% confidence level.

The results are listed as a function of methanol concentration in Table A.III.3.

Table A.III.3

Apparent Surface Tension of Aqueous Methanol Solutions (22 ± 1.5°C)

Methanol % (vol.)	Surface Tension, $\bar{P}$ (mN/m)	Standard Deviation	Confidence Interval (±)	No. of Measurements
0	72.53	0.21	0.19	7
0.1	72.12	0.06	0.15	3
0.2	71.80	0.06	0.15	3
0.5	71.25	0.06	0.16	3
1	70.73	0.06	0.15	3
2	69.00	0.10	0.25	3
4	63.38	0.06	0.15	3
8	61.20	0.08	0.13	4
12	56.70	0.08	0.20	3
15	54.40	0.11	0.18	4
18	52.90	0.21	0.26	5
21	50.80	0.14	0.22	4
24	48.51	0.06	0.15	3
27	47.67	0.08	0.20	3
30	46.13	0.10	0.25	3
33	44.21	0.11	0.27	3
38	42.60	0.11	0.27	3
42	40.73	0.13	0.32	3
45	38.52	0.14	0.22	4
48	37.71	0.10	0.25	3
51	36.95	0.08	0.20	3
54	36.08	0.10	0.25	3
57	34.25	0.14	0.22	4
60	33.78	0.15	0.23	4
63	33.25	0.16	0.25	4
66	32.30	0.12	0.30	3
72	30.52	0.15	0.24	4
80	29.79	0.20	0.25	5
85	29.45	0.14	0.22	4
90	27.60	0.12	0.30	3
95	26.52	0.20	0.25	5
100	24.6	0.15	0.16	6

Table A.III.4

Correction Factors and Surface Tension Values as a Function of Methanol Concentration

% Methanol (v.)	$\bar{P}$ (mN/m)	ρ_ℓ (g/cm^3)	ρ_g (g/cm^3)	$\bar{P}/(\rho_\ell-\rho_g)$	F	γ (mN/m)
0	72.53	0.9971	0.0012	72.83	1.0001	72.53
0.1	72.12	0.9969	0.0012	72.43	0.9993	72.07
0.2	71.8	0.9967	0.0012	72.12	0.9988	71.71
0.5	71.25	0.9964	0.0012	71.59	0.9979	71.10
1	70.73	0.9957	0.0012	71.12	0.9972	70.53
2	69.0	0.9945	0.0012	69.47	0.9942	68.60
4	63.38	0.9915	0.0012	64.02	0.9850	62.44
8	61.20	0.9860	0.0012	62.14	0.9818	60.09
12	56.7	0.9810	0.0012	57.87	0.9742	55.24
15	54.4	0.9773	0.0012	55.73	0.9703	52.78
18	52.9	0.9732	0.0012	54.42	0.9634	51.20
21	50.8	0.9695	0.0012	52.46	0.9601	48.94
24	48.51	0.9618	0.0013	50.31	0.9588	46.57
27	47.67	0.9577	0.0013	49.63	0.9561	45.71
30	46.13	0.9540	0.0013	48.23	0.9525	44.1
33	44.21	0.9465	0.0013	46.40	0.9498	42.11

Cont'd...

.....Table A.III.4 Cont'd.

% Methanol (v.)	$\bar{P}$ (mN/m)	ρ_ℓ (g/cm^3)	ρ_g (g/cm^3)	$\bar{P}/(\rho_\ell - \rho_g)$	F	γ (mN/m)
38	42.60	0.9465	0.0013	45.07	0.9498	40.46
42	40.73	0.9405	0.0013	43.37	0.9462	38.54
45	38.52	0.9352	0.0013	41.25	0.9418	36.28
48	37.71	0.9300	0.0013	40.61	0.9406	35.47
51	36.95	0.9250	0.0013	40.00	0.9394	34.71
54	36.08	0.9200	0.0013	39.30	0.9377	33.83
57	34.25	0.9141	0.0013	37.52	0.9341	32.00
60	33.78	0.9090	0.0014	37.22	0.9334	31.53
63	33.25	0.9019	0.0014	36.92	0.9328	31.02
66	32.30	0.8955	0.0014	36.13	0.9310	30.07
72	30.52	0.8800	0.0014	34.74	0.9280	28.32
80	29.79	0.8600	0.0014	34.70	0.9278	27.64
85	29.45	0.8450	0.0014	34.91	0.9284	27.34
90	27.60	0.8275	0.0014	33.41	0.9250	25.53
95	26.52	0.8100	0.0014	32.80	0.9236	24.49
100	24.6	0.7867	0.0014	31.33	0.9202	22.64

Table A.III.5

Temperature Dependence of the Surface Tension for the Water-Methanol System

% Methanol (vol.)	T(°K)	γ (mN/m)
	283.4	74.0
Dist.	293.0	72.7
Water	298.4	71.5
	307.7	70.0
	313.4	69.1
	277.7	71.1
	280.5	70.8
	286.5	69.6
2	291.4	69.3
	297.2	68.3
	300.4	67.8
	281.6	62.6
	289.8	61.4
	295.8	60.9
8	301.9	59.9
	309.0	58.9
	315.6	58.1
	277.7	54.8
	283.7	54.0
	288.7	53.5

Cont'd....

....Table A.III.5 cont'd.

% Methanol (vol.)	T(°K)	γ (mN/m)
18	293.2	52.8
	300.0	51.8
	305.2	51.2
	309.2	50.6
40	280.6	42.0
	293.7	40.6
	298.0	40.3
	300.6	39.6
	308.1	39.0
	313.3	38.6
57	281.2	34.8
	286.7	34.3
	291.7	33.7
	297.8	33.3
	303.3	32.3
	314.6	31.6
~100	280.6	23.5
	286.2	22.9
	292.8	22.7
	297.9	22.2
	300.7	21.7
	305.6	20.9

Table A.III.6

Apparent Surface Tension of Decyl Xanthate Solutions*

Concentration (g mol./l.)	$\bar{P}$ (mN/m)	SD	CI(±)	n
5×10^{-6}	73.92	0.36	0.89	3
4×10^{-5}	71.68	0.40	0.64	4
2×10^{-4}	68.92	0.34	0.84	3
5×10^{-4}	62.9	0.65	1.03	4
1×10^{-3}	58.55	0.48	0.76	4
2×10^{-3}	51.98	0.71	1.13	4
5×10^{-3}	48.90	0.36	0.57	4
1×10^{-2}	40.84	0.38	0.60	4
3.6×10^{-2} (N.S.)	37.80	0.63	1.00	4

*Freshly prepared solution.

(N.S.); Nearly saturated solution.

Table A.III.7

Surface Tension of Potassium Decyl Xanthate Solutions*

(Using a Platinum ring with C = 6.005 cm; r_r/r_w = 53.7937)

Conc. (M)	$\bar{P}$ (mN/m)	ρ_ℓ (g/cm^3)	$\bar{P}/(\rho_\ell - \rho_g)$†	F	γ (mN/m)
5×10^{-6}	73.92	0.9971	74.81	0.9348	69.10
4×10^{-5}	71.68	0.9971	71.98	0.9326	66.85
2×10^{-4}	68.92	0.9972	69.20	0.9299	64.09
5×10^{-4}	62.9	0.9972	63.15	0.9239	58.11
1×10^{-3}	58.55	0.9974	58.77	0.9194	53.83
2×10^{-3}	51.98	0.9976	52.17	0.9124	47.43
5×10^{-3}	48.90	0.9985	49.03	0.9090	44.45
1×10^{-2}	40.84	0.9998	40.90	0.8999	36.75
3.6×10^{-2} (N.S.)	37.80	1.0069	37.58	0.8961	33.87

*Freshly prepared solutions.

†ρ_g = 0.0012 g/cm^3; (N.S.); Nearly saturated solution

Table A.III.8

Surface Tension of Lignosol-XD Solutions*

(Using a Platinum ring with C=6.005 cm; r_r/r_w=53.7937)

Conc. (g/ℓ)	$\bar{P}$ (mN/m)	SD	CI (±)	ρ_ℓ (g/cm^3)	$\bar{P}/(\rho_\ell-\rho_g)$†	F	γ (mN/m)
0.005	74.41	0.36	0.57	0.9971	74.72	0.9353	69.59
0.01	73.12	0.41	0.65	0.9971	73.42	0.9340	68.30
0.02	71.09	0.38	0.60	0.9971	71.38	0.9321	66.26
0.04	70.41	0.45	0.72	0.9971	70.70	0.9314	65.58
0.06	69.50	0.28	0.45	0.9971	69.79	0.9305	64.67
0.12	65.24	0.48	0.76	0.9972	65.50	0.9263	60.43
0.24	60.00	0.21	0.33	0.9974	60.23	0.9209	55.25
0.48	57.62	0.28	0.45	0.9979	57.81	0.9184	52.92
0.96	56.44	0.23	0.37	0.9981	56.62	0.9172	51.76

*Freshly prepared solutions, $\bar{P}$; average of 4 measurements

†ρ_g = 0.0012 g/cm^3

Table A.III.9

Surface Tension of Syntex Solutions*

(Using a Platinum ring with C=6.005 cm; r_r/r_w=53.7937)

Conc. (g/ℓ)	$\bar{P}$ (mN/m)	SD	CI (±)	ρ_ℓ (g/cm^3)	$\bar{P}/(\rho_\ell-\rho_g)$†	F	γ (mN/m)
0.0025	72.45	0.44	0.71	0.9971	72.75	0.9334	67.62
0.0125	66.82	0.29	0.46	0.9971	67.10	0.9278	62.00
0.025	62.40	0.82	1.30	0.9971	62.66	0.9234	57.62
0.135	46.53	0.60	0.95	0.9972	47.72	0.9065	42.18
0.225	41.80	0.63	1.00	0.9973	41.96	0.9011	37.67
0.400	38.10	0.30	0.48	0.9975	38.24	0.8968	34.17
1.00	37.15	0.50	0.80	0.9981	37.27	0.8957	33.27
1.50	36.45	0.28	0.45	0.9986	36.55	0.8948	32.62
2.50	34.63	0.39	0.62	0.9996	34.69	0.8926	30.91

*Freshly prepared solutions, $\bar{P}$; average value of 4 measurements

†ρ_g = 0.0012 g/cm^3.

D - Calculation of Surface Excess Values and the Area Occupied per Methanol Molecule Adsorbed at the Solution-Gas Interface

The surface excess (or adsorption density) values were calculated from the Gibbs equation (section 3.4.2.). The differential part of the equation, $(d\gamma/d\ell n\alpha)$ was evaluated by taking the derivative of the expression $\gamma = f(\ell n\alpha)$ which was obtained by polynomial regression. The coefficients of the regression equation (5th degree) were as follows:-

$$\gamma = a(\ell n\alpha)^5 + b(\ell n\alpha)^4 + c(\ell n\alpha)^3 + d(\ell n\alpha)^2 + e(\ell n\alpha) + f$$

a =	0.8165783×10^{-1}	d =	0.1619673×10^{2}
b =	0.1310581×10^{1}	e =	-0.2220520×10^{1}
c =	0.7455407×10^{1}	f =	0.2402931×10^{2}

The standard error of estimate was lowest (0.83371) for the 5th degree regression. The coefficients obtained were based on 24 sets of data. The data and a comparison between observed and estimated surface tension values are given in Table A.III.10.

The area per methanol molecule adsorbed at each concentration is equal to the reciprocal of the surface excess value.

The area per molecule adsorbed = $\frac{1}{\Gamma \cdot N_A}$ [cm^2/molecule] where N_A is the Avogadro number (6.023×10^{23}). The area may be expressed in $\mathring{A}^2$ by multiplying the equation by 10^{16}.

The results of calculations are given in Table A.III.11.

Table A.III.10

Data for the Polynomial Regression and a Comparison with Estimated Surface Tensions

No. of Data	$\ell n a$	γ	$\gamma_{Est.}$	Residual
1	-4.7751	70.5	70.9	-0.4
2	-4.0950	68.6	67.3	1.3
3	-3.4113	62.4	63.9	-1.5
4	-2.7239	60.0	59.5	0.5
5	-2.3251	55.2	55.8	-0.6
6	-1.9294	51.2	51.0	0.2
7	-1.7803	48.9	49.0	-0.1
8	-1.6512	46.6	47.0	-0.4
9	-1.5380	45.7	45.3	0.4
10	-1.4365	44.1	43.6	0.5
11	-1.3444	42.1	42.1	0.0
12	-1.2604	42.0	40.7	1.3
13	-1.1585	40.0	38.9	1.1
14	-1.0436	36.3	37.0	-0.7
15	-0.9798	35.5	35.9	-0.4
16	-0.9189	34.7	34.8	-0.1
17	-0.8608	33.8	33.9	-0.1
18	-0.8046	32.0	32.9	-0.9
19	-0.6967	31.0	31.2	-0.2
20	-0.6442	30.0	30.4	-0.4
21	-0.5404	28.3	28.9	-0.6
22	-0.3996	27.7	27.7	0.6
23	-0.2117	25.5	25.2	0.3
24	-0.1092	24.5	24.5	0.0

Table A.III.11

Surface Excess Values of Methanol at the Solution-Gas Interface

X_n	% (vol.)	γ (mN/M)	$\ell n\, a_m$	$\partial\gamma/\gamma \ell n\, a_m$	$\Gamma \times 10^{10}$ (moles/cm^2)	Area (A$^{\circ 2}$) per Molecule adsorbed
0.0090	2	68.6	-4.950	-4.9912	2.0135	82.5
0.0181	4	62.4	-3.4113	-5.2684	2.1253	78.2
0.0371	8	60.0	-2.7239	-7.9834	3.2205	51.6
0.0570	12	55.2	-2.3251	-10.5892	4.2717	38.9
0.0887	18	51.2	-1.9294	-13.3596	5.3893	30.8
0.1054	21	48.9	-1.7803	-14.4825	5.8423	28.4
0.1228	24	46.6	-1.6512	-15.2954	6.1702	26.9
0.1408	27	45.7	-1.5380	-15.9247	6.4241	25.8
0.1596	30	44.1	-1.4365	-16.4030	6.6170	25.1
0.1792	33	42.1	-1.3444	-16.7513	6.7576	24.6
0.1996	36	42.0	-1.2604	-16.9857	6.8521	24.2
0.2281	40	40.0	-1.1585	-17.1470	6.9172	24.0
0.2661	45	36.3	-1.0436	-17.1425	6.9154	24.0
0.2903	48	35.5	-0.9798	-17.0437	6.8755	24.2
0.3157	51	34.7	-0.9189	-16.8788	6.8090	24.4
0.3422	54	33.8	-0.8608	-16.6525	6.7177	24.7
0.3701	57	32.0	-0.8046	-16.3755	6.6059	25.1
0.4301	63	31.0	-0.6967	-15.6101	6.2972	26.4
0.4625	66	30.0	-0.6442	-15.1384	6.1069	27.2
0.5326	72	28.3	-0.5404	-13.9874	5.6426	29.4
0.6394	80	27.7	-0.3996	-11.9181	4.8078	34.5
0.7995	90	25.5	-0.2117	-8.1250	3.2777	50.7
0.8939	95	24.5	-0.1092	-5.4981	2.2179	74.9

Table A.III.12

Surface Excess and Deficiencies at the Aqueous Methanol Solution-Gas Interface According to Gibbs and Guggenheim-Adam Conventions

X_m	Γ_M	$\Gamma_M^{(N)}$	$\Gamma_M^{(M)}$	$\Gamma_M^{(V)}$	$-\Gamma_W^{(V)}$ †	$-\Gamma_W^{(M)}$ *	$-\Gamma_W^{(N)}$
0.0090	2.0135	1.9954	1.9811	1.9731	4.4498	3.5244	1.9954
0.0181	2.1253	2.0868	2.0583	2.0405	4.6018	3.6617	2.0868
0.0371	3.2205	3.1010	3.0140	2.9630	6.6824	5.3619	3.1010
0.0570	4.2717	4.0282	3.8569	3.7592	8.4781	6.8615	4.0282
0.1054	5.8423	5.2265	4.7301	4.6158	10.4099	8.5920	5.2265
0.1408	6.4241	5.5196	4.9729	4.6906	10.5785	8.8424	5.5196
0.1792	6.7576	5.5466	4.8682	4.5281	10.2120	8.6605	5.5466
0.2281	6.9172	5.3394	4.5338	4.1509	9.3613	8.0657	5.3394
0.2903	6.8755	4.8795	3.9801	3.5763	8.0655	7.0806	4.8795
0.3422	6.7177	4.4189	3.4890	3.0911	6.9713	6.2070	4.4189
0.4301	6.2972	3.5888	2.6886	2.3305	5.2560	4.7830	3.588
0.5326	5.6426	2.6374	1.8642	1.5806	3.5647	3.3164	2.6374
0.6394	4.8078	1.7337	1.1573	0.9618	2.1690	2.0588	1.7337
0.7995	3.2777	0.6572	0.4049	0.3280	0.7397	0.7204	0.6572
0.8939	2.2179	0.2353	0.1387	0.1109	0.2501	0.2468	0.2353

† $-\Gamma_W^{(V)} = \left(\frac{X_W \cdot V_M}{\bar{V}}\right) \Gamma_M$; * $-\Gamma_W^{(M)} = \left(\frac{X_W \cdot M_M}{\bar{M}}\right) \Gamma_M$; $-\Gamma_W^{(N)} = \Gamma_M^{(N)}$

All the Γ values are in moles/cm^2 x 10^{10}

Table A.III.13

Bubble Size Distributions in Methanol Solutions

Bubble* Diameter (cm)	% Methanol (by vol.) 0.0	0.1	0.2	0.5	1	2	8	12
0.00/0.02	67	22	52	89	73	51	36	46
0.02/0.04	65	18	49	79	110	100	63	75
0.04/0.06	47	24	41	36	181	229	233	237
0.06/0.08	29	14	21	37	120	78	90	85
0.08/0.10	17	11	12	24	72	44	17	23
0.10/0.12	13	6	10	17	26	16	4	3
0.12/0.14	15	6	11	17	9	8	2	1
0.14/0.16	8	6	7	12	5	4		
0.16/0.18	10	4	8	8	2	2		
0.18/0.20	9	8	6	6				
0.20/0.22	13	8	7	3				
0.22/0.24	7	5	5	2				
0.24/0.26	12	3	2					
0.26/0.28	14	1	2					
0.28/0.30	7	1						
0.30/0.32	11							
0.32/0.34	4							
0.34/0.36	3	1						
0.36/0.38	2							
0.38/0.40	1							
0.40/0.42	2							
0.42 <	1							
Total no. of bubbles counted	357	138	233	390	598	532	445	470
No. of photos taken	6	4	4	3	4	3	2	2

*With respect to the unit square (a = 0.62 mm) of the grid at the background.

Cont'd.

Table A.III.13 Cont'd.

Bubble	% Methanol (by vol.)								
Diameter (cm)	18	27	40	48	63	72	80	95	~ 100
0.00/0.2	52	46	40	43	26	45	40	17	14
0.02/0.04	68	67	65	53	50	60	80	50	68
0.04/0.06	244	265	290	223	171	149	49	22	12
0.06/0.08	78	89	94	111	90	67	14	7	8
0.08/0.10	23	31	41	50	53	53	9	5	5
0.10/0.12	3	5	5	8	13	20	7	5	4
0.12/0.14	2	2	2	1	4	11	4	6	4
0.14/0.16				1	3	6	3	4	4
0.16/0.18					1	2	2	4	2
0.18/0.20							2	2	2
0.20/0.22							4	2	2
0.22/0.24							1		1
0.24/0.26								1	1
0.26/0.28									
0.28/0.30									1
0.30/0.32								1	
0.32/0.34									1
0.34/0.36									
0.36/0.38								2	2
0.38/0.40									
0.42/0.44									1
0.44 <									1
Total no. of bubbles counted	470	505	537	490	411	413	215	128	133
No. of photos taken	2	2	2	2		2	2	2	2

Table A.III.14

Number of Bubbles Produced per cm^3 of Methanol Solution

% Methanol (by vol.)	C_M (g.mole/ℓ)	log C_M	No. of bubbles/cm^3 all sizes	0.04/0.06
0	0	-	20	
0.1	2.46×10^{-2}	-1.61	28	5
0.2	4.91×10^{-2}	-1.31	52	9
0.5	1.23×10^{-1}	-0.91	116	28
1	2.46×10^{-1}	-0.61	289	88
2	4.91×10^{-1}	-0.31	414	178
8	1.96	0.29	417	217
12	2.96	0.47	458	229
18	4.42	0.65	417	217
27	6.63	0.82	403	212
40	9.82	0.99	371	199
48	11.79	1.07	300	138
63	15.47	1.19	243	102
72	17.68	1.25	183	66
80	19.64	1.29	81	19
95	23.33	1.37	46	8
100	24.55	1.39	31	3

E - Velocity of Ascent and Dimensionless Parameters for Bubbles in Aqueous Methanol Solutions

The rising velocity of the air bubbles was calculated using the following equation which was developed by Concha and Almendra (1979).

$$v = \frac{20.52\ \mu}{d \cdot \rho_\ell} \left[\left(1 + 0.0921\ \left(\frac{d}{J}\right)^{3/2}\right)^{1/2} - 1 \right]^2$$

where,

$$J = \left[\frac{3}{4}\ \frac{\mu^2}{(\rho_\ell - \rho_g)\rho_\ell\ g} \right]^{1/3}$$

v = velocity of bubbles (cm/s.)

d = bubble diameter (cm)

g = acceleration due to gravity (cm/s^2)

ρ_ℓ, ρ_g = density of liquid and gas ($g./cm^3$)

μ = viscosity of liquid (g./cm-s)

Table A.III.15. lists the viscosity and density values (Carr and Riddick, 1955), and the velocity of the air bubbles (d=0.05 cm) calculated as a function of methanol concentration.

The following dimensionless parameters are considered to be important in flotation systems since they relate capillary forces to viscosity, gravity, and flow (inertia) forces (Leja, 1982).

$$\text{Eotvos (or Bond) number, } E_o\ (Bo) = \frac{d^2 \rho_\ell}{\gamma \cdot g}$$

(ratio of acceleration or gravity to surface tension forces)

$$\text{Reynolds number, } Re = \frac{d\,\rho_\ell\,v}{\mu}$$

(ratio of viscous to inertia forces)

$$\text{Weber number, } \quad We = \frac{d\rho_\ell v^2}{\gamma}$$

(ratio of inertia to surface tension forces)

$$\text{Capillary number, } Cap = \frac{\mu\,v}{\gamma} = \frac{We}{Re}$$

The availability of the required data for aqueous methanol solutions permits the calculation of these dimensionless numbers. The results for the air bubbles of 0.05 cm are listed as a function of methanol concentration in Table A.III.16.

Table A.III.15

Some Physical Parameters of the Water-Methanol System

Methanol Con'n % (by vol.)	Surface Tension, γ (10^{-2}mN/cm)	Viscosity, μ (10^{-2}mN-S/cm^2)	Density, ρ_ℓ (g/cm^3)	v* (cm/s.)
0	72.5	0.00894	0.9971	5.93
0.5	71.1	0.00900	0.9965	5.91
1.0	70.5	0.00923	0.9954	5.84
2.0	68.6	0.00950	0.9940	5.76
8.0	60.0	0.01070	0.9860	5.43
12.0	55.2	0.01178	0.9804	5.17
18.0	51.2	0.01308	0.9720	4.89
21.0	48.9	0.01355	0.9695	4.79
24.0	46.6	0.01457	0.9618	4.59
30.0	44.1	0.01509	0.9572	4.49
33.0	42.1	0.01540	0.9540	4.43
36.0	42.0	0.01581	0.9492	4.36
38.0	40.5	0.01602	0.9458	4.32
40.0	40.0	0.01613	0.9441	4.30
42.0	38.5	0.01634	0.9405	4.26
45.0	36.3	0.01661	0.9352	4.20
48.0	35.5	0.01670	0.9297	4.18
51.0	34.7	0.01657	0.9259	4.18
54.0	33.8	0.01626	0.9201	4.21
57.0	32.0	0.01590	0.9141	4.25
60.0	31.5	0.01550	0.9082	4.30
63.0	31.0	0.01508	0.9019	4.35
66.0	30.0	0.01461	0.8955	4.41
69.0	29.2	0.01410	0.8887	4.48
72.0	28.3	0.01354	0.8816	4.56
80.0	27.7	0.01174	0.8603	4.85
90.0	25.5	0.00884	0.8266	5.47
95.0	24.5	0.00742	0.8100	5.87
100.0	22.6	0.00557	0.7867	6.55

*Rising velocity (v; cm/s) was calculated for bubbles with average diameter of 0.05 cm.

Table A.III.16

Dimensionless Parameters for Bubbles of 0.5 mm Diameter in Aqueous Methanol Solutions

Methanol Concentration % (by vol.)	Eotvos (Bond) Numb. $Eo(Bo) \times 10^{-8}$	Reynolds Number Re	Weber Number We	Capillary Number $Cap \times 10^{-4}$
0.5	3.57	32.72	0.024	7.33
2.0	3.69	30.13	0.024	7.97
8.0	4.19	25.02	0.024	9.59
18.0	4.84	18.17	0.023	12.49
24.0	5.26	15.15	0.022	14.52
33.0	5.77	14.00	0.022	15.71
38.0	5.95	12.75	0.022	17.09
42.0	6.23	12.25	0.022	18.09
48.0	6.67	11.64	0.023	19.66
51.0	6.80	11.90	0.023	19.59
54.0	7.33	11.91	0.024	20.26
57.0	7.28	12.22	0.026	21.11
60.0	7.35	12.60	0.027	21.15
63.0	7.41	12.66	0.028	21.74
66.0	7.61	13.52	0.029	21.47
69.0	7.76	14.12	0.031	21.63
72.0	7.94	14.85	0.032	21.81
80.0	7.91	17.77	0.034	18.99
90.0	8.26	25.57	0.048	18.77
95.0	8.43	36.00	0.057	15.82
100.00	8.87	46.26	0.075	16.14

APPENDIX IV

Table A.IV.1

Wettability Data for Minerals in Aqueous Methanol Solutions

γ_{lv}*	θ**	$\gamma_{lv}\cos\theta$***	γ_{lv}	θ	$\gamma_{lc}\cos\theta$
Sulphur Crystal			Sulphur Disc		
72.5	86.5	4.45	72.5	62.0	34.04
62.4	81.0	9.59	60.9	55.3	34.67
52.9	74	14.58	52.9	51.5	33.28
42.0	60.5	20.68	42.0	35.0	34.40
36.3	54.5	21.10	35.0	26.0	31.46
30.5	35	25.00	-	-	-
Molybdenite Face			Molybdenite Disc		
72.5	80.5	11.97	72.5	4.47	51.6
60.0	76.5	14.01	60.9	38.0	48.0
52.9	68.5	19.39	52.9	29.5	46.0
46.6	62.6	21.40	46.6	22.0	43.2
36.3	42.0	26.93	42.0	~ 0	42.0
Stibnite (Fracture Face)			Stibnite (Polished)		
72.5	50.2	46.4	72.5	30.5	62.5
68.6	49.7	44.4	62.4	28.0	55.1
60.0	45.6	42.0	52.9	20.5	49.5
51.2	40.2	39.1	46.6	17.5	44.4
42.0	30.5	36.2	-	-	-
Graphite Face			Coal (Polished)		
72.5	79.0	13.83	72.5	50.0	46.6
60.0	69.3	21.18	68.6	48.5	45.46
52.9	62.2	24.70	62.4	47.5	42.18
46.6	53.5	27.72	55.2	40.0	42.29
36.3	30.9	31.14	48.9	34.4	40.36

*mN/m; **Degrees; ***mN/m

Table A.IV.2

Wettability Data for Stibnite and Molybdenite in Decyl Xanthate Solutions

$\gamma_{\ell v}$*	θ**	$\gamma_{\ell v}\cos\theta$***	$\gamma_{\ell v}$	θ	$\gamma_{\ell v}\cos\theta$
Stibnite (Polished)			Molybdenite Edge		
72.50	30.5	62.47	72.50	0	72.50
66.85	52.6	40.60	66.85	59.0	34.40
64.09	59.6	32.43	64.09	69.6	22.34
58.11	69.5	20.35	58.11	71.4	18.53
53.83	69.7	18.68	53.83	73.3	15.47
47.43	74.8	12.44	47.43	73.5	13.47
44.45	66.0	20.87	44.45	66.5	17.72
36.75	20.0	34.53	36.75	0/20	36.8/34.5

Table A.IV.3

Wettability Data for Molybdenite Face in Aqueous Syntex Solutions

$\gamma_{\ell v}$*	θ**	$\gamma_{\ell v}\cos\theta$***
74.5	83.5	8.5
72.5	80.3	12.22
67.62	77.0	15.21
62.00	64.2	27.00
57.62	58.0	30.53
42.18	43.3	30.70
37.67	35.5	30.65
34.17	26.3	30.63

*mN/m; **Degrees; ***mN/m

Table A.IV.4

Separation Efficiencies (SE) of Binary Mixtures of Inherently Hydrophobic Minerals

Sulphur & Graphite (50:50)

$\gamma_{\ell v}$	Conc. (S+C)	Conc. (C)	R_S(%)	R_C(%)	SE(%)
30	0.1094	0.0011	43.32	0.44	42.9
32	0.2340	0.0105	89.40	4.20	85.2
33.8	0.2620	0.0165	98.20	6.60	91.6
34.7	0.2795	0.0313	99.28	12.52	86.8
36.3	0.3222	0.0737	99.40	29.48	69.9
38.5	0.3643	0.1165	99.12	46.60	52.5

Talc & Molybdenite (50:50)

$\gamma_{\ell v}$	Conc. (T+M)	Conc.(T)	R_T(%)	R_M(%)	SE(%)
32	0.0638	0.0422	16.88	8.64	8.2
34.7	0.1333	0.1188	47.52	5.80	41.7
36.3	0.2011	0.1946	77.84	2.60	75.2
39.5	0.2284	0.2176	87.04	4.32	82.7
40.5	0.2540	0.2395	95.80	5.80	90.0
44.1	0.3212	0.2400	96.00	32.48	63.5
45.7	0.3307	0.2414	96.56	35.72	60.8

Sulphur & Molybdenite (50:50)

$\gamma_{\ell v}$	Conc. (S+M)	Conc. (M)	R_S(%)	R_M(%)	SE(%
30	0.1764	0.0210	62.16	8.40	53.8
31	0.2263	0.0103	86.40	4.12	82.3
31.5	0.2470	0.0084	95.60	3.36	92.2
32	0.2540	0.0068	99.25	2.72	96.5
33.8	0.2578	0.0080	99.52	3.40	96.1
34.7	0.2815	0.0335	99.20	13.40	85.8
40.5	0.3106	0.0609	99.88	24.36	75.5

Feed: 500 mg.

Table A.IV.5

Induction Periods According to Sutherland's Equation

Methanol (% v)	γ_ℓ (mN/m)	K (s^{-1})	N(#/cm^3)	v(cm/s)	Sech($\frac{3v\lambda}{4R}$)	λ (ms)
			Sulphur			
72	28.3	0.0021	185	4.56	0.039	28.7
63	31.0	0.0298	237	4.35	0.134	20.7
57	32.0	0.0800	255	4.25	0.214	17.4
54	33.8	0.0469	285	4.21	0.492	10.6
51	34.7	1.136	298	4.22	0.749	6.3
			Talc			
72	28.3	0.0023	185	4.56	0.041	28.5
60	31.5	0.007	246	4.30	0.064	26.7
48	35.5	0.0277	310	4.18	0.115	22.7
36	42.0	0.2607	382	4.36	0.312	14.0
21	48.9	2.8183	410	4.79	0.944	2.4
			Molybdenite			
72	28.3	0.0003	185	4.56	0.015	35.8
51	34.7	0.0011	298	4.18	0.023	35.6
26	42.0	0.0047	382	4.36	0.042	29.5
21	48.9	0.0188	410	4.79	0.077	22.7
12	55.2	0.0665	458	5.17	0.132	17.5

APPENDIX V

UV Analysis of Liberated Sulphur on $CuFeS_2$, PbS and AsS

Standard Solutions

10 mg of elemental sulphur (Orthorhombic, 99.999% pure) was dissolved in 200 ml of absolute ethanol (Consolidated Alcohols Ltd.). This stock solution was used to prepare standard solutions of 2 to 50 ppm sulphur. The absorbance values of the standard solutions observed at 262 mμ and 275 mμ are listed in Tables A.V.1 and A.V.2.

Table A.V.1

Absorbance Values of UV by Elemental Sulphur in Ethanol (at 275 mμ)

Standards (ppm)	Absorbance 1	Absorbance 2	Corrected Average Adsorbance
Blank 1	0.012	0.012	-
2.0	0.066	0.068	0.055
3.5	0.105	0.109	0.095
5.0	0.144	0.146	0.133
7.5	0.210	0.214	0.200
10.0	0.268	0.270	0.257
12.5	0.340	0.344	0.330
15.0	0.398	0.397	0.385
20.0	0.543	0.541	0.530
25.0	0.633	0.636	0.623
30.0	0.790	0.794	0.780
35.0	0.870	0.875	0.861
50.0	1.249	1.254	1.240
Blank 2	0.012	0.013	-

Table A.V.2

Absorbance Values of UV by Elemental Sulphur in Ethanol (at 262 mμ)

Standard (ppm)	Absorbance 1	Absorbance 2	Corrected Average Absorbance
Blank 1	0.016	0.016	-
2.0	0.070	0.072	0.055
3.5	0.110	0.110	0.111
5.0	0.153	0.154	0.137
7.5	0.220	0.219	0.220
10.0	0.278	0.279	0.262
12.5	0.365	0.369	0.351
15.0	0.410	0.409	0.393
20.0	0.569	0.571	0.570
25.0	0.656	0.657	0.641
35.0	0.903	0.905	0.888
50.0	1.262	1.264	1.247
Blank 2	0.016	0.017	-

Reference Solvent Cuvette
Sample Solution Cuvette
} Far UV 'TSL' cells

$$\text{Corrected Average Absorbance} = \left[\left(\frac{\text{Abs.1} + \text{Abs.2}}{2}\right) - (\text{Average blank abs.})\right]$$

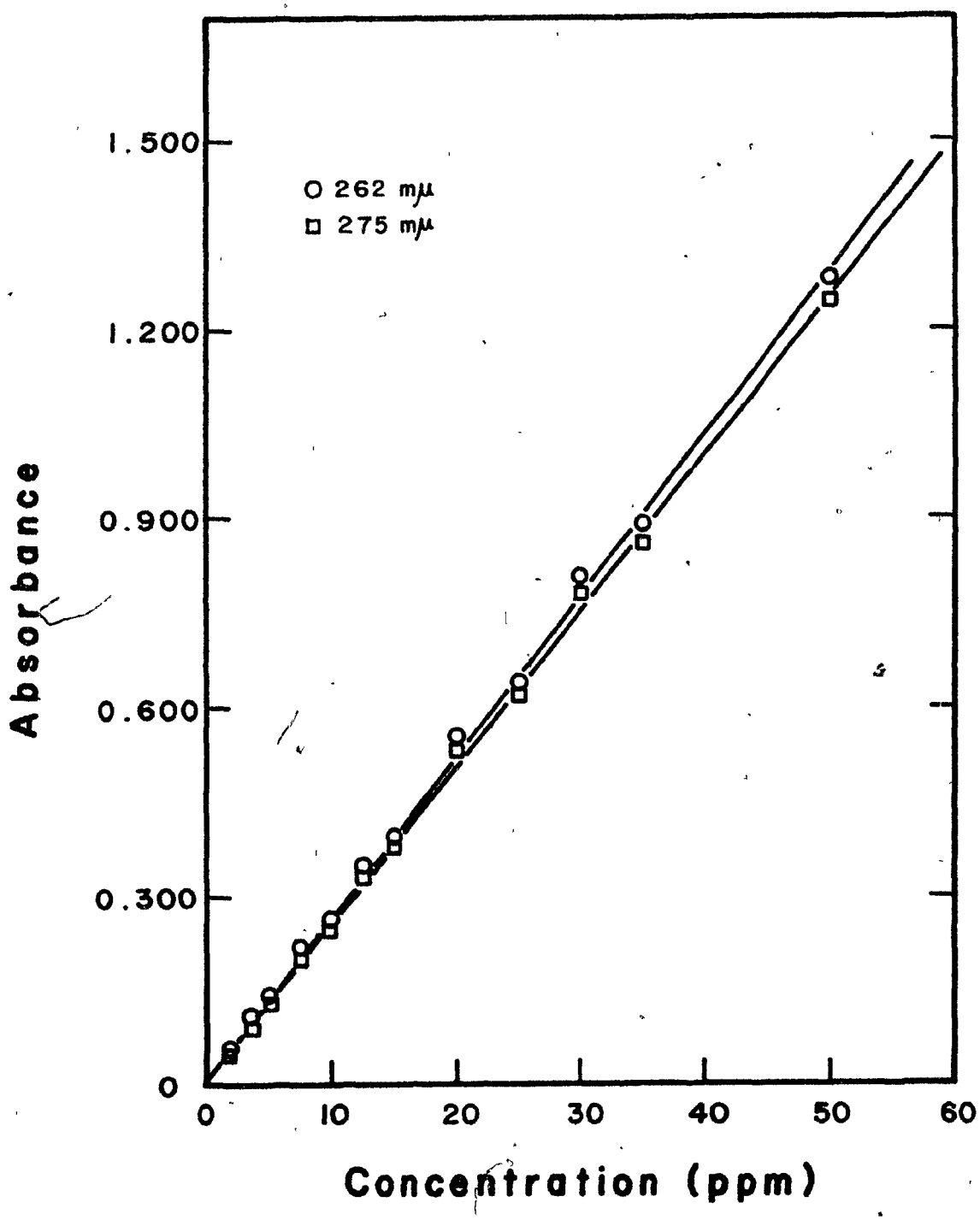


Figure A.V.1 Calibration Curve for the Determination of the Concentration of Sulphur in Ethanol Using UV Spectrophotometer

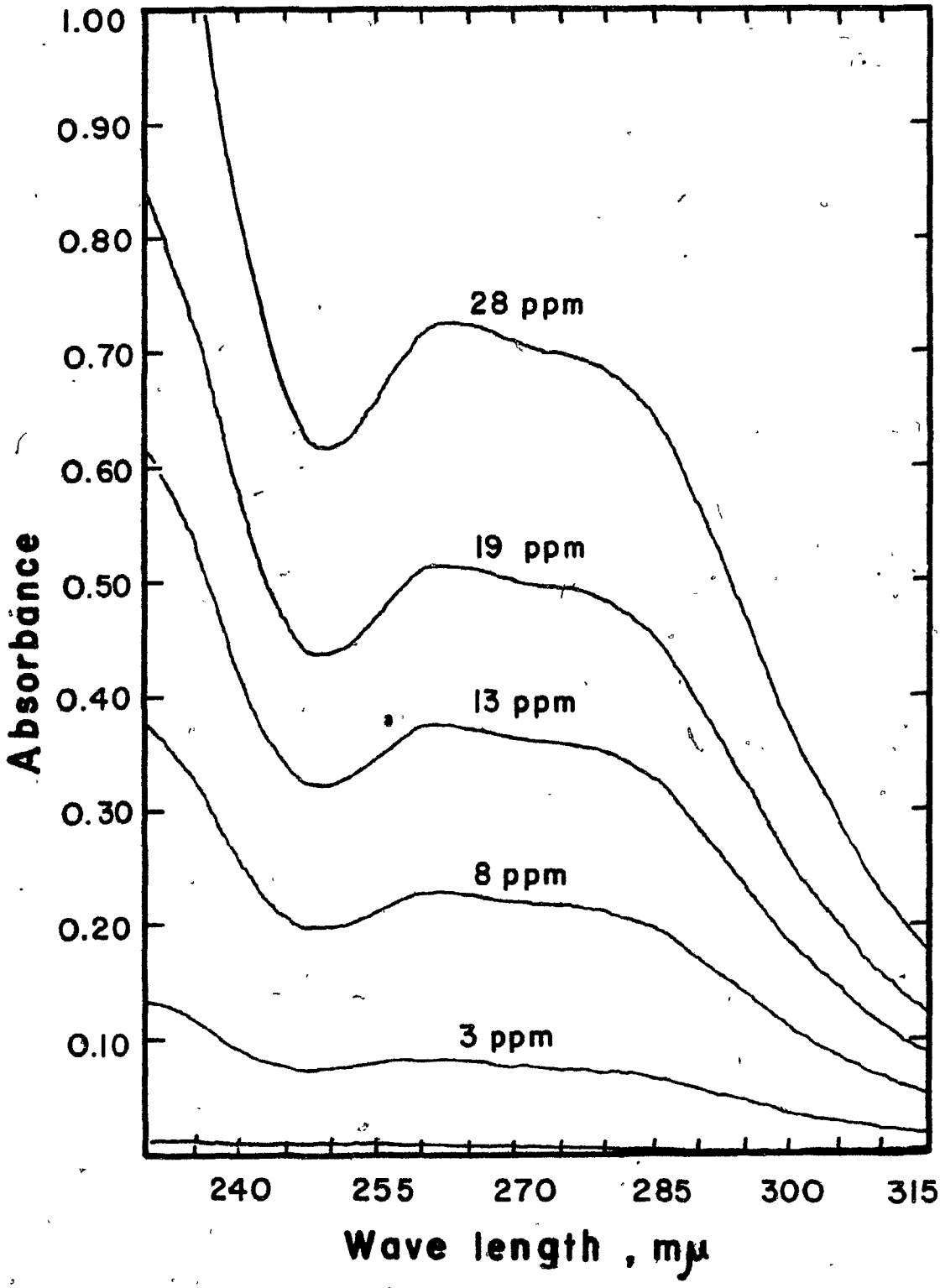


Figure A.V.2 Typical UV Spectra of Sulphur in Ethanol

Sample Calculation for Liberated Sulphur Concentration on Sulphide Minerals

Sample = Freshly ground (dry) Chalcopyrite

Specific Surface Area = $0.0614\ m^2/g = 0.614 \times 10^{20}$ Sq.A°/g

Extracted Sulphur = 0.0674 mg/g.

S° = 32.064 g./Atom

Packing Area of Sulphur = 8.62 sq. A°

Avogadra's Number = 6.023×10^{23}

$$\text{Total Hypothetical Area} = \frac{0.0674 \times 10^{-3}}{32.064} \times 6.023 \times 10^{23} \times 8.62$$

$$= 1.0913 \times 10^{19} \text{ Sq.A°/g}$$

$$\text{Equivalent Sulphur Monolayers} = \frac{1.0913 \times 10^{19}}{0.0614 \times 10^{20}}$$

$$= 1.8$$

APPENDIX VI

A - Preparation and Purification of Alkyl Xanthates

Introduction

Xanthates are dithiocarbonates. The general structural formula of a potassium alkyl xanthate may be represented by:-

$$R\text{-}O\text{-}C(=S)\text{-}S^{-}K^{+} \quad , \quad R \equiv C_nH_{2n+1} \qquad 1$$

where R is the alkyl group, the length of which is determined by the number of carbon atoms, n.

Xanthates containing one or more than five carbon atoms are not commercially available. Those which are available (i.e. with n ranging 2 to 5) require several purification steps prior to being used for research purposes. Since the present investigation involved the use of a large number of n-alkyl xanthates in a homologeous series, their synthesis was necessary. The reagents used in the preparation and/or purification are listed in Table A.VI.1. A primary alcohol (i.e. alkan-1-ol) is the essential ingredient to react with carbon disulphide to produce the desired molecule. In fact, the name of the xanthates are based on the alcohol used in their synthesis. Thus, normal butyl xanthate is produced from normal butyl alcohol.

Method

Potassium alkyl xanthates are produced according to the following reactions:-

$$R\text{-}OH + KOH \longrightarrow R\text{-}OK + H_2O \qquad 2$$

$$R\text{-}OK + CS_2 \longrightarrow ROCSSK \qquad 3$$

Table A.VI.1

Chemical Reagents Used in the Preparation and Purification of Potassium Alkyl Xanthates

Alcohols	Source and Grade
Methanol	Fisher Sci., Certified
Ethanol	Consolidated Alcohols Ltd., Absolute
n-Propanol	J.T. Baker Co., Reagent
n-Buthanol	Fisher Sci., Certified
n-Hexanol	J.T. Baker Co., Reagent
n-Octanol	Fisher Sci., Certified
n-Decanol	Eastman Kodak
n-Dodecanol	J.T. Baker Co., Reagent
Others	
Carbon disulphide	Anachemia, Reagent
Potassium hydroxide	Fisher Sci., Pellets
Acetone	Anachemia, Reagent
Acetone	Am. Chem. Ltd., Spectrograde
Benzene	Fisher Sci., Reagent
Petroleum ether	B.D.H., Analar Reagent
Ethyl ether	Fisher Sci., Lab Grade
Potassium Pentyl (Amyl) Xanthate	Cyanamid

The method of preparation is essentially similar to that described by Foster (Rao, 1971) for ethyl xanthate.

From Equations 2 and 3, the amount of alcohol, potassium hydroxide and carbon disulphide was stoichiometrically determined to obtain between 15 and 20 grams of xanthate. To the alcohol in a 400ml beaker was added potassium hydroxide in the form of a saturated aqueous solution. While the mixture was stirred and cooled using an ice-bath carbon disulphide was introduced slowly. The stirring was continued for about 10 minutes. By that time, the fluid mixture had turned into a nearly solidified state, a thick orange mass which contains yellowish xanthate and reddish polysulphides formed by side reactions. The polysulphides and impurities were removed initially by filtering under suction, and later by dissolving in acetone (reagent grade) and separating all the reddish polysulphide phase using a separatory funnel. The yellow phase containing the solution of xanthate in acetone was transferred to a conical flask which was connected to the suction system by a water pump and the xanthate was crystalized in a relatively short time. The crystals were filtered and washed with petroleum ether. Then the washed material was redissolved in acetone (spectro grade) and reprecipitated by petroleum ether. To improve the purity this was repeated twice. When petroleum ether was not available reprecipitation was done using benzene or ethyl ether for some xanthates. The final precipitate was filtered, washed with ether and stored in a vacuum desiccator.

Potassium pentyl xanthate (cyanamid) available in the laboratory, was subjected to the purification stage only.

Bulk lead xanthates were prepared according to the following reaction between potassium alkyl xanthate and lead chloride:-

$$2\ ROCSSK + PbCl_2 \longrightarrow Pb(ROCSS)_2 + 2KCl \qquad 4$$

The lead xanthate precipitate obtained was filtered, washed with ether, dried and stored in a vacuum desiccator until required. In general, the xanthates were used within two weeks after their preparation.

Table A.VI.2

The Contact Angle and Adhesion Tension Data for Xanthated Galena in Aqueous Methanol Solutions

Methanol %(vol.)	γ_{lv} (mN/m)	Contact Angle (Θ) (degrees)							$\bar{\theta}$	$\gamma_{lv}\cos\bar{\theta}$ (mN/m)
Methyl-Xanthated Galena										
0	72.5	51/50	51/50	51.51	50/50	49/50	50/49	51/49	50.1	46.5
2	68.6	50/48	50.49	48/48	48/47	47/48	47/47	48/47	48.0	46.9
4	62.4	49/47	49/50	48/47	47/47	48/50	46/47	46/47	47.8	41.9
12	55.2	42/43	41/40	43/41	41/43	43/44	42/43	43/43	42.3	40.8
18	51.2	36/35	35/34	36/38	36/35	35/37	38/36	36/35	35.9	41.5
27	45.7	30/30	29/30	30/31	31/32	31.30	30/31	29/30	30.3	39.5
36	42.0	25/25	25/26	25/25	26/25	25/26	26/25	26/27	25.6	37.9
45	36.3	22/23	22/20	23/22	21/23	22/22	23/22	23/23	22/2	33.6
57	32.0	18/18	18/19	19/17	18/19	18/19	18/17	-	18.2	30.4
66	30.1	14/15	13/14	0	15/13	0	0	15/14	14.1	29.1
0	72.5	47/48	45/49	50-45	48/49	47/46	45/47	-	47.2	-
Ethyl-Xanthated Galena										
0	72.5	50/60	61/60	60/60	61/60	59/59	59/60	60/59	59.9	36.4
2	68.6	58/57	59/59	58/60	59/60	59/59	57/58	58/59	58.6	35.7
4	62.4	55/55	54/55	55/57	54/56	54/56	53/55	54/54	54.8	36.0
12	55.2	53/52	52/53	51/53	52/52	50/51	51/52	51/52	51.8	34.1
18	51.2	47/48	47/49	48/48	47/46	48/46	46/47	47/48	47.3	34.7
27	45.7	41/43	42/40	41/41	42/43	41/43	41/42	42/43	41.8	34.1
36	42.0	36/38	35/37	37/36	35/36	36/36	38/36	-	36.3	33.8
45	36.3	28/27	26/28	27/27	25/27	25/25	26/25	28/27	26.5	32.5
57	32.0	18/18	17/18	0	18/18	0	0	0	-	30.5
66	30.1	0	0	0	13/14	0	0	0	-	30.1
0	72.5	58/57	58/59	60/61	59/59	58/60	-	-	-	-

Table A.VI.3

The Contact Angle and Adhesion Tension Data Cont'd.

Methanol % (vol.)	$\gamma_{\ell v}$ (mN/m)	Contact Angle (θ) (degrees)							$\bar{\theta}$	$\gamma_{\ell v}\cos\bar{\theta}$ (mN/m)
Propyl-Xanthated Galena										
0	72.5	66/68	67/67	65/66	67/68	67/67	66/67	67/66	66.7	28.7
2	68.6	67/67	65/65	66/68	65/65	66/65	65/67	67/66	66.0	27.9
4	62.4	63/64	64/63	63/62	63/64	63/63	63/64	63/63	63.0	28.1
12	55.7	61/59	58/60	57/57	57/58	58/58	57/57	58/57	58.0	29.5
18	51.2	55/53	54/53	52/54	54/52	52/54	-	-	53.0	30.6
27	45.7	50/48	47/49	48/49	49/48	49/48	48/46	-	48.3	30.4
36	42.0	40/42	42/42	38/41	39/40	37/41	37/37	-	39.7	32.4
45	36.3	34/35	34/34	33/33	34/34	32/33	32/33	32/33	33.3	30.4
57	32.0	20/21	0	0	21/20	20/20	0	0	20.3	30.0
66	30.1	14/17	0	0	0	0	0	0	0	30.1
0	30.1	64/61	61/65	66/67	57/55	48/45	61/50	-	58.0	-
Butyl-Xanthated Galena										
0	72.5	75/76	75/76	74/76	76/75	76/74	75/75	-	75.2	19
2	68.6	75/75	74/73	73/73	73/75	74/75	75/76	75/74	74.3	18.6
4	62.4	70/71	71/68	71/71	69/71	68/71	69/70	68/71	69.9	21.5
12	55.7	64/64	63/65	64/66	65/64	65/66	64/65	64/65	64.6	23.9
18	51.2	61/60	60/61	59/60	60/60	61/60	59/61	61/61	60.3	25.4
27	45.7	55/54	56/54	55/55	55/53	55/54	56/53	54/55	54.6	16.5
36	42.0	48/49	47/49	46/49	47/48	48/48	48/48	46/48	47.8	28.2
45	36.3	42/43	43/41	43/42	42/43	43/40	41/41	41/51	41.9	27.0
57	32.0	32/31	32/32	31/32	33/33	31/31	31/31	31/33	31.7	27.2
66	30.1	24/25	24/24	24/25	25/24	25/24	24/23	25/24	24.3	27.4
0	72.5	73/75	72/74	76/75	76/73	74/75	76/77	-	74.7	-

Table A.VI.4

The Contact Angle and Adhesion Tension Data Cont'd.

Methanol % (vol.)	$\gamma_{\ell v}$ (mN/m)	Contact Angle (θ) (degrees)							$\bar{\theta}$	$\gamma_{\ell v}\cos\bar{\theta}$ (mN/m)
Pentyl-Xanthated Galena										
0	72.5	87/84	87/85	85/86	86/87	86/85	86/87	87/86	85.9	5.1
2	68.6	87/84	87/85	85/86	83/83	86/84	82/83	81/83	82.7	8.7
4	62.4	78/80	81/80	79/78	80/79	78/79	79/78	78/80	79.0	11.9
12	55.7	70/71	72/73	74/73	72/71	73/71	71/73	71/71	71.9	17.3
18	51.2	68/68	67/67	69/69	68/69	68/67	66/66	66/66	67.4	19.7
27	45.7	62/61	61/60	62/63	60/62	62/62	60/62	62/62	61.5	21.8
36	42.0	58/56	59/56	59/56	56/57	57/57	56/55	56/56	56.5	23.1
45	36.3	47/49	49/50	48/49	49/50	49/50	48/48	50/50	49.0	23.8
57	32.0	36/36	36/36	35/35	36/36	36/36	36/38	35/37	36.0	25.9
0	72.5	71/70	76/78	73/73	83/84	85/86	73/74	-	77.2	-
Hexyl-Xanthated Galena										
0	72.5	91/92	91/93	92/92	91/92	89/91	92/90	91/91	91.3	-1.6
2	68.6	88/90	90/90	90/90	89/90	89/89	90/90	89/90	89.6	0.5
4	62.4	85/86	86/87	86/88	85/86	88/86	85/87	86/86	86.2	4.1
12	55.7	81/80	79/81	81/82	81/80	81/81	80/82	81/81	80.8	8.9
18	51.2	75.74	76/76	78/76	77/77	76/75	78/75	75/75	75.9	12.5
27	45.7	70/70	69/70	69/69	70/70	71/72	69/70	72/72	70.3	15.4
36	42.0	66/66	64/66	64/66	65/66	63/64	65/66	64/65	65.1	17.7
45	36.3	54/54	53/53	54/55	56/54	57/56	56/56	56/57	55.1	20.8
57	32.0	42/44	42/43	45/44	45/47	44/45	46/44	45/45	44.4	22.9
66	30.1	31/32	30/29	32/30	31/29	30/30	29/30	32/31	30.5	25.9
0	72.5	90/90	89/88	90/91	90/90	90/90	-	-	89.8	-

Table A.VI.5

The Contact Angle and Adhesion Tension Data Cont'd.

Decyl-Xanthated Galena

Methanol %(vol.)	$\gamma_{\ell v}$ (mN/m)	Contact Angle (θ) (degrees)						$\bar{\theta}$	$\gamma_{\ell v}\cos\bar{\theta}$
0	72.5	100/102	101/101	101/102	103/103	102/103	100/101	101.6	-14.6
4	62.4	97/98	95/96	92/93	94/96	96/97	-	95.4	- 5.9
12	55.7	91/89	89/89	89/87	89/89	89/90	90/90	89.3	0.7
18	51.2	84/85	86/85	83/85	85/83	85/84	90/90	84.5	4.9
27	45.7	79/80	77/78	80/81	80/79	80/79	81/80	79.5	8.3
36	42.0	76/77	74/75	75/74	74/75	75/75	76/75	75.1	10.8
45	36.3	66/66	67/68	69/67	65/66	66/66	67/67	66.7	14.4
57	32.0	56.54	54.55	55/55	55/55	54/55	-	54/8	18.4
66	30.1	42/43	45/44	44/46	43/43	43/43	43/43	43.5	21.8
80	27.6	27/24	26/26	29/25	25/27	27/24	26/23	25/8	24.8
0	72.5	86/90	80/85	83/93	95/90	92/93	-	88.7	-

Table A.VI.6

The Polar Component of the Surface Free Energy of Xanthate Coatings on Galena

Xanthate Coating	Octane Contact Angle (degrees)						Mean Value	γ_s^P
Methyl -	80/79	79/80	79/79	79/78	79/80	78/78	79.0	18.0
Ethyl -	96/95	93/94	94/94	95/94	96/95	94/94	94.5	10.8
Propyl -	104/104	105/103	104/105	104/103	105/103	103/104	103.9	7.3
Butyl -	118/120	121/119	118/119	118/118	117/119	-	118.7	3.4
Pentyl -	135/134	134/134	134/135	135/133	134/133	133/133	133.9	1.2
Hexyl -	141/144	142/141	142/140	141/140	140/140	-	140.8	0.6
Oxtyl -	152/151	151/152	152/152	152/152	152/152	-	151.9	0.2
Decyl -	173/173	174/173	172/174	172/173	-	-	173.0	0.001